Metal Oxide Substituted Polyurethane foams for enhanced craniofacial bone repair

Exploring the properties of Cerium, Zirconium and Copper doped Zinc oxide nanoparticles as potential additive for bone regeneration and angiogenesis.

Hafsah Akhtar

Registration No. 170138448

Thesis submitted in partial fulfilment of the requirements for the degree of Doctor of Philosophy

Department of Material Science and Engineering

University of Sheffield

United Kingdom

September 2021

Awards and Conferences

Awards

Learned Society University of Sheffield Travel Grant WBC Glasgow	2020
Learned Society University of Sheffield Travel Grant BioMedEng	2019
Armours and Brasiers Travel Grant Travel Grant TERMIS EU MEETING	2019
Learned Society University of Sheffield Travel Grant TERMIS EU MEETING	2019
University College London travel and research grant	2018

Posters

BiomedEng Sheffield, UK	September 2021
7th International symposium on Biomedical Materials Science and Technology Innovation and the Knowledge Economy Lahore, Pakistan	11-12 December, 2019
Bioengineering Lancaster conference, UK	october 15 2019
BioMedEng London, UK	(5th – 6th September) 2019
2nd Year Postgraduate Poster Presentation Sheffield, UK (Runners Up)	2019
Insigneo Showcase Sheffield, UK	(17th May,2019
Christmas Conference Lancaster , UK	(18th Dec 2018)
Christmas Conference Lancaster , UK	(18th Dec 2018)

Podium

11th World Biomaterials Congress, Glasgow, UK	December 2020
Nanomaterials for biosensors and biomedical applications – Jurmala Latvia	(2nd- 4th July-2019)

TERMIS EU 2019 Meeting -Rhodes Greece	(27^{th} – 31^{st} May 2019)
Engineering Research Symposium (1^{st} - Materials), Sheffield, UK	2019

Attendee

Research and Development Conference , UK	24^{th} May, 2018

Dedication

To my parents M. Akhtar and Samina Khanum ….

I could not have done this without you

Acknowledgements

I am highly indebted to University of Sheffield-Doctoral Academy for awarding me scholarship to support my PhD. I would like to say thanks to my Supervisor Prof. Gwendolen Reilly for her valuable advices whenever I needed. Your appreciation and enthusiasm motivated me to push my limits and complete within time limit. I would like to thank my co supervisors Prof. Ihtesham Ur Rehman and Dr. Aqif Anwar Chaudhry for their guidance during project design. Some of the work was conducted at UCL; for that I am grateful to Prof. Jawwad Darr and Dr. Thomas Ashton for supporting my research visit financially and intellectually. I am thankful to my mentor and friend Dr. Ather, who listened to my pointless worries patiently and guiding me during tough times especially during the start of my PhD.

I would like to say thanks to my friends Rabia Sanam Khan, Yasir and Fahad for their moral support and energy booster activities to keep me going towards my goals. I would like to thank my lab members Julie, Ballad, Tugba, Deepak, Jose, Rasmus and Alice for providing me with a good lab and office environment to survive long working hours. I enjoyed my PhD because of my friends and colleagues.

I would like to pay my gratitude to Post Doc Ihtesham Raza and Ana for providing me training for cells handling and research discussions regarding cell culture data as I was new to this field. Many thanks to everyone in Biomaterials and Tissue engineering laboratory at university for Sheffield for organising Research in Innovation talks at Kroto and Insigneo which really helped me learn and improve my research.

My deepest appreciation goes to my husband for understanding and supporting my thesis writing journey. This seemed a never-ending journey and I could not have done this without your love and support. I would like to thank my mom for listening my everyday stories about failed experiments or lost time which I am sure she had no idea but still she was there to support me and tell me that I can do this.

Finally, I would like to pay my gratitude again to my supervisor Prof. Gwendolen Reilly for providing me with excellent research and social environment during this PhD which helped me become an independent researcher and a team player.

Table of Contents

Table of Contents

List of Figures

List of Tables

Abstract

Zinc oxide containing bone regenerative scaffolds have great potential in bone tissue engineering since zinc oxide has multifunctional properties and is one of the most researched metal oxide. Zinc oxide have been synthesized via different methods and in different morphologies such as nanowires, rods and nanoparticles. It is a known antibacterial agent and can promote cell growth, differentiation, and angiogenesis. Within this thesis, cerium, zirconium and copper doped zinc oxides were synthesized using eco-friendly continuous hydrothermal flow system. The nanoparticles were characterized and change in particle size and morphology was seen. The zirconium doping resulted in smallest particle size i.e. from 83 nm (ZnO_2) to 45 nm (ZrZnO5). The porous polyurethane-hydroxyapatite scaffolds containing doped zinc oxides were fabricated using freeze extraction salt leaching process. The 1% CeZnO5, ZrZnO5 and CuZnO5 was added to polyurethane-hydroxyapatite scaffold. The cell seeding efficiency data revealed 60% cell adhesion for PU-HA-CeZnO5 scaffold, 45% cell adhesion for PU-HA-ZrZnO5 and 80% for PU-HA-CuZnO5 scaffolds when compared with PU only or PU-HA and PU-HA-ZnO_2. The cell metabolic activity assay revealed highest cell metabolic activity for scaffolds incorporated with doped zinc oxide nanoparticles. The raised ALP levels were also detected with doped zinc oxide incorporated scaffolds which is an early marker for bone regeneration. The current data suggested that the doped zinc oxide nanoparticles can be used as additives for bone regenerative applications and angiogenesis.

1.1 Introduction

Craniofacial Bone is a highly vascularized tissue and its repair and regeneration is challenging, especially when the network of blood vessels is disrupted due to disease or injury making the healing extremely difficult. Such injuries result mainly from trauma, which disrupts the complex network of blood vessels, resulting in lack of blood supply to bone-forming osteoblasts and a delay in the healing process. Currently, scaffold implantation when undertaken for the purpose of bone repair induces an inflammatory healing response, which usually takes weeks to form a network of blood vessels (Bramfeld et al., 2010). The currently available scaffolds for craniofacial reconstruction do not induce angiogenesis (formation of blood vessels) instead they rely on the inflammatory healing response that results in insufficient oxygen and nutrient supply, hence resulting in non-uniform cell differentiation and cell death (Bramfeld et al., 2010; Malda et al., 2004; Rouwkema et al., 2008).

Bone tissue engineering is a therapeutic strategy to combine different ceramic and polymeric materials to obtain a graft or scaffold having the ability to induce bone cell adhesion, proliferation and leading to bone repair. The scaffold is basically a three-dimensional porous structure that is used to guide the cells towards bone formation. This process is dependent on the surface properties of the scaffold as it comes into direct contact with the biological environment. The major challenge is to mimic the extracellular (ECM) environment for ideal bone repair. Researchers are identifying different biomaterials which fulfil some requirements of ECM. Creating composites by combining different materials with different properties might help with successful bone regeneration applications.

A biomimetic bone scaffold material should be osteoconductive, osteoinductive and osteogenic (Vo et al., 2012) along with necessary properties, such as, biocompatibility, bioresorbability and reasonable mechanical strength, mainly compressive strength (Butscher et al., 2011). Osteoconduction requires enough porosity for cell adhesion and migration, osteoinductive properties promote stem cell differentiation towards osteoblast formation and osteogenesis. This involves stem cell metabolism, upregulation of growth factors and bone regeneration (Gong et al., 2015).

Zinc oxide has recently caught attention in the field of nanomaterials for its ability to induce upregulation of fibroblast growth factor (FGF) and vascular endothelial growth factor

(VEGF) which result in angiogenesis and osteogenesis (Augustine, Dominic, et al., 2014b). β-TCP and zinc oxide containing scaffolds have been found to upregulate bioactivity and improve mechanical strength when compared with β-TCP scaffold alone (Feng et al., 2014; Macchetta et al., 2009). Nano-Hydroxyapatite mimics natural bone mineral, addition of HA to scaffolds has been shown previously to upregulate osteogenic gene expression and osteogenic cell attachment to surfaces (Huang et al., 2013; Im et al., 2012). HA when combined with β-TCP results in more hard bone with upregulation of the Collagen type I gene, resulting in more calcification as compared to HA alone (Sulaiman et al., 2013). Copper is a pro-angiogenic metal, Cerium and Zirconium are reported to enhance cell attachment properties of material.

In the following thesis, I propose synthesis of novel composite materials made from polyurethane, hydroxyapatite and doped zinc oxide nanoparticles. The dopants used in this study are cerium, zirconium and copper. This thesis is focussed on exploring the role of doped zinc oxides on cell metabolic activity and scaffold properties. This is the first study reporting the cell metabolic activity of doped zinc oxide nanoparticles and their comparison between themselves. The cerium, zirconium and copper doped zinc oxide incorporated scaffolds were tested for cytotoxicity, metabolic activity, and potential bone regenerative materials. In this research, we aim to identify the change in lattice properties by incorporation of above-mentioned dopants followed by evaluation of variation in cell metabolic activity. This project links the tailored chemistry approach with tailored biology.

One of the key objectives of this thesis was to identify easy and inexpensive methods for synthesis of nanoceramics and scaffolds containing nanoceramics. In this study, the continuous hydrothermal flow system is utilised for synthesis of zinc oxide and doped zinc oxide which works on the principle of green technology and is highly efficient. Fabrication of craniofacial scaffolds will be carried out using a solvent casting-salt leaching process.

In addition, it is envisaged that copper, cerium and zirconium would interact with the lattice structure of zinc oxide which may alter its ability to produce reactive oxidative species or hypoxia in the biological environment which might help in inducing the process of angiogenesis and osteogenesis.

1.2 Hypothesis

Polymer/Apatite scaffolds loaded with doped zinc oxide can be synthesised with appropriate morphology to act as a bone tissue engineering scaffolds. Such scaffolds will be non-toxic to differentiating bone cells and support the cellular synthesis of the pro-angiogenic growth factor VEGF.

It is hypothesised that incorporation of zinc oxide and doped zinc oxide i.e. cerium doped zinc oxide, copper doped zinc oxide and zirconium doped zinc oxide will result in a change in properties compared to those of zinc oxide alone, which would lead to a unique biological properties of the final scaffold. Doped zinc oxide will upregulate cell metabolic activity of osteogenic precursor cells and raise ALP activity, an early marker for osteogenesis.

1.3 Aims and Objectives

1.3.1 Global Aim:

To design and test a set of composite scaffolds using ceramic particles known to be inhibitors of bacterial growth and facilitators of angiogenesis, with the ability to induce osteogenesis. A set of scaffolds will be produced that will be ready to progress to angiogenic/osteogenic bone repair and pre-clinical testing.

1.3.2 Aim:

The main aim of the work presented in this thesis was to explore the properties of the doped zinc oxide developed by a continuous hydrothermal flow system. The cytoxicity or cell metabolic activity analysis of cerium, zirconium and copper zinc oxide nanoparticles have not previously been evaluated. In This research, the cell growth kinetic and cytoxicity in response to doped zinc oxide nanopowders will be evaluated. Furthermore, the influence of powders containing different ionic dopings within porous scaffolds on cell growth, adhesion efficiency and metabolic activity will be investigated. This contributes to the long-term goal of fabricating a porous flexible scaffold incorporated with ceramic nanoparticles with potential of osteogenesis and angiogenesis for craniofacial repair and regeneration.

To achieve the aim of the research, the project was divided into following objectives:

1. Synthesis and characterisation of zinc oxide and doped zinc oxide nanoparticles.

a. Two different concentrations of precursors were used to obtain tuneable sized nanoparticles.

b. Different mole percentages of dopants were introduced during synthesis i.e 1, 3 and 5.

c. Characterisation of nanoparticles was performed to understand the effect of dopant introduction.

d. Cell metabolic activity analysis was performed using nanoparticle suspensions in cell culture media. The nanoparticle samples that resulted in high cell metabolic activity were selected for scaffold synthesis.

2. Porous scaffold synthesis.

a. The freeze extraction salt leaching process was used for scaffold synthesis.

b. The soluble products released from scaffolds were tested for cytotoxicity.

c. Cell attachment, seeding efficiency, growth kinetics were studied.

d. Alkaline phosphatase activity and VEGF ELISA were also performed to identify the osteogenic potential of the scaffolds.

e. A comparison between cerium, zirconium and copper doped zinc oxide was performed to identify potential nanoparticles for future work.

1.4 Literature review

1.4.1 Craniofacial Bone Anatomy and Physiology

Human adult bones are classified into cortical bone or compact bone and cancellous or trabecular bone depending upon the porosities. The porosity level of the bone is different in different regions of the bone in response to mechanical needs. Mechanical forces are also one of the triggers for adjustment of total bone mineral density through the process of bone remodelling. Cortical bone is basically compact bone with dense structure and is less porous however, the cancellous bone is highly porous (Wolff, 1870).

Compact Bone: Compact bone mainly contains osteons, which are composed of concentrically arranged osteocytes around a central canal which contains blood vessels that supply blood to osteons and deep bone tissue. Compact bone is thickest and withstands forces along the axis of alignment.

Trabecular or cancellous bone: Trabecular bone is also known as spongy bone because of high porosity. Trabecular bone is composed of meshwork fibres called trabeculae. Red bone marrow is present between the trabeculae which produces red blood cells, the blood vessels present in this tissue region provides the nutrients to trabeculae and remove the waste (Fig 1.1). This bone type is present in regions that are subject to lower mechanical forces because it is much lighter compared to compact bone and it reduces the weight of skeleton to allow the smooth movement of bones (Hollinger et al., 2004). Depending on where it is in the body, trabecular bone may also contain yellow bone marrow; adipose tissue cells which act as energy reservoir for the body.

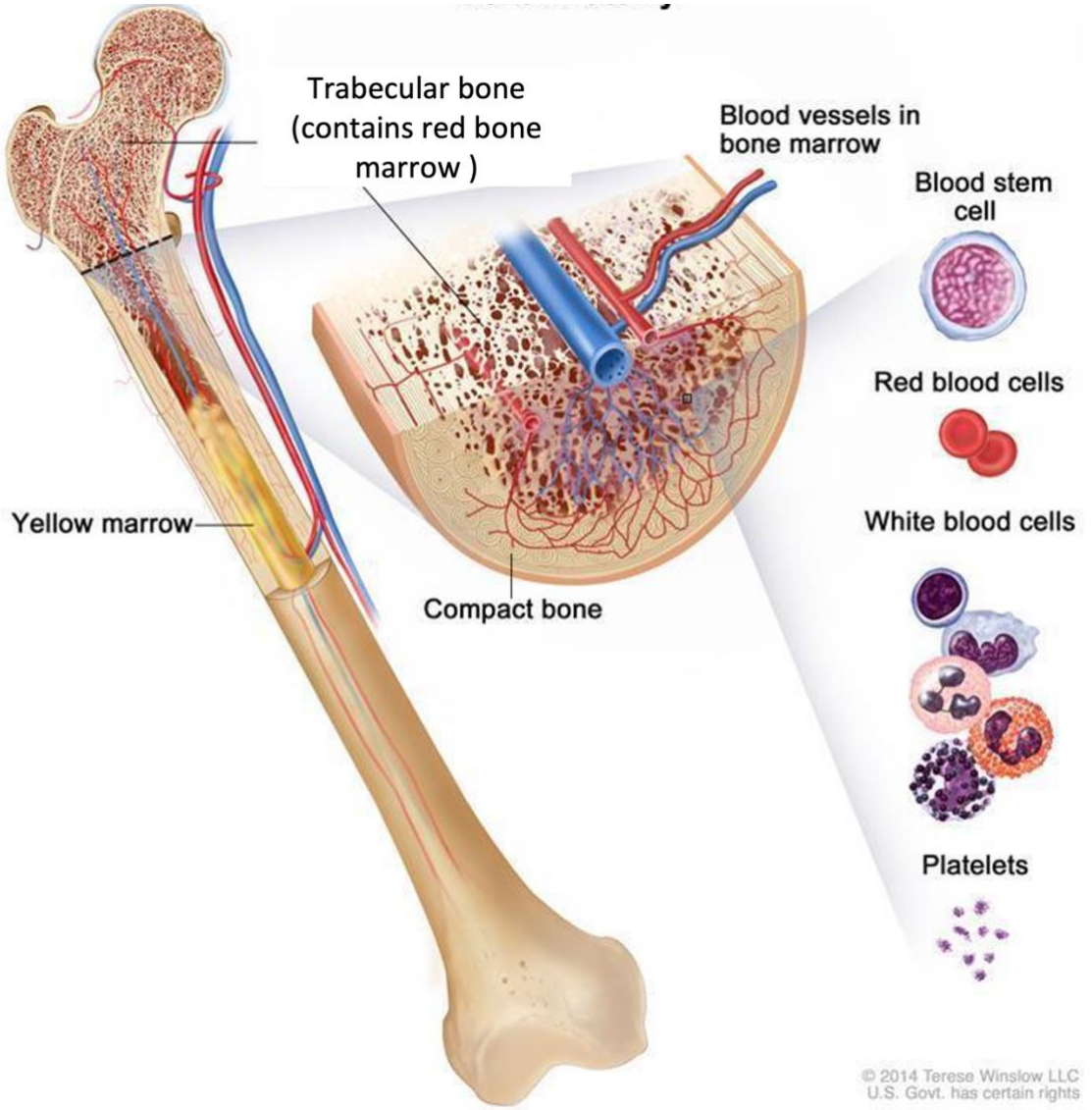

Figure 1.1: *A diagram of a human femur (thigh bone) illustrating the microstructure of compact and trabecular bone. Image used with kind permission of Terese Winslow.*

The skull is a complex 3D bony structure that houses the brain which is an essential functional part of the human body. The skull acts as a protective barrier for soft tissue and protects it from external forces that can lead to deformities. It is composed of compact and trabecular bone in the form of three layers. The two rigid bony layers formed of compact bone sandwiching trabecular in between are also known as dipole (DeSaix et al., 2013; Hollinger et al., 2004)(fig 1.2).

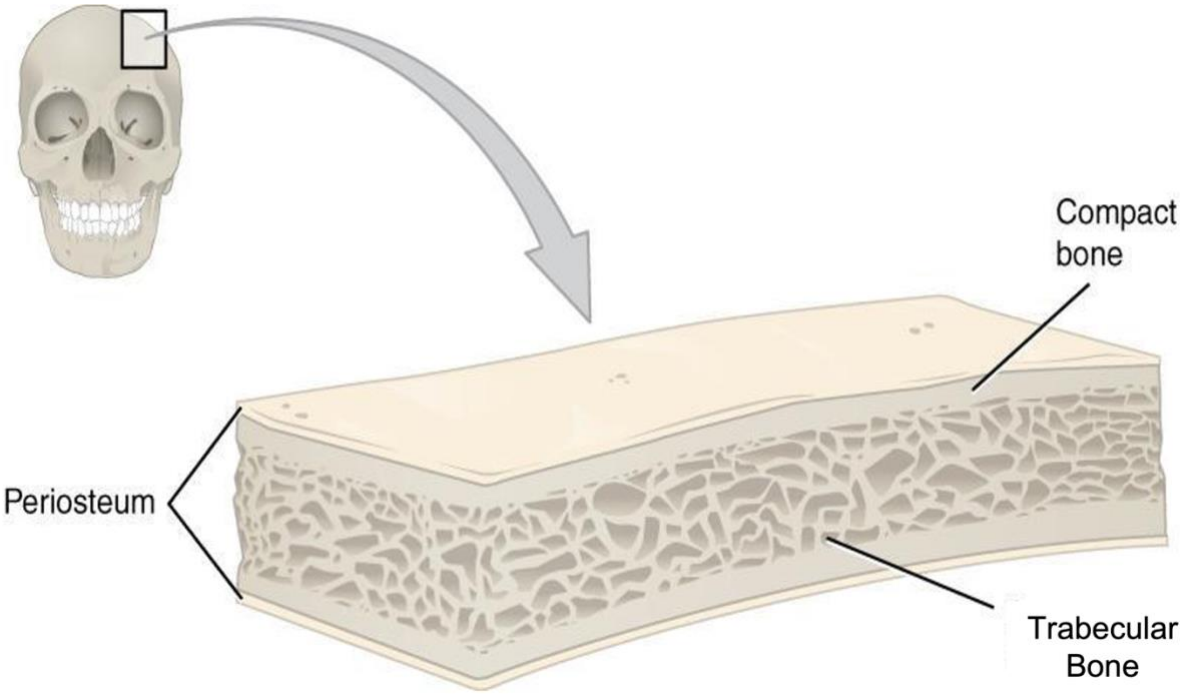

Figure 1.2: *Three layered skull bone structure. Reprinted under Creative Commons Attribution License 4.0 license* (DeSaix et al., 2013).

The skull is divided into frontal, occipital, temporal and parietal regions. The temporal and parietal regions of the skull are involved in the absorption of external forces. The temporal region is thinner in comparison to the other regions because of medially concave geometry and the parietal region is convex. The temporal and parietal regions are constitutively identical despite variations in geometry (fig. 1.3). During aging, the bones of the body reduce in density, but that's not the case for skull bones. The skull bones are composed of a high proportion of compact bone, which is less affected by bone resorption than cancellous bone (Yoganandan & Pintar, 2004).

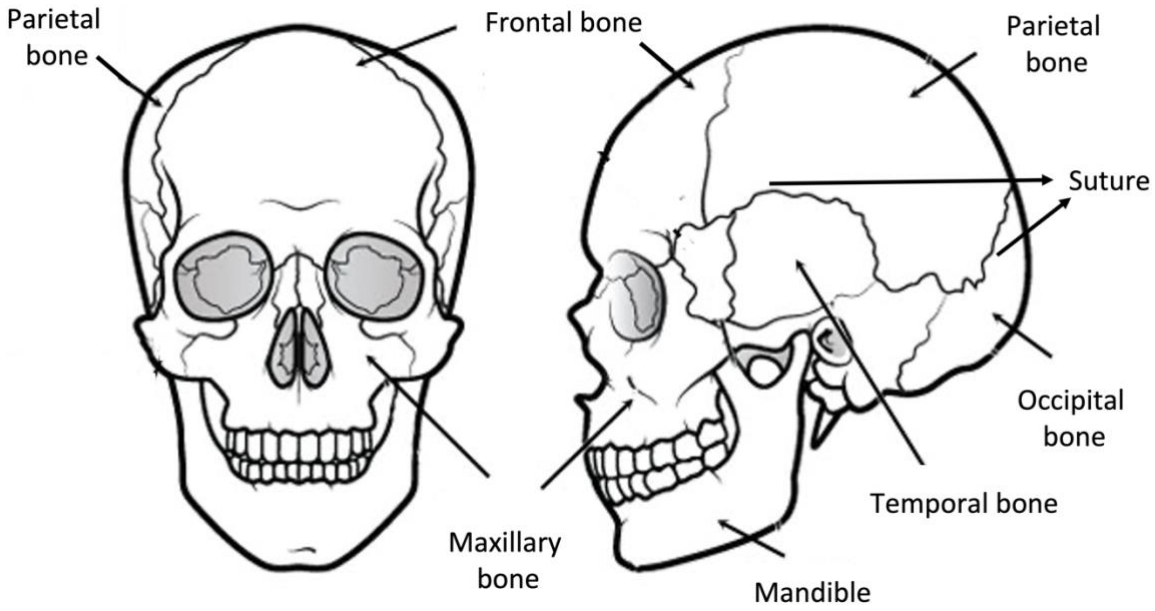

Figure 1.3 : Skull diagram showing location of Frontal, Parietal, Occipital and temporal regions.

1.4.2 Bone Structure and Osseous Tissue:

1.4.2.1 Bone Structure

Bone is a strong three-dimensional structure which can tolerate a reasonable range of compression, bending and twisting forces. It is composed of matrix and cells. The cells are classified as osteocytes, osteoblasts, osteogenic cells, and osteoclasts (fig.1.4). The bone tissue or osseous tissue is supporting connective tissue containing specialized cells and protein fibres. The tissue is solid and very dense in nature due to the presence of the hydroxyapatite-based calcium salts around and embedded in the collagen fibres. The osseous matrix contains bone cells-osteocytes which are present within lacunae and lacunae are present around the blood vessels (Rizzo, 2015).

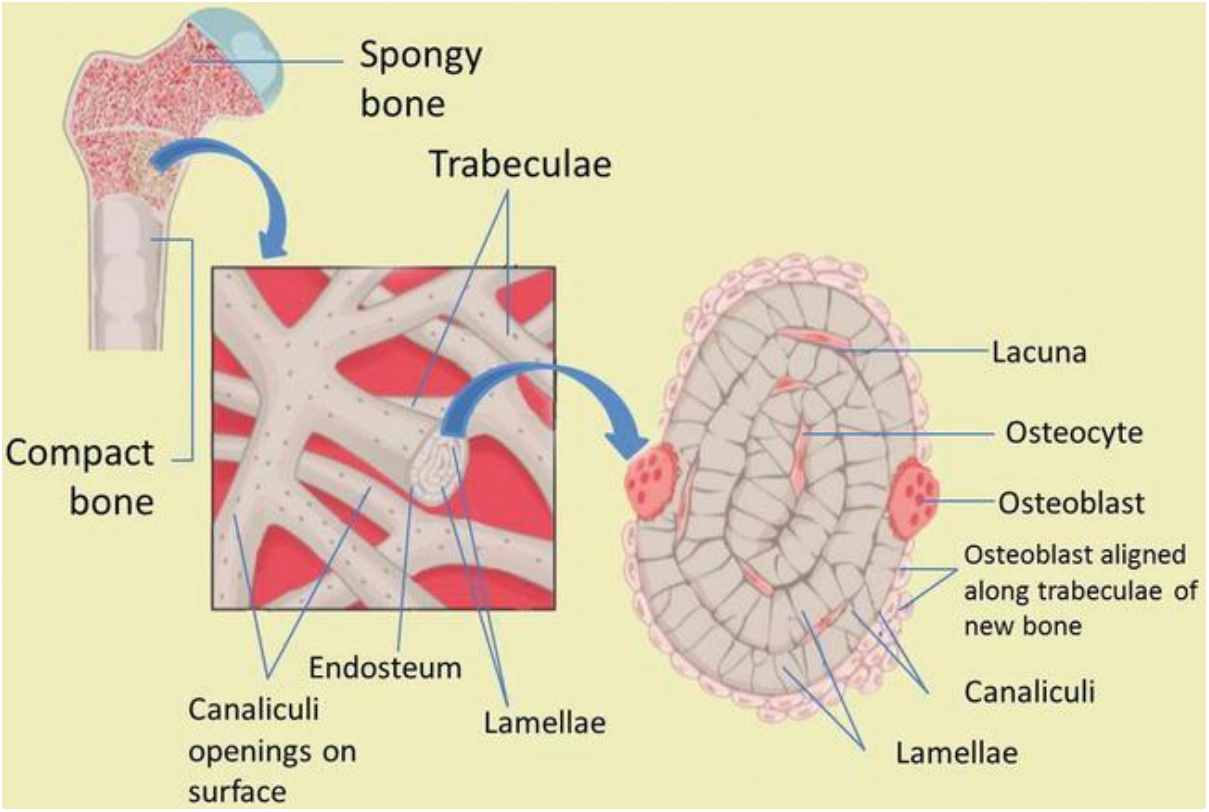

Figure 1.4: *The microstructure of trabecular bone. Reprinted under Creative Commons Attribution 3.0 License* (Setiawati & Rahardjo, 2019).

1.4.2.2 Bone Matrix

Two third (2/3 by weight) of bone matrix is composed of calcium phosphate ($Ca_3(PO_4)_2$) containing mineral. The calcium phosphate reacts with Calcium hydroxide ($Ca(OH)_2$) to form Hydroxyapatite crystals.

$$Ca_3(PO_4)_2 + Ca(OH)_2 \longrightarrow Ca_{10}(PO_4)_6(OH)_2$$

Formation of physiological hydroxyapatite crystals induces the incorporation of other calcium salts and ions such as Calcium Carbonate, Sodium ion, Magnesium Ion and Fluoride Ions. Hydroxyapatite crystals are strong and withstand high compression forces but are inflexible and brittle which makes them unfavourable for bending and twisting forces. However, one third (by weight) of bone is composed of collagen which is the organic part of the bone. Collagen provides the bone with flexible and tough properties. It is present in the form of long protein fibres which allow the deposition of Hydroxyapatite crystals in a geometrical fashion (Kołodziejska et al., 2020)(plates and rods) (Fig 1.5). This protein crystal

complex enables bone to tolerate compression, tension and bending/twisting forces, hence prevents it from shattering under loading.

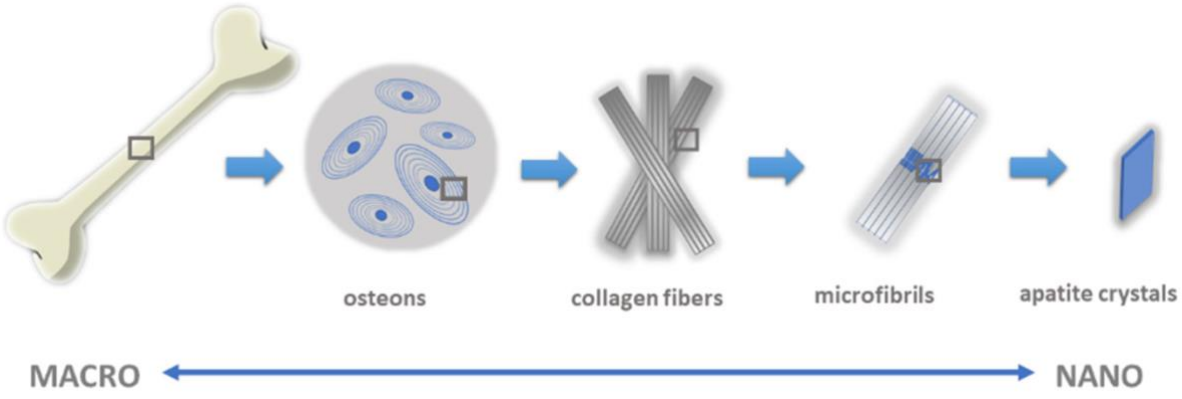

Figure 1.5: *Arrangement of apatite crystals on collagen fibres. Image is used under Creative Common CC BY licence* (Kołodziejska et al., 2020).

Hydroxyapatite synthesis and different substitutions in hydroxyapatite are being carried out to find a bone substitute close to natural bone for reconstruction and regeneration (Alhamoudi et al., 2021). Carbonated hydroxyapatite is available commercially and used as a moldable bone substitute. Photo-acoustic Fourier transform infrared (FTIR) spectroscopy was used to compare hydroxyapatite and carbonated hydroxyapatite to identify the differences (Rehman & Bonfield, 1997). Carbonated apatite is a low order crystalline biomaterial that resembles natural bone. carbonate apatite as bone substitute resulted in hardened fully functional bone in less time. Carbonated apatite was found to be a better alloplastic material as compared to hydroxyapatite for craniofacial reconstruction (Baker et al., 2002). It has been found to degrade at low acidic environments via osteoclast resorption and promotes bone regeneration within the bone graft without the formation of fibrous tissue (Rahyussalim et al., 2019).

1.4.2.3 Bone Cells

Bone can undergo resorption or formation according to the need, this phenomenon is known as bone remodelling. There are four types of bone cells: osteocytes, osteoblasts, osteogenic cells and osteoclasts. Osteoclasts are present in the blood and recruited when

bone resorption is required, however, the osteocytes, osteoblasts and osteogenic cells are all present in the bone. The bone cells are responsible for normal bone function.

Mature human bone morphology is in the form of layers called lamellae, in between lamella, pocket like structures are present called lacunae inhabited by osteocytes. One osteocyte resides in each lacuna. Osteocytes are basically mature bone cells and lack the ability to divide. All lacunae are connected with one another, with the matrix and to the vascular system (Fig 1.4). The vascular system is composed of a network of nerves, veins, and arteries responsible for nutrient and oxygen exchange (Fig 1.1). This system is connected via a small tubular network of canaliculi which contain the cytoplasmic extensions of osteocytes. Neighbouring osteocytes are connected by the gap junctions at the ends of these processes for ions and small molecular exchange, such as hormones and nutrients. The interstitial fluid surrounding the cells is also involved in the diffusion of the nutrients and waste products (Setiawati & Rahardjo, 2019).

Osteogenic cells or osteoprogenitor cells: Osteogenic cells or osteoprogenitor cells originate from mesenchymal stem cells (MSCs), present in a small number in bone tissue. These stem cells differentiate into bone, fat, cartilage and muscle. So far no identifying markers have been detected for stem cells to differentiate into bone (Pignolo, Robert J., Kaplan, 2008). MSCs differentiates into osteogenic progenitor cells which later differentiate into osteoblasts (Hollinger et al., 2004; Setiawati & Rahardjo, 2019).

Osteoblasts: The osteoblasts are differentiated form of osteoprogenitor cells which originate from pluripotent mesenchymal stem cells of the bone marrow (Mohamed, 2008). Osteoblasts are immature bone cells which are involved in new bone matrix formation, a phenomenon known as ossification or osteogenesis. In active state they are in cuboidal shape and involve in synthesis of proteins and other organic components to create the early stage organic matrix called osteoid. Osteoid is then mineralised by deposition of the calcium phosphate-based salts (DeSaix et al., 2013; Kołodziejska et al., 2020). Osteoblasts promote the local increase of the calcium phosphates above solubility level to aid their deposition in the organic matrix. This process converts osteoid to mineralised bone. Osteoblasts differentiate to osteocytes as they become embedded in this matrix (Hollinger et al., 2004). Osteoblasts, in general, facilitate mineralization which results in bone formation. They do so by three developmental stages;

proliferation, matrix maturation and mineralisation (Karsdal et al., 2002; Katagiri & Takahashi, 2002).

Bone lining cells and Osteocytes: When is bone it in resting state i.e. it is not undergoing formation or resorption, it is covered by flattened bone lining cells which prevent the bone from osteoclast activity. These are post proliferative osteoblasts which can become active osteoblasts in response to adequate bone formation signal (injury etc.). The osteocytes are post-proliferative mature osteoblasts which are entrapped inside the bone. About 90% of all bone cells are osteocytes. These are present in lacunae and finely distributed via. Canaliculi in all directions. The distribution is in perpendicular to bone surface direction. The interconnected distribution of osteocytes acts as main mechanoreceptor of the bone and involve in secretion of paracrine factors such as insulin-like growth factor-I (IGF-I) and express *c-fos* in response to mechanical forces (Mohamed, 2008). Osteocytes are involved in maintaining the protein and mineral content of the bone matrix. Osteocytes are mature bone cells and lack the ability to divide(Wolff, 1870) .Some researchers believe that osteocytes induce the dissolution of adjacent matrix to release minerals which enter the circulation, and they are involved in rebuilding the matrix by deposition of hydroxyapatite crystals. However, this still needs more research to be accepted as a general fact. They are also involved in bone repair in the case of injury, osteocytes can convert to less specialized cells such as osteoblasts, upon release from lacunae (Hollinger et al., 2004).

Osteoclasts: Osteoclasts are derived from macrophage-monocyte cell. Osteoclasts are the large multinucleated phagocytic cells which are responsible for bone resorption. They migrate from bone marrow to required specific skeletal site, either fuse with existing osteoclasts or remain as mononuclear cells for future recruitment (Mohamed, 2008). These cells secrete protein digesting enzymes which break down the protein matrix and acid to dissolve the stored minerals. These are then released into the vascular system to maintain the calcium and phosphate ratio in the body fluids. The process is known as osteolysis or resorption.

In normal bone metabolism osteoblasts and osteoclasts work in a strict balance. Osteoclasts continuously degrade bone matrix; however, osteoblasts are continuously involved in bone formation. If the balance is disrupted, the bone either becomes weak or compact (Florencio-Silva et al., 2015; Setiawati & Rahardjo, 2019).

1.4.3 Phenomenon of Bone Growth:

Osteoblasts and osteoclasts are continuously working to meet functional requirements of the bone. Bone development is divided into two main processes: **Intramembranous ossification:** this happens in the development of the mandible, maxilla and skull bones; where bones form from mesenchymal connective tissue.

Endochondral Ossification: In this type of ossification pre-existing hyaline cartilage is replaced by bone tissue (DeSaix et al., 2013; Florencio-Silva et al., 2015; Setiawati & Rahardjo, 2019).

Ossification begins at the centre of the porous bony structure. The osteoid layer is formed on top of the porous structure leading to formation of calcified bone. The cells present in between the periosteum differentiate into osteoblasts and an increased quantity of alkaline phosphatase is reported. The osteoblasts rearrange and begin synthesis of collagen fibres around them resulting in trabeculae formation. This process makes the bone multi-layered. The rate of formation of primary bone and the calcification process is variable in different bone types (Hollinger et al., 2004). Fibroblast growth factor receptors (FGFR) 1 and 3 are reported to have a regulatory role in the production of extracellular matrix and chondrocyte proliferation and differentiation respectively in endochondral ossification, mutations in FGFR3 lead to dwarfism. Bone development is a well-coordinated event which results due to VEGF, FGF, BMPs and other signalling pathways (Setiawati & Rahardjo, 2019; Wolff, 2010).

Bone growth is initiated by perichondrium and tissue forming interzones which lead to an increase in intercellular matrix and multiplication of cartilage cells. Immature bone cells are localized at the ends of the bone where most growth occurs; such cells are small in size and lack specific arrangement. Upon growth signals, the cells start to proliferate and form a closely packed cluster of flattened cells which start to produce matrix resulting in an increase in intercellular matrix. The cells start to become larger and vesicular and then differentiate into hypertrophic chondrocytes.

Hypertrophic Chondrocytes act as regulatory cells for bone growth process in long bones. They are involved in localised mineralisation, induction of vascularisation by producing

vascular endothelial growth factor (VEGF) and recruit chondroclasts which are associated with matrix digestion. Hypertrophic chondrocytes induce the production of osteoblasts from adjacent perichondral cells. Osteoblasts secrete bone matrix and start the process of bone formation. The hypertrophic cells at this stage undergo apoptosis. The cartilage matrix then acts as scaffold for osteoblasts, the bone and vessel ingrowth occur resulting in a porous bony structure.

1.4.4. Regulation of Bone formation:

The regulation of bone formation was described by Julius Wolff in 1892. According to wolff's law, the bone density and organisation of bone trabeculae correlate with the magnitude and direction of tensile and compressive stresses of loading. It is a known fact that the bone is mechanosensitive and adapts to mechanical loading such as internal strain. Internal strain within the bone results in four tissue level outcomes. 1) net mineral loss, 2) mineral homeostasis, 3) net mineral gain, or 4) damage formation. Everyday mechanical strains are expressed in terms of microstrains. The strains lie between minimum and lower effective strains which were calculated to be approximately 1500-2500με and 50-200με respectively (Fuchs et al., 2009). Within this window bone resorption equalled bone formation during normal circumstances. When a fracture happens, stress shielding effect plays an important role for complete healing. After bone union is performed successfully, the bone starts to adapt to new mechanical environment. According to Wolff's law, the density of new bone formation is dependent on the stress conditions bone is under. If the stress is below than normal physiological stress levels, the newly forming bone will have reduced bone density hence leading to reduced strength (Wolff, 1870).

The fracture nature in paediatrics and adults is similar and so is the healing in terms of healing phases. The fractured bone go through three phases 1) inflammation, 2) reparation and 3) remodelling, before it is completely healed. The difference lies between the density of the bone. The paediatric bone is more porous due to presence of haversian canals on a greater portion of the bone as compared to adult bone. This makes the paediatric bone more flexible

and very well vascularised. The presence of a dense layer of vascular connective tissue (periosteum) allows the environment to be oxygen rich hence reducing the fracture healing time as compared to adults. The paediatric bone is in growing phase which means the osteogenic processes are already ongoing hence it accommodates the fracture healing process quickly, however, in adults the bone structure is mature and in case of fracture the osteogenic environment has to be created by the body in order to start the healing process (Lindaman, 2001).

The bone fixatives used for bone union (for fracture repair) are crucial as they must have optimal rigidity or mechanical stiffness close to natural bone. The stainless-steel implants for lower load-bearing extremities is recommended to have 43-53% of fixation, while for forearm it is approximately 30%. Inappropriate use of bone implants for fracture repair may lead to abnormal stress shielding, leading to failure of fixation or refracture of the bone after implant removal (Burke & Goodman, 2008). In case of paediatric fractures, the bone union step must be taken immediately in order to obtain the correct healing regime.

The process of bone formation is a controlled mechanism which involves a number of growth factors and enzymes working together. As soon as the mechanical signal is received, the fracture site undergoes a cascade of chemical signals. As a result, a number of growth factors are released which affect the osteoblasts' regulation and differentiation. Some important growth factors are described below.

1.4.4.1 Bone Morphogenetic Protein (BMPs)

These are among the most widely studied growth factors. About 15 different BMPs have been identified in vertebrates which play important roles in bone repair and regeneration. The growth factors are secreted primarily by osteoprogenitor cells and mature osteoblasts. Upon secretion they act as activators for differentiation of cells. The most significant BMPs are BMP-2, BMP-4 and BMP-7 (Karsdal et al., 2002; Katagiri & Takahashi, 2002). It has been studied that the BMP-2 poses a significant impact on healing of critical sized bone defects in animal species which makes it promising for bone tissue engineering (Lieberman et al., 2002).

1.4.4.2 Transforming Growth Factor β (TGF β)

TGF β is mainly secreted by platelets and it is known to interact with specific receptors on osteoblasts which under certain circumstances aid cell differentiation. But the process overall is complicated and not clear. It was analysed that to provide significant differentiation a very high concentration of TGF β is required. Limited information about the process and requirement of higher concentrations makes it less favourable for bone tissue engineering (Bonewald, 2002; Karsenty, 1999).

1.4.4.3 Fibroblast growth Factor (FGF), Insulin Like Growth Factor (IGF-1) & Platelet derived growth factor (PDGF)

Bone formation involves a cascade of processes involving FGF, IGF-1 and PDGF as assistive factors. FGFs specifically FGF-2 and FGF-18 are involved in promoting osteoblast proliferation. FGFs have no role in osteoblastic differentiation. However, IGF-1 and PDGF are involved in osteoblastic proliferation and differentiation (Kubota et al., 2002; J.-Y. Lee et al., 2002; Shimoaka et al., 2002).

1.4.5 Development of the Mandible

Mandible development requires an altered ossification process with respect to bone growth patterns and orientation of trabeculae. The central mandible plates develop at a faster rate with the borders of the bone being smooth.

Mandible reconstruction is a very complex process because of the presence of teeth and their migration, along with maintaining a proper coordination between the mandible and the maxilla. Endochondral ossification begins with the expression of the SOX9 gene by chondrocytes which induces cellular proliferation. Hypertrophic chondrocytes produce Type X Collagen and VEGF which lead to the onset of endochondral ossification and vascularisation

respectively. Parathyroid hormone related protein (PTHrP) induces the differentiation of mesenchymal cells into chondroblasts and osteoblasts.

A study performed on embryonic chicks demonstrated that there are three types of mesenchymal cells; Myogenic cells, which migrate from other regions to the mandible region and are associated with muscular functions. Chondrogenic and Osteogenic cells originate on site and are involved in bone formation. Osteogenic cells are associated with the formation of thick mouth epithelium which act as a ground for enamel organ in mammals. Further, Meckel's cartilage starts to form at 6th week in human embryonic development, which undergoes ossification to become the mandible. At the end of the embryonic period, the mandible is well defined, and ossification begins to spread to the posterior regions. The process of foci calcification in the extracellular matrix occurs due to the expression of the extracellular matrix protein osteopontin by chondrocytes, leading to periosteal bone formation on upper and lateral regions of cartilage. At this point the functional vascular penetrations occur and similarly, intramembranous ossification happens. It was reported that the higher levels of VEGF leads to more bone formation (Karsenty, 1999; Katagiri & Takahashi, 2002).

1.4.6. Parietal and Frontal Bone

Skull bone development starts from the outer skeletogenic membrane. The sutures present between the membrane bones of the skull are the active growth centres for skull bone development because they house proliferating osteogenic stem cells. Osteogenic cells are located at the periphery of membranes and on the inner and outer surfaces. The continual skull growth during embryonic development depends on proliferation of osteogenic stem cells and their differentiation to mature bone cells. The frontal occipital growth is induced by the coronal suture which is present between frontal and parietal bones.

At suture edges, the osteoprogenitor cells proliferate and higher expression of FGF2 occurs. However, at the midsutural mesenchymal region, *twist* expression was reported which is not associated with proliferation or differentiation. The area acts as a buffer zone between the frontal and parietal proliferating region which connects to the region of cells co-expressing both genes, FGF2 and *twist*. Low levels of FGF are associated with the proliferation

of osteogenic stem cells, whereas the higher FGF1 levels are involved in their differentiation (particularly FGF1). Once the differentiation is well established, FGF is downregulated. Cell differentiation is a multi-step process involving several regulatory pathways which work in a sequential manner. Osteonectin and alkaline phosphatase activity are differential indicators which are generally found in regions of proliferation in preosteoblasts and osteoblasts at earlier stages, however, osteopontin expression is recorded in mature osteoblasts in contact with the osteoid. FGFR1 functions until the completion of differentiation. The parietal bones grow rapidly till they reach a definitive shape, followed by slow growth till birth time. The frontal sinuses are formed postnatally (Karsenty, 1999).

1.4.7. Angiogenesis

In the last decade, enormous research is being carried out regarding the importance of vascularisation in bone tissue engineering. It has been investigated and believed that the modification of the angiogenesis phenomenon can be a promising way to deal with life threatening diseases such as cancer, cardiovascular abnormalities, wound healing etc. as well as bone defect repair and regeneration.

Angiogenesis is defined as the propagation of blood vessels from a pre-existing network of blood vessels. The process starts in the embryo and continues till death and ensures that each metabolically active tissue is close to the capillary network (a few hundred microns far) to aid exchange of nutrients and waste effectively. The change in hemodynamic factors and tissue requirements changes the pattern of angiogenesis such as physical activities, leading to angiogenesis in skeletal muscles. However, lack of exercise reduces the renewal of blood vessels in the regions hence making it poorly vascularised over a period leading to cardiovascular or muscular disorders (Bielenberg & D'Amore, 2008; Figg & Folkman, 2008).

1.4.8. Origin of Angiogenesis

The first organ that develops in an embryo is the cardiovascular system and circulatory system which matures at quite early stages. The circulatory system is derived from mesoderm which provides mesodermal stem cells that differentiate to give rise to hematopoietic stem cells and angioblasts. Hematopoietic stem cells are blood forming cells; however, angioblasts are undifferentiated endothelial cells due to lack of potential endothelial cell marker. The Angioblasts act as precursor for the development of blood vessels in the embryo; the process is known as vasculogenesis (fig.1.6). It undergoes complex cell to cell and cell to extra cellular

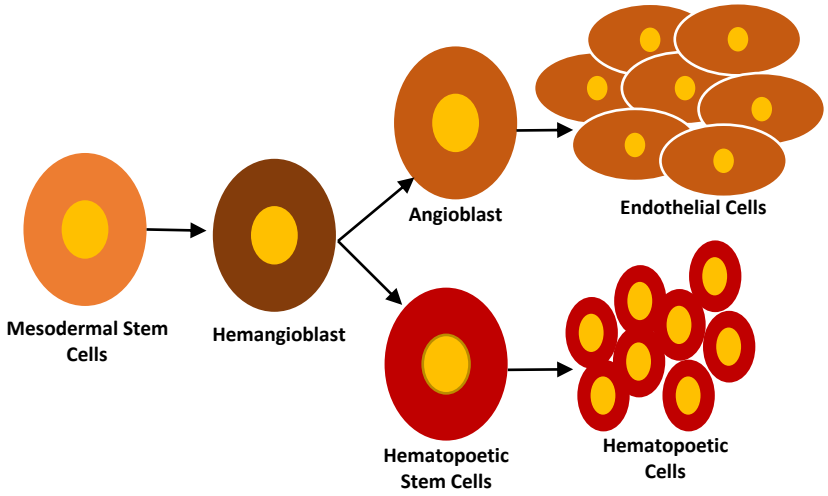

Figure 1.6: *The process of vasculogenesis. The mesodermal cells differentiates into endothelial cells resulting in tube/vessel formation.*

matrix (ECM) interactions, followed by growth factors and morphogens leading to formation of clusters of angioblasts and hematopoietic stem cells. The angioblasts with further Growth factor signalling differentiate into endothelial cells and results in formation of de novo blood vessel synthesis called vasculogenesis (Risau, 1997; Schmidt et al., 2007).

1.4.9 Types of Angiogenesis

1.4.9.1 Sprouting Angiogenesis

Sprouting angiogenesis is characterised by formation of an endothelial sprout at the end of a capillary towards angiogenic stimulus. The angiogenic stimulus is generally vascular endothelial growth factor (VEGF) which is a vascular permeability factor and acts as a proangiogenic. Sprouting is initiated in response to a hypoxic environment i.e., whenever a tissue is deprived of oxygen it induces hypoxia signals which enable parenchymal cells to secrete VEGF which further initiates the sprouting angiogenesis process. The process is composed of several steps.

a. Enzymatic degradation of capillary basement membrane.
b. Proliferation of Endothelial Cells
c. Directed migration of Endothelial cells
d. Tubologenesis
e. Vessel Fusion
f. Vessel pruning
g. Pericyte stabilization

The sprouting starts with two types of cells; tip cells which are non-proliferating and endothelial cells that lack a lumen and Filopodia which are thin cytoplasmic projections that are involved in directed angiogenesis. Tip cells control capillary sprouting towards the stimulus via the extracellular matrix. Filopodia on tip cells secrete various proteolytic enzymes associated with the VEGF receptors. VEGF receptors sense the VEGF and catalyse proteins in line towards the stimulus to allow sprout elongation. Endothelial cells proliferate and migrate at the growing sprout and there is elongation of capillary towards the stimulus. Once sufficient elongation is achieved the lumen is developed within endothelial cells and the sprout converges and fuses at the VEGF source. The lumen becomes continuous and oxygenated blood starts to flow through it. The hypoxic tissue is supplied with oxygenated blood followed by a reduction in hypoxia which reduces the elevated levels of VEGF to normal. Furthermore, capillary maturation occurs with the help of pericytes and deposition of extracellular matrix in response to shear stress and mechanical signals. Pericytes are basically

supporting cells present along the walls of endothelial cells lining the capillaries, and help in cell-cell signalling (Carmeliet et al., 2009; Chien, 2007; Gerhardt, 2008; Horowitz & Simons, 2008; Ruhrberg et al., 2002; Small et al., 2002; Van Hinsbergh & Koolwijk, 2007).

1.4.9.2. Intussusceptive Angiogenesis

Intussusceptive angiogenesis is also known as splitting angiogenesis which is characterised by the splitting of an existing single vessel into two. This process is time efficient as compared to sprouting angiogenesis. It requires reorganisation of existing endothelial cells instead of *de novo* vessel formation. It is a common type of angiogenesis in an embryo as well as throughout the life. It can only initiate at a site having existing capillaries and involves the formation of capillaries, vein bifurcation, pruning of larger vessels and arteries.

Intussusceptive angiogenesis commonly occurs in choroid of eye, vascular baskets around glands, intestinal mucosa, kidney, ovary, uterus, skeletal muscle, heart, and brain (Burri et al., 2004; Kurz et al., 2003).

1.4.10. Influence of Metabolic Factors on Angiogenesis

The vasculature in general depends on metabolic activity, increased metabolic activity, increased oxygen and nutrient demand leads to increased vessel formation to fulfil the demands of the tissue. Extensive studies have been performed on skeletal muscles with reference to angiogenesis and it is concluded that the capillary density is directly proportional to metabolism of the tissue; the higher the tissue metabolism the higher would be the growth of the vessels and vice versa.

The process of angiogenesis was studied in endurance training; it increased the metabolic activity of the skeletal muscles which stimulated angiogenesis. Long-term muscle inactivity reduced skeletal muscle metabolism and lead to deterioration of muscle vasculature (Terjung et al., 2002; Wagner, 2001). The effect of oxygen on angiogenesis was studied in developing chick embryos; when the chick was exposed to a hypoxic (low oxygen) environment, the micro vessel growth and chorioallantoic membrane was stimulated along with major artery formation in the embryo. However, micro vessel growth was inhibited when the chick was exposed to a hyperoxic (high oxygen) environment (Adair et al., 1990; Strick et al., 1991). Similar results were obtained for avian and rodent models. An investigation of

infants exposed to a hyperoxic environment demonstrated reduced retinal vasculature. Oxygen levels are critical for stimulation and regulation of proangiogenic factors and receptors to which they attach for functional activation. These include Vascular Endothelial Growth Factor (VEGF) and its receptors, Placental Growth factor (PGF), Angiopoietin, Fibroblast growth factor-2 (FGF-2), Transforming Growth Factor beta (TGF-β), Hypoxia inducible factor-1 (HIF-1) and inducible nitric oxide synthase (iNOS). An oxygen deficient environment can also control anti angiogenic factors such as endostatin and thrombospondin-1 (Adair & Montani, 2010).

1.4.11. Reactive Oxygen Species (ROS) in Angiogenesis

At a cellular level, reactive oxygen species are formed as a result of by products produced by processes such as mitochondrial electron transport, NADPH oxidase, xanthase oxidase and Nitric oxide synthase. ROS chemically are super oxides or hydrogen peroxides which are involved in producing oxidative stress which is known to have pro angiogenic or anti angiogenic properties depending upon the levels and times of release, the process is complex and limited success has been achieved regarding the modulation of ROS as a therapeutic agent. At low levels of ROS, it triggers FGF-2 release and induces the binding of growth factors to their receptors which lead to angiogenesis signalling initiation. Along with angiogenesis, ROS also enhances endothelial cell permeability and cell adhesion. However, higher ROS levels are involved in inhibition of angiogenesis, necrosis and apoptosis (Bhadada et al., 2011; Carmeliet, 2003; Simons, 2005).

1.4.12. Angiogenesis and Osteogenesis

A functional vascular system is very important for any process in the human body. Angiogenesis is linked with skeletal development and bone damage repair. Once the bone damage happens, the requirement of osteoblast progenitor cells is fulfilled by functional blood vessels. So, the increased number of blood vessels increases the cascade of osteoblast progenitors, which later mature, and speeds up the bone formation process. The blood vessels in bone not only provide oxygen and nutrients at the defect site but also supply building blocks such as calcium and phosphate for the mineralisation process. Angiogenesis

and osteogenesis work in coordination for successful bone repair. The low oxygen levels in bone and marrow play an important role in the activation of Hypoxia inducible Factors (HIF) which results in Vascular endothelial growth factor (VEGF) release. VEGF acts in two ways towards osteogenesis. Osteoblasts and Endothelial cells both express VEGF receptors (VEGFR). VEGF accumulation directly promotes osteogenesis through VEGFR on osteoblasts and indirectly through endothelial cells (fig. 1.7). The endothelial cells upon activation induce angiogenesis which results in recruitment of growth factor, O_2, nutrients and bone building minerals on site which indirectly induce osteogenesis (Schipani et al., 2009; Stegen et al., 2015).

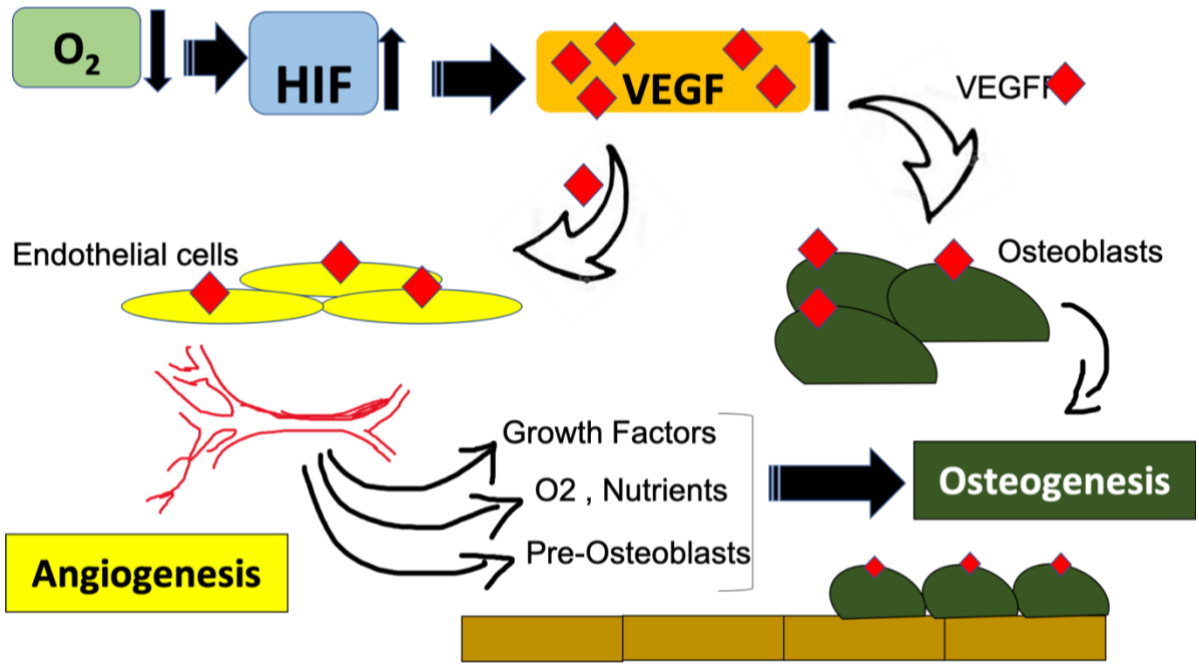

Figure 1.7: *Regulation of angiogenesis and osteogenesis in response to oxygen. The low oxygen levels activate the HIF leading to VEGF accumulation. The VEGF binds to VEGFR on endothelial cells and osteoblasts inducing direct and indirect osteogenesis. The schematic shows the coordinated function of angiogenesis and osteogenesis for successful bone repair.*

1.4.13. The need for bone tissue engineering scaffolds:

Road accidents are the main cause of craniofacial injuries. Statistics reported that more than a half of the craniofacial trauma is the result of severe road accidents. Almost 4000 people die and almost 8000 people are disabled. Injuries at work, while playing sports or due

to falls also contribute to cranium injuries (Jones, 1997). The increase in incidence of facial fractures has also been reported in England, Germany, Netherlands, and Norway; it is increasing by 7% in terms of admissions to hospitals for skull or facial fractures (Rizzo, 2015). These injuries happen either by being hit by a moving object or static object such as when a motorbike crashes on the road with speed. The fractures can be divided into 1) Skull fractures and 2) facial fractures.

1.4.13.1 Skull fractures

Skull injuries leading to cracking or breakage of the bone most likely occur because of trauma. The fractures can be of varying types such as linear, comminuted, depressed or stellate form which are mainly caused by the bruising process. Cranial fractures can allow a route for infection which can lead to meningitis. So, the treatment strategy is designed to prevent the infection. It is suggested that treatment should be provided within 24 hours which is debridement of the wound and removal of the loose bone fragments.

1.4.13.2 Facial Fractures

The fractures to the facial region are classified by their anatomical position. These can be scalp and skull fractures, infra-orbital fractures, and maxilla-mandibular fractures (Rizzo, 2015).

Over the past decades, significant advances have been carried out in terms of research and management for trauma patients suffering from craniofacial injuries. Such injuries are a leading cause of death, disability, and psychological effects. The craniofacial region has significant importance in terms of function and aesthetics. Therefore, the approaches based on advanced techniques for the survival and repair of congenital deformities along with maintaining the aesthetic and functional aspects of the facial region are the focus of surgeons and biomaterials scientists.

1.4.14 Role of growth factors for bone repair and regeneration

Growth factors play an important role in the recruitment of necessary cells, inducing the bone formation cascade and differentiation of cells at the injury site. The delivery of growth factors directly at the site is a challenge and not very well understood yet. Several studies have been performed on the use of growth factors for fracture repair and regeneration. Transforming growth factor-Beta TGF-β is present in bone, platelets and cartilage and has been found in increased levels during the early fracture healing period. The effect of TGF-β on fracture repair was investigated on tibia fractures in thirty rabbits. 1 or 10 μg TGF-β was administered for a duration of six weeks and a significant increase in callus formation was recorded. However, no difference was seen in bone mineral content or bone thickness. With a dose of 1 μg of TGF-β, significant increases in normal bending strength were seen as compared to controls (Lind et al., 1993). Another study reported the use of 4 or 40 ng TGF-β injected into rats with tibia fractures. The group which received 40 ng demonstrated a significant increase in ultimate strength as compared to the group which received 4 ng (Nielsen et al., 1994). It was also reported that stable mechanical construct is also necessary along with the TGF-β dose. Absence of stable mechanical construct led to minimal cartilage and bone formation even with a high dose of TGF-β (600 ng) (Critchlow et al., 1995). The current research involved different models and different doses; hence it is difficult to conclude the clinical significance of TGF-β (Lieberman et al., 2002).

BMP-2 is a member of TGF- β which has a huge impact in field of bone regeneration as it induces osteogenesis when implanted in extra skeletal soft tissue. It was discovered by Marshall R. Urist in 1965. BMP-2 and BMP-7are being employed for clinical studies. BMP-2 injection at a fracture site in a rat model resulted in accelerated healing. Recombinant human BMP-2 was found to be effective for patients with resistant non-unions. Recombinant BMP-2 was delivered, bound to allogenic bone (Johnson et al., 1992). BMP-2 was FDA approved as an alternative to autograft for tibial nonunions and maxillofacial reconstructions. In united States, 2002 onwards the use of BMP-2 drastically increased from 0.7% to 24.9% and by 2007 it further increased to 50% (Ong et al., 2010). Another study reported recombinant BMP-2 as an additive for a collagen sponge (Govender et al., 2002; Nordsletten, 2006). The BMP-2

loaded collagen sponge resulted in speedy fracture healing in open tibial fractures. Recombinant BMP-7 was reported to have an 82% successful healing rate in the United Kingdom (653 subjects), which included open fractures, non-unions, periprosthetic fractures, free fibular grafts etc (Giannoudis & Tzioupis, 2005). The BMP administration was also associated with stimulation of angiogenesis and reduced onset of infection (Nordsletten & Madsen, 2006). Further, it was associated with the reduced operation and recovery time which lead to exponential rise in use of BMP-2 as an alternative to autografts (Garrison et al., 2007).

FDA approved 1.5mg/ml BMP-2 concentration for effective fracture healing, however, the frequent use of BMP-2 lead to side effects such as ectopic bone formation (Carragee et al., 2011; James et al., 2016). This happens due to premature leakage of BMP-2 out of fracture site. Another common side effect of BMP-2 treated spinal surgeries is activation of osteolysis. The osteoclast activity is increased leading to formation of osteolytic cystic lesions, implant loosening or displacement (Burkus et al., 2002; James et al., 2016). Bone cyst formation, inflammatory complications and risk of tumor formation were also recorded as adverse effects of BMP-2. Though the administration of growth factors was found to be effective in many studies but still the autologous bone grafts is considered to be a gold standard (Gautschi et al., 2007). The current data shows that use of growth factors with an appropriate carrier (collagen, polymer etc) can lead to the development of a non-invasive bone regenerative technique. Further clinical studies and dose optimisation of growth factors is required (Devescovi et al., 2008; Lieberman et al., 2002).

1.4.15 Biomaterials in Tissue engineering

Biomaterial or biomedical material is defined as “a material designed to take a form that can direct, through interactions with living systems, the course of any therapeutic or diagnostic procedure”. And the tissue engineering is defined as “the use of cells, biomaterials and suitable molecular or physical factors, alone or in combination, to repair or replace tissue to improve clinical outcomes”. Tissue engineering and biomaterials are correlated.

Tissue engineering using biomaterials having functional properties such as porosity to promote cell attachment and regeneration is a key therapeutic approach for regenerative medicine. Scaffold materials must be designed in a way that favours cell adhesion and attachment on the surface as well as migration into the material and thus promotes proliferation. The material architecture should provide a favourable microenvironment for nutrient and growth factor transport. The scaffold material plays an important role in eliciting the appropriate biological response. If the surface topography, degree of porosity and interconnectivity is adequate it should result in enhanced tissue regeneration at the defect site (Hollister, 2005; Hollister et al., 2005; S. Wu et al., 2014). Furthermore, properties such as cytotoxicity, biocompatibility and biodegradation are also to be considered for designing an ideal scaffold for specific applications. Depending upon the intended application, the proposed materials need to be screened for chemical and physical properties. Nanoparticles are defined as materials having at least one dimension of a size of <100 nm. Studies have shown that nanosized particles have enhanced properties when compared with the same material with particle sizes in millimetres. Recent advancement in research have been focussed on controlled synthesis of biomaterials and investigations to better understand the chemical and physical properties. biomaterials have many applications in a broad range of fields such as cancer therapy, drug delivery systems, medical imaging, and electronics field (Roduner, 2006; Tsuzuki, 2009).

1.4.16 Effect of Biomaterials on Bone Cell Differentiation and angiogenesis

Biomaterial properties such as surface properties play a significant role in interactions with the biological environment. Surface properties can be divided into chemical and morphological; morphological properties are very well studied and play a significant role in implant integration. The biomaterial surface is capable of inducing or inhibiting cell adhesion or proliferation for example a rough, porous surface facilitates cell attachment. Biomaterial interactions with the biological environment are basically the interaction between surface, cells, and proteins (matrix). This complex is of significant importance because it is the basis for mineralisation. Surface properties of a biomaterial are involved in cytocompatibility, it is

known that the same material with different surface treatments can lead to different responses in a biological environment (Anselme, 2000).

High surface roughness is a morphological feature which assists cell adhesion. Better cell adhesion generally assists better proliferation and matrix formation. Finally, bone mineralisation happens as a result of enzyme and cell mediated processes. It is believed that increased surface area (high surface porosity or roughness) of the biomaterial will promote osteoblast proliferation and differentiation. Some studies performed on titanium implants demonstrate higher surface roughness leading to better osteoblast attachment to implants, and higher alkaline phosphatase, osteocalcin and TGF β activity which favour osteoblast differentiation (Boyan et al., 2001; Morra, 2001). Studies of fibroblast cell culture on Polystyrene & Poly (4-Bromostyrene) reported that moving from microscale to nanoscale surfaces, cell adhesion and gene upregulation is increased. Nanoscale surface roughness further improves the surface to promote osteointegration in bone tissue engineering.

Surface chemistry plays a significant role in cell adhesion and proliferation. Bioglass is a perfect example of surface chemistry assisting cellular responses (Xynos et al., 2000). Bioglass, when exposed to aqueous buffer solution undergoes a series of reactions which results in formation of a layer of carbonated Hydroxyapatite. The layer changes the surface chemistry of the bioglass and promotes osteoblast proliferation on site. Surface chemistry can also affect protein adsorption and protein activity on the site which has profound effect on osteoblast adhesion and proliferation. It is reported that the addition of a fluorapatite layer over a hydroxyapatite surface changes the orientation of some proteins which are involved in calcium binding, this process enhances cell attachment (Rezania & Healy, 2000). The material sterilisation process is also of significant importance as inadequate sterilisation techniques can alter surface properties. Thus, materials used in bone tissue engineering must present appropriate signals at appropriate time scale. Surface properties should be homogenous in order to induce effective cell attachment and functional differentiation (McFarland et al., 2000; Rezania & Healy, 2000; Stephansson et al., 2002; Xynos et al., 2000).

1.4.17 Synthesis of Nanoparticles

Nanoparticles can be synthesized *via* two approaches; Top down and bottom up. The top-down approach depends upon the structural decomposition of bulk materials to synthesise nano sized materials such as mechanical grinding, milling, etching and lithography but these processes have limited control over the size of the particles, are energy intensive and imprecise (Cao, 2004; Hornyak et al., 2008; Sebastian et al., 2014; Yu et al., 2013). The bottom-up approach initiates at an atomic or molecular level. It utilizes precursors which chemically interact and form nano sized particles. Such methods include dry methods, wet methods, and high temperature processes. The dry methods include solid state and mechanochemical methods, these processes promise high crystallinity but are limited to micron sized particles. Wet methods include chemical precipitation, hydrolysis, and sol-gel, these are most commonly used methods for nanoceramic synthesis as they give nanosized particles, but limitations lie in terms of crystallinity which is variable and often difficult to control. High temperature processes include the combustion method and pyrolysis methods, they do give high crystallinity and nanosized particles but require high energy (Sadat-Shojai et al., 2013). Such methods enable precise size control of morphology, hence the research advancement is focussing on bottom up approaches for synthesis of biomaterials (Cushing et al., 2004; Hornyak et al., 2008).

1.4.17.1 Zinc oxide Synthesis

Zinc oxide exists in a range of morphologies having high surface areas (sizes from micrometres to nanometres). The morphologies may be in the form of thin sheets, nanorods, nanowires, nanobelts, nanotubes, nanorings, flower like, multipods and tetrapods (Abd-Ellah et al., 2016; Calestani et al., 2010; Chen et al., 2010; Gazia et al., 2012; Laurenti et al., 2014; Pacholski et al., 2002; Shi et al., 2012). Zinc oxide is very easy to synthesise using various synthesis techniques such as sol-gel, hydrothermal and sonochemical. To obtain nanorods & nanowires generally a hydrothermal system is used and to obtain thin sheets solgel is used (Baruwati et al., 2006; Dumontel et al., 2017; Kandjani et al., 2008). Zinc oxide has been recognised as a safe material by the Food and Drug Administration, it is classified as GRAS (generally recognised as safe substance). The FDA has approved the use of zinc oxide as skin

protectants, color additive for drugs and cosmetics and food fortification. Zinc oxide can be found in food products such as breakfast cereals, nutrition drinks/bars, food supplements etc. Due to the ease of synthesis, biosafety and functional properties, zinc oxide is used commercially in a number of cosmetics, health care products such as baby creams and sun screens (Rasmussen et al., 2010). Furthermore, due to the optical properties of zinc oxide, it is also used in the fabrication of biosensors. It has also been investigated that the electrical properties of zinc oxide plays and important role in adsorption-desorption of biomolecules which can be exploited for different biomedical applications and targeted therapy (Miccoli et al., 2016; Sanginario et al., 2016; Zhu et al., 2016).

1.4.17.2 Zinc oxide in biological systems

Biocompatibility plays an important role when it comes to use of biomaterials. Biocompatibility is defined as "the ability of a material to perform with an appropriate host response in a specific application". To evaluate biocompatibility of zinc oxide several biological tests have been reported. A human osteoblast cell line was used to evaluate the effect of microphase and nanophase zinc oxide, it was reported that the cells' adhesion and metabolic activity was significantly improved in the presence of nanophase zinc oxide which further led to improved protein interaction due to high surface area (Colon et al., 2006). In another study, zinc oxide nanoflower morphology and zinc oxide flat thin films were compared for improved biological response in the form of lamellipodia, filopodia, DNA content and Alkaline Phosphatase Activity. The cell line MC3T3-E1 osteoblasts were incubated with both morphologies of zinc oxide for up to 4 days and it was noted that active filopodia formation occurred on the zinc oxide nanoflowers morphology. The cell adhesion and proliferation was improved in the case of nanoflowers (Z. Li et al., 2008). Porous zinc oxide films were cultured with NIH 3T3 fibroblasts, it was observed that a high degree of porosity significantly improved the cells' viability via protein adsorption (H.-J. Wang et al., 2011). Such findings depict the significance of topography of zinc oxide in biological environment. The differentiation of mesenchymal stem cells into osteoblasts in the presence of zinc oxide nanoparticles was also investigated using real-time PCR, alkaline phosphatase activity and the expression of osteopontin and osteocalcin. The cells were exposed for 15 days, and evidence of osteoblast formation was reported at optimum levels of zinc oxide (30 µg/ml) (Foroutan,

2014). Such investigations conclude that zinc oxide is a biocompatible and significantly important material in field of bone tissue engineering.

1.4.17.3 Zinc oxide and Angiogenesis

Angiogenesis is an important mechanism and manipulating angiogenesis is a developing therapeutic approach for a number of physical or pathophysiological conditions. Proangiogenic growth factors or cytokines are being employed to treat conditions such as cardiovascular disorder and ischemia. Proangiogenic factors such as vascular endothelial growth factor are effective in the promotion of angiogenesis, but they are expensive and have reduced stability which makes their use limited in the field of tissue engineering. Current research is focussed on finding materials which are cost effective and can be used in place of angiogenic growth factors.

The proangiogenic potential of flowerlike zinc oxide particles was studied. The Microwave technology was used to synthesise the zinc oxide particles followed by *in vitro* and *in vivo* investigations to evaluate the proangiogenic potential of metal oxides. Zinc oxide internalisation, cell cycle & proliferation and chick embryo angiogenesis assay were analysed, and a significant difference was observed. Cell cycle analysis demonstrated a significant number of cells in S phase which involved DNA and centrosomes. TEM investigations confirmed that the zinc oxide particles penetrated the cells while cells were healthy and proliferating (Fig.1.8). Finally, chick embryo angiogenesis assay confirmed that zinc oxide nanoflowers initiated the formation of new blood vessels from pre-existing ones (Barui et al., 2012).

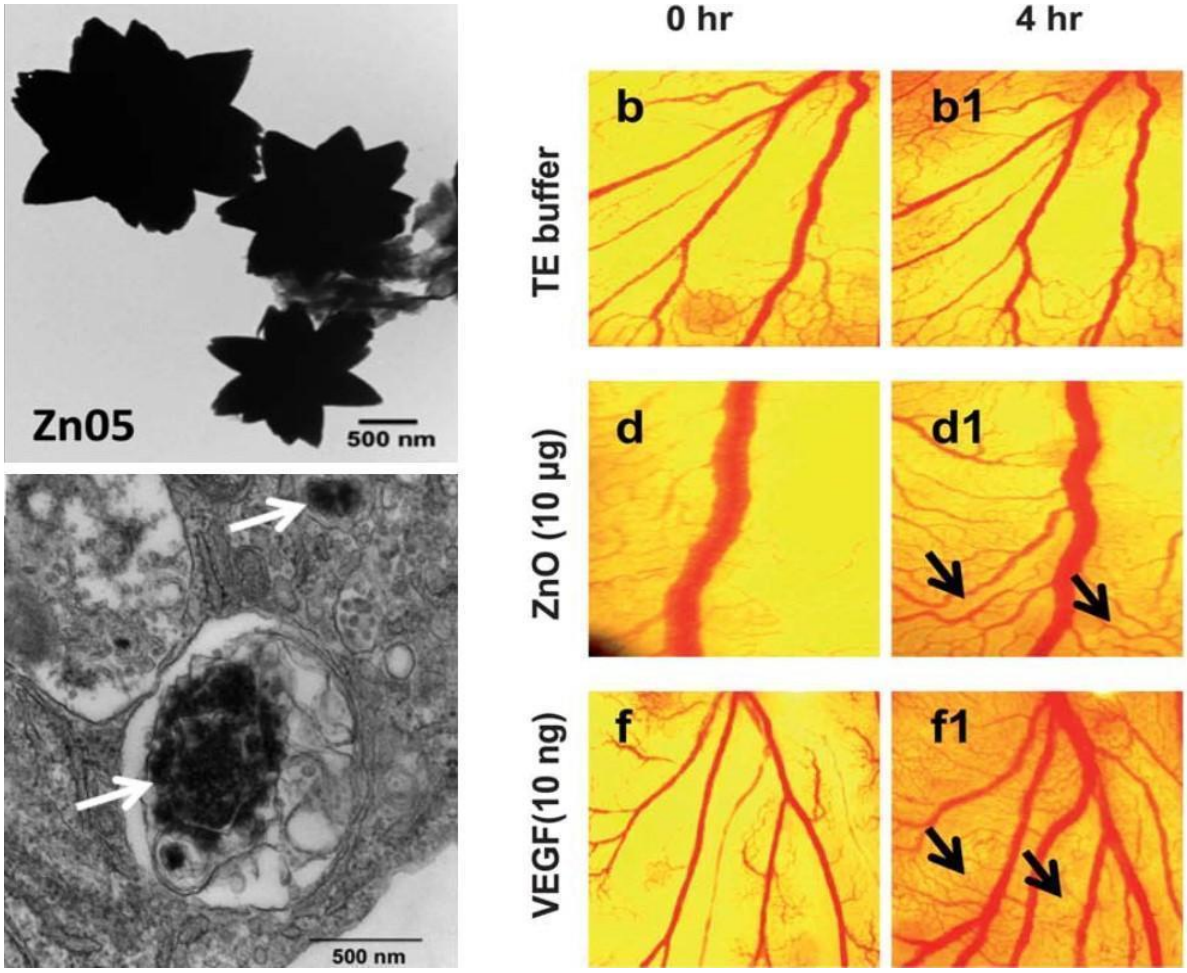

Figure 1.8: *The acceleration of angiogenic process in response to flower shaped Zinc oxide. The flower shaped Zinc oxide particles were internalised by the cells (shown by white arrows). The increase in vessel formation with 10ng Zinc oxide (d1 black arrows). The positive and negative controls are VEGF 10ng and TE buffer respectively. Republished with permission of the Royal Society of Chemistry, from* (Barui et al., 2012). *Permission conveyed through Copyright Clearance Center, Inc.*

The phenomenon behind angiogenesis is generation of hydrogen peroxide which leads to ROS followed by initiation of angiogenic process. An investigation was performed to evaluate the chemical factor of zinc oxide which plays an important role in angiogenesis. Zinc oxide is a n-type semiconductor having free electrons associated with anion vacancies in the zinc oxide crystal lattice. Due to which zinc oxide, upon interaction with cells, chemisorbs oxygen as O_2 by receiving electrons from oxides and forms hydrogen peroxide in an aqueous

environment which, as discussed above, leads to oxidative stress hence triggering a natural angiogenic process (Augustine et al., 2014b). The oxidative stress triggers expression of VEGF and FGF to initiate the cascade reactions leading to angiogenesis and improved cell adhesion. In another study, poly caprolactone-zinc oxide electrospun composite scaffolds were synthesised with varying percentages of zinc oxide (0.5%, 1%, 2%, 4%, 6% by wt), it was observed that the presence of zinc oxide in the scaffolds significantly improved cell attachment and 1wt% zinc oxide (Fig 1.9) supported the formation of mature blood vessels with highly branched capillaries (Augustine, Dominic, et al., 2014a).

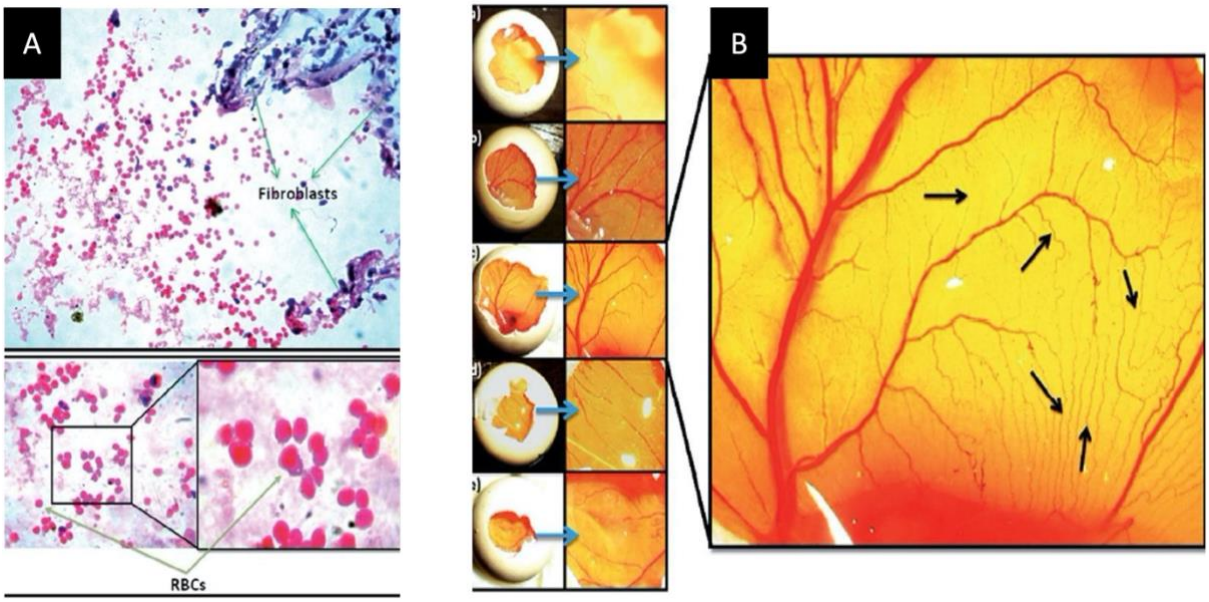

Figure 1.9: *The optimal level of zinc oxide that is suitable for cell migration and angiogenesis. A) fibroblast migration from sides of scaffolds was observed (purple dots) The vessel sprouting was initiated with 1% Zinc oxide implantation in guinea pigs. The circular arrangements of Red blood cells (RBS) indicates the initiation of angiogenesis. B) The maximum vessel formation was recorded for 2% zinc oxide in CAM. The number of vessels markedly increased (shown by black arrows).* Republished with permission of Royal Society of Chemistry, from (Augustine, Dominic, et al., 2014b); permission conveyed through Copyright Clearance Center, Inc.

Further, it was proposed that the electron transfer mechanism from zinc oxide to O_2 leading to the formation of hydrogen peroxide and angiogenesis (Fig. 1.9) (Ahtzaz et al., 2017). Electrospun poly(vinylidene fluoride-trifluoroethylene)/zinc oxide nanocomposites were

analysed with varying percentages of zinc oxide (0%, 0.5%, 1%, 2%, and 4% w/w with respect to the polymer) and it was observed that maximum cell attachment/proliferation and angiogenesis was seen in samples having 2% zinc oxide (fig. 1.9) (Augustine et al., 2017).

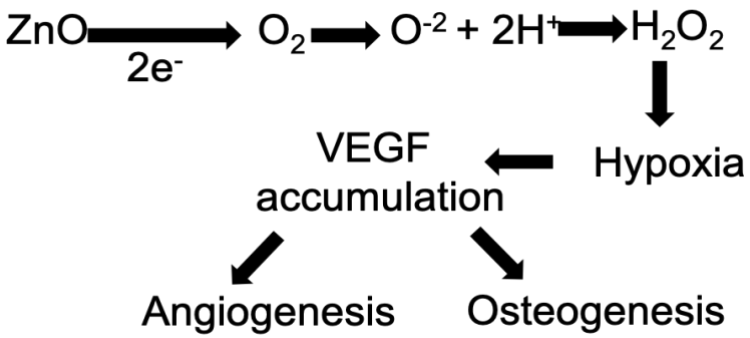

Figure 1.10: *Mechanism of zinc oxide induced angiogenesis and Osteogenesis.*

The ROS and O2 production in mitochondria were studied in response to ZnO exposure. 25µg/ml and 50µg/ml ZnO was introduced and significant increase in ROS was observed. Upregulation of four oxidative stress responsive genes; Aldehyde oxidase 1, Heme oxygenase 1, Neutrophil cytosolic factor 2 and Superoxide dismutase 3 in zinc oxide nanoparticles treated HEK-293 cells for up to 48hours. Aldehyde oxidase 1 is a xenobiotic metabolizing protein which promoted cell damage and fibrogenesis however, the other three genes are responsible for antioxidative and anti-inflammatory properties. The higher levels of zinc oxide nanoparticles promoted the release of excess production of ROS in mitochondria resulting in mitochondrial dysfunction and cell death. Excess exposure of zinc oxide nanoparticles (25µg/ml & 50µg/ml) was reported to have genotoxic effects resulting in DNA fragmentation and nuclear condensation (Choudhury et al., 2017). Genotoxic behaviour of zinc oxide makes the dose a critical aspect in tissue engineering.

The material properties of nanoceramics are of significant importance, as mentioned above, and surface topography plays an important role in particle internalization. Currently, studies are being carried out to investigate the influence of surface charge, zeta potential and lattice properties in the biological environment. Titanium thin films were synthesised and functionalised with different functional groups (CH CH_2, NH_2 and COOH groups) in order to create a different zeta potential for every sample, which was measured using XPS analysis.

Results revealed that a lower the zeta potential would result in lower protein adsorption (Cai et al., 2006). Similarly, Cerium oxide nanoparticles with varying zeta potential were evaluated for adsorption of fetal bovine albumin and cellular internalization in adenocarcinoma lung cells and it was revealed that the positive zeta potential was favourable for albumin adsorption and negative zeta potential aided uptake of nanoparticles into the cells (Patil et al., 2007). The results report preliminary studies, and more data is required to confirm the role of surface charge in the biological environment.

1.4.18 Selection of Dopants

1.4.18.1 Cerium

Cerium doped zinc oxide is a known photocatalyst. A number of studies have been performed where successful cerium doping has been carried out for a number of applications such as enhanced ionic and ferroelectric properties (Sinha et al., 2014), breadth sensor to detect the levels of acetone and ethanolamine at room temperature which are biomarkers for diabetes mellitus and carcinoma (Kulandaisamy et al., 2016), detection of hazardous chemicals (Dar et al., 2012), enhanced optical and photoelectrochemical properties (Jinghai Yang et al., 2008; Yousefi et al., 2011) and efficient photocatalysts (Rezaei & Habibi-Yangjeh, 2013). A number of studies reported that cerium in the biological environment is nontoxic and also has bacteriostatic properties. It was investigated that cerium introduction into bioactive glass scaffold increases the *in vitro* bioactivity which makes it favourable for bone tissue engineering (Deliormanlı, 2015; Shruti et al., 2013). A few studies have been published on the angiogenic potential of CeO_2, and results revealed that it is proangiogenic and upregulates Hypoxia inducible factor 1 α which leads to angiogenesis. It was also reported that the size and morphology of the particles play a significant role in oxygen modulation within the cells which leads to hydrogen peroxide production leading to angiogenesis (Das et al., 2012; Nethi et al., 2017). Studies demonstrate that cerium incorporation results in zinc oxide lattice expansion, reduced grain size and increased bandgap (Kulandaisamy et al., 2016; Sinha et al., 2014).

1.4.18.2 Copper

Copper is an emerging element in field of tissue engineering. It has been investigated that copper ions interact with receptors on cells which are involved in angiogenic pathways. Copper is involved in the upregulation of expression of fibroblast growth factor (FGF) and vascular endothelial growth factor (VEGF). A study performed on magnesium-copper alloys revealed that the copper ions and Mg-Cu alloys pose no cytotoxic effects to HUVECs and MC3T3-E1 cells. Cu improved the biodegradation property of magnesium and stabilised it in the cellular environment. Furthermore, the alloy enhanced osteogenesis and angiogenesis in invitro so that they can be used in orthopaedic applications (Liu et al., 2016). In another study, Cu- doped bioglass (a family of bioactive glasses composed of silicon dioxide, sodium oxide, calcium oxide and phosphorus pentoxide) was investigated to have increased VEGF secretion as compared to undoped bioglass (Bejarano et al., 2017). The doped bioglass also revealed antibacterial and increased bioactive properties which reduced the chance of infection as well as biofilm production compared to orthopaedic implants (Bari et al., 2017). Copper is a promising element in the field of bone tissue engineering, it has been reported that copper doping in zinc oxide improves the electrical properties of zinc oxide and makes the grain size more uniform (Shafi et al., 2013).

1.4.18.3. Zirconium

Zirconium substitution in hydroxyapatite and bioglass is widely reported to improve the mechanical properties for orthopaedic applications. Zirconium dioxide and Hydroxyapatite composite have been synthesised and results suggested that incorporation of ZrO_2 leads to uniform porosity and enhanced cellular compatibility (An et al., 2012). Incorporation of zirconia into bioactive glasses has been reported to provide radiopacity to the final composite which is promising for injectable bone cements which can be visualised with the help of fluoroscopic control (Tallia et al., 2014). ZrO_2 is also known to have to high wear resistance and is frequently used in hip or joint replacement implants (Chevalier, 2006; B. Wang et al., 2012). Multi layered composite scaffolds using biphasic calcium phosphate and ZrO_2 were successfully synthesised, and it was reported that there was a significant improvement in collagen incorporation which led to bone regeneration without any immunogenic reactions (Linh et al., 2015), ZrO_2 significantly improves the mechanical strength specifically the compressive strength and osteointegration of the scaffold (Benic et al., 2017;

Sapkal et al., 2017). In this research we plan to investigate the role of zirconium incorporation in zinc oxide for angiogenic applications.

1.4.19 Polyurethane as a biomaterial

Polyurethane is a synthetic polymer which has been used in biomedicine since 1958 as material for implantable medical devices such as intra-aortic balloons, heart valves and stents (Grad et al., 2003). It has been demonstrated to have long durability under the biological environment and have been examined to have adequate biodegradability, biocompatibility, biostability, good hydrolytic and processability properties and mechanical strength for bone regenerative applications (S. A. Guelcher, 2008; S. a. Guelcher et al., 2004). A range of properties from flexible to rigid scaffolds and from fast degrading to slow degrading scaffolds can be prepared by varying the concentrations and choice of basic materials (Zdrahala & Zdrahala, 1999). The mechanical properties of a scaffold are a significant factor which need to be controlled depending upon the application, in the case of polyurethane the microphase between the soft segment and hard segment enables stress resistance, improved mechanical resilience, and allows proliferation of osteoprogenitor cells under mechanical cycle conditions (Sittichockechaiwut et al., 2009; Sittichokechaiwut et al., 2010; G. Tetteh et al., 2014). It also demonstrates mechanical stability under cyclic loading by providing a high yield strain and fatigue which is a significant factor in craniofacial bone tissue engineering. Such promising properties makes it significant in the field of bone tissue engineering as it can be tailored to withstand cyclic loading and fatigue which are very important mechanical properties for craniofacial bone grafts (Gorna & Gogolewski, 2003).

1.4.20 Polyurethane and zinc oxide composite materials for tissue engineering applications:

Polyurethane and zinc oxide separately are biocompatible and researched well for tissue engineering purposes. Recently composite materials have gained much attention, especially combining polymers with nanoceramics to obtain added functionality for desired applications. 3D porous scaffolds and nanofibers have attracted attention in the field of tissue

engineering due to their potential for a number of applications such as repair and regeneration of complex 3D skull fractures or load bearing fractures, bone tumours, bone defects or for drug delivery (Frenot & Chronakis, 2003). Polyurethane containing calcium phosphate sponges were prepared. The resultant sponge/scaffold was three dimensional and microporous (500 µm-800 µm). The study reported that the porosity obtained was interconnected. As the scaffold contained calcium phosphate, it might be a good candidate for bone tissue engineering. Improved interconnected porosity and compressive strength was reported but no cell culture studies were performed (Park et al., 2006). Another study reported zinc oxide doped polyurethane nanofibers synthesised via the electrospinning process. The composite was made using 10% polyurethane and 5% zinc oxide and electrospun to obtain fibres of around 400 nm diameter. Fibroblasts were culture and MTT assay was performed at Days 3, 5 and 7. The cells adhered really well and proliferated in presence of zinc oxide as compared to the control (Amna et al., 2013).

Zinc oxide has the ability to generate Reactive Oxidative species (ROS), and the role of ROS in cell growth and wound healing is very well established. The zinc ion is a trace element which is present naturally in the body and plays a role in DNA and RNA synthesis which lead to cell growth, differentiation and cell transcription. 10% Polycaprolactone and (0.1% - 0.9%) and (1-6%) zinc oxide electro spun fibres were synthesised and evaluated for antimicrobial and fibroblast cell attachment and proliferation. Cell viability assay was performed to analyse cell proliferation. Lower zinc oxide percentage (0.1-0.9 %) resulted in smooth fibres (fig. 1.11), however as the percentage of zinc oxide was increased the fibre morphology became rough and zinc oxide agglomerates were spotted on the fibres. With the increase of zinc oxide content over 6 wt%, the solution viscosity was increased and fibre formation was difficult (Augustine, Dominic, et al., 2014a).

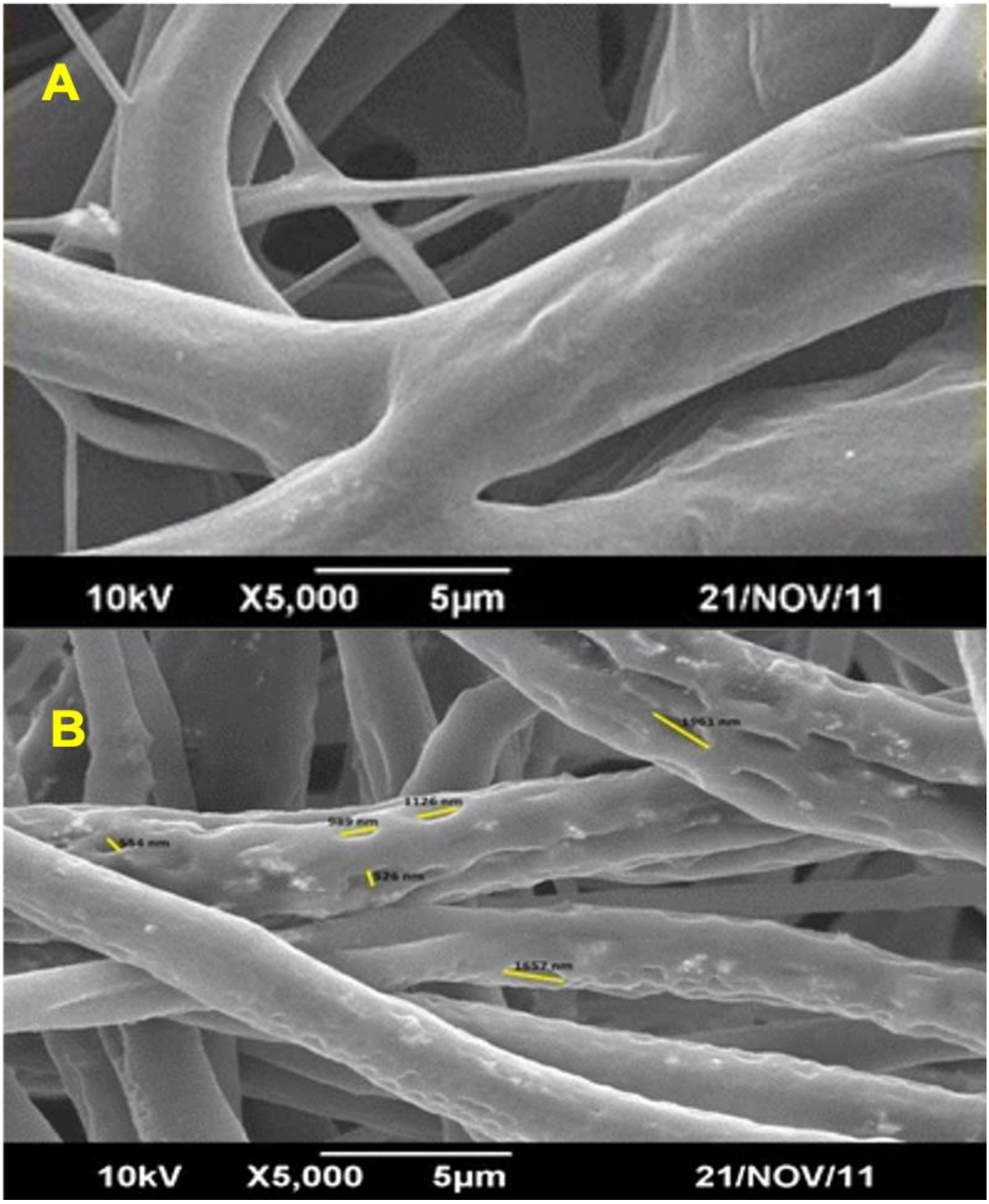

Fig 1.11: *The morphology difference between 1% zinc oxide and 2% zinc oxide incorporated electrospun fibres. Small pores within fibres were observed with 2% zinc oxide incorporates electro spun fibres. Republished with permission of Royal Society of Chemistry, from (Augustine, Dominic, et al., 2014b); permission conveyed through Copyright Clearance Center, Inc.*

When cell viability with a fibroblast cell line was evaluated, 1 weight % zinc oxide containing nanofibers increased the cell viability, however fibres containing more than 1 wt % of zinc oxide showed considerable reduction in cell attachment and proliferation (Augustine, Malik, et al., 2014). PLGA nano zinc oxide composites were found to have antimicrobial properties against Gram-positive bacteria *Staphylococcus aureus*, *Staphylococcus epidermidis*, and *Bacillus subtilis* and the Gram-negative bacteria *Escherichia coli*, *Klebsiella pneumoniae*, *Salmonella abony* and *Pseudomonas aeruginosa*, and the yeast *Candida albicans*. Such properties along with being biocompatible make zinc oxide a better candidate for biomedical applications (Stanković et al., 2016). Another study on electrospun fibres was reported where polyurethane (8%) was incorporated with zinc oxide (0.2%) and carbon nanotubes (0.4%). Randomly oriented fibres were used to perform biomineralization and antibacterial studies. The results showed the formation of a hydroxyapatite layer at the end of the SBF study. The bio-composite was subjected to antibacterial evaluation and the results were favourable when compared to control i.e. 148% and 158% higher than the mats containing only PU against S. Aureus and E coli. The antimicrobial activity was related to the production of ROS which is destructive for bacterial cell membrane and disintegrates the lipids and proteins present the in membrane in a short time. The bio-composite was also cytocompatible with cells of the MC3T3-E1 cell line. The cells adhered, proliferated and differentiated in a healthy manner. The composite also raised ALP levels and collagen type I production (Shrestha et al., 2017).

Shitole et al., (2019) synthesised Polycaprolactone, hydroxyapatite and zinc oxide composite scaffolds and evaluated the physical, chemical and biological properties. The in vitro cell viability assay was performed using the MG-63 cell line and 1% - 5% zinc oxide containing scaffolds increased the cell viability, however 10%-30% zinc oxide content caused cytotoxic effects. Alkaline phosphatase Activity assay revealed that 1%-5% zinc oxide raised ALP levels which were further backed up by a mineralisation assay (Shitole et al., 2019). Thermoplastic polyurethane and zinc oxide composite foams with increasing zinc oxide content (1%, 2%, 5% and 10%) were synthesised for wound dressing applications. Human adipose-derived stem cells (hASC) were used for cell viability and improved cell response was recorded with 1%-5% zinc oxide incorporated foams and no significant improvement was seen with 10% zinc oxide. It was also revealed that 10% zinc oxide made the cells lose their

fibroblast-like shape and become more rounded and they formed tighter groups (Bužarovska et al., 2019). Solution casting shape memory polyurethane and zinc oxide composites with zinc oxide concentrations 0, 0.5, 1.0, 1.5 and 2.0% were synthesised. The cytocompatibility assay was performed using mouse fibroblasts - L929 and Cell Counting kit-8 (CCK-8) assay was performed. The assay is a sensitive colorimetric determination of viable cells in proliferation assays. The results suggested improved cell viability upon introduction of zinc oxide (Y. Wang et al., 2020).

Finally, Polyurethane zinc oxide composite has been investigated to have important antifungal properties as well which are very important in biomedical applications. As antimicrobial antifungal properties are very important to avoid the infections related to implant and prevents the implant failure (Vlad et al., 2012).

1.5 Summary

Antibacterial and angiogenic properties of zinc oxide are well established, however the pathway by which zinc oxide induces angiogenesis is still not very clear. Low levels of zinc oxide in the form of composite scaffolds have been found to increase cell metabolic activity, improve seeding efficiency and angiogenesis. A few studies are published on polyurethane and zinc oxide composites concluding that 1-2% of zinc oxide increases cell adhesion and proliferation. Cerium, zirconium, and copper doped zinc oxide have previously been synthesised for photocatalytic applications but for bone tissue engineering these nanoparticles have never been tested. This thesis will elaborate the properties of doped zinc oxide as potential bone regenerative additive.

Chapter 2. Material and Methods

2.1 Materials

Table 2.1 List of materials used in the experiments:

	Reagents	**Supplier**
1	Zinc nitrate hexa hydrate Zn(NO3)2.6H2O	Alfa Aesa,
2	Potassium hydroxide KOH	EMSURE
3	Cerium (III) Nitrate hexahydrate 99.5%	ACROS Organics
4	Zirconyle (IV) Nitrate hydrate 99.5%	ACROS Organics
5	Copper (III) Nitrate hemi(pentahydrate) (Cu(NO3)2.2H2O) 99.9%	Merck
6	Hydroxyapatite commercial grade	Finceramica
7	Dimethyle sulfoxide (DMSO)	Sigma Aldrich
8	DMF	Sigma Aldrich
9	1,4 Dioxane	Sigma Aldrich
10	Ethanol	Honeywell
11	IMS	Honeywell
12	Avalon 85AE	Supplied by Huntsman Holland BV, Netherlands
13	Avalon 85AB	Supplied by Huntsman Holland BV, Netherlands
14	Irogran CA117-200	Supplied by Huntsman Holland BV, Netherlands
15	Sodium Chloride	Sigma Aldrich
16	Alpha Modified Eagles Medium ((α-MEM)	Lonza UK
17	Fetal Bovine Serum (FBS)	Gibco Life Technologies
18	L-glutamine (L-G)	Sigma-Aldrich, UK

19	Penicillin and streptomycin (P/S)	Sigma-Aldrich, UK
20	Gelatine	Sigma-Aldrich, UK
21	Human Embryonic Stem Cell-derived Mesenchymal Progenitor (hES-MP) cells	Cellartis, Sweden
22	Phosphate buffer saline (PBS)	Sigma-Aldrich, UK
23	Trypsin/EDTA (0.25%/0.02%)	Sigma-Aldrich, UK
24	Haemocytometer	Sigma-Aldrich, UK
25	Minimum Essential Medium Eagle (MEME)	Sigma-Aldrich, UK
26	Murine Lone Bone Osteocyte-A5 (MLO-A5)	Donated by Professor Lynda Bonewald
27	human vascular endothelial growth factor (hVEGF) ELISA kit	Bio-techne
28	0.2 M NaOH:MeOH (1:1)	Sigma-Aldrich, UK
29	3.7% formaldehyde	Sigma-Aldrich, UK
30	5% v/v perchloric acid	Sigma-Aldrich, UK
31	Alizarin Red dye	Sigma-Aldrich, UK
32	Phosphate buffer saline (PBS)	Sigma-Aldrich, UK
33	Sirius Red dye	Sigma-Aldrich, UK
34	4', 6-diamidino-2-phenylindole dihydrochloride (DAPI) fluorescent dye	Sigma-Aldrich, UK
35	Immunocytochemistry (ICC) buffer (1% BSA, 0.1% Triton X-100 in PBS)	Sigma-Aldrich, UK
36	Phalloidin-Tetramethyl Rhodamine Isothiocyanate (TRITC) fluorescent dye	Thermo Fisher Scientific
37	Phosphate buffer saline (PBS)	Sigma-Aldrich, UK

2.2. Methods

2.2.1 Synthesis of zinc oxide; continuous hydrothermal flow system (CHFS):

An eco-friendly green technology was used to synthesise the nanoparticles. The first step was synthesis of zinc oxide and doped zinc oxide nanoparticles. Cerium, zirconium and copper were selected as dopants due to their potential benefits for bone regeneration and angiogenesis, as discussed in chapter 1. The synthesis of nanoparticles was performed at School of Chemistry, University College London.

The figure 2.1 shows the schematic of the CHFS pilot plant that was used for synthesis of nanoparticles. The pilot lab scale plant was used which was comprised of three pumps to supply pressurised precursor feeds into the system. Pump 1 (P1) was used to feed deionized water at flow rate of 80 ml/min (supercritical water at 450°C), Pump 2 (P2) was used to feed Potassium Hydroxide (KOH) Solution and Pump 3 (P3) was used to feed Zinc nitrate Solution at flow rate of 40ml/ml respectively. Supercritical water was produced by pumping water through Pump 1 (P1) with flow rate of 80 ml/min, passed through heating chamber where it was heated at 450˚C/240 bar in order to keep a temperature of about 335˚C at the reaction centre.

The process was initiated by preparation of precursor solution at room temperature. The magnetic stirrer was used to prepare KOH and zinc nitrate solution in deionised water. The concentration of precursor solutions was increased to obtain larger particles. 0.2M KOH and 0.1M Zn precursor solutions were used to synthesise group 1 bigger nanoparticles. 1M KOH and 0.5M Zn solutions were used to obtain relatively small nanoparticles called group 2. Table 2.2 shows the concentrations of precursor solution and dopants used (Table 2.2). To synthesize doped zinc oxides, pre-weighed dopant sources [$Ce(NO_3)_3.6H_2O$, copper nitrate and zirconium nitrate] were added to zinc nitrate solution which was under continuous stirring. (For Amounts See table 2.2)

The precursor solutions prepared at room temperature were pumped through pumps P2 and P3 (Fig.2.1) at a flow rate of 40 ml/min. Both the solutions were pumped through Polytetrafluoroethylene (PTFE) tubing which was connected with a 3/4inch SS-316L T-piece serving as reaction mixer. The mixture was pumped to the reaction centre (R) where it came

into contact with supercritical water which acted as crystallisation medium. The zinc salts were converted into zinc oxides due to rapid hydrolysis and dehydration. The resultant product was cooled to 40˚C by passing through a pipe in the cooler chamber. The cooled product or slurry was then passed through back pressure regulator (BPR) in order to maintain the pressure in the system. The resulting nanoparticles in the form of a slurry were collected in a beaker at 25˚C.

The slurry was washed with deionised water twice and suspended in deionised water. The washing process was undertaken by suspending the particles in deionised water followed by centrifugation to obtain sedimentation of nanoparticles. The nanoparticles were again suspended in deionised water and packed in dialysis tubes. The dialysis tubes were sealed carefully and left in a tank filled with deionised water to remove any soluble impurities or salts present in the slurry. After 24 hours the slurry was separated from deionised water and freeze dried (Virtis Genesis 35XL) by slowly heating the samples from −60˚C to 25˚C for 24 hours at vacuum of <13.3 Pa to obtain nanopowders. The copper doped zinc oxide powders were grey to black in colour. The reason might be presence of copper oxide (black colored oxide) along with zinc oxide. The further characterisation details will be discussed in later chapters. The powders were stored in glass tubes, labelled and stored at room temperatures for further experiments (fig. 2.2).

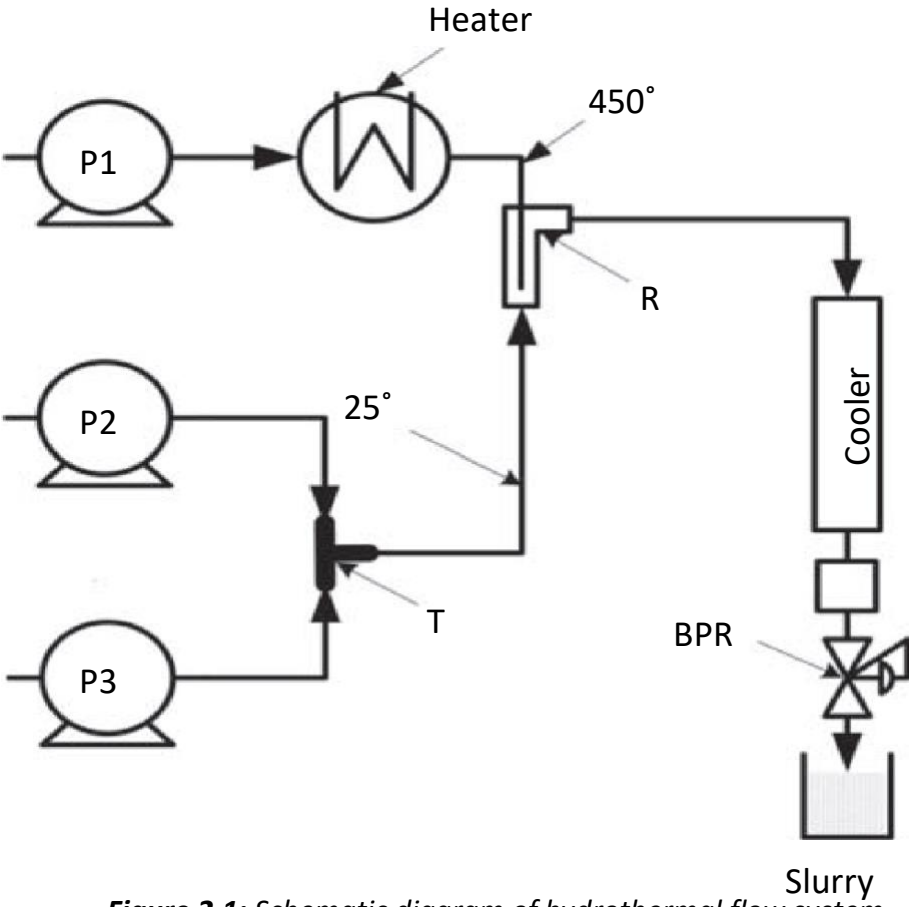

Figure 2.1: *Schematic diagram of hydrothermal flow system.*

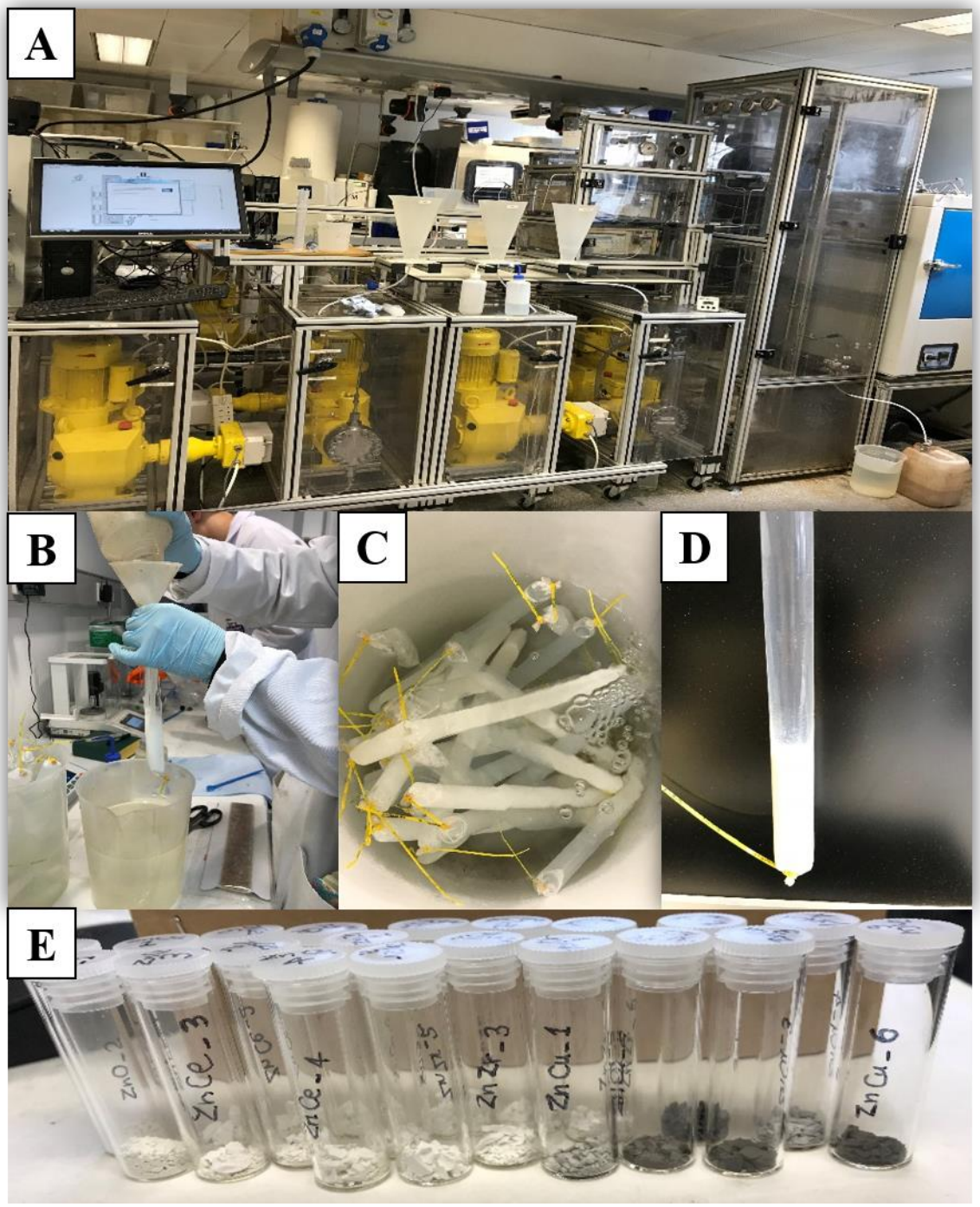

Figure 2.2: *The continuous flow system used for nanoparticle synthesis. A) Lab scale pilot plant continuous flow system for nanoparticles synthesis. B) The nanoparticle suspension obtained was poured in dialysis tubes. C) Dialysis for 24 hours to remove impurities and salts. D) Nanoparticles settle down after 24 hours of dialysis. E) Freeze dried samples obtained.*

Table 2.2: *The concentrations of precursor solutions and dopant quantities used to synthesise Zinc oxide, cerium doped Zinc oxide, zirconium doped Zinc oxide and copper doped Zinc oxide.*

NAMES	[KOH] (M)	[Zn]* (M)	M precursor	[M]	Volume (L)	Mass Zn* (g)	Mass (g)
ZnO_1	0.2	0.1	N/A	0	1	29.75	0.00
ZnO_2	1	0.5	N/A	0	0.5	74.37	0.00
ZrZnO1	0.2	0.099	$ZrO(NO_3)_2.6H_2O$	0.001	1	29.45	0.30
ZrZnO2	0.2	0.097	$ZrO(NO_3)_2.6H_2O$	0.003	1	28.85	0.89
ZrZnO3	0.2	0.095	$ZrO(NO_3)_2.6H_2O$	0.005	1	28.26	1.49
ZrZnO4	1	0.495	$ZrO(NO_3)_2.6H_2O$	0.005	0.5	73.62	0.74
ZrZnO5	1	0.485	$ZrO(NO_3)_2.6H_2O$	0.015	0.5	72.14	2.23
ZrZnO6	1	0.475	$ZrO(NO_3)_2.6H_2O$	0.025	0.5	70.65	3.72
CeZnO1	0.2	0.099	$Ce(NO_3)_3.6H_2O$	0.001	1	29.45	0.43
CeZnO2	0.2	0.097	$Ce(NO_3)_3.6H_2O$	0.003	1	28.85	1.30
CeZnO3	0.2	0.095	$Ce(NO_3)_3.6H_2O$	0.005	1	28.26	2.17
CeZnO4	1	0.495	$Ce(NO_3)_3.6H_2O$	0.005	0.5	73.62	1.09
CeZnO5	1	0.485	$Ce(NO_3)_3.6H_2O$	0.015	0.5	72.14	3.26
CeZnO6	1	0.475	$Ce(NO_3)_3.6H_2O$	0.025	0.5	70.65	5.43
CuZnO1	0.2	0.099	$Cu(NO_3)_2.3H_2O$	0.001	1	29.45	0.24
CuZnO2	0.2	0.097	$Cu(NO_3)_2.3H_2O$	0.003	1	28.85	0.72
CuZnO3	0.2	0.095	$Cu(NO_3)_2.3H_2O$	0.005	1	28.26	1.21
CuZnO4	1	0.495	$Cu(NO_3)_2.3H_2O$	0.005	0.5	73.62	0.60
CuZnO5	1	0.485	$Cu(NO_3)_2.3H_2O$	0.015	0.5	72.14	1.81
CuZnO6	1	0.475	$Cu(NO_3)_2.3H_2O$	0.025	0.5	70.65	3.02

2.2.2 Characterisation of nanoparticles:

The nanopowders synthesised using CHFS were subjected to chemical and physical characterisation. The aim of characterisation step was to explore if the nanopowders obtained had incorporated the dopants and to assess whether the compositions contained impurities i.e. oxides etc.

2.2.2.1 Dynamic Light scattering Measurements

Dynamic light scattering is a process which uses nanoparticle suspension in deionised water to determine the hydrodynamic diameter of the particles. The suspension was introduced into the machine in a closed cuvette. Electromagnetic light waves were passed through the suspension inducing oscillations of electrons in the particles which lead to path deviation for the incident light. The scattered light was collected to obtain the diffusion rate. The environmental conditions such as temperature have to be the same for all the samples as it affects the Brownian motion which is indirectly proportional to the size of the particles.

Dynamic Light scattering was used to obtain the hydrodynamic diameter of the synthesised particles using a Zeta Ziser Nanoseries (fig. 2.3). The nanoparticles were sonicated in 1 ml water for 5min and readings were obtained.

The hydrodynamic diameter is the diameter of a solid sphere that is created around the nanoparticle which in this case is the sphere or bubble created by water molecules around the nanoparticles (fig. 2.3). Generally, DLS provides an output value as a range, where the boundaries of the range can be smaller or larger than the average value obtained. Overall, this average of the range given will be larger than the actual particle size because of suspension in water. The DLS analysis is a preliminary method to identify a range of sizes in which the nanoparticles lie. It was performed soon after synthesis to check the particle size.

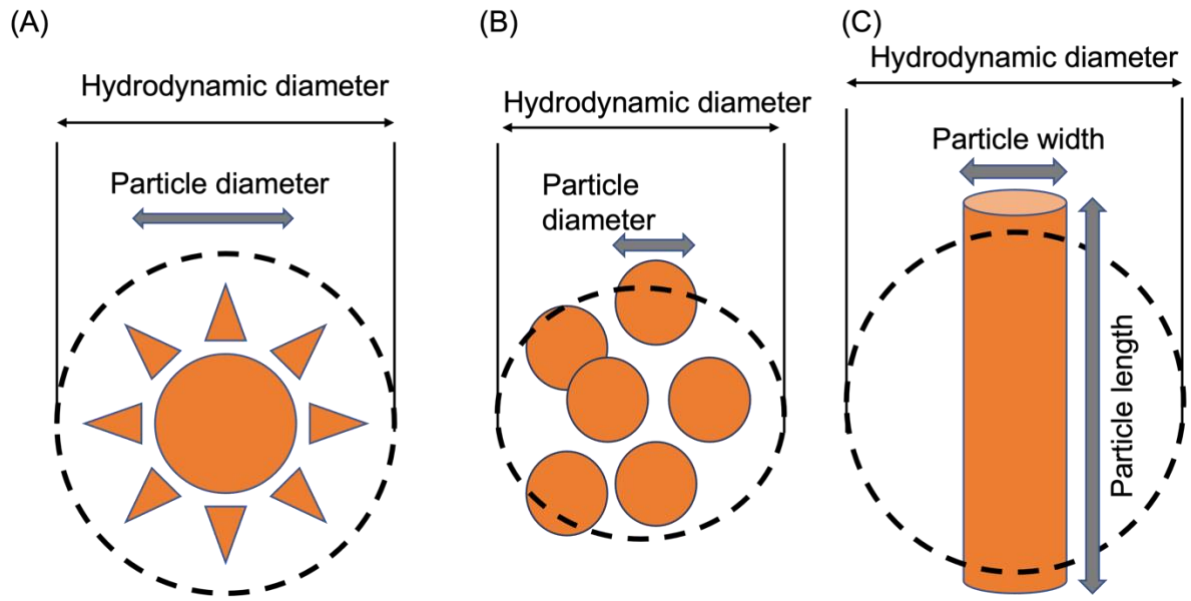

Figure 2.3: *Theoretical concept of hydrodynamic diameter.*

The Zeta Ziser Nanoseries works on the principle of Stokes-Einstein Equation to calculate hydrodynamic diameter.

$$d_H = kT/3\pi\eta D$$

d_H = hydrodynamic diameter (m)

k = Boltzman constant (J/K)

T = Temperature (K)

η = solvent viscosity (kg/m.s)

D = diffusion coefficient (m^2/s)

It is affected by particle properties such as agglomeration which is not a precise measurement of size but provides an approximation of size range (fig. 2.3). The measurements were performed three times and a mean calculated was taken to obtain the hydrodynamic diameters of zinc oxide and doped zinc oxide nanoparticles.

2.2.2.2 Raman Spectroscopy of zinc oxide Samples

Raman characterisation was performed using Raman DXR Xi to obtain Raman spectra of the samples. The Raman spectra were obtained using laser 780 nm and Aperture 25 µm.

2.2.2.3 X-ray Diffraction (XRD)

The X-Ray Diffraction analysis was performed by using Brukner D2 Phaser. The parameters used were same for all the sample (Table 2.3).

Table 2.3: The XRD parameters used to analyse the zinc oxide samples.

Effective total time	310.8 s
Time	0.600 s
2 theta	30-80
Voltage	30V
Current	10A

The Scherrer's equation was used to calculate the crystallite size. The dominant peak at 36.4 degrees was selected to calculate crystallite size using Scherrer's equation.

$$Dp = (0.94 * \lambda)/ \beta * \cos \theta$$

Dp= average crystallite size

β = line broadening in radians

θ= Braggs angle

λ= X-ray wavelength

2.2.2.4 Brunauer-Emmett-Teller (BET)

Physical Adsorption isotherms of N_2 at -196˚C were measured by Tristar II Micrometrics. All the samples were degassed under N_2 at 150˚C for 12 hours before BET surface area from N_2 isotherms were measured. The measurements were performed at 10 points.

2.2.2.5 Scanning Electron Microscopy

The morphology of Nano powders was investigated using scanning electron microscopy Vega 3 LMU – TESCAN. The nanopowders were suspended in absolute ethanol using a sonicator followed by dropping 100 µl on an SEM Stub. The stub was left for ethanol evaporation for 5 minutes followed by gold coating with a thickness of 250 Å using a coating unit. Elemental analysis was carried out using an Oxford Instruments SSD detector attached to a VEGA3 TESCAN Scanning Electron Microscope.

2.2.2.6 Transmission Electron Microscopy (TEM)

To perform TEM, the copper palladium carbon-coated grids were glow discharged using an Agar Scientific glow discharge unit attached to Agar scientific turbo carbon coater unit (Agar Scientific Stansted Essex UK). The nanoparticles were suspended in absolute ethanol and sonicated for 2 hours. The 10 µl sample was dropped onto discharged TEM grids and left to dry for 10 minutes. The excess ethanol was removed carefully using clean filter paper (Whatman grade 1 GE HealthCare UK, Little Chalfont, UK). TEM grids were visualised using FEI Tecnai G2 Biotwin Tranmission Electron Microscope (FEI Cambridge, UK) at an operating voltage of 80kv. Micrographs were obtained using Gatan Orius 1000B digital camera. The Gatan Digital Micrograph software suite (Gatan Ltd, Corby UK) was used.

2.2.3 Cell Metabolic Activity Assay of Nanoparticles

Sterilisation of Nanoparticles: 2000 microgram nanoparticles were weighed on an electronic balance and stored in Eppendorf tubes. The Eppendorf tubes were packed in autoclave bags and sealed with autoclave tapes. The bags were autoclaved at 121°C for 30 minutes to sterilise the nanoparticles. The autoclave bags containing Eppendorf tubes were placed in drying cabinet at 70°C overnight to dry the moisture in the bags. The Eppendorf tubes containing sterilised nanoparticles were stored in a box on shelf and were only opened in cell culture hood (it is installed with HEPA filters and creates sterile environment for cell culture experiments, prevents the samples from contamination) to prevent the contamination.

2.2.3.2 Preparation of stock suspensions of nanoparticles for Cell culture:

To prepare nanoparticle stock solutions, 2000 µg nanoparticles were weighed in an eppendorf. The eppendorf tubes were autoclaved. 2000 µl of serum free media (DMEM for MG63 and Alpha MEM for hES-MPs) was added to the eppendorf tubes. The Eppendorf tubes were sonicated at room temperature for 30 minutes to create homogenous suspensions. The working solutions were prepared by taking the desired amount of stock solution and diluting it into serum free media in a sterile environment (table 2.4). The stock suspension was created in a way that 1 µl contained 2 µg of nanoparticles.

Stock Solution concentration: 2 µg/1µl

Working solution prepared in serum free DMEM or Alpha MEM.

Table 2.4: *The nanoparticle suspension preparation from stock solution for cell metabolic activity assay.*

Desired concentration	Required Suspension quantity (µl)	Suspension quantity stock solution (µl)	Amount of Serum Free Media (DMEM or Alpha MEM) (µl)
5 µg/ml	100	2.5	97.5
10 µg/ml	100	5	95

2.2.3.5 Cell metabolic activity assay or Resazurin Assay:

Preparation of Resazurin Stock Solution: 1mM Resazurin stock solution was prepared by dissolving 0.013 g in 50 ml deionised water. The resazurin salt was mixed well and filtered using a syringe filter inside the cell culture hood to maintain sterility environment. The container was wrapped with Aluminium Foil and stored at 4°C.

Preparation of Resazurin Working Solution: The resazurin working solution was prepared by making 10% stock solution in Serum free Media (table 2.5).

Table 2.5: *The type of media used for making cell metabolic activity assay working solution for different cell types used in the study.*

Cell Type	**Media used for working solution**
MG63	DMEM
Y201 cell line	DMEM with nucleotides
hES-MPs	Alpha MEM

Assay Process: The well plate to be analysed was taken out of the incubator. The media was discarded, and each well was washed at least once with PBS. Then 500 µl resazurin working solution was added to each well (24 well plate), the plate was wrapped in Aluminium foil to prevent light exposure. The plate was stored in the CO_2 incubator for 2 hours.

After 2 hours the resazurin solution was transferred into a new well plate and readings were taken in a plate reader. The original 24 well plate was washed with PBS to remove any residual resazurin solution. The cell culture media was re-introduced and well plates were returned to the CO_2 incubator. The resazurin reading was recorded at Day1, Day3, Day5 and Day 7 using the microplate reader.

2.2.3.3 Preparation of MG63 cell line for cell metabolic activity assay:

The MG63 cells belong to osteosarcoma cell line which is an experimental model of osteoblasts. The advantage of this cell line is that it proliferates rapidly as compared to primary cells and are immortal. It is the least differentiated cell line and have been in use in a number of assays while investigating biomaterials (Gogolewski & Gorna, 2007).

Media Preparation: The basal media for MG63 cell line consisted of DMEM with 10% FBS and 0.2% pencillin-streptomycin and 0.2% L-Glutamine. The media was stored in fridge at 4°C until used.

T75 Flask preparation or Cell line propagation from a frozen vial: A frozen cell Vial was taken and thawed on water bath at 37°C. Once the vial was thawed, the contents were quickly

transferred to a centrifuge tube containing 5ml media. The tube was centrifuged at 10000 rpm for 5 minutes. The supernatant was discarded, and the pellet was dissolved in fresh media. The cell suspension was introduced into a T75 flask containing 10ml prepared media which was then placed in CO_2 incubator at 37°C. The flask was visualised everyday under light microscopy for cell attachment and growth. The media was carefully changed every two days. A T75 flask takes about 3-4 days to become confluent. The flask was visualised under light microscope for confluence, if there are no spaces between cells, this indicated that the flask is confluent and is ready to use (fig. 2.4).

Cell Freezing: Freezing solution preparation: Freezing solution is prepared by mixing DMSO and fetal calf serum at a ratio of 1:9. The cell suspension that is required to be stored was counted using a haemocytometer. Cells were stored at a minimum density of 1 X 10^6 cells per ml.

2.2.3.4 Cells seeding for cell metabolic Activity Assay:

The cells were counted and suspended in the required amount of media such that there was a known number of cells in per ml of cell culture expansion media. For the experiment 24 well plates were used, and 1 X 10^4 cells were used per ml per well. The well plates were incubated for 24 hours to allow cells to attach. After 24 hours the media was removed, and cells were washed once with PBS to remove any non-attached cell and cell waste. The nanoparticle suspension was pipetted onto the cells.

Two concentrations of nanoparticle suspension were tested 5 µg/ml and 10 µg/ml. The experiment was repeated 3 times and the mean calculated. The resazurin assay was performed at Day 1, Day 3, Day 5 and Day 7. The assay is a semi quantitative assay to determine cell metabolic activity overall in the culture well, the output obtained is an indicator of cell number assuming that the metabolic activity per cell remains the same and is not affected by the test samples.

2.2.3.6 28 Day Cell metabolic activity Assay using hES-MPs

Introduction: Human Embryonic mesenchymal like stem cells were used to evaluate the cell viability of selected nanoparticles for up to 28 days. The study was aimed to analyse the long-term cell viability (28 days) in presence of nanoparticles before scaffold synthesis.

hES-MPs is a human embryonic stem cell-derived mesenchymal progenitor cell line. The advantage of this cell line is reduced risk of donor site morbidity and ample availability for in vitro cell culture for tissue engineering experimentations. These cells are capable to differentiate towards osteogenic lineages in presence of osteogenic supplements. This property makes these cells a good choice for investigation of osteogenic potential of biomaterials (Delaine-Smith et al., 2012).

Media Preparation: The α MEM, PS and FBS were placed in water bath at 37°C. The 10% FBS (50ml in 450ml αMEM) and 5ml PS was added to αMEM. The ingredients were mixed well and stored at 4°C.

hES-MPs Expansion: The hES-MPs were grown from a frozen vial. The vial was kept at 37°C until it melted. The cell solution was transferred to a centrifuge tube containing 10 ml of basal/expansion media. The tube was centrifuged at 1000 RPM for 5minutes. The supernatant was discarded, and the pellet was resuspended in 3ml media. A T75 flask was used for cell expansion, 12 ml Media was introduced in the flask followed by introduction of re-suspended cells. The flask was kept at 37°C in a CO_2 incubator for at least 5 days until the cells became confluent. The media was changed every two days.

Once the flask was 100% confluent, the cells were transferred to a flask or in a well plate depending upon the requirement. In order to do that, the media was removed from a T75 flask, followed by PBS washing twice (to remove any debris or dead cells). 3.5 ml of trypsin was added and incubated at 37°C for 90 seconds. The flask was given a gentle jerk to promote cell detachment. The trypsin was deactivated by the addition of 7ml of cell culture basal media (double the amount of Trypsin). The content was transferred to a centrifuge tube for centrifugation at 1000 RPM for 5min. The supernatant was removed, and the pellet was resuspended in 3ml media.

The haemocytometer was used to count the cells. The 10 µl cell suspension was used and introduced to a clean haemocytometer. The cells were counted under a light microscope.

The cell seeding plan is shown in fig 2.4. Only the selected nanoparticles were tested with hES-MPs from the previous cell metabolic activity assay performed with MG63. The 10 µg/500 µl was used for 28 day cell metabolic activity assay.

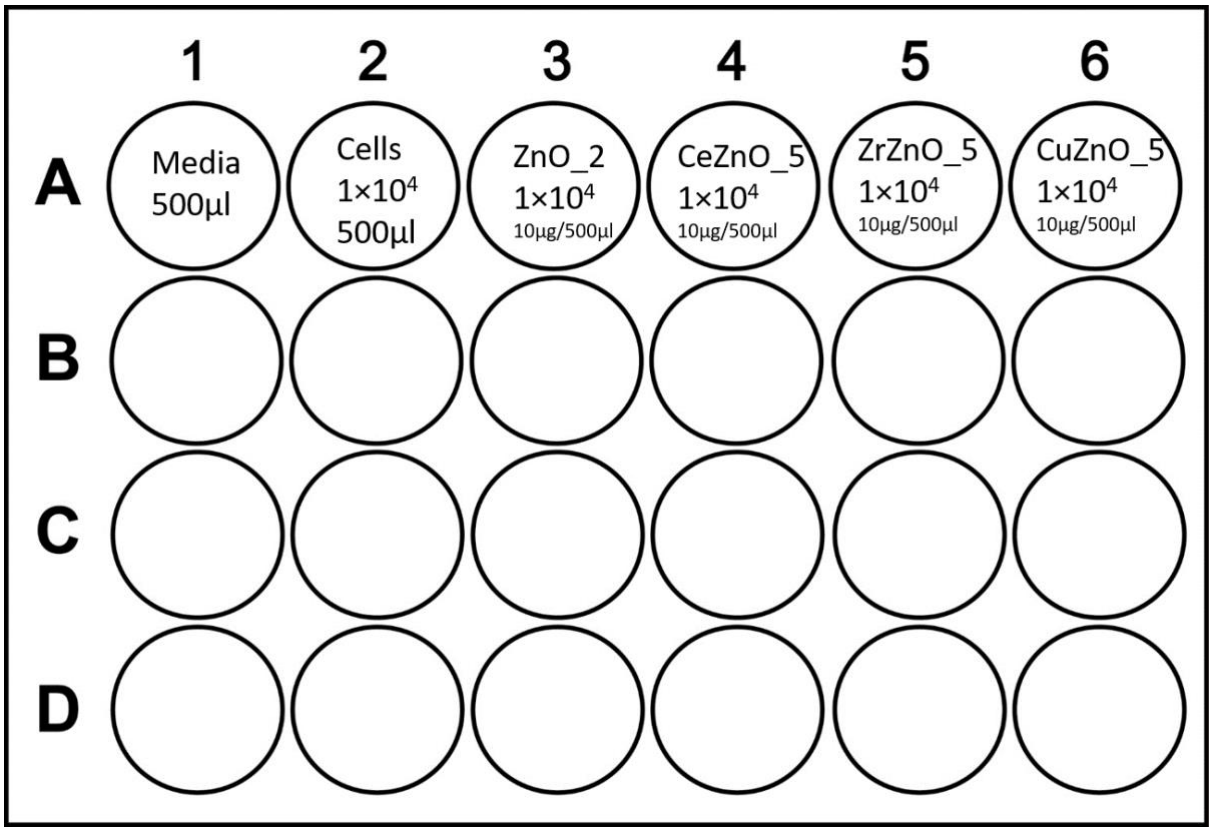

Figure 2.4: *Experimental plan for Cell viability Assay of selected nanoparticles with hES-MPs*

2.2.4 Scaffold Synthesis: Method Development troubleshooting

The solvents; 1,4 Dioxane, Dimethyle Sulfoxide and Dimethyle formamide were tested with three different polyurethane types; Avalon 85AE, Avalon 85AB and Irogran CA117-200. A 10% PU solution was made up in each solvent and a total of 36 samples was prepared (table 2.6). Each polymer mixture was poured into a petri dish to obtain identical scaffolds. The petri dishes were frozen at -20°C or -80°C (table 2.6) for 24 hours. The frozen petri dishes were

transferred to 10% ethanol water for salt leaching for 10 days. The ethanol water was changed once every 24 hours. The resultant scaffolds were dried in a drying cabinet at 60°C for 24 hours to obtain PU foams. At this stage qualitative analysis was performed, mainly to identify a better solvent. The scaffold strength and porosity were seen visually to identify which ones seem better for scanning electron microscopy analysis.

Table 2.6: *The method development for scaffold synthesis. A number of scaffolds were synthesised and tested to identify the appropriate solvent, polymer, salt/porogen concentration and freezing temperature.*

	Type of solvent	Type of Polymer (Polymer concentration 10% by weight)	Freezing Condition (°C)	Salt quantity (g)	Sample name
1	1,4 Dioxane	Avalon 85AE	-20	7	DX 1
2	1,4 Dioxane	Avalon 85AB	-20	7	DX 2
3	1,4 Dioxane	Irogran CA117-200	-20	7	DX 3
4	1,4 Dioxane	Avalon 85AE	-20	14	DX 4
5	1,4 Dioxane	Avalon 85AB	-20	14	DX 5
6	1,4 Dioxane	Irogran CA117-200	-20	14	DX 6
7	1,4 Dioxane	Avalon 85AE	-80	7	DX 7
8	1,4 Dioxane	Avalon 85AB	-80	7	DX 8
9	1,4 Dioxane	Irogran CA117-200	-80	7	DX 9
10	1,4 Dioxane	Avalon 85AE	-80	14	DX 10
11	1,4 Dioxane	Avalon 85AB	-80	14	DX 11
12	1,4 Dioxane	Irogran CA117-200	-80	14	DX 12
13	Dimethylformamide	Avalon 85AE	-20	7	DMF 1
14	Dimethylformamide	Avalon 85AB	-20	7	DMF 2
15	Dimethylformamide	Irogran CA117-200	-20	7	DMF 3
16	Dimethylformamide	Avalon 85AE	-20	14	DMF 4
17	Dimethylformamide	Avalon 85AB	-20	14	DMF 5
18	Dimethylformamide	Irogran CA117-200	-20	14	DMF 6

19	Dimethylformamide	Avalon 85AE	-80	7	DMF 7
20	Dimethylformamide	Avalon 85AB	-80	7	DMF 8
21	Dimethylformamide	Irogran CA117-200	-80	7	DMF 9
22	Dimethylformamide	Avalon 85AE	-80	14	DMF 10
23	Dimethylformamide	Avalon 85AB	-80	14	DMF 11
24	Dimethylformamide	Irogran CA117-200	-80	14	DMF 12
25	Dimethylsulfoxide	Avalon 85AE	-20	7	DMSO 1
26	Dimethylsulfoxide	Avalon 85AB	-20	7	DMSO 2
27	Dimethylsulfoxide	Irogran CA117-200	-20	7	DMSO 3
28	Dimethylsulfoxide	Avalon 85AE	-20	14	DMSO 4
29	Dimethylsulfoxide	Avalon 85AB	-20	14	DMSO 5
30	Dimethylsulfoxide	Irogran CA117-200	-20	14	DMSO 6
31	Dimethylsulfoxide	Avalon 85AE	-80	7	DMSO 7
32	Dimethylsulfoxide	Avalon 85AB	-80	7	DMSO 8
33	Dimethylsulfoxide	Irogran CA117-200	-80	7	DMSO 9
34	Dimethylsulfoxide	Avalon 85AE	-80	14	DMSO 10
35	Dimethylsulfoxide	Avalon 85AB	-80	14	DMSO 11
36	Dimethylsulfoxide	Irogran CA117-200	-80	14	DMSO 12

2.2.4.1 Choice of Solvent:

DMF was ruled out as a solvent because its freezing temperature is -61°C. It was not possible to completely freeze the polymer mixture even at -80°C in 24 hours. The visual appearance of the scaffold was the main criterion for solvent selection. Such as if the thickness of the scaffold is uniform, no big pores as a result of air bubbles and if the scaffold is fragile etc. DMSO was able to produce foam like porous 3D scaffolds. 1, 4 dixoane were not appropriate as the scaffolds stuck to the mould and tore apart upon removal (fig 2.5).

Figure 2.5: *Scaffold appearance using different solvents.*

2.2.4.2 Choice of Polymer:

SEM was performed to evaluate the porosity of the three polymers. Avalon AE and Avalon AB were appropriate because of foam like texture and visible porosity, however, irogran CA 117-200 was found rough and fragile as compared to other two (fig. 2.6 & 2.7).

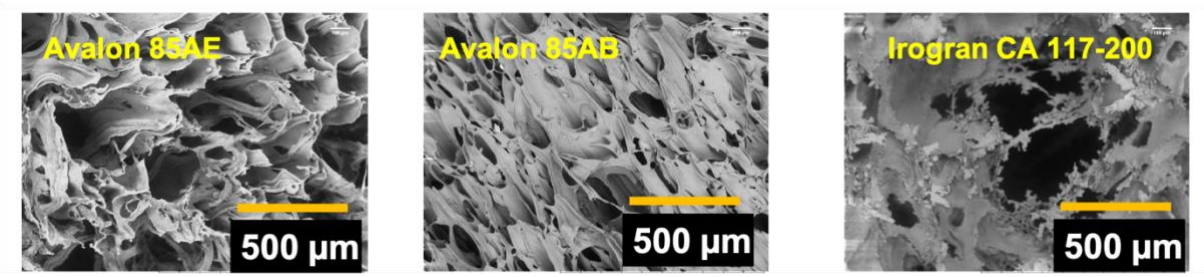

Figure 2.6: *SEM micrograph of porous scaffolds synthesised using different polyurethane types. The Avalon 85AE and Avalon 85AB was foam like highly porous without gaps, however Irogran CA 117-200 was fragile.*

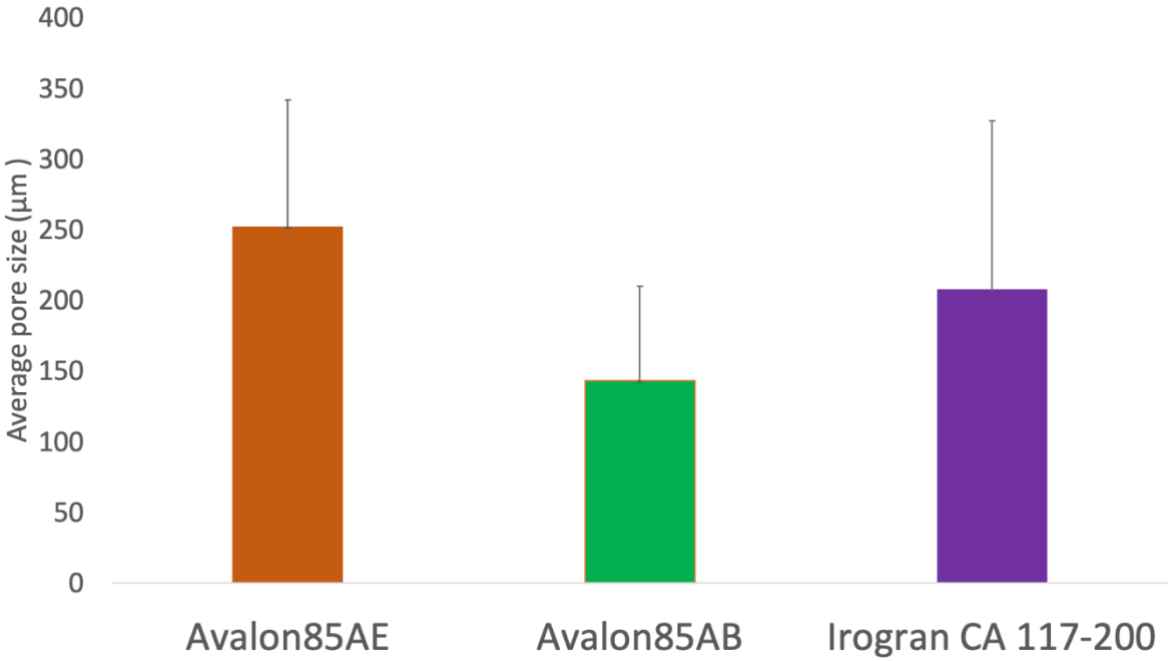

Figure 2.7: *Pore size comparison of different polymers. The pore size was calculated in Image J. A total of 25 pores were measured and data was compared to select appropriate polymer type.*

2.2.4.3 Amount of Salt:

7g or 14g salt was used per 50ml of polymer solution. The SEM was performed, and Image J was used to calculate the pore size. The porosity and physical appearance were not much different because of salt concentration. The 14g salt settled more quickly and the scaffold was more dense on one side than the other, however, the porosity when compared was the same. Therefore, 7g salt quantity was selected for further scaffold synthesis (fig. 2.8).

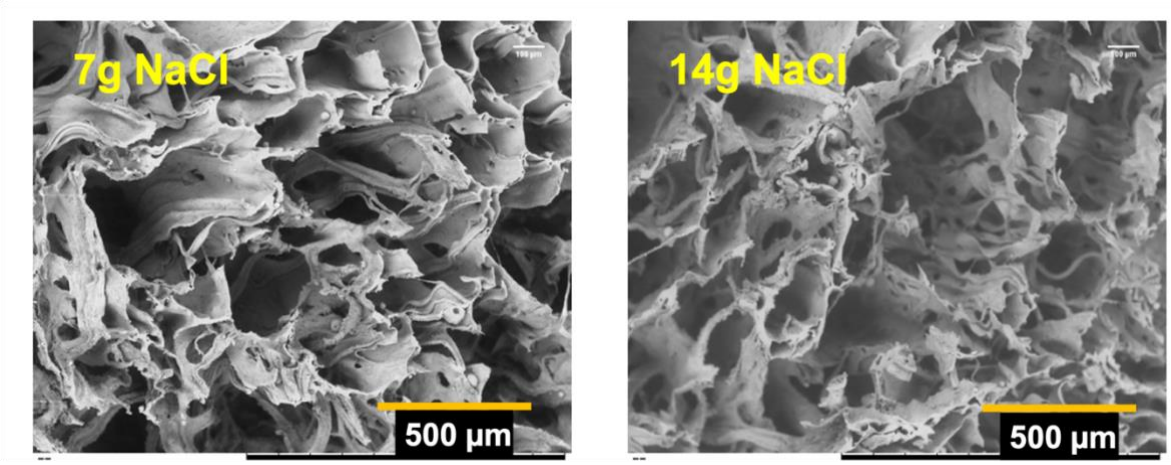

Figure 2.8: *SEM micrograph of porous scaffolds synthesised using 7 g and 14 g Sodium Chloride porogen. The porosity was not affected by quantity of salt.*

2.2.4.4 Freezing temperature:

The -80°C and -20°C freezing temperature were used. -20°C was found to be appropriate as -80°C yielded fragile scaffolds. The rigorous mixing of polymer solution with salt resulted in a suspension with a lot of air bubbles due to highly viscous nature of polyurethane solution. -80°C temperature resulted in quick freezing, hence not allowing the air bubbles to come on the surface. This resulted in void spaces in middle of the dried scaffold resulting in a fragile structure. On the other hand, -20°C resulted in slow freezing as compared to -80°C, allowing ample time for air bubbles to escape from the surface.

2.2.5 Optimised Scaffold Synthesis

Apparatus: Round Bottom Flask, Condenser, Oil Bath, Hot plate, magnetic stirrer, thermometer, spatula, weighing balance, weighing boats, measuring cylinder, Drying cabinet (Fig 2.10).

Materials: Degradable polyurethane Avalon 85AE, Dimethyle Sulfoxide, Sodium Chloride, 10% Ethanol.

2.2.5.3 Process:

PU Scaffolds (control): The 10% polyurethane solution in DMSO was used for scaffold synthesis. The 5g PU was weighed carefully and added to the round bottom flask, followed by addition of 50ml DMSO. The apparatus was set as shown in fig 2.10. The temperature of the oil bath was maintained at 70-80°C. The PU was left on continuous stirring for 24 hours.

After 24 hours, a viscous PU Solution was obtained. The solution was poured into a beaker and 7g salt was introduced followed by rigorous mixing with a spatula for about 2-4 minutes. Once the salt was uniformly distributed, the mixture was divided into two Petri dishes and stored at -20°C for 24 hours. Once the mixture was completely frozen, the petri dishes were transferred to 500ml 10% ethanol water for salt and solvent leaching for 10 days. The ethanol water was changed once every 24 hours. The scaffolds were dried in a drying cabinet at 60°C for 24 hours to obtain PU foams (Fig 2.9).

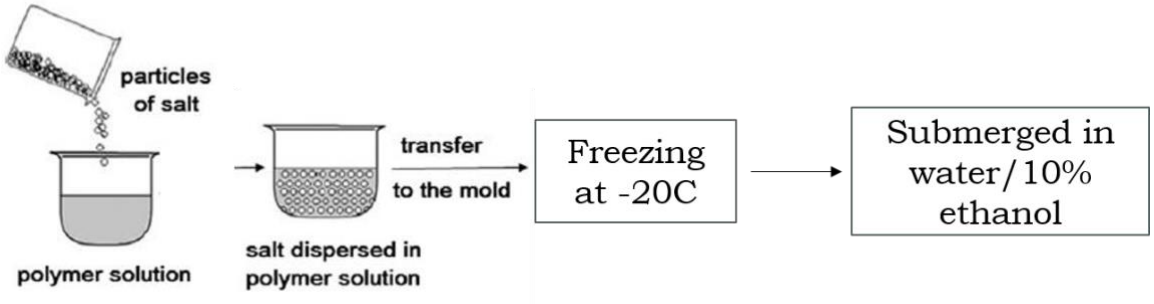

Figure 2.9: *The freeze Extraction-salt leaching process used for Scaffold synthesis.*

Figure 2.10: *Experimental setup for Scaffold Synthesis*

PU hydroxyapatite Scaffold: The 10% PU solution was prepared as mentioned above, after 24 hours of dissolution 5% HA (2.5g) was added and left for dissolution for 24 hours before freezing. Once a complete homogenous solution was obtained, salt was added and mixed well. The solution was poured into petri dishes followed by freezing and Salt/Solvent leaching as mentioned before.

PU HA ZnO Scaffold: In order to make composite scaffolds, the 5g PU was dissolved in 45 ml DMSO, and zinc oxide or doped zinc oxide was added to 5ml DMSO and left for stirring for 24 hours in a glass reagent bottle separately. Once a homogenous DMSO zinc oxide solution was obtained, it was added to the PU/HA mixture and left on continuous stirring for 24 hours before freezing. The solution was transferred to Petri dishes and frozen at -20°C followed by Salt/Solvent leaching for 10 Days.

Scaffolds were prepared PU, PU-HA, PU-HA-ZnO_2, PU-HA-CeZnO5, PU-HA-ZrZnO5 and PU-HA-Cu ZnO5. The aim was to identify the effect of different dopings within the composite on cell metabolic activity. 1%, 3% and 5% weight percent nanoparticles were loaded during scaffold synthesis to identify the dose effect on cells.

2.2.6 Scaffold Characterisation

2.2.6.1 FTIR

The Polyurethane and Polyurethane composite scaffolds were characterised using ATR Nicolet iS5 ThermoScientific in the Diamond Building, University of Sheffield. The resolution was kept 8 and 128 scans were recorded per sample.

2.2.6.2 Tensile Testing

The scaffolds were cut in 8cm strips with 3cm width. Shimadzu 5 kN Universal Testing Machines (Tension, Compression, Flexural) was used for tensile testing. 500N/minute load was used for the testing (fig. 2.11).

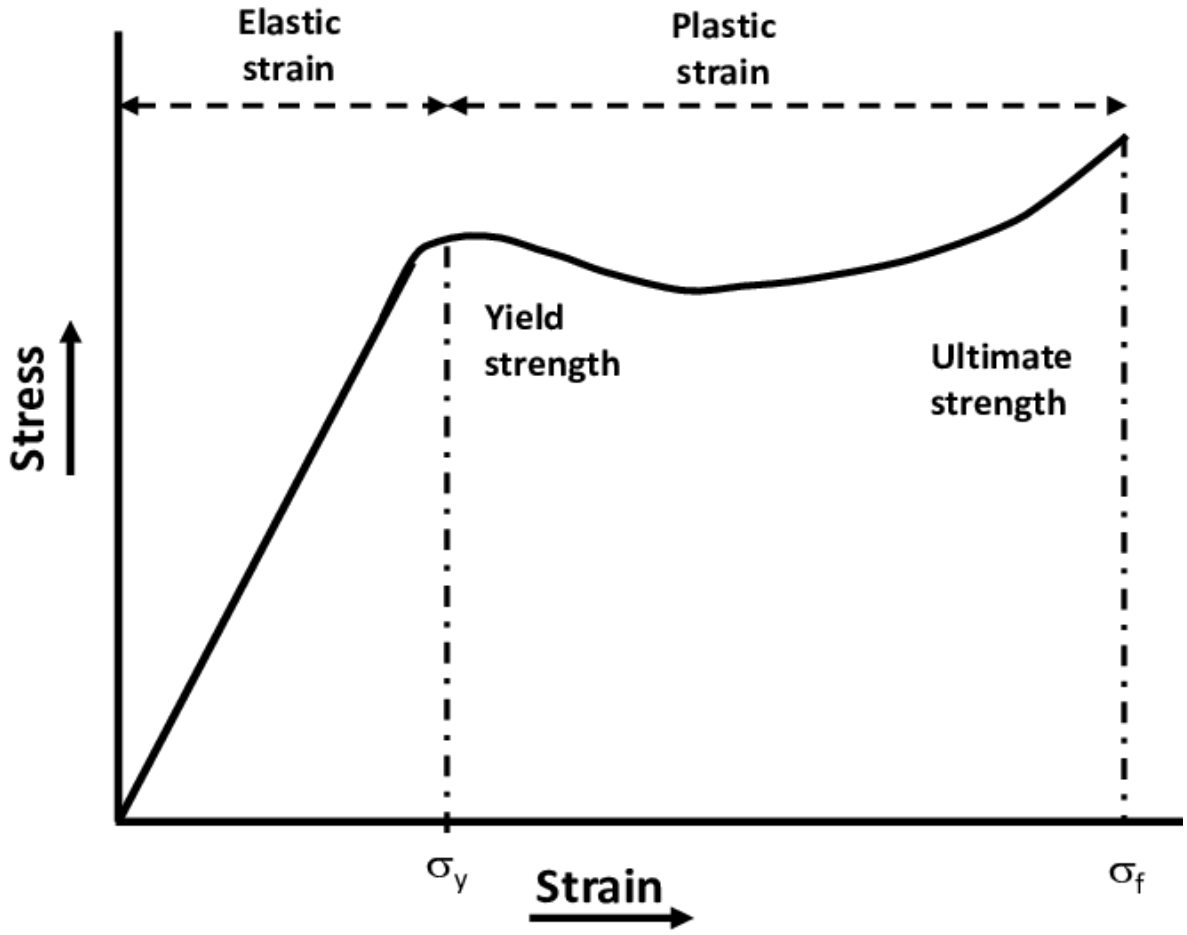

Figure 2.11: *The standard stress strain curve was used to calculate the yield strength and Ultimate strength/tensile strength.*

2.2.6.3 Scanning Electron microscopy

The scaffolds were cut into 10mm*10mm squares and were gold coated. A Hitachi TM3030Plus Tabletop Scanning Electron Microscope (SEM) was used for taking images at different magnifications.

2.2.7 Cell Culture Evaluation of synthesised scaffolds

2.2.7.1 Scaffold Sterilisation

The scaffolds were cut into 5m*5mm squares using paper cutter. The measurement was performed using Vernier callipers. Scaffold squares were sterilised using two alternative methods to identify the appropriate one.

Ethanol/UV sterilisation: Fresh 70% ethanol in water was prepared. The scaffolds were placed in a labelled 24 well plate. 1ml 70% ethanol was added to each scaffold. The plate was sealed using parafilm and placed on a rocker for 2 hours. After 2 hours the parafilm was removed inside the cell culture hood and ethanol was aspirated. The scaffolds were left to dry inside the cell culture hood overnight to avoid any contamination. The dried scaffolds were washed with PBS thrice and once with expansion media.

After the process, the scaffolds were submerged in expansion media in a 24 well plate overnight in the fridge. The well plate was sealed using parafilm to avoid any contamination to the samples. The cell seeding process was performed the next day.

Autoclave method: The scaffolds were cut and sealed in autoclave bags. Labelled and tagged with autoclave tape to ensure the sterilisation process. The bags were autoclaved at 121°C for 30 minutes. The samples were left in a drying cabinet at 50°C overnight for drying.

The autoclaved samples were opened inside a cell culture hood and submerged in the cell culture expansion media overnight in the fridge. The cell seeding process was done the next day.

2.2.7.2 Evaluating the effect of soluble products on cell viability from scaffolds

The analysis was performed to evaluate the effect of released substances from scaffolds on hES-MPs and Y201 cell lines.

Y201 Cell line: The Y201 cell line is also known as bone marrow derived mesenchymal stromal cell line. It is derived from stem cells and is capable of differentiation into adipigenic, chondrogenic and osteogenic lineages depending upon environment such as chemical induction. The advantage of this cell line is that it is immortalised through over expression of telomerase reverse transcriptase. This makes it to grow exponentially and prese nt surface markers as that of MSCs. The research showed no evidence of tumorigenicity, hence making this cell line popular for experiments in tissue engineering.

The 5mm×5mm scaffolds were submerged in cell culture expansion media (1ml per well) in a 24 well plate (fig. 2.12). The well plate was stored at 37°C in a CO_2 Incubator. The same conditions were used as for cell expansion. The media was frozen at Day 1, Day 7, Day 14 and Day 21 (Fig 2.12), this media is scaffold-conditioned media. The process was performed for both Alpha MEM and DMEM for hES-MPs and Y201 cell lines.

The hES-MPs and Y201 were seeded in a 96 well plate at a seeding density of 1×10^4 per well (Fig 2.13). The well plates were incubated at 37°C in a CO_2 incubator for 24 hours to allow cell attachment. The light microscope images were recorded to make sure that the cells were attached by visual inspection. The media was aspirated and frozen conditioned media of Days 1, 7, 14 and 21 of incubation was introduced. The well plate was incubated for 48hours, followed by a resazurin reading.

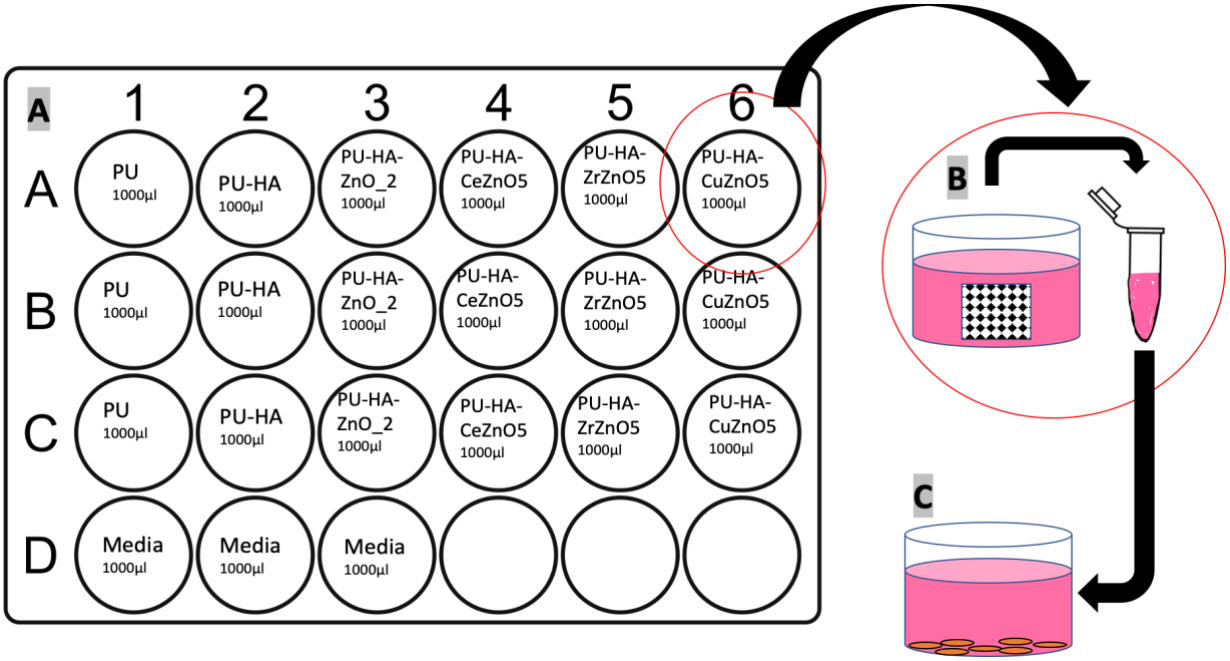

Figure 2.12: *A: The 5mm×5mm scaffolds were submerged in cell culture expansion media. B: The medium was collected in eppendorf tubes at Day 1, Day 7, Day 14 and Day 21 to create scaffold-conditioned media. The collected media was stored at -20°C. C: The frozen conditioned media was used for cell expansion in 96 well plates to evaluate the effect of soluble products on cell metabolic activity.*

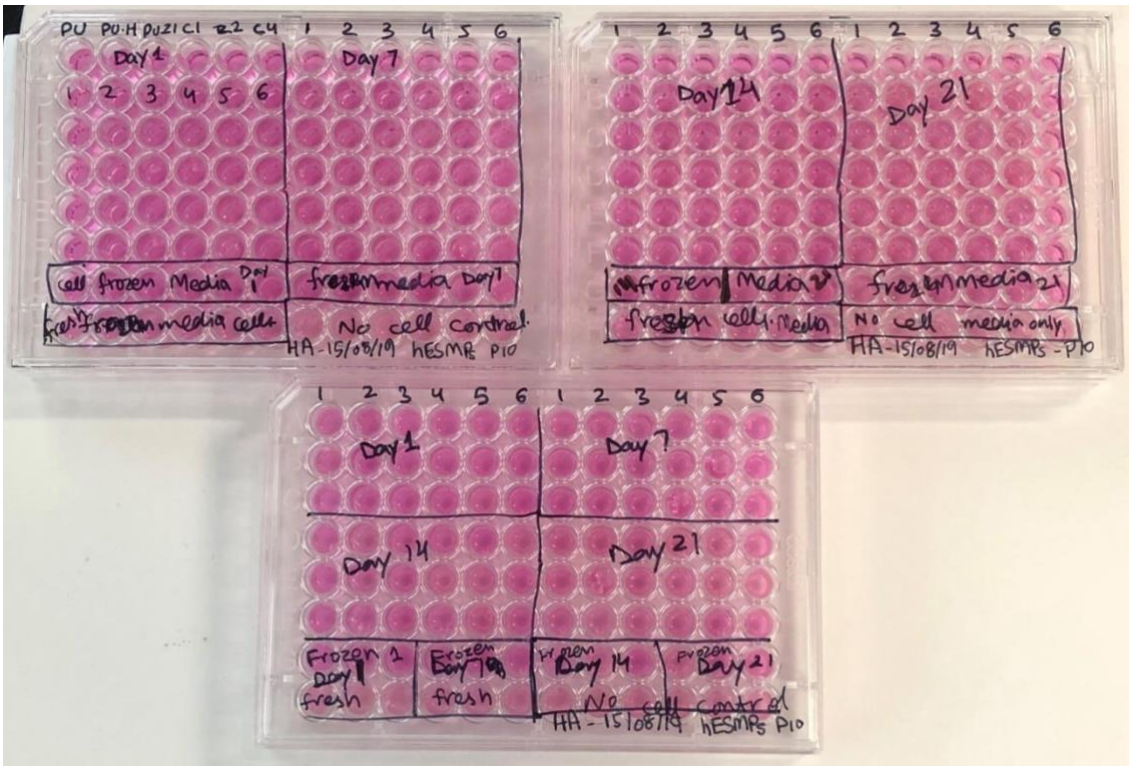

Figure 2.13: *Cell Seeding plan for evaluating effect of soluble products released from the scaffolds.*

2.2.7.3 Cell Seeding Efficiency:

The scaffolds were cut into 5m*5mm squares and sterilised. 48 well plates were used for this experiment. The wells were carefully labelled, and scaffolds were transferred to the well plate and fixed at the bottom. 1×10^5 cells per scaffolds were seeded. The cells were seeded in a way that 10 µl of expansion media contained 1×10^5 cells to allow the cells to interact with scaffold surface. The well plates were incubated for 4 hours followed by the addition of 500 µl expansion media. The well plates were incubated in the CO_2 incubator at 37°C.

After 24 hours, one set of the scaffolds were transferred to a new well plate and resazurin assay was performed on both plates (fig. 2.14). The other set of scaffolds were washed with PBS and fixed for scanning electron microscopy analysis. The 2.5% glutaraldehyde solution was used as fixative. The washed scaffolds were submerged in 2.5% glutaraldehyde for 2 hours at 4°C. The scaffolds were washed and dehydrated using a series of ethanol solutions (20%, 40%, 60%, 80%, 96% and absolute ethanol) three times in each for 3 minutes. The scaffolds were immersed in hexamethyldisilazane (HMDS) in a fume hood (exhaust provides local ventilation to prevent the worker/lab from exposure of toxic chemicals) overnight. The SEM micrographs were taken the next day.

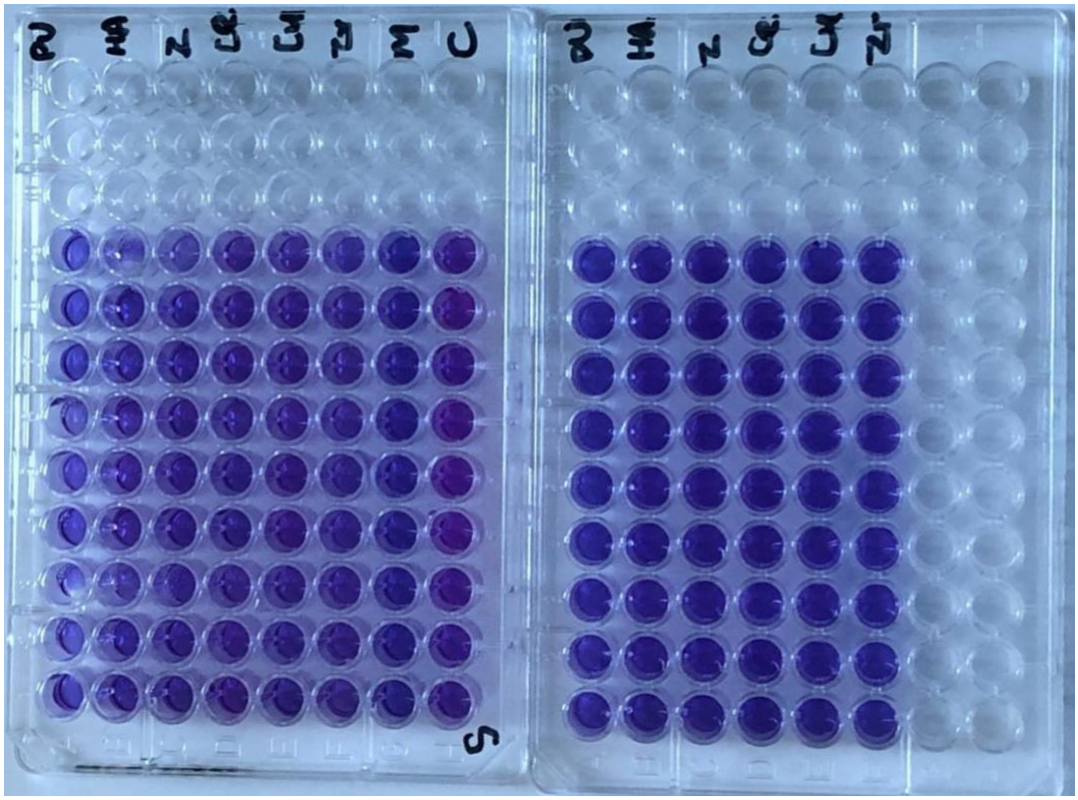

Figure 2.14: *The resazurin assay performed after 24 hours to investigate cell seeding efficiency.*

2.2.7.4 Growth Kinetic analysis using resazurin assay for 30 days:

The scaffolds were cut into 5mm*5mm squares and sterilised and scaffolds were transferred to the wells of a 48 well plate and fixed at the bottom by pressing down the scaffolds before cell seeding. 1×10^5 cells per scaffolds were seeded. The well plates were incubated for 4 hours followed by the addition of 500 µl expansion medium a CO_2 incubator at 37°C.

The scaffolds were transferred to a new well plate on Day 3. The resazurin readings were recorded at day 3, 7, 14, 21 and 30 (fig. 2.15).

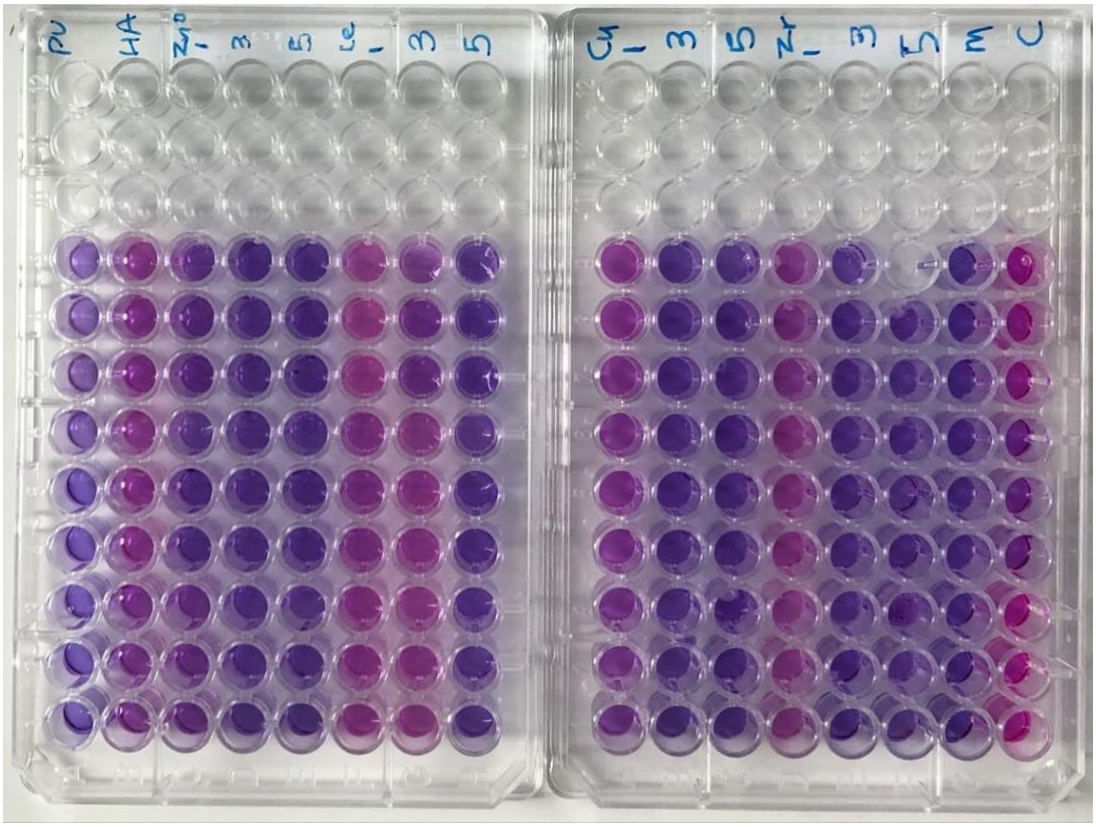

Figure 2.15: *Resazurin assay reading plate just before recording the reading at day 30.*

2.2.7.5 Comparison of growth kinetics and differentiation markers in Basal media and Osteogenic media:

Basal Media Composition: The basal media was basically the conventional media that is used for HTERT-BMSCs Y201 cell line. DMEM with Glutamax, 10% FBS (Gibco) and 10,000 U/mL penicillin, and 10,000 U/mL streptomycin (Life Technologies) were mixed together at room temperature in sterile environment. The media bottle was stored at 4°C and consumed within 2 weeks.

Osteogenic Media Composition: The osteogenic media is supplemented with the ingredients that promote osteogeneis or cell differentiation. The media was prepared by adding 0.01 μM dexamethasone, 50 μg/mL ascorbic acid and 10 mM sodium β-glycerophosphate (Gibco BRL) to basal media in a sterile environment. The media was labelled and stored at 4°C and consumed within 2 weeks.

For cell seeding, the same process was used as section 2.2.3.4. Once the cell seeding was undertaken, one group had basal media and the other had osteogenic media added after 4

hours of incubation. The media was changed every two days. The resazurin assay was performed at Day 5, Day 10, Day 15, Day 20 and Day 25.

2.2.7.6 Alkaline Phosphatase Activity (ALP):

For ALP activity analysis the experiment was stopped at Day 20. The scaffolds were washed with PBS twice followed by cell lysis. The cell lysis was performed to extract the cellular components from cells attached on the scaffolds. Cell lysis solution was prepared using Trizma hydrochloride solution (CAB), autoclaved H_2O and Triton X. To make 20 ml cell lysis solution, 3ml CAB, 17ml H_2O and 200 µl Triton X was used. The Vortex was used to mix the ingredients well. Once the cell lysis buffer was ready, the well plate containing scaffolds were washed with PBS and 500 µl of cell lysis buffer was added to all the scaffolds. The well plate was incubated at room temperature inside a cell culture hood for 30 minutes and at 4°C overnight.

The freeze thaw cycles were performed three times, for this the well plate was frozen at -80°C for 15minutes followed by thawing at 37°C (15minutes) in an egg incubator on an orbital shaker. The process was repeated three times to ensure sufficient cell lysate was extracted. The buffer was transferred to Eppendorf tubes, labelled and stored at -80°C until used for DNA and ALP analysis.

For ALP/DNA analysis, Quant-iT ds DNA Assay Kit and a black 96 well plate was used. The kit was brought to room temperature and reagents were prepared as per kit instructions. The first step was to prepare the working solution for HS reagent by diluting the HS reagent in HS buffer at a of ratio 1:200. 90 µl of working solution was added into each well in black 96 well plate followed by the addition of 10 µl lysate solution. The wells were carefully labelled. The plate was read in microplate reader with a 10 second shaker function to ensure proper mixing of buffer and lysate before recording the reading. The plate was read at **λ**ex : 485nm, **λem : 535 nm (fig 2.16).** A standard curve of DNA 0-60 ng was also run. 10 µl standard was added to 90 µl working reagent in the same well plate.

All the samples and standard were run in triplicate and average (mean) was taken.

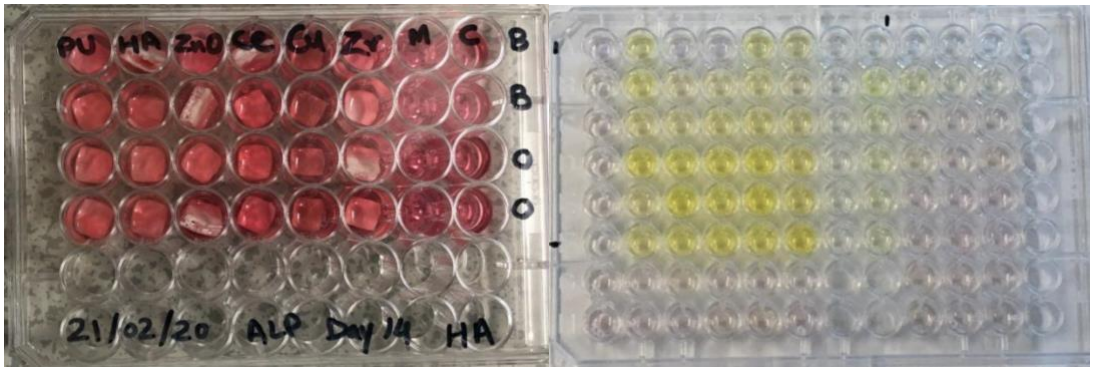

Figure 2.16: *The cell seeding for ALP analysis (left). The ALP analysis plate just after recording the reading in microplate reader (right).*

The well plate prepared for ALP analysis with basal media and osteogenic media comparison (left image). The colour change as a result of mixing of lysate and HS reagent working solution.

ALP Activity Analysis: PNPP Phosphatase Substrate kit was used to record ALP activity. The reagents were prepared as per kit instructions. The substrate was prepared by dissolving the tablet in deionised water & buffer mixture (4:1). 1 tablet was dissolved in 5ml deionised water & buffer mixture. 180 µl of substrate solution was added to clear 96 well plate. 20 µl cell lysate was added and wells were carefully labelled. The plate was closed and incubated at room temperature until a slight colour change happened from clear to slightly yellow or for 30 minutes. The microplate reader was used to record the reading.

The ALP activity is expressed in nmol of p nitrophenol per minute (nmol pNP/min). 20 µl lysate was analysed for DNA, ALP activity was normalised to DNA by dividing the ALP values with respective DNA values the resultant value was ALP activity per ng of DNA.

2.2.7.7 'Quantine' ELISA VEGF Assay using Cell Culture supernatants:

The Cell culture supernatants were stored from the experiment Growth Kinetic analysis section 2.2.7.3.2 at Day 20. The cell culture media were transferred to labelled eppendorf tubes and stored at -80°C until used for ELISA.

The Quantine ELISA VEGF kit was used, and the reagents were prepared as per kit instructions. The wash buffer was prepared (for 500 ml wash buffer solution, 20 ml wash buffer concentrate was mixed in 480 ml deionised water). Human VEGF standard was dissolved in 1ml RDSK and mixed carefully to avoid bubbles. Once the VEGF was dissolved,

serial dilutions were prepared using RDK5. In order to perform serial dilutions, 7 Eppendorf tubes were labelled and 500 µl of RDK5 was added to all the tubes. 500 µl of standard VEGF was added to tube 1 and mixed well. Followed by extraction of 500 µl from tube 1, which was added to tube 2 and so on (Fig 2.17).

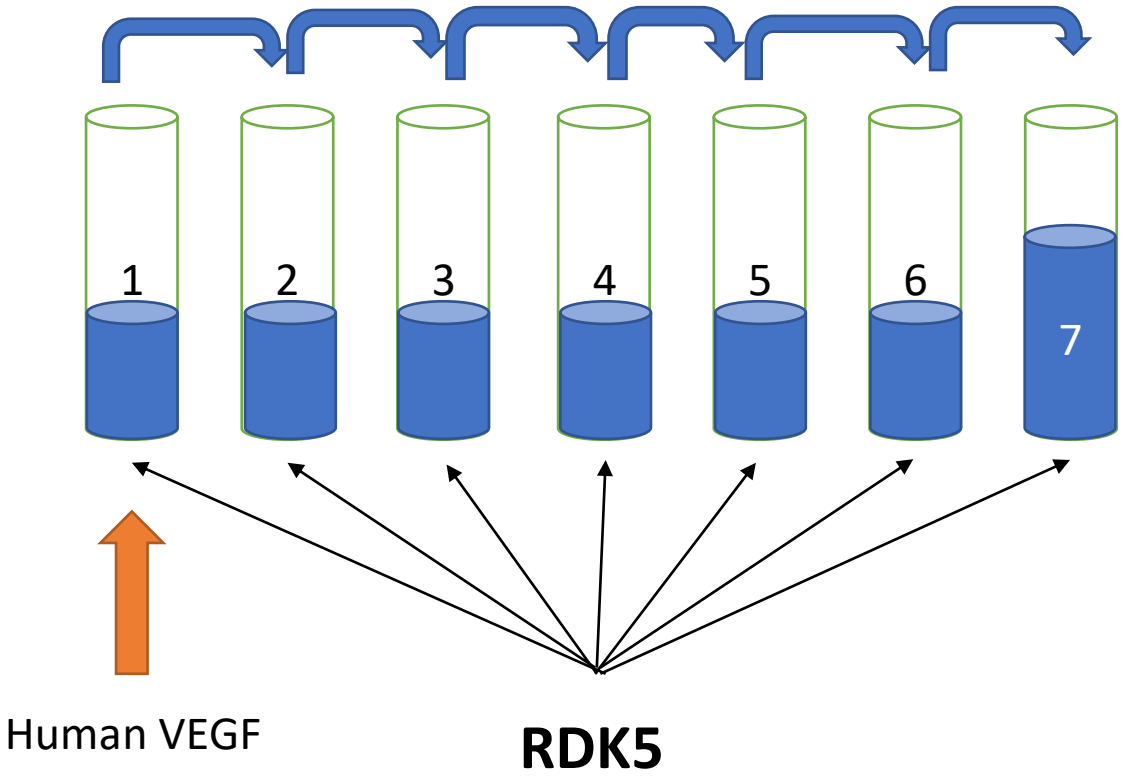

Figure: 2.17: *Serial dilution of Human VEGF standard for VEGF ELISA analysis***.**

The cell culture supernatants were brought to room temperature and centrifuged at 1000 RPM for 5 minutes. VEGF ELISA strips were arranged in the holder and labelled. 50 µl assay diluent RD1W was added to all the wells. 200 µl standard and cell culture supernatant were added. The wells were covered with adhesive tape and placed on an orbital shaker at room temperature for 2 hours. After 2 hours all the wells were aspirated and 300 µl wash buffer was added to each well and aspirated. This step was repeated three times. 200 µl of human VEGF conjugate was added to each well and covered by adhesive tape. The plate was incubated at room temperature on an orbital shaker for 2 hours. Washing with wash buffer was performed three times, followed by the addition of 200 µl of substrate solution. The plate was covered with aluminium foil and incubated for 20 minutes on an orbital shaker then 50 µl

stop solution was added to all the wells. The plate was tapped gently to mix the stop solution to allow uniform colour change (fig. 2.18). The microplate reader was used to record the optical density at **λ450 nm.**

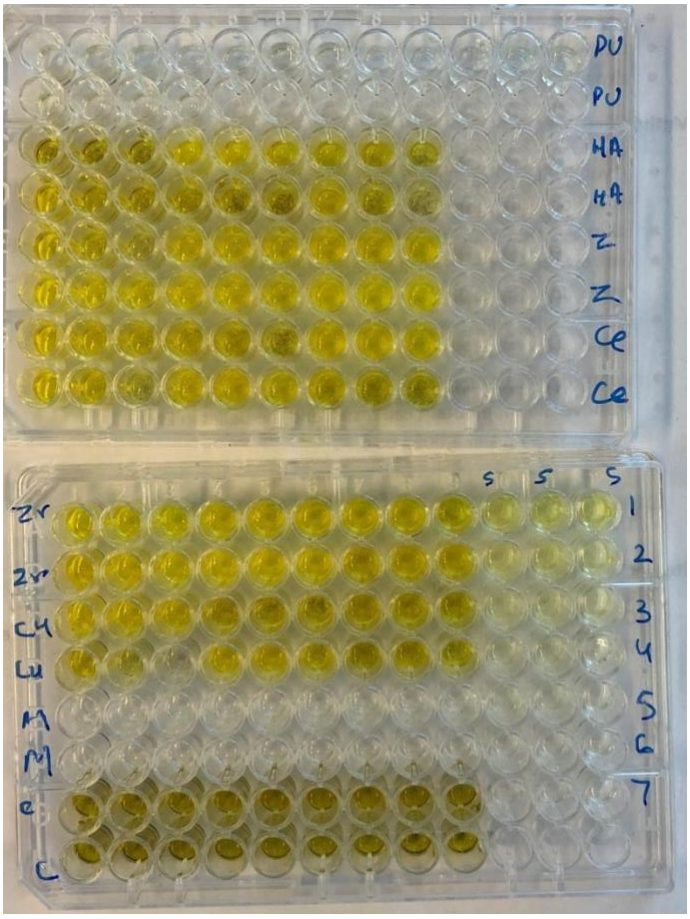

Figure 2.18: *The colour change after adding stop solution VEGF ELISA last step.*

Chapter 3 Identifying working range of cerium doped zinc oxide substituted bioactive scaffolds for craniofacial bone regeneration and vascularisation

3.1 Introduction

A key requirement of craniofacial bone regeneration is a highly vascularised tissue. Vascularisation is disrupted due to disease or injury making the healing extremely difficult. Such injuries happen mainly due to trauma, which disrupts the complex network of blood vessels in bone and the surrounding soft tissues, resulting in a lack of blood supply to bone cells which delays the healing process. The currently available scaffolds for craniofacial reconstruction do not induce angiogenesis (formation of blood vessels) instead they rely on an inflammatory healing response that results in insufficient oxygen and nutrient supply, hence resulting in non-uniform cell differentiation and cell death (Bramfeld et al., 2010; Malda et al., 2004; Rouwkema et al., 2008). Barui, A.K *et al* reported the proangiogenic potential of flowerlike zinc oxide particles. Microwave technology was used to synthesise the zinc oxide particles followed by *in vitro* and *in vivo* investigations to evaluate the proangiogenic potential of metal oxides. zinc oxide internalisation, cell proliferation and VEGF assay were analysed, and significant differences were observed between different samples (Barui et al., 2012).

On the other hand, several studies reported that cerium in the biological environment is nontoxic and has bacteriostatic properties. It was investigated that cerium introduction into bioactive glass scaffolds increases the *in vitro* bioactivity which makes it favourable for bone tissue engineering (Deliormanlı, 2015; Shruti et al., 2013). A few studies are published on the angiogenic potential of CeO_2, and results revealed that it is proangiogenic and upregulates hypoxia inducible factor 1 α which leads to angiogenesis. It was also reported that the size and morphology of the particles play a significant role in oxygen modulation within the cells which lead to hydrogen peroxide production leading to angiogenesis (Das et al., 2012; Nethi et al., 2017). Studies demonstrated that cerium incorporation resulted in zinc oxide lattice

expansion, reduced grain size and increased bandgap (Kulandaisamy et al., 2016; Sinha et al., 2014). These findings from previous studies enabled us to select cerium as the dopant. This chapter is focussed on synthesis and characterisation of cerium doped zinc oxide nanoparticles and explores the biological properties of cerium doped zinc oxide nanoparticles in form of nano-powders as well as within a porous composite scaffold.

3.2 Aims and Objectives

Zinc oxide has proangiogenic potential *in vitro* & *in vivo* (CAM) and CeO_2 is bioactive *in vitro*. Cerium doped zinc oxide has been shown to cause zinc oxide lattice expansion and reduced particle size, however to my knowledge no biological analysis has been carried out to date. **The aim of this chapter is to evaluate appropriate cerium doped zinc oxide nanoparticle samples for use in scaffold synthesis and *in vitro* cell culture analysis.** To achieve this, the following objectives were addressed in this chapter.

1) Synthesise and characterise nano-sized cerium doped zinc oxide nanoparticles with different concentrations of cerium.

2) Analyse and compare cell metabolic activity of cells when exposed to zinc oxide and cerium doped zinc oxides, at varying concentrations of cerium.

3) Fabricate cerium doped zinc oxide containing composite scaffolds with polyurethane and explore their potential as bone tissue graft substitutes.

3.3 Materials and methods

Zinc oxide and cerium doped zinc oxide nanoparticles were synthesised using a hydrothermal flow system, followed by characterisation using XRD, SEM, TEM and cell metabolic activity assay using the MG63 cell line. CeZnO5 was selected for scaffold synthesis and further study. The freeze extraction salt leaching technique was used to fabricate porous polyurethane foams substituted with nano hydroxyapatite and ZnO_2 or CeZnO5. Human Embryonic Stem Cell-Mesenchymal progenitors (hES- MPs) and Bone Marrow Stromal cells

from the Y201 cell line were used to evaluate the effect of soluble products from the scaffolds. Cell metabolic activity, cell adhesion and cell seeding efficiency was evaluated using Y201 cells. These methods are all described in detail in Chapter 2 (Heading no. 2.2.7).

3.4 Results

3.4.1 Dynamic Light Scattering (DLS) for Hydrodynamic diameter measurements:

The hydrodynamic diameters of all the samples were measured at room temperature (Table 1). The hydrodynamic diameter of nanoparticles was observed to be in a range between 21 nm to 134 nm (Table 3.1). It was observed that varying the concentration of precursor solutions i.e. potassium hydroxide and zinc nitrate led to notable differences in hydrodynamic diameter size. But a less notable difference was observed when samples were introduced with cerium, copper and zirconium. Furthermore, it was observed that increasing the dopant amount led to bigger particle sizes (table 3.1).

Table 3.1: *The mean surface area and mean particle size of zinc oxide and cerium doped zinc oxide nanoparticles obtained using Dynamic Light scattering, Brunauer–Emmett–Teller (BET), and X-Ray Diffraction Analysis. n=3*

	Sample Name	**Hydrodynamic Diameter (nm)**	**BET Surface Area m2/g**	**Crystallite Size (Scherrer Equation) (nm)**	**Average Particle size (calculated from TEM imaging) (nm)**
1	ZnO_1	21.02	6.76	32.35	83.16
2	ZnO_2	134.50	11.35	31.70	45.23
3	CeZnO1	100.70	15.64	31.38	88.45
4	CeZnO2	88.88	12.88	32.45	67.30
5	CeZnO3	101.70	13.68	31.41	49.88

6	CeZnO4	70.49	12.32	31.23	79.21
7	CeZnO5	98.95	13.68	31.30	51.67

3.4.2 Brunauer–Emmett–Teller (BET):

The preliminary DLS findings were further confirmed by using BET surface area analysis. The change in precursor solution concentration led to significant variation in surface area in the case of pure zinc oxide, but for doped zinc oxide no notable difference was seen (Table 3.1).

3.4.3 Raman spectral analysis of zinc oxide and cerium doped zinc oxide

Live Raman spectral analysis was performed to investigate the Raman scattering of zinc oxide nanoparticles and the influence of Cerium doping on characteristic zinc oxide Raman scattering. All the spectra were recorded at room temperature. Zinc oxide synthesised *via* Hydrothermal flow was characterised as wurtzite (crystal structure having hexagonal unite cell), zinc oxide because of the presence of eight characteristic optical phonon modes at the centre of Brillouin Zone (Γ point). Figure 3.1 represents room temperature Raman spectra of pure zinc oxide.

$$\Gamma = 1A1 + 2B1 + 1E1 + 2E2$$

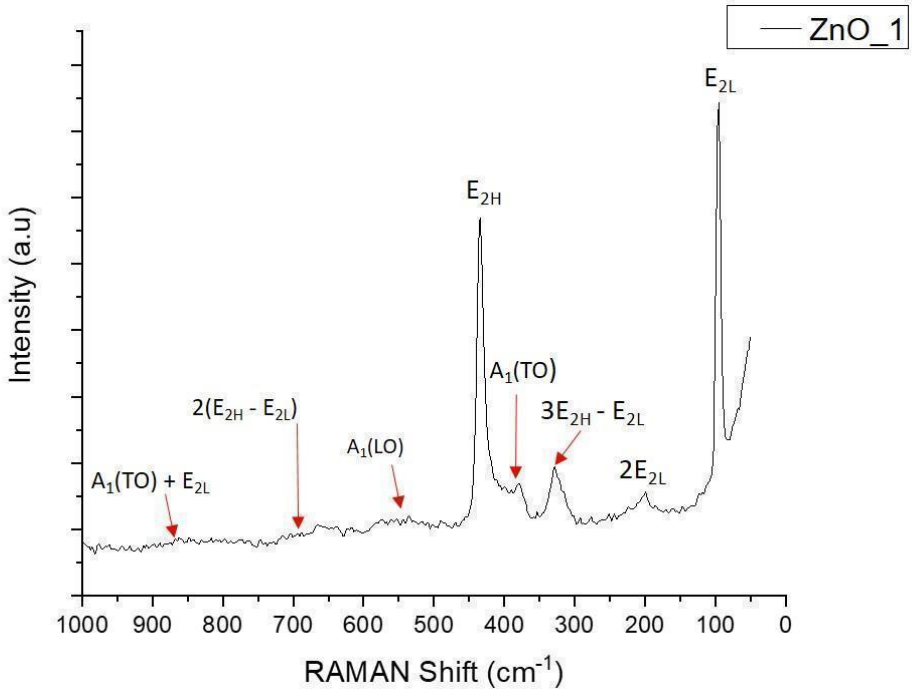

Figure 3.1: *Raman spectral analysis of synthesised ZnO_1.* The peaks are labelled.

The spectra demonstrated the four characteristic peaks at 100, 380, 437 and 580 cm^{-1} which are characteristic phonon modes of hexagonal zinc oxide. The peaks were characterised as E_{2L}, A1(TO), E_{2H}, and A1(LO) respectively (Table 3.2).

Table 3.2: *The Raman spectra peak characterisation*

	Wave number (cm^{-1})	Assignment	References
1	100	E_{2L}	(Zeferino et al., 2011)
2	380	A_1	(Zeferino et al., 2011)
3	437	E_{2H}	(Zeferino et al., 2011)
4	580	A_1(LO)	(Zeferino et al., 2011)
5	465	F_{2g}	(Chouchene et al., 2016)

A1, E_1 and E_2 were characterised as Raman active modes. A_1 and E_1 were categorised as polar branches. The polar branches divide into longitudinal Optical (LO) and transversal optical components which were associated with different frequencies due to LO phonons associated electric fields. The E_2 Raman nonpolar mode associated with low frequency was classified as E_{2L} which depicted a heavy Zn sub lattice. However, nonpolar high frequency mode E_{2H} only involved oxygen atoms (Zeferino et al., 2011).

The spectra demonstrated the appearance of Raman active mode F_{2g} (Fig. 3.2) which is the characteristic peak for the CeO_2 cubic structured lattice. The remaining peaks associated with the zinc oxide hexagonal structure were found at the same position. The F_{2g} corresponded to a ceria (CeO_2) vibrational unit which shows the oxidation of Ce^{3+} during hydrothermal synthesis. This confirmed the presence of two phases in the sample zinc oxide and CeO_2 respectively (Chouchene et al., 2016).

Cerium Oxide (CeO_2) belongs to the group of cubic fluorite structures. In samples in which cerium was introduced into zinc oxide, the first order Raman active phonon mode F_{2g} appeared as shown in Figure 3.2. with reduced amounts of cerium there (fig. 3.2) there was no longer evidence of the Raman characteristic peak of zinc oxide at 380 cm^{-1} A1(TO) which is one of three characteristic vibration modes of wurtzite zinc oxide with P63mc symmetry (Fig 3.2) (Chouchene et al., 2016; Zamiri et al., 2015; Zeferino et al., 2011).

ZnO_1 and ZnO_2 shows Raman spectra of pure zinc oxide, moving upwards CeZnO1 to CeZnO3 is one cerium group and CeZnO4- CeZnO6 is another cerium group having cerium content 1 mole %, 3 mole % and 5 mole % respectively (fig 3.2).

As the cerium content was increased the partial oxidation of Ce^{+3} happened during the hydrothermal process at 335°C leading to formation of cubic CeO_2. It was observed that the peak intensities for characteristic wurtzite zinc oxide reduced as the cerium content was increased (shown by purple dots), however, the Raman active mode for ceria F_{2g} increased as the cerium content was increased (indicated by the green triangle-fig 3.2) (Chouchene et al., 2016).

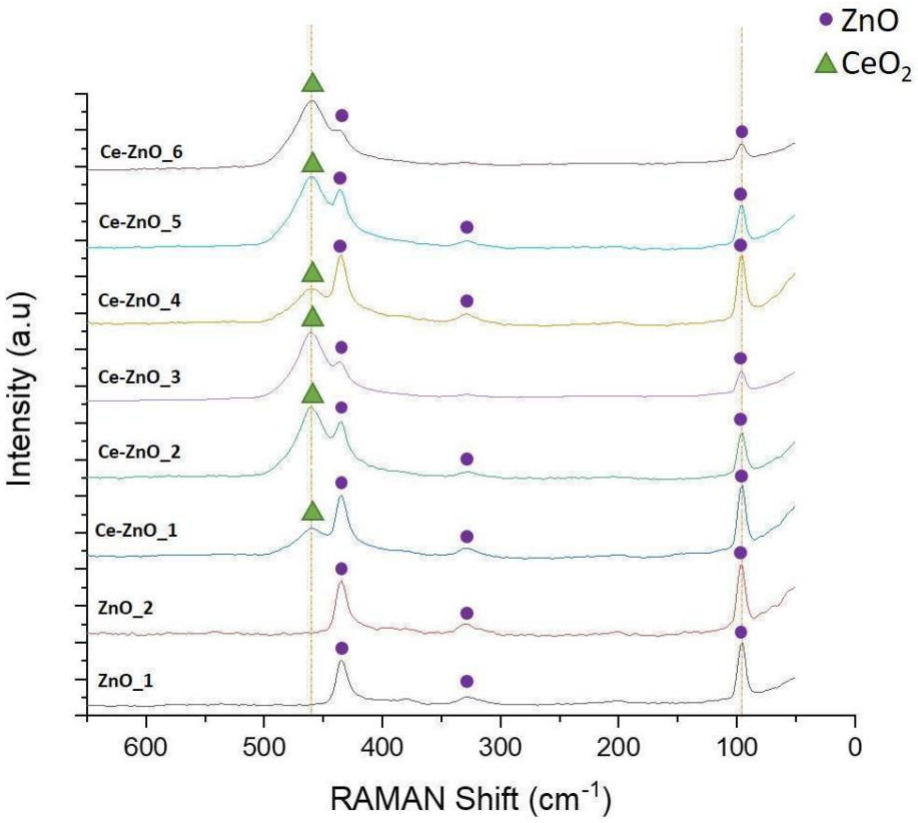

***Figure 3.2**: Comparative analysis of pure zinc oxide as control and Cerium doped zinc oxide in varying concentrations*.

3.4.4. X-Ray Diffraction Analysis (XRD):

Zinc oxide and Cerium doped zinc oxide group was analysed using X-ray diffraction patterns to investigate the composition and crystal properties of synthesised nanoceramics.

Figure 3.3 shows the pure zinc oxide, synthesised via the hydrothermal process, match with PDF 00-036-1541. The diffraction pattern matched exactly to the zinc oxide PDF pattern which confirmed the successful synthesis of zinc oxide (fig 3.3), the pattern showed very sharp peaks which indicated the high crystallinity and hexagonal wurtzite crystal structure of the sample (Chouchene et al., 2016; Zeferino et al., 2011). However, the addition of cerium content resulted in the appearance of a signal at 33 degrees which was attributed to cerium oxide (CeO_2) (figure 3.3), after matching with the PDF 00-067-0123 (figure 3.3) (Bueno-Ferrer et al., 2010).

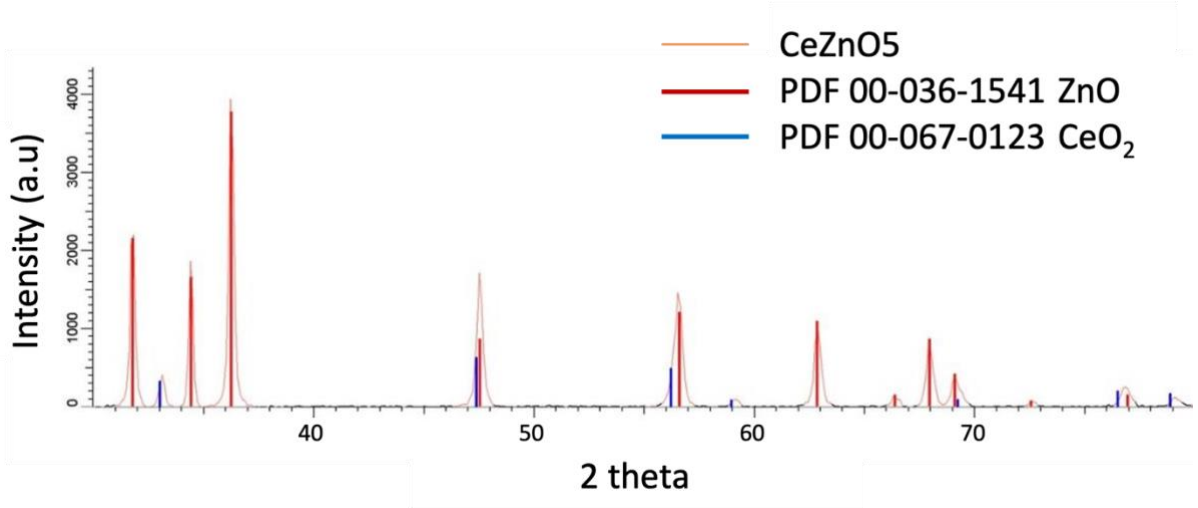

Figure 3.3: *Peak match of Cerium doped Zinc oxide synthesised via Hydrothermal Flow with XRD library PDF 00-036- 1541 and PDF 00-067-0123.*

The peak at 33 degrees was observed as a weak signal at lower (1mole%) concentration of cerium but was more evident with higher addition of cerium (figure 3.4). The peak at 33 degrees is negligible in CeZnO1 but with an increase in Cerium concentration the intensity of the peak increased (CeZnO2 & CeZnO3). A similar pattern was observed in other

cerium groups (CeZnO4, CeZnO5 & CeZnO6). The sharpness of the peaks remained the same even after doping which confirmed good crystallinity (figure 3.4).

Further, the peak at 47.5 degrees resulted in increased intensity with an increase in cerium content. This peak is associated with the zinc oxide & CeO_2 lattices, which demonstrated the change in geometry of the overall crystal structure. PDF 00-067-0123 matching demonstrated the cubic fluorite like structure, increase in intensities of the peaks associated with CeO_2 confirmed the presence of two phases; hexagonal and cubic (ZnO & CeO_2) but the dominant phase observed was hexagonal due to maximum intensity (figure 3.2) (Bueno-Ferrer et al., 2010; Zeferino et al., 2011).

The crystallite/grain size was observed to be almost the same for all the samples, no significant change in size was observed with variations in precursor concentrations or doping concentrations (Table 3.1).

3.4.5 Transmission Electron Microscopy (TEM)

A TEM study was performed to analyse the change in physical properties of nanoparticles with increase in doping concentration. For pure zinc oxide, the structure was rod shaped and the size was around 100 nm-150 nm. However, with addition of cerium content, the shape remained rod like, but the size of the rods reduced significantly. The size range for CeZnO1 is 50 nm- 100 nm. With increase in cerium content, 2 morphologies were observed (CeZnO2), rounded particles and rod like particles. At a further, increase in cerium content (CeZnO3) most particles were spherical, and size reduced (table 3.1) significantly (Figure 3.4). The introduction of ions resulted in expansion of the zinc oxide lattice which resulted in a reduction in grain size and increase in bandgap (Kulandaisamy et al., 2016; Sinha et al., 2014). It is evident that doping resulted in a change in particle size and, partly, particle morphology.

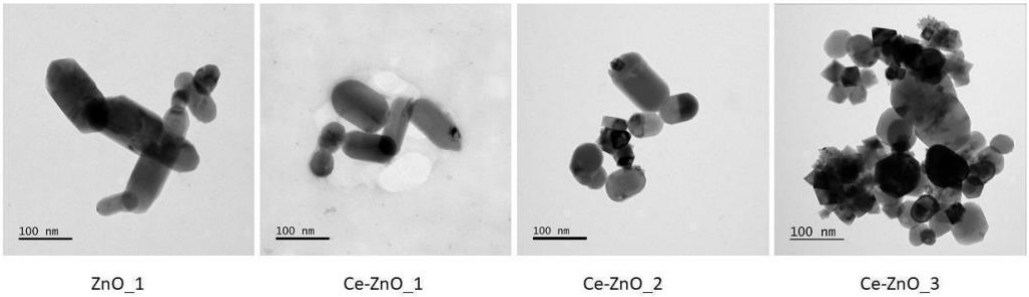

Figure 3.4: *TEM imaging of particles fabricated with concentrations of Cerium*

3.4.6 Cell Metabolic Activity Assay with a Human Osteoblast like cell line (MG63)

The test was performed using 5 µg/ml and 10 µg/ml nanoparticle suspensions in cell culture media for 7 days using cells from the human osteosarcoma cell line (MG63). At day 1 (24 hours), using a 5 µg/ml nanoparticle suspension in contact with cells, no cell inhibition or morphological changes were observed. Different concentrations of cerium doped ZnO showed different cell metabolic activity. ZnO_1 and CeZnO2 showed improved response and similarly ZnO_2 and CeZnO5 increased cell proliferation up to day 7. In order to check the dose response, increased nanoparticle concentrations were used. The results showed the same trend with CeZnO2 and CeZnO5 showing maximum cell viability for up to 7 days (fig 3.5). No nanoparticle was found toxic or inhibited cell proliferation when compared with only cell control. Tukey's multiple comparison test was performed to evaluate if the differences are significant or not.

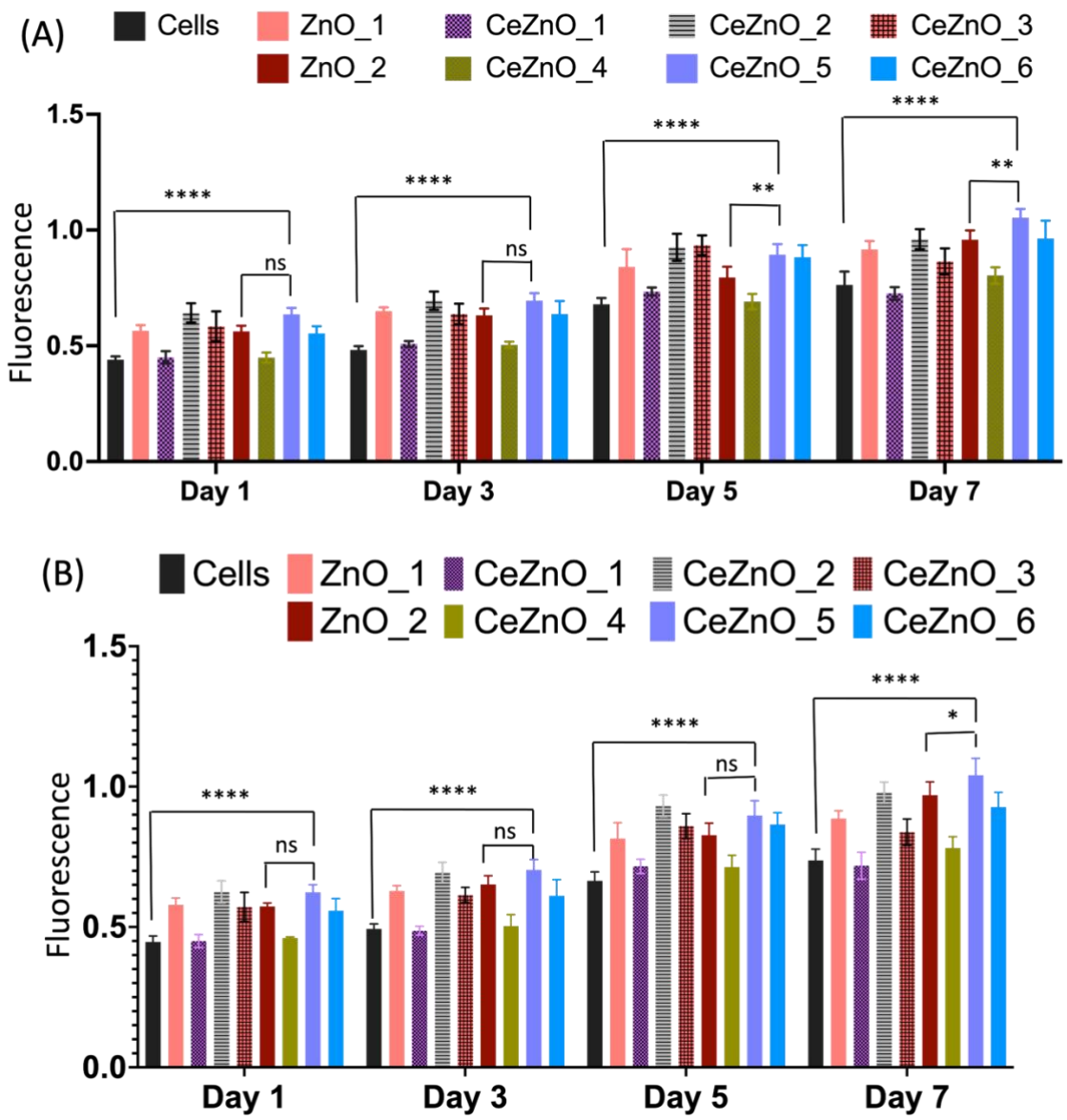

Figure 3.5: *7-Day Cell viability assay using nanoparticle suspension. (A) 5 µg/ml nanoparticle suspension. (B) 10 µg/ml nanoparticle suspension. Data represents ± mean SD, n=3*3, *= p<0.05.*

3.4.7 28- Day cell metabolic activity assay using cells from the hES-MPs cell line (10 µg/ml nanoparticle suspension):

Human embryonic mesenchymal like stem cells (hES-MPs) were selected for a 28 day study in order to evaluate the long-term contact effect on cells and to ensure the safe use of cerium doped Zinc oxide for craniofacial bone scaffolds. ZnO_2 and CeZnO5 were selected for further investigations based on nanoparticle size (ZnO_2 and CeZnO5 have a smaller particle size (Table 3.1) and preliminary improved cell viability response.

At Day 1, there was no significant difference between control and ZnO_2, CeZnO5 (Fig 3.6). The cells were attached to tissue culture plastic and no adhesion impairment was observed under the microscope. At Day 7, ZnO_2 and CeZnO5 improved cell metabolic activity significantly as compared to the cells only control, however no notable difference was observed between ZnO_2 and CeZnO5. A similar pattern was observed for days 14, 21 and 28. ZnO_2 and CeZnO5 clearly improved the cell proliferation for up to Day 28 (Fig 3.7). Tukey's multiple comparison test was performed to evaluate whether CeZnO5 has significantly improved cell metabolic activity, it was confirmed that the difference is significant (p value 0.0198) as compared to the cells only control for both ZnO_2 and CeZnO5. However, no significant difference was observed between ZnO_2 and CeZnO5 (Table 3.3).

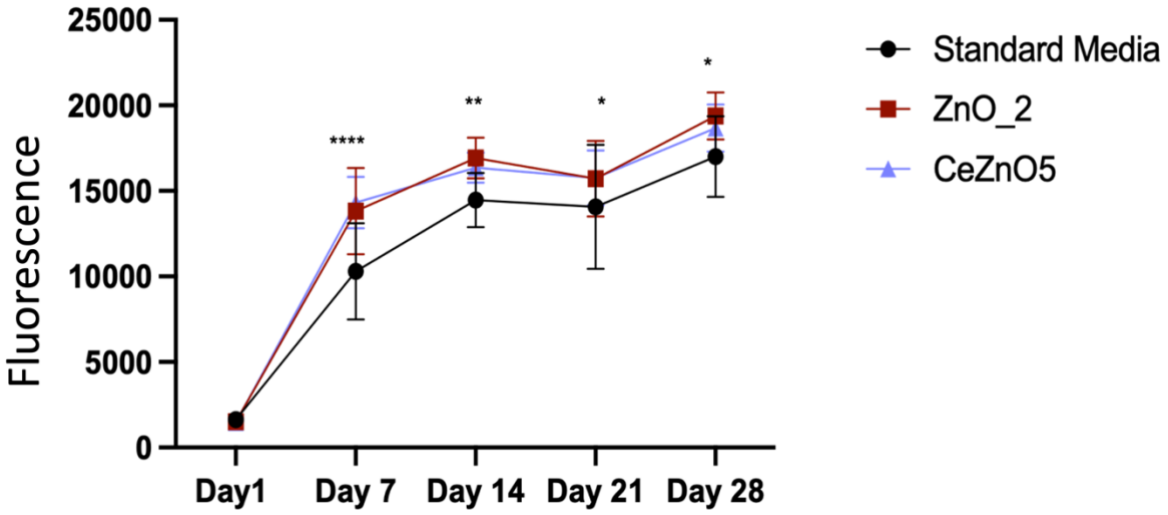

Figure 3.6: *28-Day cell viability assay using 10 µg/ml nanoparticle suspension in cell culture media. Data represents ± mean SD, n=3*3, *= p<0.05.*

Table 3.3: *Cell metabolic Activity difference on hES-MPs due to CeZnO5 nanoparticle suspension as compared to only cells with standard media and ZnO_2 suspension.*

Analysis Time point	Comparison of ZnO_2 and CeZnOwith Standard media	P Value
Day 1	Standard media Vs CeZnO5	0.9558 ns
	ZnO_2 Vs CeZnO5	0.9978 ns
Day 7	**Standard media Vs Ce**ZnO**5**	**<0.0001 ******
	ZnO_2 Vs CeZnO5	0.6952 ns
Day 14	**Standard media Vs Ce**ZnO**5**	**0.0061 ****
	ZnO_2 Vs CeZnO5	0.6361 ns
Day 21	**Standard media Vs Ce**ZnO**5**	**0.0188 ***
	ZnO_2 Vs CeZnO5	0.9971 ns
Day 28	**Standard media Vs Ce**ZnO**5**	**0.0198 ***
	ZnO_2 Vs CeZnO5	0.4942 ns

Conclusions; Nanoparticle Analysis:

The CeZnO5 nanoparticles were investigated to have two phases: hexagonal zinc oxide and cubic CeO_2. The average particle size was calculated as 78 nm. The nanoparticle suspension in cell culture media was used to analyse cell metabolic activity assay with MG63 and hES-MPs, the results suggested increased metabolic activity with CeZnO5 suspension in comparison to standard cell culture media. Therefore, CeZnO5 was selected for scaffold synthesis and further evaluations.

3.5 Cell Culture investigation of porous composite scaffolds incorporated with cerium doped zinc oxide:

Introduction to the PU scaffolds:

Porous scaffolds were synthesised using a solvent casting salt leaching technique. Polyurethane was used as polymer base and 2.5% hydroxyapatite as the. ZnO_2 and CeZnO5 were used in composite scaffolds. The aim of this section was to identify the working concentration of CeZnO5 for the scaffold and if the cerium doped zinc oxide increases the cell's response. The details of scaffold synthesis are described in Chapter 2 (Heading no. 2.2.5).

3.5.1 Evaluating the effects of soluble products released from scaffolds over time on cell metabolic activity from scaffolds:

Cell metabolic activity levels were found to be statistically similar compared to those cultured with either frozen media or fresh media. Metabolic activity was statistically similar and there was no evidence of a cytotoxic response for collected media at Day 14 (Figure 3.7).

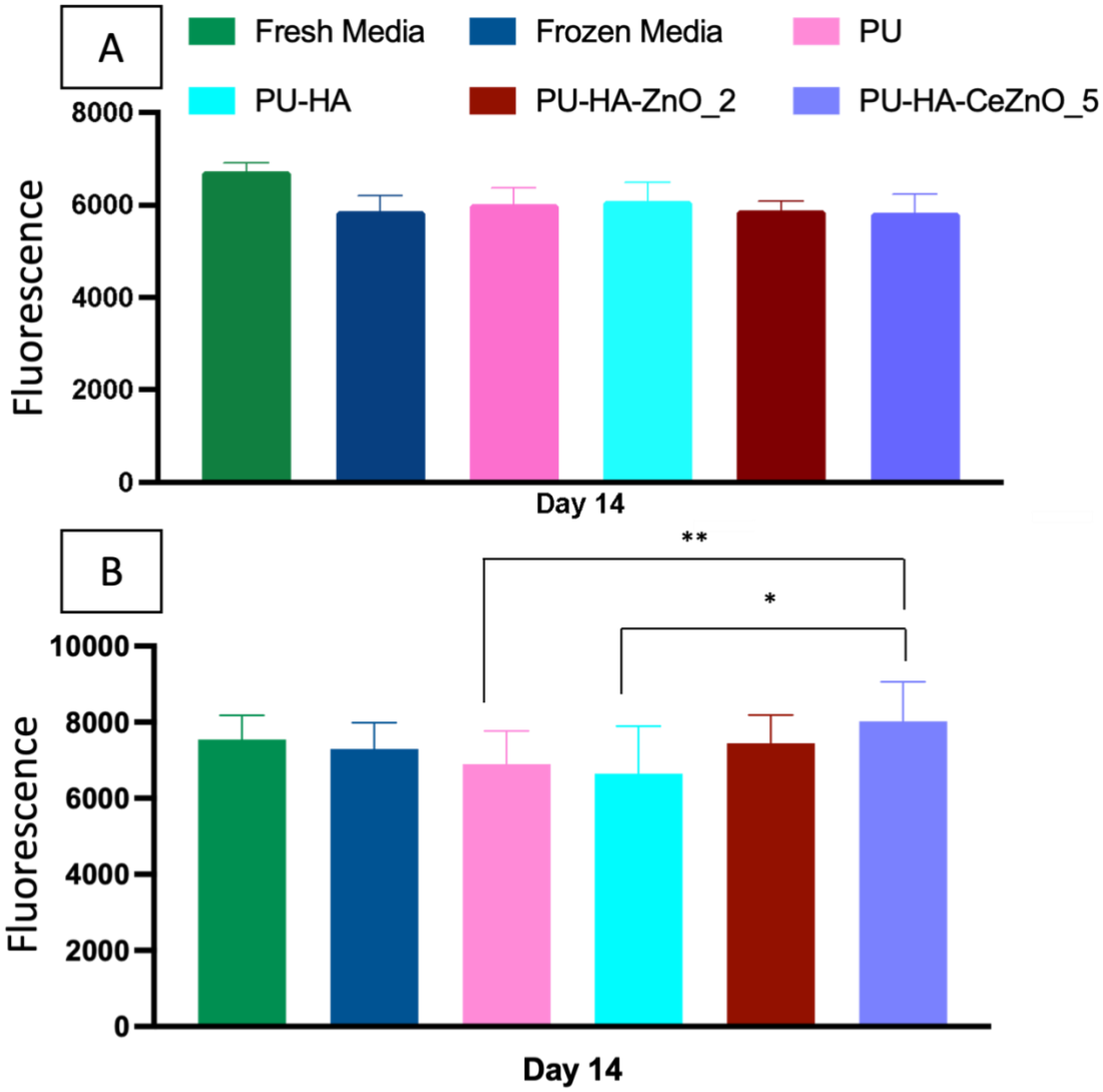

Figure 3.7: *Effect of soluble products (when submerged in media for 14 days) from scaffolds. (A) hES-MPs cells data. (B) Y201 cells data. Data represents ± mean SD n=3*3*

3.5.2 Cell Seeding Efficiency

The Scaffolds incorporated with CeZnO5 showed notably higher cell attachment as compared to the other scaffolds (Fig 3.). Approximately 60% cells adhered to the scaffolds incorporated with CeZnO5 and 40% to scaffolds incorporated with ZnO_2. However, PU and PU-HA retained less than 40%.

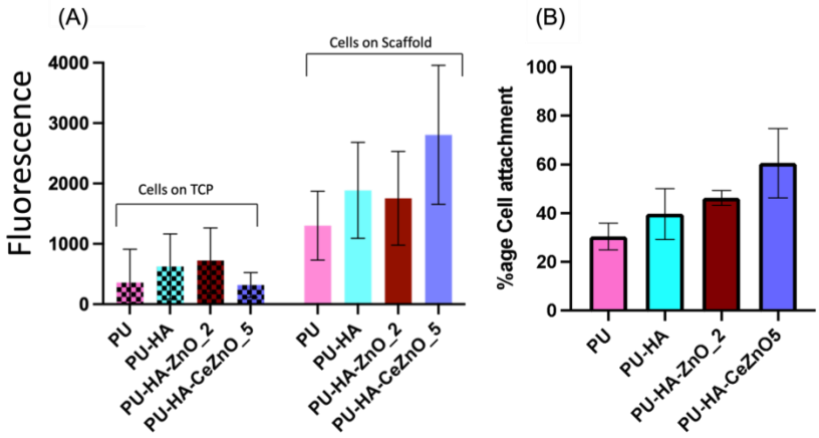

Figure 3.8: *Cell Seeding efficiency as measured by comparing the metabolic activity of cells attached on surrounding tissue culture plastic (TCP) with cells attached to scaffolds. A). The scaffolds were transferred to a new well plate before performing resazurin assay to evaluate the cell metabolic activity on TCP and scaffolds. B) the percentage cell attachment is shown using cells that were seeded in parallel on TCP in monolayer as the 100% marker. CeZnO5 incorporated scaffolds showed over 60% cell attachment. Data represents ± mean SD n=3*3.*

3.5.3 Y201 cells growth kinetics with porous composite scaffolds

Figure 3.9 shows the cell metabolic activity of the Polyurethane scaffolds incorporating Hydroxyapatite only, Hydroxyapatite-ZnO_2 and Hydroxyapatite-CeZnO5. The Y201 cells were cultured for 30 days. Cells were seeded on the sterilised scaffolds and resazurin assay was performed to record cell viability. The Y201s attached and proliferated on all the scaffolds except PU only foams. At Day 3 and Day 7, some cell attachment was observed, and cells proliferated up to day 7, however the adhesion was weak or impaired after Day 7 and cell number seemed to drop (Fig 3.9). The scaffolds incorporating with HA, ZnO_2 and CeZnO5 showed better attachment and cell proliferation for up to 30 days when compared with PU only. At Day 3, no significant difference was observed between PU-HA and ZnO_2 (table 3.4), however significantly improved cell metabolic activity was seen with scaffolds incorporated with CeZnO5. With increasing time, the cell growth became significantly higher for ZnO_2 and CeZnO5 as compared to PU_HA. At Day 30, the CeZnO5 supported a significantly higher number of Y201 cells compared to PU-HA and ZnO_2 hence making the CeZnO5 a better scaffold in terms of cell attachment and proliferation for up to 30 days. Neither ZnO_2 nor CeZnO5 were found to be toxic or posed inhibitory effects for cell attachment or proliferation during the complete duration of experiment.

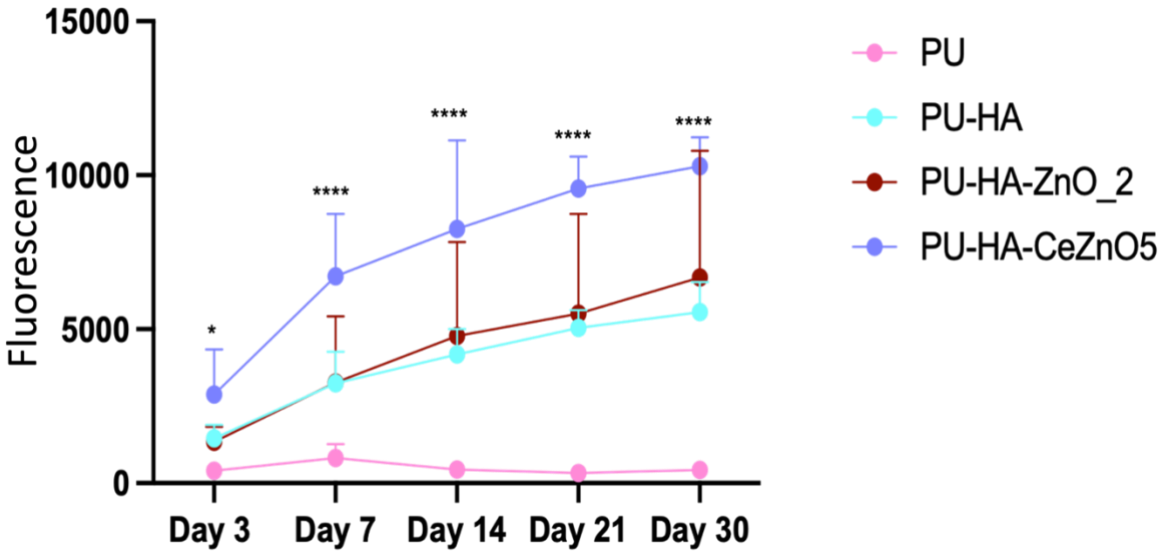

Figure 3.9: *Cells attachment and growth analysis using resazurin cell viability assay on synthesised porous scaffolds for 30 days. Data represents ± mean SD n=3*3.* **<0.0001 ****.**

Table: 3.4: *Cell metabolic Activity differences between Y201 cells on porous scaffolds incorporating HA & CeZnO5 nanoparticles in comparison with scaffolds containing only HA or HA and ZnO_2 as controls.*

Analysis Time point	Comparison of PU-HA-ZnO_2, PU-HA-CeZnO5 1% and PU-HA	P Value
Day 3	PU-HA Vs PU-HA-CeZnO5 1%	0.0741 ns
	ZnO_2 Vs PU-HA-CeZnO5 1 %	**0.0445 ***
Day 7	**PU-HA Vs PU-HA-CeZnO5 1%**	**<0.0001 ******
	ZnO_2 Vs PU-HA-CeZnO5 1 %	**<0.0001 ******
Day 14	**PU-HA Vs PU-HA-CeZnO5 1%**	**<0.0001 ******
	ZnO_2 Vs PU-HA-CeZnO5 1 %	**<0.0001 ******
Day 21	**PU-HA Vs PU-HA-CeZnO5 1%**	**<0.0001 ******
	ZnO_2 Vs PU-HA-CeZnO5 1 %	**<0.0001 ******
Day 30	**PU-HA Vs PU-HA-CeZnO5 1%**	**<0.0001 ******
	ZnO_2 Vs PU-HA-CeZnO5 1 %	**<0.0001 ******

3.6 Discussion

Angiogenesis in bone tissue engineering has gained much attention as it is believed it is required for speedy bone regeneration. The initiation of neovascularization and angiogenesis at a defect site is an important strategy to recruit osteoblasts at the fracture site and leads to new bone growth. Zinc oxide is known to generate reactive oxidative species which initiate the process of angiogenesis with the help of growth factor mediated mechanisms. The use of metal oxides in tissue engineering scaffolds for the purpose of angiogenesis was first reported in 2014 and since then it has gained attention as vascularisation is prerequisite for most repair or regeneration applications (Augustine, Dominic, et al., 2014b, 2014a; Augustine, Malik, et al., 2014). ROS production leads to expression of VEGF and FGF which are key proangiogenic factors. Considering the properties of zinc oxide, based on the literature, this chapter focussed on the synthesis of cerium doped zinc oxide. The resultant oxides were characterised and differences in size, morphology and biological properties were evaluated in comparison with pure zinc oxide. The research was aimed to synthesise phase pure and Cerium doped zinc oxide nanoparticles and introduce them into the scaffolds. It was envisaged that the resultant composite will result in unique lattice and surface properties which would affect biological performance of the final scaffold.

The first task was to select a nanoceramic synthesis method which can yield nanosized particles and give reproducible results. A number of popular methods such as solgel, liquid phase synthesis, gas phase synthesis and several physical methods are being used specifically for synthesis of zinc oxide nanoparticles (Naveed Ul Haq et al., 2017). However, all of them have limitations, such as not being able to achieve nanosized particles in a reproducible manner, difficulty of controlling the morphology of the particles, and the high costs of these methods. The continuous hydrothermal flow system uses supercritical water (at temp. 200-400°C) which interacts with the metal salt at room temperature and causes crystallisation of inorganic materials within seconds to a few minutes duration. The precipitated nanoparticles are then washed and dried to obtain nanopowders. The process is eco-friendly as it only uses water rather than organic solvents (Darr et al., 2017). The technique is reproducible and has been reported in a number of studies. The reaction parameters were adjusted to obtain nanosized zinc oxide and cerium doped zinc oxide particles. The results indicated that the

change in concentration of precursor reactant solutions i.e. potassium hydroxide and zinc nitrate resulted in a change in size of particles. To obtain nanosized particles was a key aim at this stage as the particles will be used in polymeric scaffolds and cell culture experiments. It has been previously established that the smaller the size of nanoparticles, the lower are the chances that the cells will detect them as foreign bodies and create adverse effects. Nanosized particles have higher surface areas hence it is easier for them to cross the cell membrane in a concentration and time- dependent manner through the process of endocytosis (Panyam & Labhasetwar, 2003; Salatin et al., 2015). The particles of less than 100 nm have shown greater cellular uptake than microparticles. Caco-2 cells were treated with 100 nm and 1-10 µm particles and results demonstrated 150-250 times higher particle internalisation for 100 nm nanoparticles. It was reported that microparticles tend to stay in epithelial lining however, nanoparticle uptake allowed penetration and distribution throughout submucosal layers (Desai et al., 1996). Also, nanoparticles can be administered into systemic circulation as they are tiny and can't block fine blood capillaries. Nanoparticles have been reported to have higher efficiency for cellular uptake based on data with different cell lines i.e. Hepa 1-6, HepG2 and KLN 205 (Zauner et al., 2001). The concentrated reactant solutions resulted in smaller particle sizes in the case of control samples (ZnO_1 & ZnO_2).

The shape of nanoparticles is equally important in tissue engineering applications as it affects the biodistribution, residence time and circulation inside a living cell. Achieving elongated particle morphology such as rods or needles is highly efficient for cell attachment as they have higher surface area and aspect ratio specifically for endothelial cells (Salatin et al., 2015). The nanoparticles were further subjected to Raman Analysis to investigate the role of cerium incorporation on Raman Scattering of zinc oxide nanoparticles. The analysis further supported the hypothesis that cerium incorporation poses changes in lattice structure which continually change upon increase in concentration (Srisuvetha et al., 2020). The data also supported the BET surface area analysis as doping resulted in change in size of particles. So, the initial plan of changing the concentration of precursor solutions to obtain different sized nanoparticles was achieved as hoped. The technique can be explored further to optimise the particle size for customised nanoparticles.

The chemical limitation of the synthesis method was detection of cerium oxide phase along with zinc oxide. While analysing XRD data, the presence of more than one oxide phase is generally considered to be an impurity. The doping involves incorporation of ions to the lattice for functional modification; however, substitution is replacing an ion with another one. The synthesis aim was to dope cerium ion into the zinc oxide lattice to obtain added functional benefits, but the result obtained was CeO_2 and zinc oxide. It was concluded that the final nano powder might contain two types of particles: rod shaped zinc oxide and cubic or rounded CeO_2 (Srisuvetha et al., 2020). The conclusion was made based on XRD and TEM data, as TEM micrographs also spotted rounded particles and rod like particles. The presence of another phase can be called unsuccessful doping. However, this chemical synthesis limitation was found not to inhibit biological activity at this stage. The cell metabolic activity of MG63 was recorded to be higher for CeZnO5 and CeZnO6 as compared to ZnO_1 or ZnO_2.

CeO_2 nanoparticles as additives to the scaffolds are reported to facilitate cell proliferation and differentiation of human mesenchymal stem cells (hMSCs). CeO_2 nanoparticles act as a free radical scavenger when loaded in low concentrations. Higher CeO_2 loading in PLGA scaffolds (20%) led to agglomeration of nanoparticles hence reducing the scavenging activity. In another study, PLGA composite with 6 wt% TiO_2 and CeO_2 nanoparticles respectively were compared, better cell attachment and proliferation was recorded for PLGA CeO_2 composite scaffolds (Hosseini & Mozafari, 2020). The CeO_2 is thought to have better biochemical interaction with the cells as compared to TiO_2 as CeO_2 is in trivalent state which is more stable and acts as antioxidant which plays an important role in enhanced cell proliferation. When free radicals are generated within the cells they interfere with the cells' normal growth. CeO_2 is a free radical scavenger, which scavenges oxygen molecules. This oxygen molecule scavenging significantly improved bone regeneration. The superoxide radicals when in contact with CeO_2 are converted into peroxides, such peroxides are attached to the surface of CeO_2 stronger than that of Oxygen molecule. In this way, CeO_2 nanoparticles regulate oxygen within the cells which is the key factor for cell growth and proliferation (Hosseini & Mozafari, 2020). The synthesis method was in agreement with the reported literature in terms of size and shape of particles obtained. Based on literature, the particles with CeO_2 phase were the better combination for cell culture studies.

CeO_2 also known as Ceria on its own promotes angiogenesis and bone regeneration by upregulating the proliferation of vascular endothelial cells and Alkaline phosphatase activity. Ceria also plays an important role in cell migration and osteogenic differentiation of BMSCs by the Smad1/5/8 signalling pathway. Ceria containing bioglasses were found to act as anti-inflammatory and no cytotoxicity was recorded in mouse osteoblast 7F2 cells nor in human mesenchymal stem cells (HMSCs) (Hosseini & Mozafari, 2020).

The CeZnO5 incorporated scaffolds were tested for cell metabolic activity and clearly the cell metabolic activity was higher in samples containing CeZnO5. In light of the literature, the presence of CeO_2 might have an impact on cell attachment and migration leading to proliferation. However, investigating the PCR based markers for bone regeneration and angiogenesis is required. A cell differentiation study is also required to make conclusions about bone regenerative potential of CeZnO5.

3.7 Conclusions

The CeZnO5 incorporated scaffolds showed better cell metabolic activity than scaffolds without cerium with no obvious cell growth inhibition. The cell attachment was recorded to be 60% for these scaffolds and the cell growth kinetics was significantly higher than the control for up to 30 days. PU-HA-CeZnO5 is a novel composite scaffold that can further be explored for bone tissue regeneration and angiogenesis.

Chapter 4: Synthesis and characterisation of Zirconium doped Zinc oxide and identification of a working range of Zirconium doped Zinc oxide for craniofacial bone regeneration and vascularisation

Chapter Objectives:

1) Characterise the Zinc oxide and zirconium doped zinc oxide nanoparticles.

2) Assess biological properties of zirconium doped zinc oxide as nanoparticles and in the form of porous composite scaffolds.

3) Investigate if the porous composite ZrZnO5 containing scaffolds have potential for bone regeneration.

4.1 Introduction:

Biomaterials are important in the field of tissue engineering, especially implantable materials including fixatives, replacements, or reconstruction of damaged bone tissue. A number of metal oxides have been introduced into the field of biomaterials based on properties such as mechanical strength and chemical & physical properties that are compatible with the biological environment. In the previous chapter, the properties of cerium doped zinc oxide were discussed. Cerium doped zinc oxide incorporated scaffolds were found to have better biological properties as compared to scaffolds incorporating only zinc oxide or Hydroxyapatite. The basic cell seeding efficiency and growth kinetics resulted in significant improvement compared to controls. Zirconia is also a promising ceramic candidate due to its mechanical properties in load bearing applications. Zirconia based implants are used in orthopaedics for femoral heads for total hip and knee replacements due to toughness and corrosion resistant properties (Tosiriwatanapong & Singhatanadgit, 2018). This chapter investigated the properties of Zirconium doped zinc oxide nanoparticles as a potential candidate for bone regeneration. The particle morphology, size and surface area were analysed, and porous scaffolds were synthesised. The scaffolds were subjected to cell culture analysis to explore the effect of zirconium doped zinc oxide on cell growth in order to identify if zirconium doped zinc oxide has potential for bone tissue engineering applications.

4.2 Materials and methods

Zinc oxide and zirconium doped zinc oxide nanoparticles were synthesised using a hydrothermal flow system, followed by characterisations. ZrZnO5 was selected for scaffold synthesis and further study. The scaffold synthesis was done using freeze extraction salt leaching technique. Human Embryonic Stem Cell-Mesenchymal progenitors (hES-MPs) and Bone Marrow Stromal cells Y201 cells were used to evaluate the effect of solubility products from scaffold. Cell metabolic activity, cell Seeding efficiency and the ability of scaffolds to support cell adhesion was evaluated using Y201 cells. These methods are all described in detail in Chapter 2 (Heading no. 2.2.7.)

4.3 Results

4.3.1 XRD

The XRD results for zirconium doped zinc oxide showed sharp peaks when analysed with XRD which demonstrated high crystallinity of the nanopowders. The Zr doped zinc oxide (Fig 4.1) was found to be similar to hexagonal wurtzite zinc oxide. No oxide or any other phases were spotted. However, the increase in Zr content led to a shift of the spectra slightly, to the lower angle. This effect was associated with the increased ionic size of Zr^{+4} than Zn^{+2}, upon substitution Zr^{+4} crystal lattice distortion happened which resulted in reduced particle size as the Zr content was increased (Table 4.1). The peak shift to a lower angle as the concentration (fig 4.2) was increased confirmed the substitution of Zr into the zinc oxide (Zhang et al., 2011). Similar data was observed in other Zr doped zinc oxide groups as well, which determined that the change in reactant concentration doesn't have much effect on nano-powder chemistry or properties.

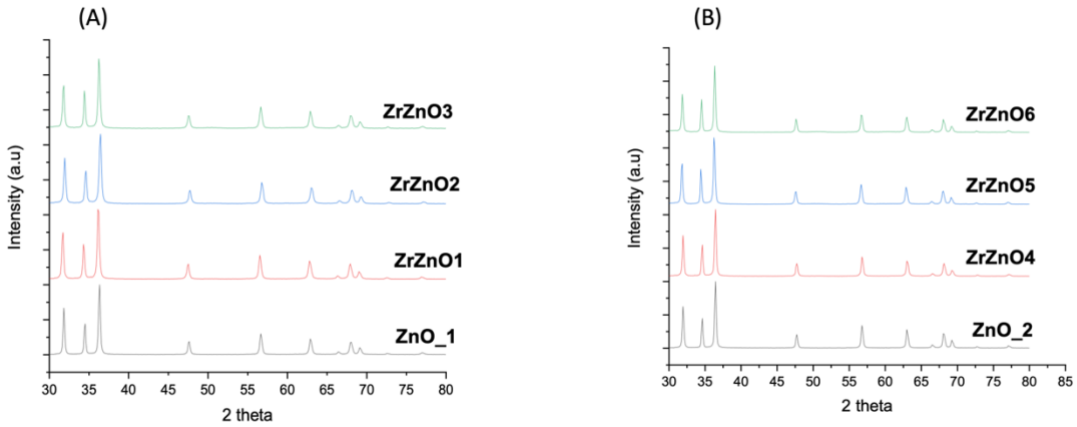

Figure 4.1: *XRD patterns of Zinc oxide and Zirconium doped Zinc oxide A) 0.2 M KOH B) 1M KOH as precursor.*

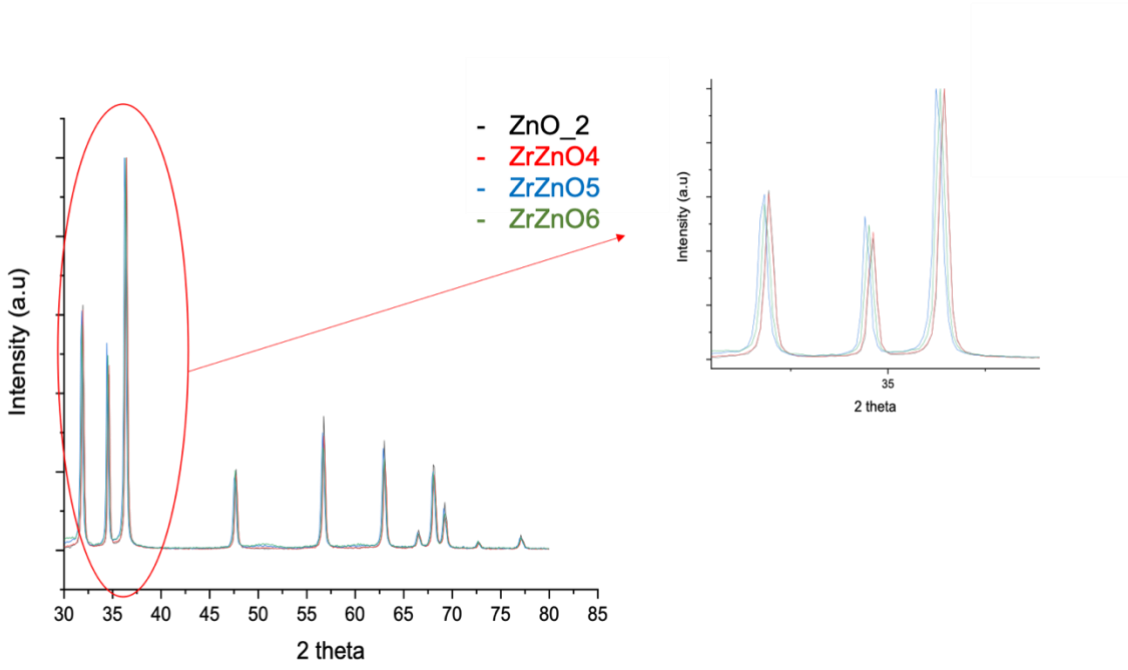

Figure 4.2: *The XRD peak shift due to Zirconium incorporation into the zinc oxide lattice during the synthesis process.*

4.3.2 Brunauer–Emmett–Teller (BET):

The BET data showed that the change in precursor solution concentration led to significant variation in surface area in the case of pure zinc oxide but for doped zinc oxide no significant variation was seen (Table 4.1).

Table 4.1: *Physical properties of nanoparticles*

Sr. no.	Sample Name	BET Surface Area m^2/g	Crystallite size (Scherrer Equation) nm	Average particle size (calculated from TEM imaging) nm
1	ZnO_1	6.77	32.35	83.16
2	ZnO_2	11.35	31.70	45.23
3	ZrZnO1	16.99	29.04	43.32
4	ZrZnO2	24.44	25.78	42.30
5	ZrZnO3	29.07	29.12	73.50
6	ZrZnO4	16.11	31.21	49.55
7	ZrZnO5	26.18	31.20	54.39
8	ZrZnO6	29.84	32.36	58.16

4.3.3. Scanning Electron Microscopy

The nanopowders formed agglomerates of several particles (figure 4.3). The samples were sonicated before SEM analysis, but particle separation was not achieved which might be due to weak physical forces. The nanoparticles were found fused together to make micron sized particles. Even at 23Kx it was difficult to evaluate the individual particle size range due to agglomeration (Mohan & Renjanadevi, 2016). However, it was possible to confirm that the size of particles is in the nano range. To study the morphology of the particles TEM was performed.

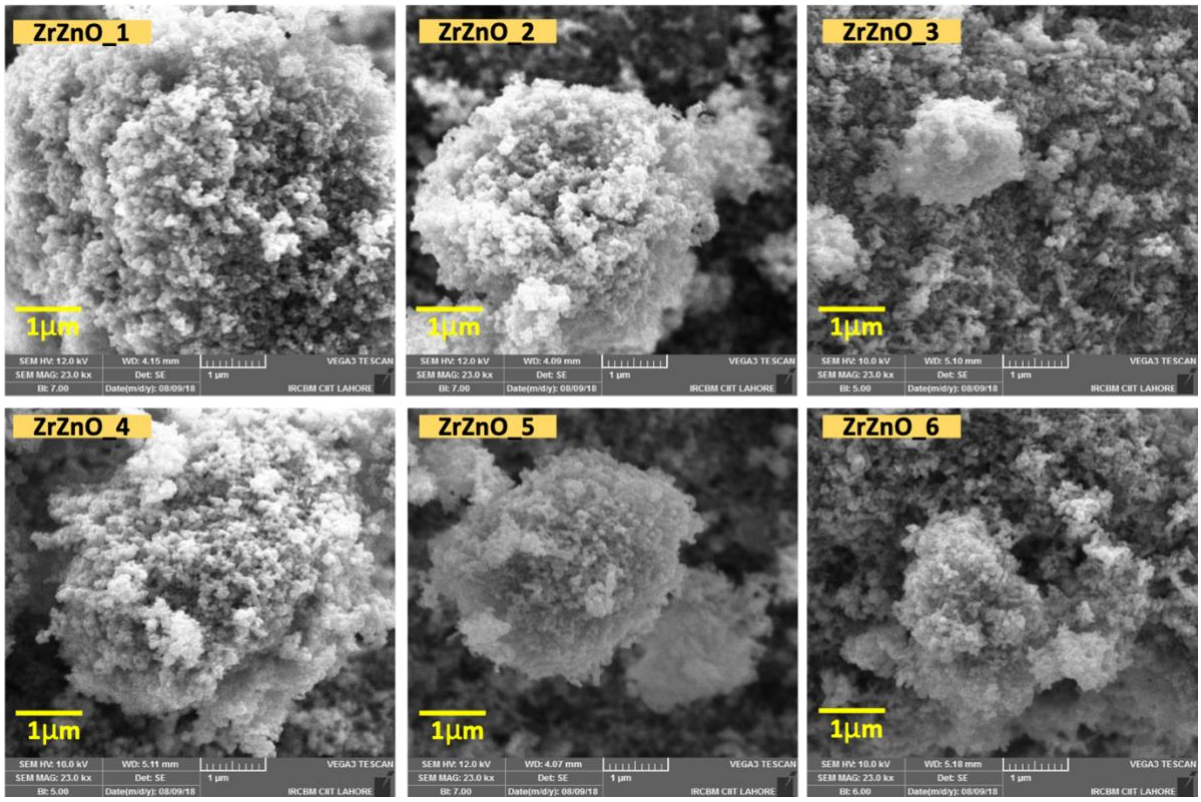

Figure 4.3: *Scanning Electron Micrographs of Zirconium doped Zinc oxide nanoparticles at 23kx magnification.*

4.3.4. Transmission Electron Microscopy

Transmission electron microscopy was performed to evaluate the change in morphology of the particles after doping. At the lowest concentration of Zirconium doping (1%) the size of particles was reduced as compared to control Zinc oxide nanoparticles. Also, less rods were spotted in ZrZnO1 and ZrZnO4. As the concentration increased agglomerates of quite small particles were spotted (approximately 3.5-4 nm) (ZrZnO2, ZrZnO3, ZrZnO5 and ZrZnO 6). The introduction of ions resulted in expansion of the zinc oxide lattice which resulted in reduction in grain size and increase in bandgap (Kulandaisamy et al., 2016; Sinha et al., 2014). It is evident that doping resulted in change in particle size and partly the particle morphology (table 4.1)(fig 4.4).

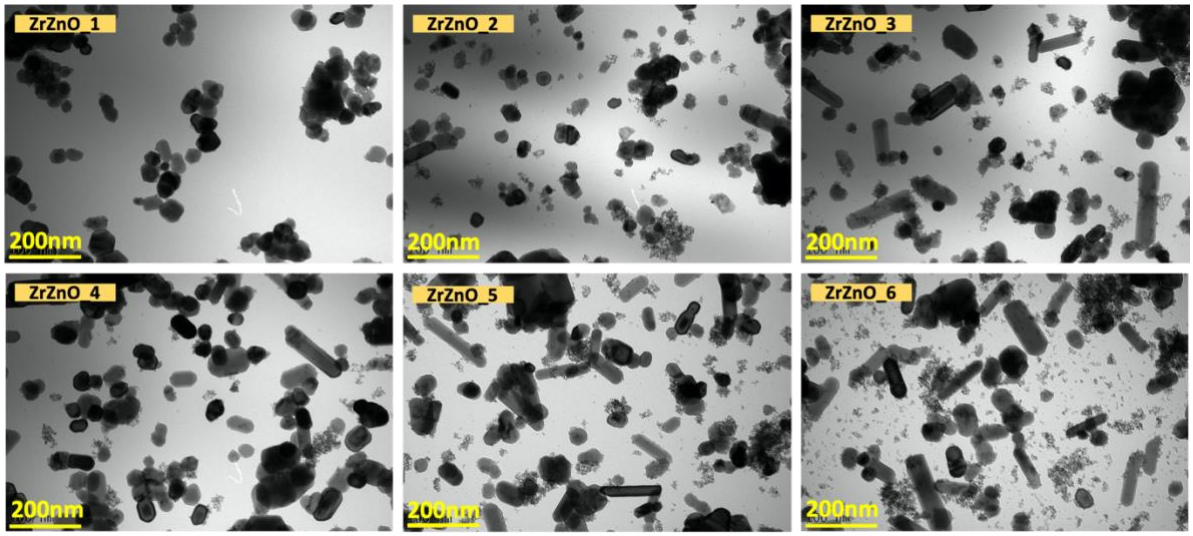

Figure 4.4: *Transmission Electron Micrographs revealing morphology of ZnO nanoparticles and effect of Zirconium doping on nanoparticle morphology. A) ZnO_1 B) ZnO_2 C) ZrZnO1 D) ZrZnO2 E) ZrZnO3 F) ZrZnO4 G) ZrZnO5 H) ZrZnO6*

4.3.5 Nanoparticles cell culture

4.3.5.1 Cell Metabolic Activity investigation using MG63

The Direct contact cell metabolic activity assay was performed as a preliminary evaluation of nanoparticles with 5 µg/ml and 10 µg/ml nanoparticle suspensions for 7 days using cells from the human osteosarcoma cell line (MG63). At day 1 (24 hours), cells exposed to the 5 µg/ml nanoparticle suspension did not appear to have any morphological changes were observed. Different concentrations of Zirconium doped zinc oxide supported distinctive cell metabolic activity. ZnO_1 and ZrZnO2 showed improved response (fig 4.5) and similarly ZnO_2 and ZrZnO5 increased cell growth up to day 7. In order to check the dose response, increased nanoparticle concentrations were used. The results showed the same trend with ZrZnO2 and ZrZnO5 supporting the highest cell viability for up to 7 days. No nanoparticle

chemistry was found to be toxic or inhibited cell proliferation when compared with cells grown in standard culture media as a control. Tukey's multiple comparison test was performed to evaluate if the differences are significant or not.

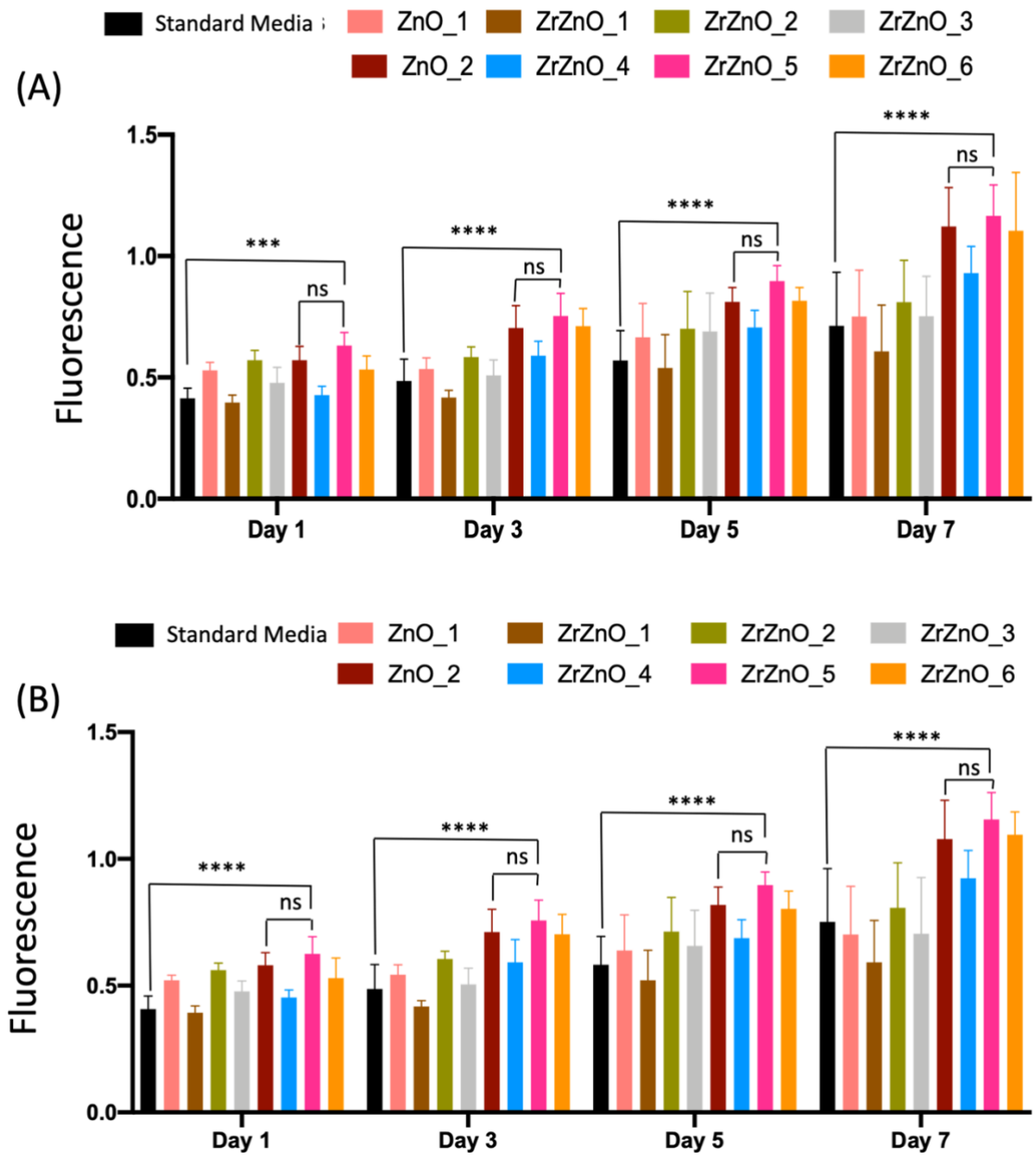

Figure 4.5: *Cell Metabolic Activity of MG63 cultured in nanoparticle media suspension A)5 µg/ml, B) 10 µg/ml , expressed with absorbance units, mean ± S.D, n=3*3, **** <0.0001.*

4.3.5.2 28- Day Cell Viability Assay (10 μg/ml nanoparticle suspension) using hES-MPs:

Human embryonic mesenchymal like stem cells (hES-MPs) were selected for a 28-day study in order to evaluate the long term effect of exposure to the particles on cells and to identify the safe use or toxicity of Zirconium doped nanoparticles at lower concentrations for craniofacial bone scaffolds. ZnO_2 and ZrZnO5 were selected for the study based on preliminary cell culture data (fig 4.5) as well as nanoparticle size (ZnO_2 and ZrZnO5 have smaller particle sizes (Table 4.1).

At Day 1, there was no significant difference between control and ZnO_2, ZrZnO5 (Fig 4.6). The cells were attached to tissue culture plastic and no adhesion impairment was observed under a microscope. At Day 7, ZnO_2 and ZrZnO5 improved cell metabolic activity significantly as compared to the cells-only control, however no significant difference was observed between ZnO_2 and ZrZnO5. A similar pattern was observed for days 14, 21 and 28. ZnO_2 and CeZnO5 clearly improved the cell proliferation for up to Day 28 (Fig 4.6). From Day 14 to Day 21 a steady growth phase was seen for cells and ZnO_2, however a continuous increase in cell metabolic activity was observed for ZrZnO5. Tukey's multiple comparison test was performed to evaluate if ZrZnO5 has significantly improved cell metabolic activity, it was confirmed that the cell metabolic activity was 17% higher than the standard media and 4% higher than the ZnO_2. A significant difference was seen between standard media and ZrZnO5, but no significant difference was observed between ZnO_2 and ZrZnO5 (Table 4.2).

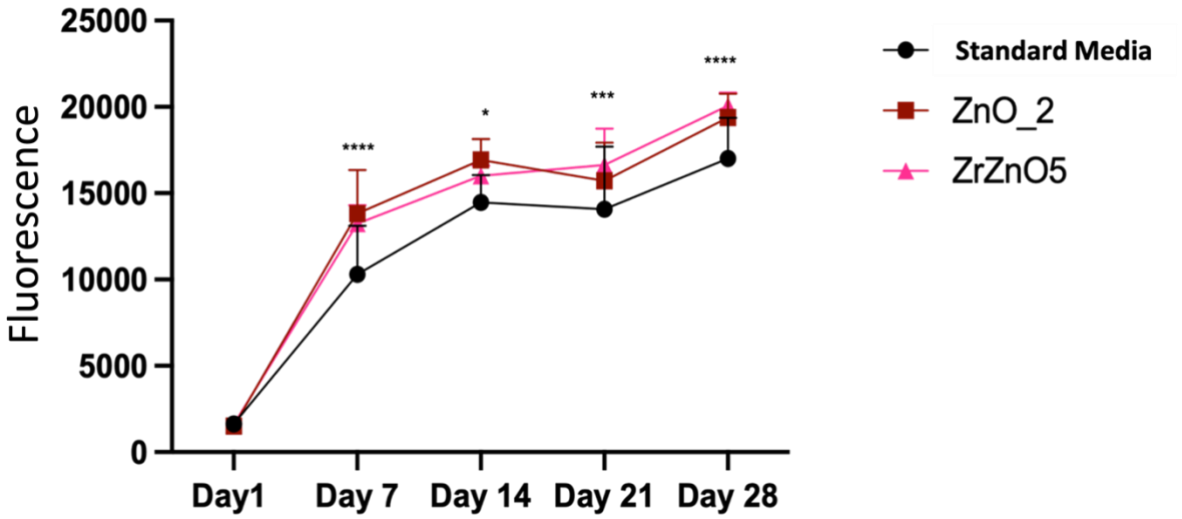

Figure 4.6: *Metabolic Activity of Y201 cells cultured in nanoparticle media suspension (10 μg/ml), expressed with fluorescent units at Day 1 , 7, 14, 21 and 28 days. mean ± S.D, n=3*3, **** <0.0001.*

Table 4.2: *Cell metabolic Activity difference on hES-MPs due to ZrZnO5 nanoparticle suspension as compared to only cells with standard media and ZnO_2 suspension.*

Analysis time points	**Comparison of ZnO_2, ZrZnO5 and Standard media**	**P value**
Day 1	Standard Media Vs ZrZnO5	0.9995 ns
	ZnO_2 Vs ZrZnO5	0.9792 ns
Day 7	**Standard media Vs ZrZnO5**	**<0.0001 ******
	ZnO_2 Vs ZrZnO5	0.6192 ns
Day 14	**Standard media Vs ZrZnO5**	**0.0331 ***
	ZnO_2 Vs ZrZnO5	0.2790 ns
Day 21	**Standard media Vs ZrZnO5**	**0.0001 *****
	ZnO_2 Vs ZrZnO5	0.2938 ns
Day 28	**Standard media Vs ZrZnO5**	**<0.0001 ******
	ZnO_2 Vs ZrZnO5	0.5034 ns

4.3.6 Cell Culture studies on bioactive scaffolds containing Zirconium doped zinc oxide

4.3.6.1 Evaluating effect of soluble products on cell viability from scaffolds:

The experiment was performed to evaluate if the released soluble content from scaffold over time has any toxic effects or inhibitory effects on cells' metabolic activity. The resazurin assay was performed after 48 hours. The hES-MPs and Y201 cells were used for this study to get an overview of whether cell types would respond in a similar way each day. Day 14 data are shown here.

Cell metabolic activity levels were found to be statistically similar compared to those cultured with either frozen media or fresh media. The soluble products from the scaffolds had no inhibitory effect on cell metabolic activity. The metabolic activities recorded were statistically similar and a lack of cytotoxic response was confirmed (Figure 4.7 A).

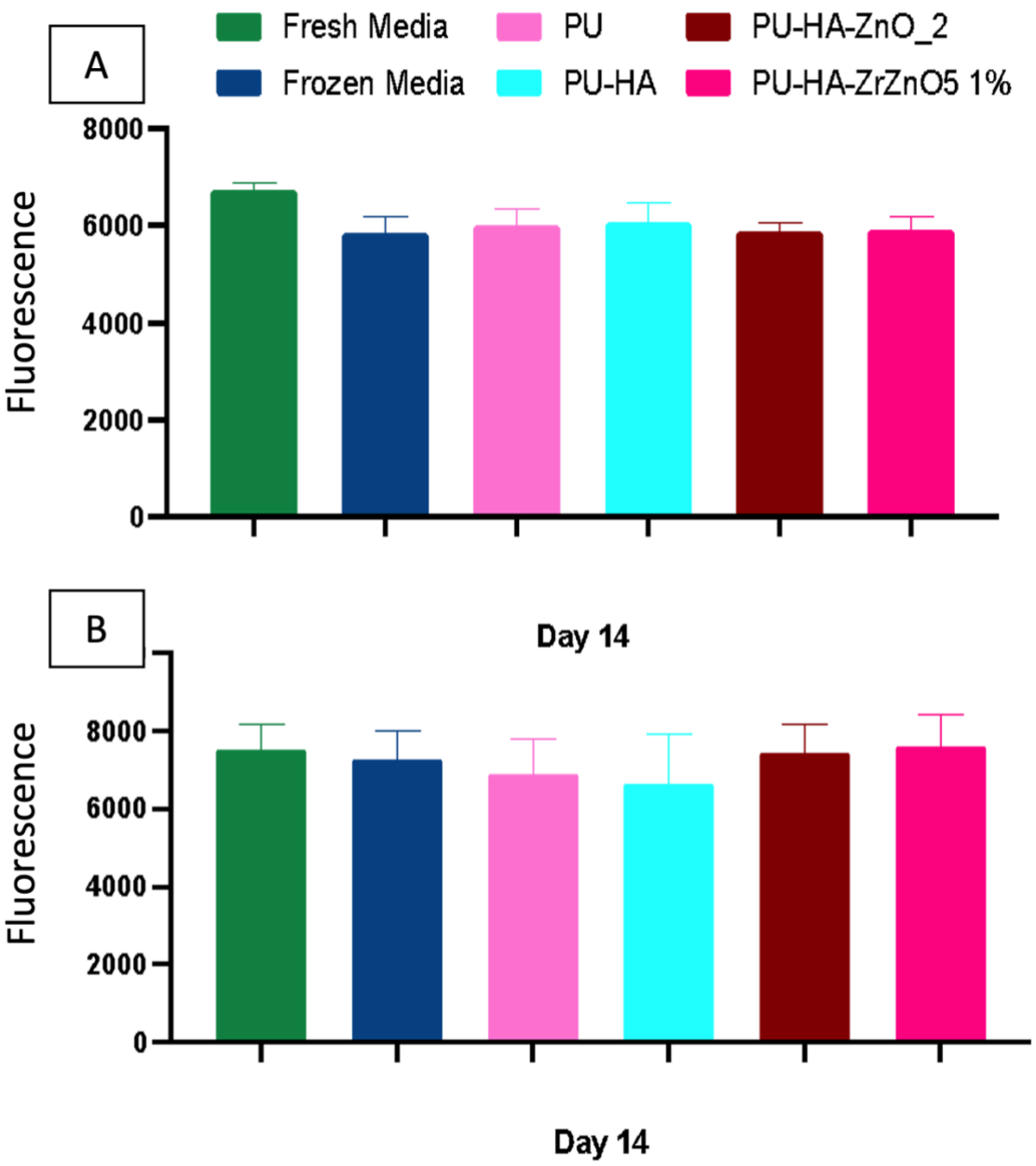

Figure 4.7: *Effect of soluble products eluted from the scaffolds (when submerged in cell culture media for 14 days) The cells were in contact with eluted media for 24 hours. A) hES-MPs, B) Y201, mean ± S.D, n=3*3,*

Similar results were recorded when the assay was performed with Y201 cells (Figure 4.7 B). Hence making it clear that the scaffolds are safe to use for further cell studies.

4.3.6.2 Cell Seeding Efficiency:

The cell seeding efficiency assay was performed using Y201 cells to evaluate if the scaffold's surface supports cell adhesion and how effectively the cells are attaching to the surface immediately after seeding. The cells were incubated for 16 hours after seeding on top of scaffolds followed by transfer of the scaffolds to a new well plate. The resazurin assay was performed on both the previous culture plate and the scaffolds in fresh plates to assess the number of cells attached on the scaffolds and that had fallen onto the surrounding tissue culture plastic. The Scaffolds incorporating HA, ZnO_2 or ZrZnO5 supported significantly higher cell attachment as compared to the control scaffold (only PU) (Fig 4.8).

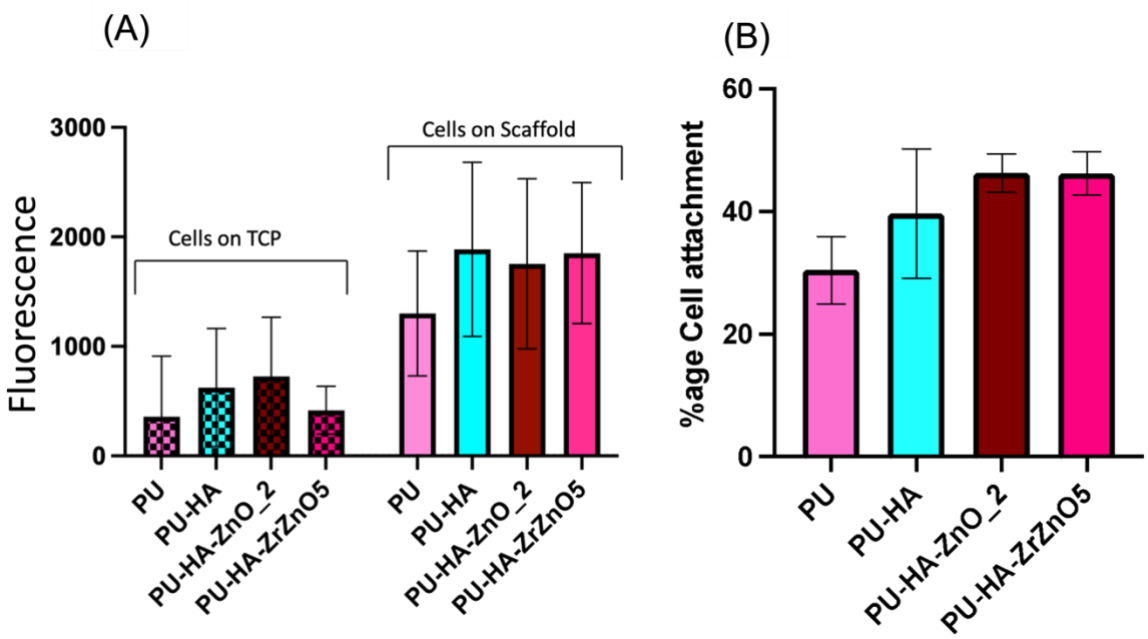

Figure 4.8: *Cell Seeding Efficiency after 16 hours incubation with Y201 cells. The metabolic activity assay was performed to identify cells attached on scaffolds and tissue culture plastic. A) The scaffolds were transferred to new well plate before performing resazurin assay to evaluate the cell metabolic activity on TCP and scaffolds. B) the percentage cell attachment is shown with control (cells with standard media) being considered 100%. ZrZnO5 incorporated scaffolds showed over 45% cell attachment. Data represents mean ± S.D, n=3*3.*

4.3.6.3 Y201 Cells growth kinetic with Bioactive scaffolds

Figure 4.9 shows the viability of cells on the Polyurethane Scaffolds incorporated with hydroxyapatite only, hydroxyapatite-ZnO_2 and hydroxyapatite-ZrZnO5. The Y201 cells were cultured for 30 days. Cells were seeded on the sterilised scaffolds and resazurin assay was performed to record cell viability. The Y201 cells attached and proliferated on the scaffolds except PU only foams. At Day 3 and Day 7, some cell attachment was observed, and cells

proliferated up to day 7, to the extent where cell number on day 7 although low was significantly higher than on day 3 however after Day 7 the cell number seemed to drop (Fig 4.9) which indicates the cells were not in a healthy state, this may be because of weak cell adhesion. The Scaffolds incorporated with HA, ZnO_2 and ZrZnO5 showed better attachment and cell proliferation for up to 30 days when compared with PU only. At Day 3, no significant difference was observed between PU-HA and ZnO_2 (table 4.3), however significantly higher cell metabolic activity was seen with scaffolds incorporated with ZrZnO5. With increasing days, the cell numbers became significantly higher for ZrZnO5 as compared with PU_HA and ZnO_2. At day 30, the ZrZnO5 had significantly higher cell metabolic activity compared to PU-HA and ZnO_2 strongly suggesting that the ZrZnO5 is a better scaffold in terms of cell attachment and proliferation for up to 30 days. Neither ZnO_2 nor ZrZnO5 were found to be toxic nor to pose inhibitory effects for cell attachment or proliferation during the complete duration of the experiment, however ZrZnO5 evidently improved the overall number of metabolically active cells above the other compositions. It can be concluded that ZrZnO5 improved the cell proliferation significantly as compared to the control scaffolds. Tukey's multiple comparison test was performed to evaluate the statistical significance of the result obtained.

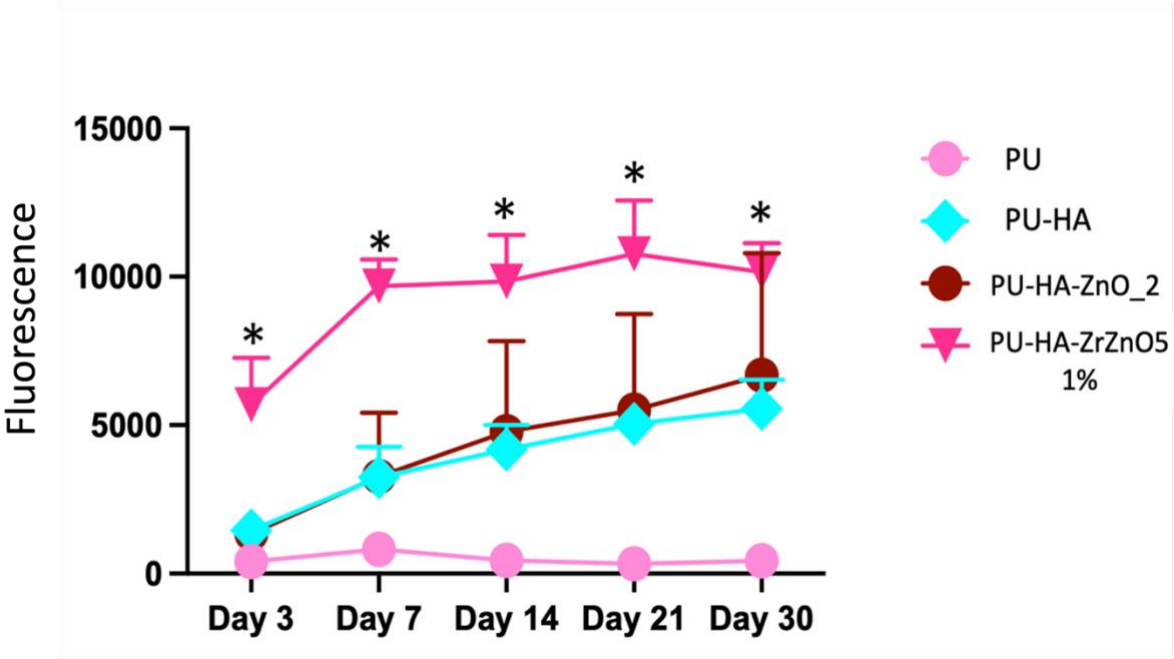

Figure 4.9: *Y201 Growth kinetic with Bioactive scaffolds containing ZnO_2 and ZrZnO5 verses control PU & PU-HA. Data represents mean ± S.D, n=3*3, **** <0.0001.*

Table 4.3: *The cell metabolic Activity difference (Y201 cells) due to ZrZnO5 incorporated scaffolds as compared to only PU-HA and PU-HA-ZnO_2 scaffolds*

Analysis time points	Comparison of PU-HA-ZnO_2, PU-HA-ZrZnO5 and PU-HA	P value
Day 3	PU-HA vs PU-HA-ZrZnO5	<0.0001 ****
	PU-HA-ZnO_2 vs PU-HA-ZrZnO5	<0.0001 ****
Day 7	PU-HA vs PU-HA-ZrZnO5	<0.0001 ****
	PU-HA-ZnO_2 vs PU-HA-ZrZnO5	<0.0001 ****
Day 14	PU-HA vs PU-HA-ZrZnO5	<0.0001 ****
	PU-HA-ZnO_2 vs PU-HA-ZrZnO5	<0.0001 ****
Day 21	PU-HA vs PU-HA-ZrZnO5	<0.0001 ****
	PU-HA-ZnO_2 vs PU-HA-ZrZnO5	<0.0001 ****
Day 30	PU-HA vs PU-HA-ZrZnO5	<0.0001 ****
	PU-HA-ZnO_2 vs PU-HA-ZrZnO5	<0.0001 ****

Another set of scaffolds was synthesised with increasing percentages of the ZnO_2 and ZrZnO5 (1%, 3% and 5%). The synthesis method and conditions were kept the same, only the quantities of the nanoparticles were increased. The (fig 4.10) experiment was repeated with a new set of scaffolds to examine the dose effect of nanoparticles. The data suggested that increasing the nanoparticle content in the scaffolds reduced the cell attachment and proliferation significantly. The increased zinc oxide probably made the scaffolds hydrophobic based on previous research and my qualitative observations of the ability of the scaffold to uptake media hence making it difficult for cells to attach. The best nanoparticle quantity of those examined was concluded to be 1%.

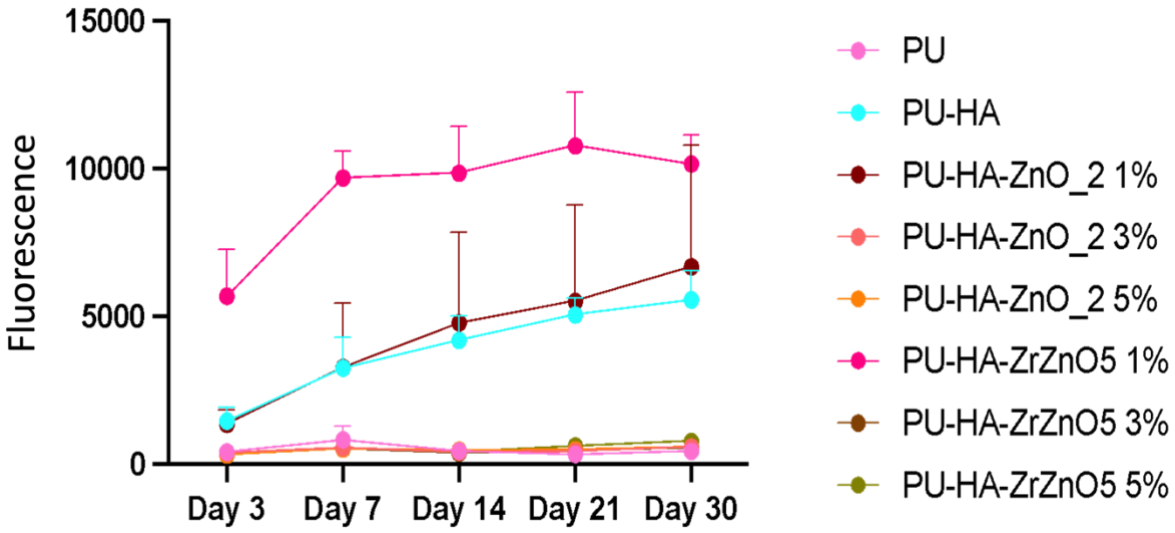

Figure 4.10: *Y201 proliferation kinetic with bioactive scaffolds containing 1%, 3% and 5% PU-HA-ZnO_2 and 1%, 3% and 5% PU-HA-ZrZnO5 verses control.*

4.4 Discussion

Nanotechnology in tissue engineering has gained a lot of attention especially for synthesis of novel scaffolds with added functionalities which may create bone graft substitutes with better clinical performance compared to autografting and allografting. In order to achieve the desired properties, the characteristics of the nanoparticles such as, morphology, size, biological aspects and surface properties are very important, as these properties affect cell adhesion, internalisation and escape from the cell's defence system to obtain the desired response. Gradual developments in nanotechnology in the field of bone tissue engineering have led to an interest in metal oxide nanoparticles due to the biological advantages they offer in the form of cements or scaffolds. Metal oxides are demonstrated to be antibacterial, anticancer, drug delivery vehicles, biosensors and cell imaging agents among other applications. Among many metal oxides, zinc oxides are predominant due to excellent physical and chemical properties. Studies are on-going to explore the potential of zinc oxide in field of biomedicine as anticancer, antibacterial, anti-inflammatory and wound healing (Jiang et al., 2018). It is important to explore the morphological, physical and chemical properties of nanoparticles and how these properties impact in a biological environment, moreover, how to customise these properties to mimic functional tissue in order to make an ideal bone tissue implant. In this chapter, zirconium doped zinc oxide was synthesised and introduced to the polyurethane hydroxyapatite composite. The morphological and physical effects of zirconium doped zinc oxide as nanoparticles and as a substitute in polymeric scaffolds were evaluated followed by evaluation of the biological effect of these nanoparticles.

Zinc oxide exhibited a wurtzite structure as evidenced by XRD analysis, no supplementary peak demonstrating any other phase or oxide was seen. This indicated either a very low quantity of secondary phase that cannot be detected or the Zirconium doping is present in the form of impurity in the zinc oxide lattice. The XRD patterns with increasing zirconium quantity were overlapped and a shift towards lower 2θ was seen. This shift indicated the presence of zirconium as an impurity, introduction of zirconium to zinc oxide caused the expansion of the zinc oxide lattice due to ionic radii mismatch (Tsay & Fan, 2008; Zhang et al., 2011). Another possible reason for the lack of zirconium peaks can be that zirconium ions are completely trapped by the zinc oxide lattice, hence making it difficult for

the diffractometer to detect it as another entity (Mansour et al., 2017). The widening or broadening of the peak was not observed in resultant nanoparticles which indicated the high crystallinity of the zirconium doped zinc oxide nanoparticles, as suppression of nanoparticle crystallinity is indicated by less intense or broad peaks (Clament Sagaya Selvam et al., 2012). There was no difference in crystallite size calculated, however previous studies have shown a reduction in crystallite size upon increase in zirconium content. In our experiments, the difference is not evident, which might be because of a small change in dopant percentages (from 1% to 5%) (Castañeda, 2013; Naik et al., 2020). A slight decrease however was recorded when the percentage was increased from 1% to 3%.

The SEM micrographs were unable to reveal much detail due to smaller particle sizes and the formation of agglomerates, making it difficult to visualise the shape and size of particles. Another study reported the same particle arrangement with Zirconium doping (Mansour et al., 2017) (fig 4.5). The TEM micrographs confirmed the reduction in particle size upon increase in zirconium content.

The toxicity of metal oxide nanoparticles directly depends on concentration, cell density, time period and cell type (Kang et al., 2013). In order to identify safe metal oxide nanopowders content for scaffold synthesis it was important to carefully evaluate these properties. A human osteoblast like cell line was used to investigate any dose dependent effect of synthesised nanoparticles on cell metabolic activity. No cell inhibition or toxicity was seen during this period of time with the concentrations examined (fig 4.6-4.7). The cells adhered to the tissue culture plastic in the presence of zirconium doped zinc oxide very well and proliferated significantly better than in standard media or media containing zinc oxide control. To confirm the findings, human embryonic mesenchymal like stem cells were used to perform the same study but for an extended period of time (28 days) (fig 4.8). The study revealed the better performance of Zirconium doped zinc oxide with respect to standard media or zinc oxide only control. No cell inhibition or detachment was observed, the cells proliferated well for up to 28 days. As reported previously, zinc oxide causes toxicity at higher concentrations such as 25 µg/ml. At this concentration zinc oxide was shown to cause dissolution of Zn^{+} ions into the cell culture media and caused cells to detach and shrink (Kang et al., 2013). In this study, zirconium doping seems to lower the release of Zn^{+} ions into the cell culture medium or cause sustained release hence preventing toxic Zn^{+} ions levels in the

culture medium for the cells, this interpretation is based on literature (Kang et al., 2013). The cells adhered and proliferated even with the cell line that better represents the cells the materials would encounter in vivo hES-MPs. The ZrZnO5 was selected for further research after evaluating its performance with 2 cell lines.

Given the promising result obtained with the powder format ZrZnO5 was selected for inclusion in composite scaffolds with the aim to create a bioactive composite. ZnO_2 was selected as a control for comparison. The 1% PU-HA-ZrZnO5 formation was found to be appropriate for cell attachment and proliferation however the other formulations inhibited the cell attachment. The 1% PU-HA-ZrZnO5 was found to have enhanced cell attachment and proliferation as compared to PU-HA-ZnO_2 and PU-HA. The porous scaffold retained the number of cells and cells proliferated at a higher rate between day 3 to day 7 due to availability of spaces over the rough surface of the scaffolds as well as within the pores. After day 7 the growth was however steady, but no cell inhibition or detachment was seen as the metabolic activity was still increasing which is due to a higher number of living cells. The attachment of cells over composite biomaterials depends on biological and chemical factors such as chemical/hydrogen bond formation, electrostatic/ionic interactions or hydrophobic/hydrophilic interactions. These factors enhance or inhibit adsorption of proteins on scaffolds, hence leading to attachment, the adsorbed proteins then initiate cell-cell signalling leading to proliferation over the biomaterial. The previous literature reported that ZrO_2 has negative zeta potential (-40 mV) and Pure ZnO also has -45.4mV zeta potential hence making the scaffold negatively charged. The ZrZnO5 containing scaffold would be less negatively charged as compared to Pure ZnO_2. The positively charged proteins can easily adsorb over negatively charged titanium implant surfaces such as lactoferrin, hence making the positively charged proteins adsorbed efficiently due to electrostatic attraction. The negatively charged proteins such as albumin precursor and fibronectin suffer electrostatic repulsion hence adsorb less effectively over titanium implants (Kusakawa et al., 2017; Yoshida & Hayakawa, 2016). The higher cell attachment and proliferation over ZrZnO5 containing scaffolds as compared to ZnO_2 containing scaffold should be associated with higher adsorption of protein such as fibronectin. Because ZrZnO5 might have lower negative zeta potential as compared to pure ZnO_2 hence causing less repulsion. Fibronectin and vitronectin are crucial extracellular proteins that control cell behaviours such as adhesion,

migration and differentiation (Parisi et al., 2020). The adhesion of these proteins is very important for cell attachment over metallic or ceramic scaffolds as it leads to cells spreading and morphological adaptation to the substrates that the proteins are attached to (Howlett et al., 1994; Kornu et al., 1996). As mentioned above, the scaffolds physical properties such as surface charge, surface area, surface roughness etc also play an important role for cell adhesion and proliferation. The cells seem to attach better on rough and porous surfaces.

In bone tissue engineering, the osteoblast cell behaviour is very important as these are the bone forming cells. It has been reported that the osteoblasts tend to adhere and proliferate better over Zirconia implants having rough surface properties just like the ones reported in this dissertation. The ZrZnO5 containing bioactive scaffolds supported significantly better cell proliferation as compared to control scaffolds for a duration of 30 days. This data supports that previously reported literature where osteoblasts were cultured with zirconia. The study also explained that the osteoblasts differentiated into osteogenic lineages and mineralised over time in presence of implanted zirconia (Josset et al., 1999).

4.5 Conclusions

The ZrZnO5 was found nontoxic when tested with MG63 cell line. The PU-HA-ZrZnO5 composite scaffold yielded better cell metabolic activity for a duration of 30 days when compared with PU-HA-ZnO_2 scaffolds. The Zirconium doped zinc oxide improved cell seeding efficiency and proliferation as compared to hydroxyapatite and zinc oxide only containing scaffolds.

Chapter 5: Synthesis and characterisation of Copper doped Zinc oxide and identifying a working range for craniofacial bone regeneration and vascularisation

Chapter Objectives:

1) Investigate whether the Copper doped zinc oxide is a better candidate for bone tissue engineering in comparison to Hydroxyapatite and zinc oxide.

2) Investigate if copper doped zinc oxide nanoparticles enhance the cell metabolic activity and select the potential nanoparticles for a bioactive scaffold.

3) Analyse the effect of copper doped zinc oxide containing scaffolds in comparison with zinc oxide-only containing scaffolds.

5.1 Introduction:

In the previous chapters, the properties of cerium and zirconium doped zinc oxide were investigated. The zirconium and cerium doped zinc oxide incorporated scaffolds were found to increase cell metabolic activity as compared to control scaffolds. The literature reported proangiogenic properties of copper. Copper is an emerging element in the field of tissue engineering due to its proangiogenic nature. It has been investigated that copper ions interact with receptors on cells which are involved in angiogenic pathways. It is involved in the upregulation of expression of fibroblast growth factor (FGF) and vascular endothelial growth factor (VEGF). A study performed on Magnesium-copper alloys revealed that the copper ions and Mg-Cu alloys pose no cytotoxic effects to HUVECs and MC3T3-E1 cells. Cu improved the biodegradation property of magnesium and stabilised it in the cellular environment. Furthermore, the alloy enhanced osteogenesis and angiogenesis in a promising way so that could be useful for orthopaedic applications (C. Liu et al., 2016). In another study, Cu- doped bioglass was investigated to have increased VEGF secretion as compared to undoped bioglass (Bejarano et al., 2017). The doped bioglass also revealed antibacterial and increased bioactive properties which reduces the chance of infection as well as biofilm

production over orthopaedic implants (Bari et al., 2017). Copper is a promising element in the field of bone tissue engineering. It has been reported that the copper doping in zinc oxide improves the electrical properties of zinc oxide and creates a more uniform grain size compared to undoped zinc oxide (Shafi et al., 2013). This chapter focuses on copper doped zinc oxide nanoparticles' synthesis and characterisation. Also, the cell metabolic activity assay was performed using copper doped compounds in the form of nanopowders as well as in the form of porous scaffolds to identify if copper doping has any effect on the biological properties of zinc oxide.

5.2 Materials and methods

Zinc oxide and copper doped zinc oxide nanoparticles were synthesised using a hydrothermal flow system, followed by characterisation using XRD, SEM, TEM and cell viability assay. CuZnO5 was selected for scaffold synthesis and further study. The Freeze extraction salt leaching technique was used to synthesise biodegradable porous polyurethane foams substituted with nano hydroxyapatite and zinc oxide or CuZnO5. Human Embryonic Stem Cell-Mesenchymal progenitors (hES- MPs) and Bone Marrow Stromal cells (Y201 cells) were used to evaluate the effect of solubility products from scaffolds. The Cell metabolic activity, Cell adhesion and Cell Seeding efficiency was evaluated using Y201 cells. *These methods are all described in detail in Chapter 2 (Heading no. 2.2.7)*

5.3 Results

5.3.1 XRD:

The X-Ray Diffraction Technique was employed to characterise the synthesised Cu-doped zinc oxide and to compare it with non-doped zinc oxide. The XRD pattern for ZnO_1 and CuZnO1, CuZnO2 and CuZnO3 are shown in Fig 5.1, and ZnO_2, CuZnO4, CuZnO5 and CuZnO6 is shown in fig 5.2. The zinc oxide spectra exhibit sharp peaks which demonstrate good crystallinity of the synthesised zinc oxide and this was indexed to wurtzite hexagonal phase (PDF 00-036-1541). Similar sharp peaks were observed of Cu doped zinc oxide also, which confirmed the high crystallinity of nano powders. CuZnO1 Spectra were found to be identical to the zinc oxide. Different characteristic peaks were observed at an angle 2 theta i.e., at 31.78°, 34.43°, 36.25°, 47.57°, 56.63° and 62.89° which correspond to the Miller Indices (100), (002), (101), (102), (110) and (103) respectively. All these peaks and Miller Indices are related to the standard hexagonal wurtzite crystal structure of zinc oxide NPs (PDF 00-036-1541). It was concluded that lower Cu concentration corresponds to tenorite-like oxide (ZnxCu1−xO) phase (Fernandes et al., 2009; Sajjad et al., 2018).

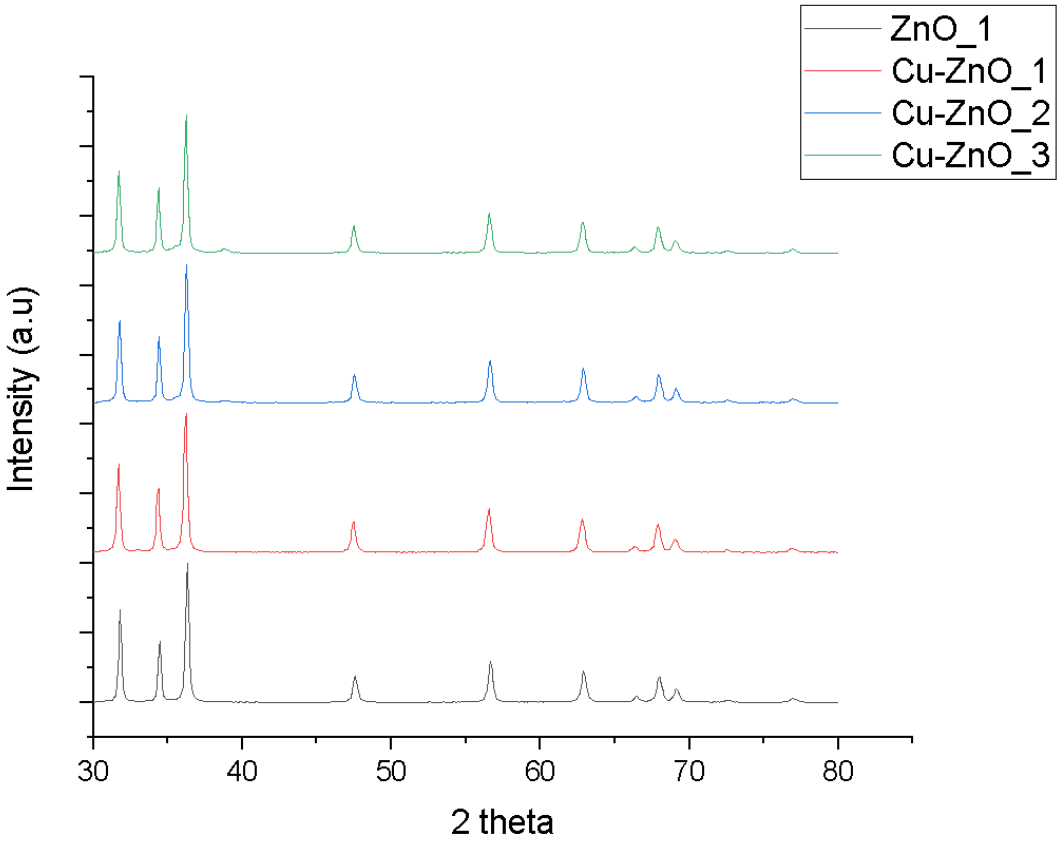

Figure 5.1: *XRD pattern of Zinc oxide and Copper Doped Zinc oxide.*

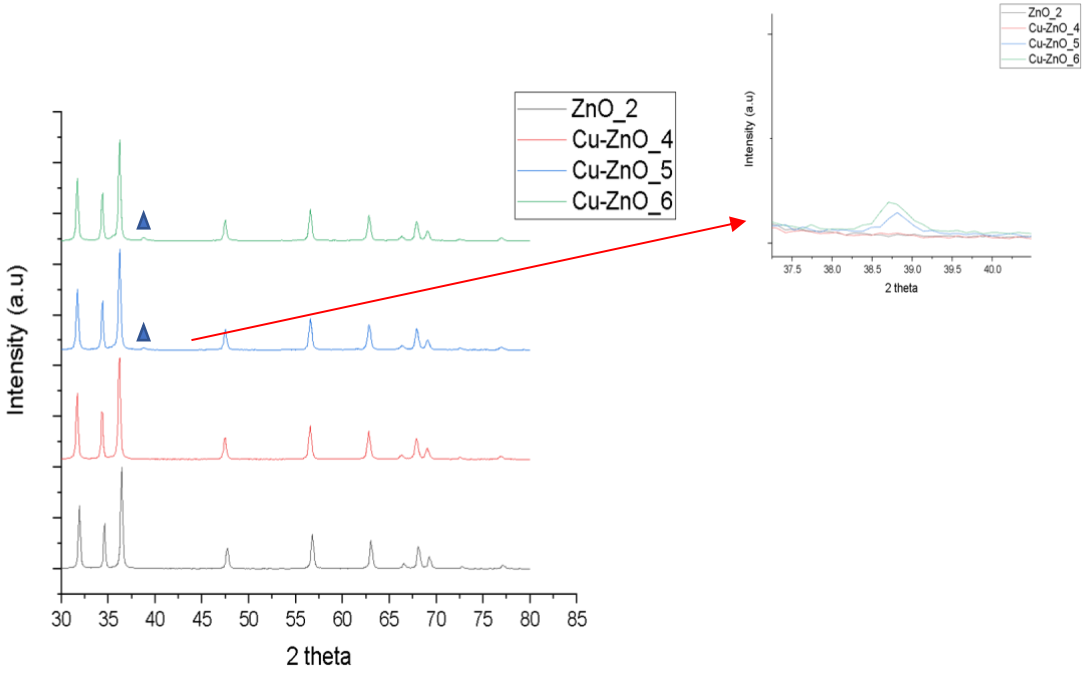

***Figure 5.2**: The appearance of another phase due to copper incorporation during the synthesis process is shown in this XRD pattern.*

At the higher copper concentration, another peak was observed (CuZnO3, CuZnO5 & CuZnO-6). The new phase was matched to PDF 00-048-1548 which was denoted CuO (Fig 5.3). The peak for CuO is not visible at lower concentrations of Cu which might be because XRD is not sensitive enough to pick up the effect of Cu incorporation (Chatkaewsueb et al., 2017)(fig 5.3).

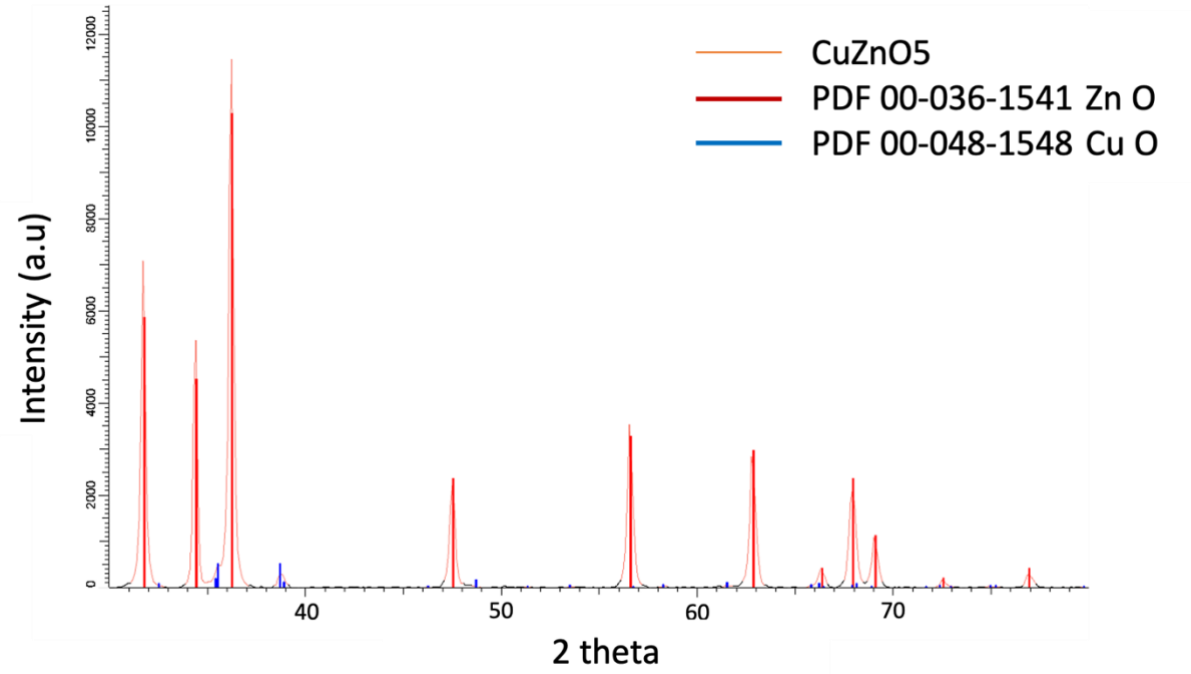

Figure 5.3: *Peak match of new Phase with PDF 00-048-158 which is referred to Copper Oxide.*

The XRD pattern depicts the zinc oxide wurtzite structure, no supplementary peak demonstrating that no other phase or oxide was seen. The data in Fig 5.1 and Fig 5.2 confirmed the incorporation of CuO in the zinc oxide as the particle size decreased the concentration of Cu increased. The trend is very much visible in CuZnO4, CuZnO5 and CuZnO6, the size decreased from 57 nm (CuZnO4), 51 nm(CuZnO5) and 53nm (CuZnO6) respectively Table 5.1. This trend has already been reported in literature (Giahi et al., 2013). The reason for the reduced particle size is linked with the coating of CuO over zinc oxide given that CuO has a smaller size as compared to zinc oxide (Widiarti et al., 2017). Zinc oxide and CuO were the only phases observed and the indices indicated the formation of a phase pure CuO/zinc oxide (Kumar et al., 2017). The sharp peaks for all the samples depicted the high crystallinity of the nanopowders (Chatkaewsueb et al., 2017). And also lower Cu concentration corresponding to a tenorite-like oxide (ZnxCu1−xO) phase (Fernandes et al., 2009; Sajjad et al., 2018).

Table 5.1 shows the calculated crystallite size of zinc oxide and copper doped zinc oxide. The crystallite/grain size was observed to be almost the same for all the samples, no

significant change in size was observed with variation in precursor concentrations or doping concentration.

5.3.2 Brunauer–Emmett–Teller (BET)

The change in precursor solution concentration led to significant variation in surface area in the case of non-doped zinc oxide but for doped zinc oxide no significant variation was seen (Table 5.1).

***Table 5.1**: The particle size calculated using different techniques.*

	Sample Name	BET Surface Area m^2/g	Crystallite size (Scherrer Equation) Nm	Average Particle size (Calculated from TEM images) nm
1	ZnO_1	6.77	32.35	83.16
2	ZnO_2	11.35	31.70	45.23
3	CuZnO1	11.86	30.11	51.21
4	CuZnO2	11.66	32.35	50.61
5	CuZnO3	12.30	30.53	60.01
6	CuZnO4	11.05	30.11	57.54
7	CuZnO5	12.16	29.11	51.74
8	CuZnO6	13.46	30.1	53.37

5.3.3 Scanning Electron Microscopy

The figure 5.4 shows the SEM micrographs of nanopowders which were found as agglomerates of several particles. The samples were sonicated before SEM analysis, but particle separation was not achieved which might be due to weak physical forces. The nanoparticles were found fused together to make micron sized particles. Even at 23Kx it was difficult to evaluate the individual particle size range due to agglomeration (Mohan & Renjanadevi, 2016), although it was confirmed that the size of particles is in the nanoscale range.

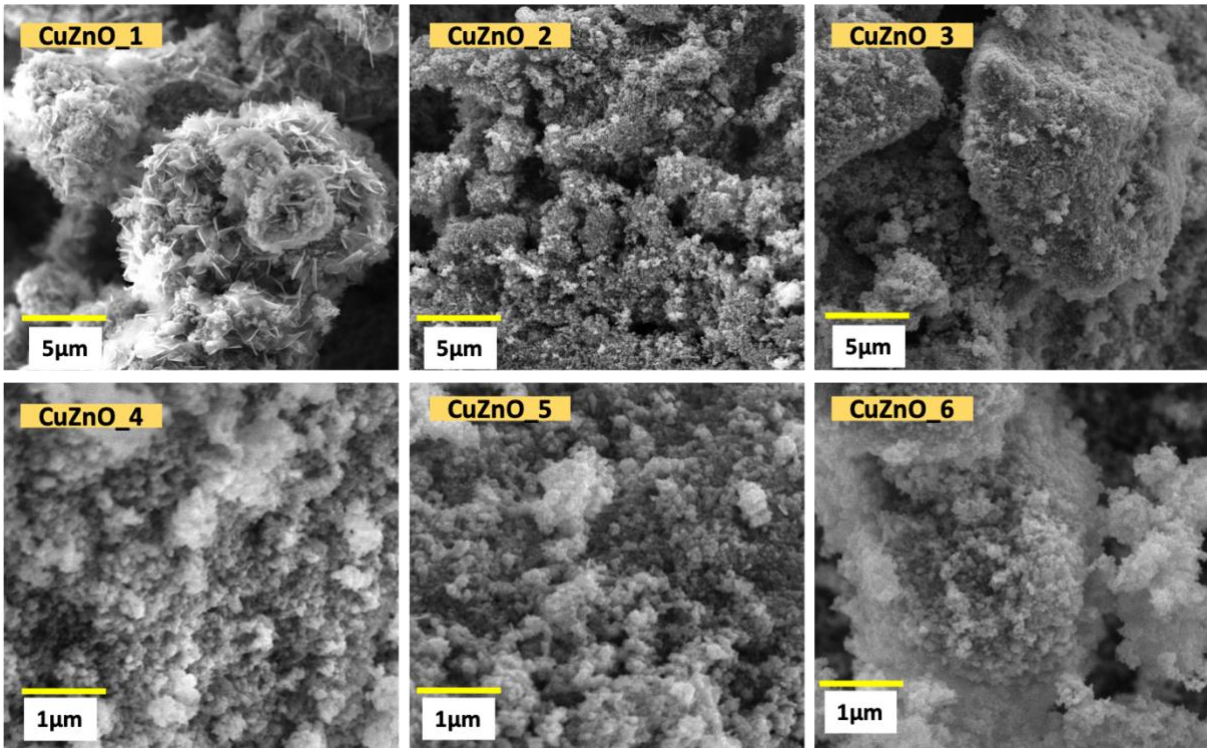

Figure 5.4: *SEM micrograph of CuZnO1, CuZnO2, CuZnO3 at 6.00kx magnification and CuZnO4, CuZnO5 and CuZnO6 at 23kx magnification.*

5.3.4 Transmission Electron Microscopy

Transmission electron microscopy was performed to visualise the particle morphology clearly. In group 1 (CuZnO1, CuZnO2 and CuZnO3) fewer rod like structures are visible, mostly rounded morphology can be seen even at higher copper concentrations. The second phase is not clearly visible which can be confirmed from XRD data. However, the Group 2 does show mixed morphology with both rod-like and spherical particles, which might explain the presence of the CuO phase along with rod-like zinc oxide nanoparticles. The particle size were calculated using image J. The average particle size ranged between 50-60nm (table 5.1).

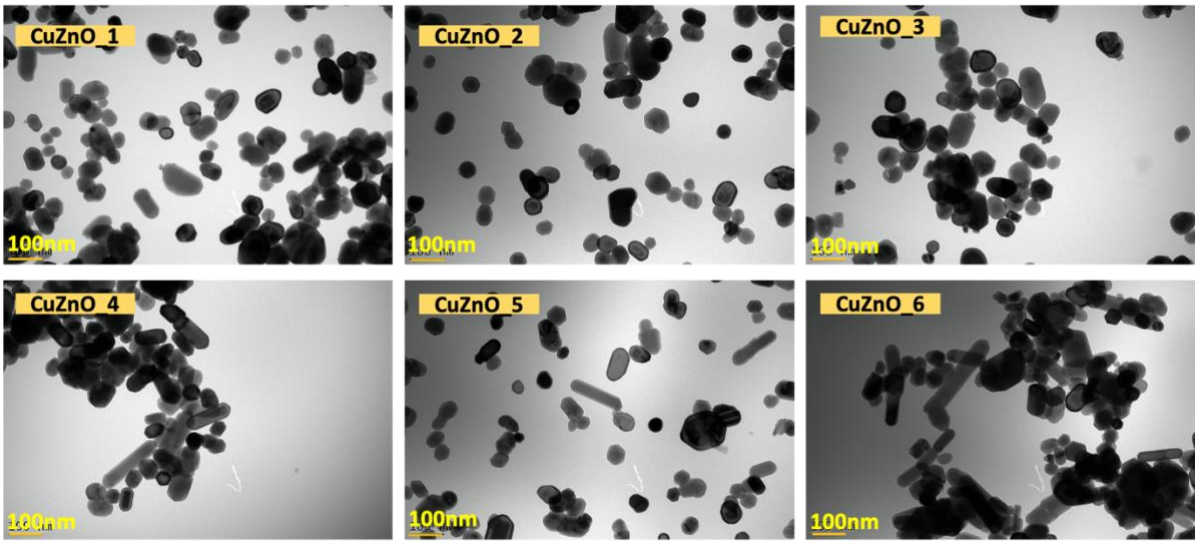

Figure 5.5: *Transmission Electron Micrograph captured at 23kx. at higher Copper contents agglomeration of nanoparticles is visible.*

5.3.5 Nanoparticles Cell Culture

5.3.5.1 Cell Metabolic Activity investigation using MG63

The Nanoparticle suspensions were used to perform direct contact toxicity tests. The cell viability assay using resazurin was performed to record the readings and the test was performed for 7 days using the Human Osteosarcoma cell line (MG63). After 24 hours of nanoparticle suspension exposure, no cell inhibition or change in morphology was observed for either concentration (5 μg/ml & 10 μg/ml). The cells cultured in CuZnO2 and CuZnO5 showed improved viability as compared to the control. A significant difference in cell viability was seen between cells grown in CuZnO5 suspension compared to cells in standard cell culture media. However, no significant difference was observed between cells grown with zinc oxide and CuZnO2 or CuZnO5 respectively. Similar results were observed for up to 7 days with no difference between different concentrations of suspension. None of the nanoparticle suspensions were found to have inhibitory or toxic effects on cells. The cells were metabolically active for the whole duration of the experiment (7 days). Tukey's multiple comparison Test was performed to evaluate if the differences are statistically significant or not.

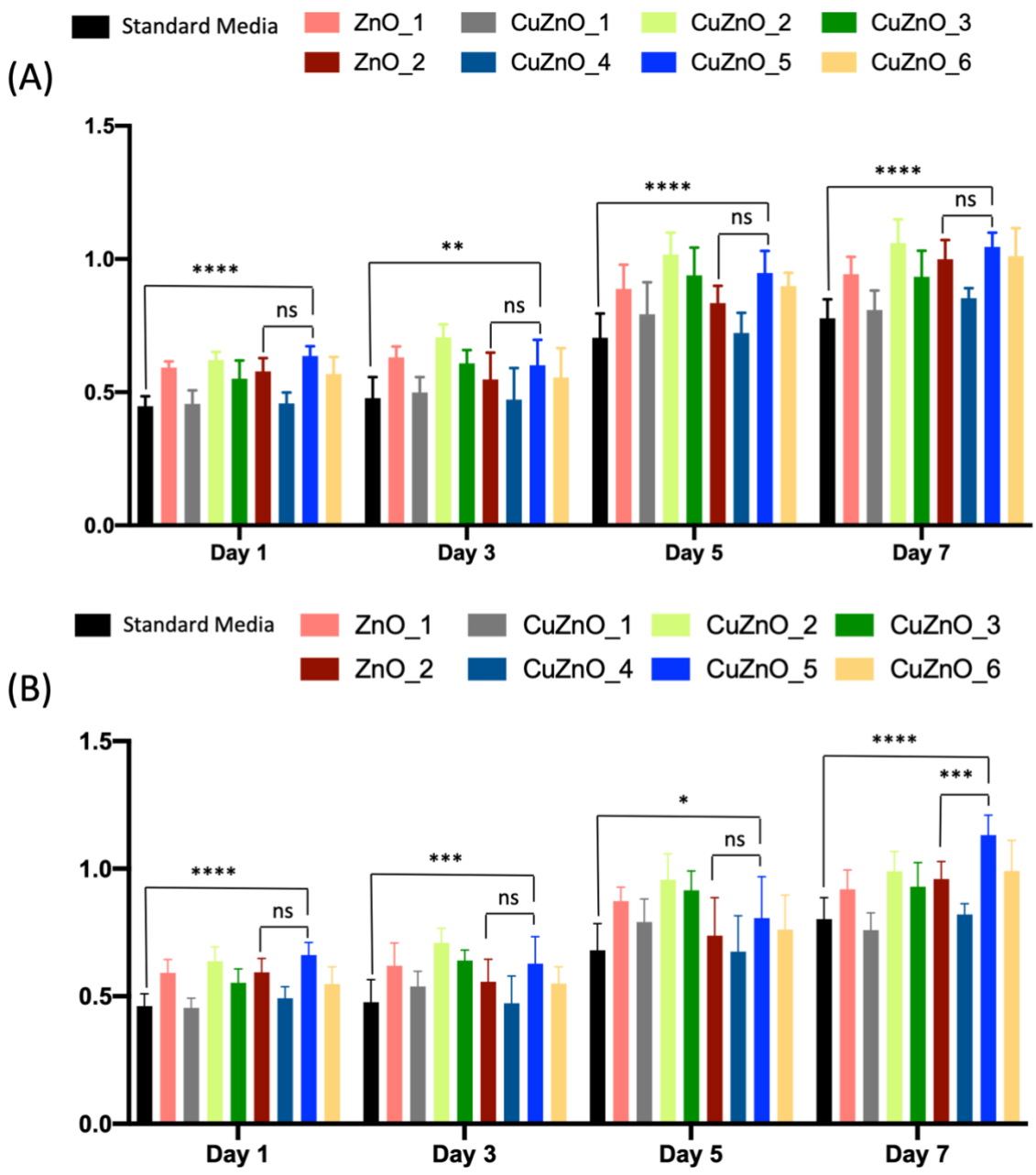

Figure 5.6: *Metabolic Activity of MG63 cultured in nanoparticle media suspension (A)(5 µg/ml),(B) (10 µg/ml), expressed as resazurin absorbance units, mean etc at Day 1, 3, 5 and 7. Data represents mean ± S.D, n=3*3.*

5.3.5.2 Cell Viability Assay over 28 days (10 µg/ml nanoparticle suspension) using hES-MPs:

Human embryonic mesenchymal like stem cells were grown with nanoparticle suspensions to evaluate the effects of long-term contact of nanoparticles with cells. ZnO_2 and CuZnO5 were selected for this study based on preliminary cell culture data (fig 5.6) as well as nanoparticle size (ZnO_2 and CuZnO5 have smaller particle size (Table 5.1).

At Day 1, there was no significant difference between CuZnO_5 and controls, however the ZnO_2 supported better cell viability than both, and this was statistically significant by Tukey's post-hoc test (table 5.2). The cells did attach and proliferate in the presence of CuZnO_5 and no adhesion impairment or cell death (based on cell metabolic activity data) was observed for up to 7 days (fig. 5.7).

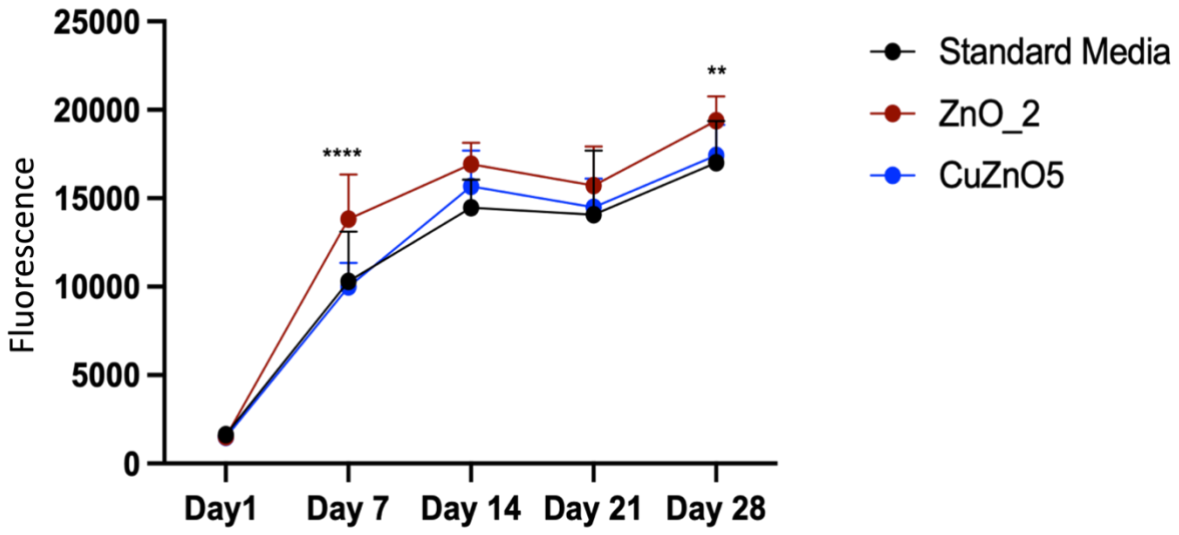

Figure 5.7: *Metabolic Activity of Y201 cells cultured in nanoparticle media suspensions (10 µg/ml), expressed as fluorescent units of resazurin at Days 1, 7, 14, 21 and 28 of culture. Data represents ± mean SD, n=3*3.*

Table 5.2: *The cell metabolic activity difference (Y201 cells) due to CuZnO5 as compared to standard media and ZnO_2.*

Analysis time points	**Comparison of ZnO_2, CuZnO5 and standard media**	**P value**
Day 1	Standard media Vs CuZnO5	0.9665 ns
	ZnO_2 Vs CuZnO5	0.9994
Day 7	Standard media Vs CuZnO5	0.8801
	ZnO_2 Vs CuZnO5	**<0.0001 ******
Day 14	Standard media Vs CuZnO5	0.1374 ns
	ZnO_2 Vs CuZnO5	0.1269 ns
Day 21	Standard media Vs CuZnO5	0.7995 ns
	ZnO_2 Vs CuZnO5	0.1356 ns
Day 28	Standard media Vs CuZnO5	0.7976 ns
	ZnO_2 Vs CuZnO5	**0.0069 ****

5.3.6 Cell Culture Studies on bioactive scaffolds containing copper doped zinc oxide.

5.3.6.1 Evaluating effect of soluble products on cell viability from scaffolds:

Cell metabolic activity levels were recorded at days 1, 7, 14 and 21. The data was found not to be statistically different compared to those cultured with either frozen media or fresh media for all the days. The data confirmed that the soluble products from the scaffolds had no inhibitory effect on cell metabolic activity. The Metabolic activities recorded were similar with no statically significant differences and lack of cytotoxic response was confirmed (Figure 5.8 A).

Similar results were recorded when the assay was performed with Y201 cells (Figure 5.8 B). Hence making it clear that the scaffolds are safe to use for further cell culture experiments.

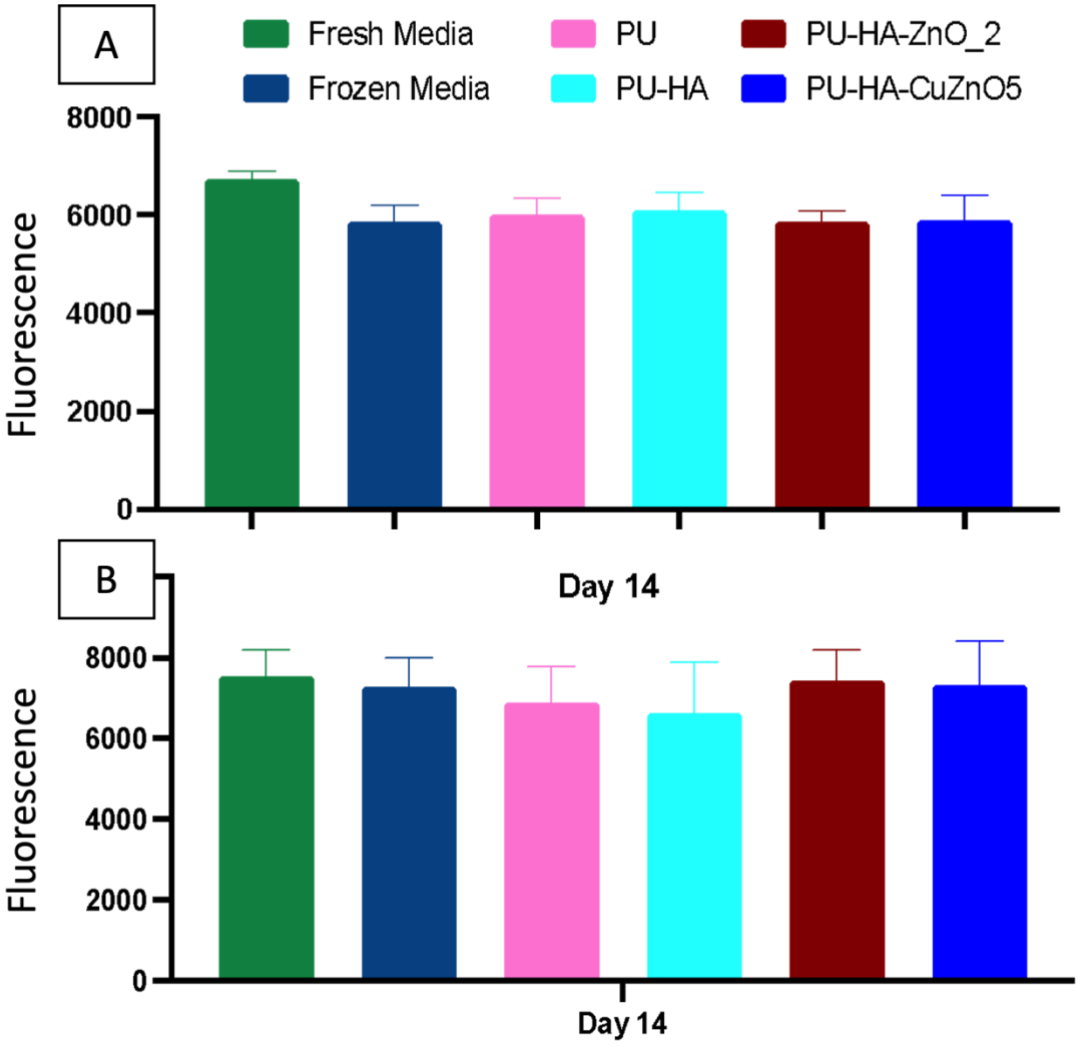

Figure 5.8: *Effect of soluble products eluted from the scaffolds (when submerged in cell culture media for 14 days) A) hES-MPs cell line. B) Y201 cell line. The data represents. mean ± S.D, n=3*3, **** <0.0001 of resazurin fluorescence units measured after 24 hours exposure with eluted media.*

4.3.6.2 Cell Seeding Efficiency

The seeding efficiency of the cells into porous scaffolds was performed using cells from the Y201 cell line. The purpose was to evaluate if the scaffold's surface has potential to

support cell adhesion. The cells were incubated for 16 hours after seeding over scaffolds followed by transferring the scaffolds to a new well plate. The cell viability assay was performed on both plates to assess the number of cells attached on the scaffolds and on the tissue culture plastic. The scaffolds incorporating HA, ZnO_2 or CuZnO5 showed significantly higher cell attachment as compared to the remaining control scaffolds (only PU) (Fig 5.9).

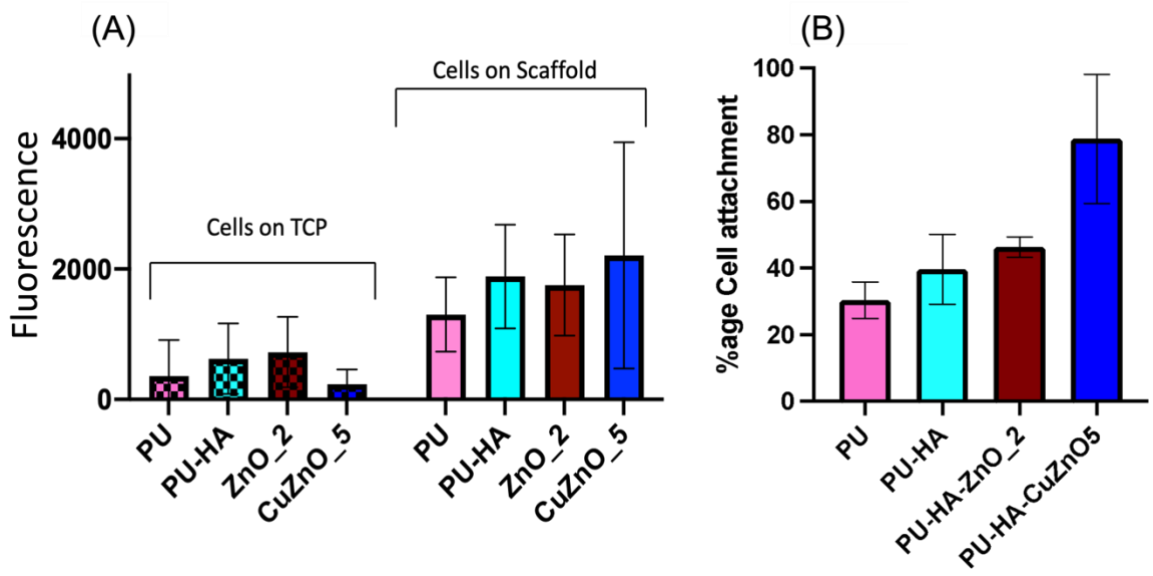

Figure 5.9: *Cell Seeding Efficiency after 16 hours of incubation with Y201 cells. The metabolic activity assay was performed to identify cells attached on scaffolds and tissue culture plastic. A) The scaffolds were transferred to new well plate before performing resazurin assay to evaluate the cell metabolic activity on TCP and scaffolds. B) the percentage cell attachment is shown with control (cell with standard media) being considered 100%. CuZnO5 incorporated scaffolds showed 80% cell attachment. Data represents mean ± S.D n= 3*3*

4.3.6.3 Y201 cells proliferation kinetic with Bioactive scaffolds

Figure 5.10 shows the cell viability of the Polyurethane Scaffolds incorporated with Hydroxyapatite only, Hydroxyapatite-ZnO_2 and Hydroxyapatite-CuZnO5. The Y201 cell line was used, and the test was performed over 30 days. The scaffolds were sterilised (details mentioned in methodology section 2.2.7.1) followed by cell seeding. The fluorescence reading was recorded using resazurin at days 3, 7, 14, 21 and 30. The Y201 cells attached and proliferated on the Scaffolds except on PU only foams. At Day 3 and Day 7, some cell attachment was observed, and cells proliferated till day 7, however the adhesion seemed weak or impaired after Day 7 and cell viability dropped which corresponds to a lower cell number (Fig 5.10). The scaffolds incorporated with HA, ZnO_2 and CuZnO5 showed better attachment and cell proliferation for up to 30 days when compared with PU only. In the case of CuZnO5 incorporated bioactive scaffolds, the cell attachment was significantly improved and a gradual increase in cell proliferation was recorded till day 21 and growth seemed to steady for next 10 days. At Day 3, only marginal difference was observed between PU-HA and ZnO_2 and CuZnO5, however significantly improved cell metabolic activity was seen with scaffolds incorporated with CuZnO5 from Day 7 till day 30. At Day 30, the CuZnO5 had significantly higher cell metabolic activity compared to PU-HA and ZnO_2 hence making the CuZnO5 a better scaffold in terms of cell attachment and proliferation for up to 30 days. Neither ZnO_2 nor CuZnO5 were found toxic or posed inhibitory effects for cell attachment or proliferation during the complete duration of experiment, however CuZnO5 evidently improved the cell viability which reflects the fact of a greater number of cells present on the scaffold. It can be concluded that CuZnO5 improved the cell proliferation significantly as compared to the control scaffolds. The tukey's multiple comparison test was performed to evaluate the significance of the result obtained.

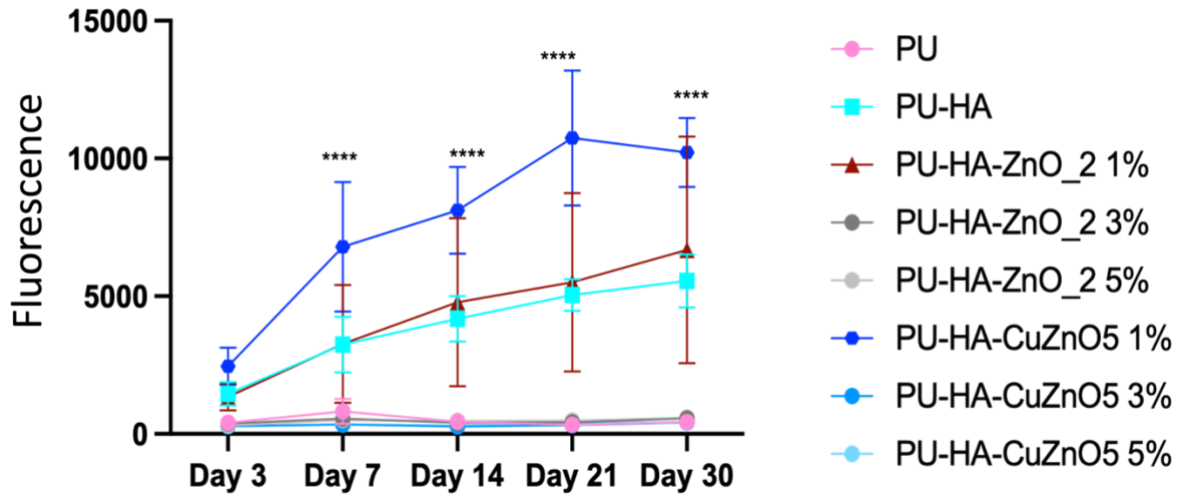

Figure 5.10: *Y201 cells Proliferation kinetic with Bioactive scaffolds containing ZnO_2 and CuZnO_5 verses control PU & PU-HA. (****p<0.0001)*

Table 5.3: *The cell metabolic activity difference (Y201 cells) due to CuZnO5 incorporated scaffolds as compared to only PU-HA and PU-HA-ZnO_2 scaffolds*

Analysis timepoints	**Comparison of PU-HA-ZnO_2, PU-HA-CuZnO5 and PU-HA**	**P Value**
Day 3	PU-HA Vs PU-HA-CuZnO5 1%	0.3217 ns
	ZnO_2 Vs PU-HA-CuZnO5 1 %	0.2269 ns
Day 7	**PU-HA Vs PU-HA-CuZnO5 1%**	**<0.0001 ******
	ZnO_2 Vs PU-HA-CuZnO5 1 %	**<0.0001 ******
Day 14	**PU-HA Vs PU-HA-CuZnO5 1%**	**<0.0001 ******
	ZnO_2 Vs PU-HA-CuZnO5 1 %	**<0.0001 ******
Day 21	**PU-HA Vs PU-HA-CuZnO5 1%**	**<0.0001 ******
	ZnO_2 Vs PU-HA-CuZnO5 1 %	**<0.0001 ******
Day 30	**PU-HA Vs PU-HA-CuZnO5 1%**	**<0.0001 ******
	ZnO_2 Vs PU-HA-CuZnO5 1 %	**<0.0001 ******

To identify the dose effect of ions released from the scaffolds on cell viability of Y201 cells, another set of scaffolds was synthesised with increasing percentages of the ZnO_2 and

CuZnO5 (1%, 3% and 5%). The synthesis method and conditions were kept identical, only the quantities of the nanoparticles were increased. The (fig 5.10) experiment was repeated with a new set of scaffolds to see the dose effect of nanoparticles. The data suggested that increasing the nanoparticle content in the scaffolds impaired the cell attachment and proliferation significantly. The increased zinc oxide content caused the scaffolds to be hydrophobic hence making it difficult for cells to attach. The optimal or safe nanoparticle quantity was concluded to be 1%.

5.4 Discussion

Nanoparticles were synthesised using a continuous hydrothermal flow system, three concentrations of copper doping were introduced during the synthesis and two groups were synthesised aiming to get different particle sizes under 100 nm. The concentrations of precursor solution were varied to obtain variable nanosized particles.

The ability of copper doped zinc oxide to support cell viability was investigated using the resazurin assay. The assay was performed to identify whether there are any cytotoxic effects of copper doped zinc oxide nanoparticles for bone tissue engineering scaffolds. The results indicated increase in cell viability suggesting increase in cell number in the presence of nanoparticles. CuZnO2 and CuZnO5 showed significantly higher cell viability compared to control, demonstrating synthesised nanoparticles are safe and do not cause cell death. CuZnO5 increased cell viability marginally as compared to CuZnO2 but the difference was not significant. CuZnO5 was selected with ZnO_2 as a control. Metallic ions released from the nanoparticles in cell culture medium such as Cu^{+}/Cu^{+2} and Zn^{+2} is safe in concentrations as no cell inhibition or cell death was recorded. The cells continued to grow in the presence of nanoparticle suspensions. The literature reported that a burst release of copper from scaffolds can reduce or impair cell proliferation and induce cell toxicity, however low concentrations stimulate endothelial cells (Jaidev et al., 2017). In the present study the cell seeding efficiency and growth kinetics was improved which might be because of a slow release of copper ions. Enhanced cells' adherence and increase in cell viability was recorded. A CuZnO5 suspension was used to test the cell viability of hES-MPs for up to 28 days in order to confirm the long-term safety of these nanoparticles *in vitro*. The ZnO_2 and CuZnO5 both were found to be safe and did not cause any cell death or toxicity for 28 days. For Bone tissue engineering scaffolds, the physical, chemical, and biological properties are very important as the combined effect of these properties leads to scaffold integration. Scaffold integration is a predominant factor as scaffold surface properties either promote or inhibit cell attachment and proliferation. The Y201 cell line was used to investigate if the scaffolds have potential for cell attachment and proliferation and to identify the effect of CuZnO5. The cell attachment study also confirmed the finding that the CuZnO5 containing scaffolds enhanced the cell adhesion (Jaidev et al., 2017). Cell attachment was significantly higher on porous scaffolds

than the tissue culture plastic as compared to only polyurethane, HA or zinc oxide scaffolds which supports the previous data that Cu ions enhance cell adherence in case of Y201s as well. The study was further advanced and cell proliferation assay revealed significant differences between scaffolds containing CuZnO5 and ZnO_2. The cells proliferated well on scaffolds, indicated by the cell viability increasing with time. The increase in cell proliferation on scaffolds containing Cu can be related to the enhanced cell attachment, as the initial cell attachment was higher so that there were more cells available for proliferation. However, only 1% CuZnO5 was found to enhance adherence and proliferation, as the concentration was increased, little or no cell attachment was observed, and no cell proliferation was seen. The finding is in agreement with the reported data that the higher concentration of copper ions reduces cell proliferation (Jaidev et al., 2017). Cu ions have also been reported to enhance recruitment and cross linking of tropoelastin precursors and promote mature fibre formation. Low levels of Cu ions induce vascularisation however 10-fold increase in ion levels i.e. 560 ng of Cu^{+2} promote wound tissue ingrowth. Cu ions are known to facilitate the release of growth factors and cytokines which help the proliferation of mesenchymal cells, towards osteogenic differentiation (Mourino et al., 2012).

Cu^{+2} is a stable oxidation and copper ions and Zn ions are very important for enzymatic functions. Copper proteins involved in normal functioning of enzymes work in three different ways. Electron transfer reactions such as DNA repair, oxygen transport and storage and transport of metals. Cu is responsible for bone metabolism and turnover. It is also involved in collagen fibre deposition and angiogenesis. Regeneration of critical sized calvarial defect in rats upon copper supplementation was also reported. The copped doped chitosan scaffold was used and compared with only chitosan. Twice the bone volume was recorded using microCT analysis (D'Mello et al., 2015).

Mesenchymal stem cells (MSCs) have the ability to induce immunomodulatory functions either by direct cell-cell contact or by secretion of cytokines. MSCs have also been reported to respond to cytokines to migrate to the site of inflammation or injury (Kyurkchiev et al., 2014; Leuning et al., 2018). The cytokine release profile from stromal MSCs depends upon microenvironment and surface topography. A study performed by seeding MSCs on 76 different bioactive surface topographies resulted in unique cytokine profiles. The data demonstrated that the alteration in microenvironment can change the release profile of

cytokines resulting in altered cellular response (Leuning et al., 2018). The change in environment or surface topography can be done using different kinds of ceramic nanoparticles to induce a cytokine response for bone regeneration and angiogenesis. The present research data showing that PU-HA-CuZnO5 composite scaffold induced cell proliferation might also be related to increased cytokine activity leading to higher cell proliferation on the scaffold. This could further be confirmed by performing cytokine detection investigations.

5.5 Conclusions

PU-HA-CuZnO5 composite scaffold was found to improve the cell seeding efficiency, metabolic activity and alkaline phosphatase activity levels as compared to control scaffolds. CuZnO5 was found to be nontoxic for MG63, hES-MPs and Y201 cells at lower concentrations.

The addition of copper into zinc oxide might have reduced the burst release of Cu ions which resulted in improved cellular response for up to 30 days, though an ion release study is required for further confirmation. 1% CuZnO5 was found to be an appropriate dose for improved cellular response. The higher concentration of CuZnO5 leads to impaired cell attachment and no proliferation.

6 Comparative analysis of Cerium, Zirconium and Copper doped Zinc oxide incorporated porous scaffolds

6.1 Chapter Objectives

1. Investigate if the introduction of doped zinc oxide changes the material properties of Polyurethane scaffolds such as porosity and tensile properties.
2. Investigate the effect of different ionic dopings on cell viability and seeding efficiency.
3. Evaluate the mineralisation and angiogenic potential of doped zinc oxide incorporated scaffolds and compare the properties of Cerium, zirconium and copper doped zinc oxide incorporated scaffolds.

6.2 Introduction

The previous chapters discussed in detail the synthesis, characterisation and biological properties of cerium, zirconium and copper separately. The metal doped zinc oxide demonstrated good seeding efficiency and cell growth kinetics. The scaffolds incorporated with the doped zinc oxide were not found to cause toxic effects on cells, neither was any kind of cell inhibition observed. The novel composites were found to increase cell metabolic activity significantly better than hydroxyapatite or zinc oxide containing scaffolds. In this chapter, the three novel composites PU-HA-CeZnO5, PU-HA-ZrZnO5 and PU-HA-CuZnO5 will be compared. The aim is to understand the benefits of different dopings and identify which ones are better than the others. Also, to identify which doping has potential for future bone regenerative studies.

Scaffold properties are highly dependent on additives added to the scaffold during the synthesis process. The addition of nanoceramics into the scaffold can enhance surface properties, mechanical properties and biological properties which are all important factors in regenerative medicine. Balancing these properties in the design of scaffolds for bone tissue engineering is very critical as all these properties may impact each other and a single property cannot be prioritised over all the others. For example, good surface properties promote

implant integration, but adequate mechanical properties are also important to avoid graft failure. Doped zinc oxide nanoparticles were added to Polyurethane-Hydroxyapatite scaffolds to explore the physical and biological properties of scaffolds. The chapter will also focus on benefits of dopings and conclude whether the doped zinc oxide incorporated scaffolds have potential for further exploration as a useful material for bone regeneration and angiogenesis.

6.3 Materials and Methods

The freeze extraction salt leaching technique was used for porous scaffold synthesis. The amount of Hydroxyapatite was kept constant and 1% zinc oxide or doped zinc oxide nanoparticles were added to the scaffolds. FTIR, SEM and tensile testing were performed to evaluate the physical and mechanical properties of the scaffolds. The semi-quantitative resazurin assay was performed to evaluate the cell metabolic activity in response to different scaffolds. Cell seeding efficiency, Alkaline phosphatase activity assay and VEGF ELISA were also performed to explore the biological properties of the scaffolds containing different ionic dopings i.e. zirconium, copper and cerium.

6.4 Results:

6.4.1 Scaffold characterisation

6.4.1.1 Fourier-transform infrared spectroscopy (FTIR)

The Fourier transform infrared spectroscopy was performed to study the composition of composite scaffolds.

The zinc oxide FTIR Spectra is shown for discussion (Fig. 6.1). The FTIR spectra of all the scaffolds was found to be similar. The characteristic peaks for Polyurethane and Hydroxyapatite were identified but no difference was seen between zinc oxide or doped zinc oxide incorporated scaffolds. The characteristic peaks for Hydroxyapatite and Polyurethane can be seen in fig 6.2. The details are stated in table 6.1. The ZnO_2, ZrZnO5, CeZnO5 or CuZnO5 were used in very small amounts that is 1 weight percent which might be completely encapsulated by Polyurethane during scaffold synthesis. The IR only analyses the surface which in this case was polyurethane. However, the hydroxyapatite was higher in concentration i.e. 5 weight percent making it more detectable by FTIR analysis.

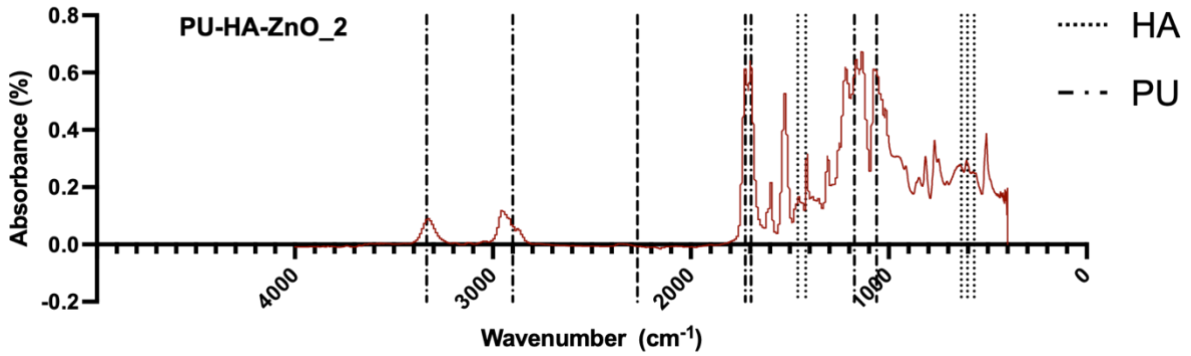

Figure 6.1: *FTIR absorbance Spectra of PU-HA-Zinc oxide_2 composite scaffold showing characteristic peaks for PU and Hydroxyapatite. Data represents mean (n=5).*

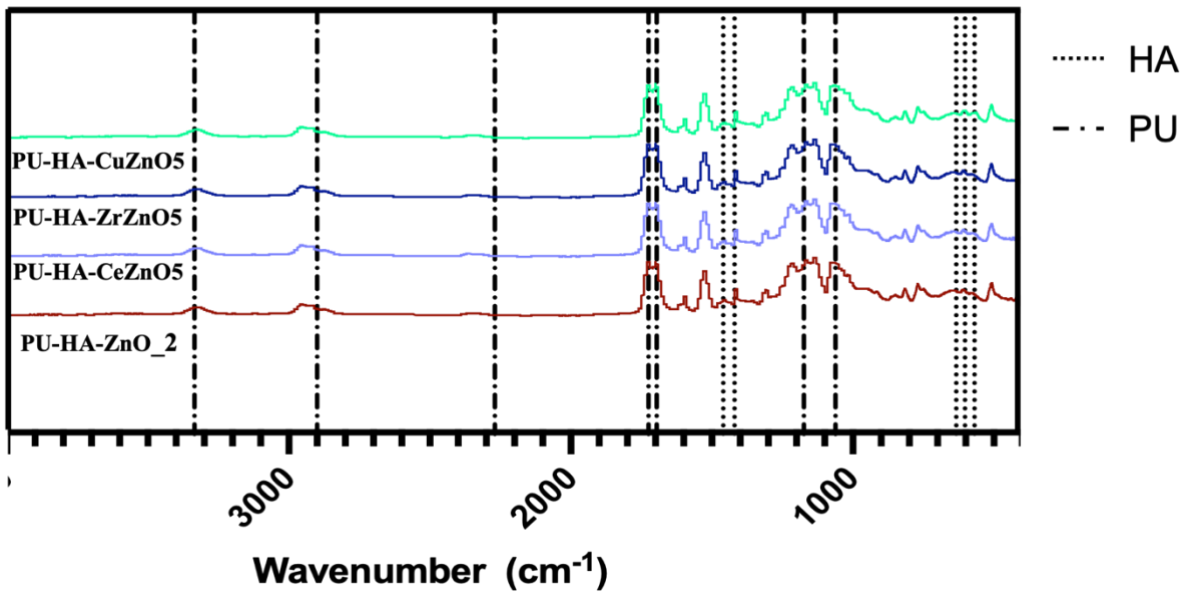

Figure 6.2: *Stacked FTIR absorbance Spectra of PU-HA-ZnO_2, PU-HA-CeZnO5, PU-HA-ZrZnO5 and PU-HA-CuZnO5 composite scaffolds. All spectra were found to have characteristic peaks for PU and Hydroxyapatite.*

Table 6.1: *The FTIR peak analysis for Polyurethane porous scaffolds.*

Hydroxyapatite characteristic peaks (cm^{-1})	**Attribution**	**Reference**
569 603	P-O bending of phosphate group V3	(G. Tetteh et al., 2014)
634	Structural OH^- group stretching and vibration	(G. Tetteh et al., 2014)
1420 1460	V_3 , asymmetric stretching & vibrations of CO_3^{-2} ions CH_2 bending a	(G. Tetteh et al., 2014; Vannozzi et al., 2017)
Polyurethane characteristic Peaks (cm^{-1})		

1725	Ester bonds	(Dias et al., 2010)
1696	Shoulder peak attributed to urethane and carbonyle groups	(Dias et al., 2010)
3335	Stretching of NH bond	(Dias et al., 2010)
2900	Alkane-CH stretching vibrations	(Dias et al., 2010)
1174	C-N & C-O stretching vibrations	(Dias et al., 2010)
1062	C-O-C symmetric stretching	(Dias et al., 2010)
2270	Absent, indicates no unreacted isocyanate groups in scaffolds.	(Dias et al., 2010)

6.4.1.3 Scanning Electron Microscopy (SEM)

The SEM Micrograph of composite scaffolds revealed that the scaffold containing only PU is highly porous and has a rough surface morphology (Fig 6.3). It can be seen that the pores are not distinct and do not have clear boundaries, the morphology is more like a mesh. However, PU scaffolds containing ceramic particles have pores with a more defined structure. The scaffold containing hydroxyapatite only exhibits a few pores with defined boundaries. Scaffolds also containing zinc oxide and doped zinc oxide have a higher number of pores of larger size.

The Zirconium doped zinc oxide, Cerium doped zinc oxide and Copper doped zinc oxide incorporated scaffolds had interconnected pores that were distributed evenly over the surface. However, a rough and highly porous surface can be seen similar to that of cancellous bone or spongy bone tissue. Such surface properties were not observed in scaffolds consisting of only PU, PU-HA or PU-HA-ZnO_2 scaffolds.

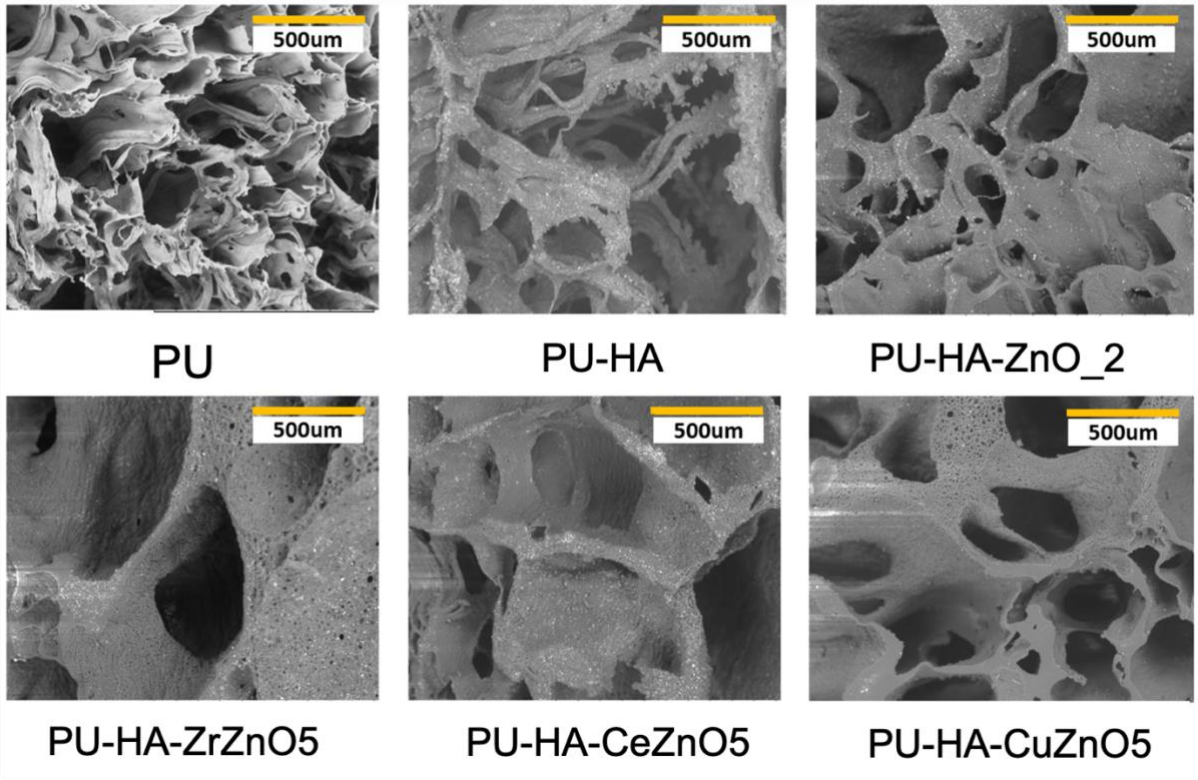

Figure 6.3: *Scanning Electron Microscope micrograph showing porosity distribution in PU, PU-HA, PU-HA-ZnO_2, PU-HA-CeZnO5, PU-HA-ZrZnO5 and PU-HA-CuZnO5*

6.4.1.2 Tensile Testing

The tensile testing analysis revealed that the incorporation of nanoceramics in polyurethane did improve mechanical properties such as yield strength and tensile strength. The hydroxyapatite incorporated scaffold improved the stress bearing capacity due to particle incorporation in the scaffold while decreasing the Young's modulus as compared to polyurethane only scaffold. The ZnO_2 and ZrZnO5 improved the tensile strength from 0.3MPa (PU porous scaffold) to 0.87MPa and 0.81MPa respectively.

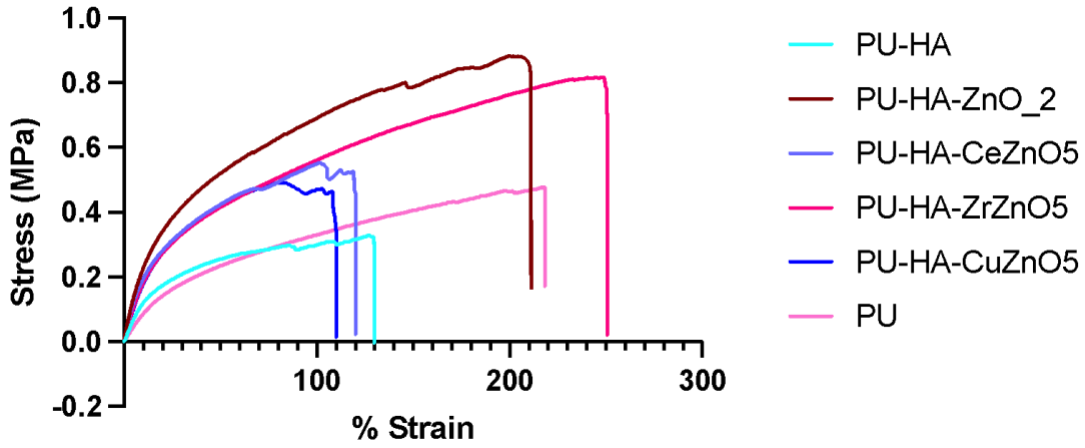

Figure 6.4 : *Tensile properties of composite polyurethane scaffolds. Stress-strain relations of cerium, zirconium and copper doped Zinc oxide incorporated scaffolds confirms differences in tensile strength compared to unmodified Polyurethane scaffolds. Stress Vs Strain curves of PU, PU-HA, PU-HA-ZnO_2, PU-HA-CeZnO5, PU-HA-ZrZnO5 and PU-HA-CuZnO5 were produced. n=5*

Table 6.2: *Mechanical properties of porous scaffolds calculated from stress strain curve.*

Sample name	Young's modulus (MPa)	Yield strength (MPa)	Tensile strength (MPa)	Elongation at break point (% Strain)
PU	0.83	0.10±0.01	0.33±0.02	240±66
PU-HA	0.54	0.17±0.09	0.29±0.09	128.6±43
PU-HA-ZnO_2	0.78	0.4±0.02	0.87±0.02	238.74±85
PU-HA-CeZnO5	0.76	0.3±0.09	0.55±0.09	141.15±24
PU-HA-ZrZnO5	0.66	0.38±0.08	0.81±0.07	249.26±89
PU-HA-CuZnO5	0.64	0.3±0.04	0.57±0.04	180.75±85

6.4.2 Scaffolds Biological properties investigations

6.4.2.1 Cell attachment assay

This is a qualitative analysis. The cell attachment was observed to be the lowest on Polyurethane only foams. The cells were seen as spheres or balled up on PU-HA, PU-HA-ZnO_2, PU-HA-CeZnO5 and CuZnO5 however, cells were spreading out and connected to each other on the scaffold surfaces of ZrZnO5 incorporated scaffolds.

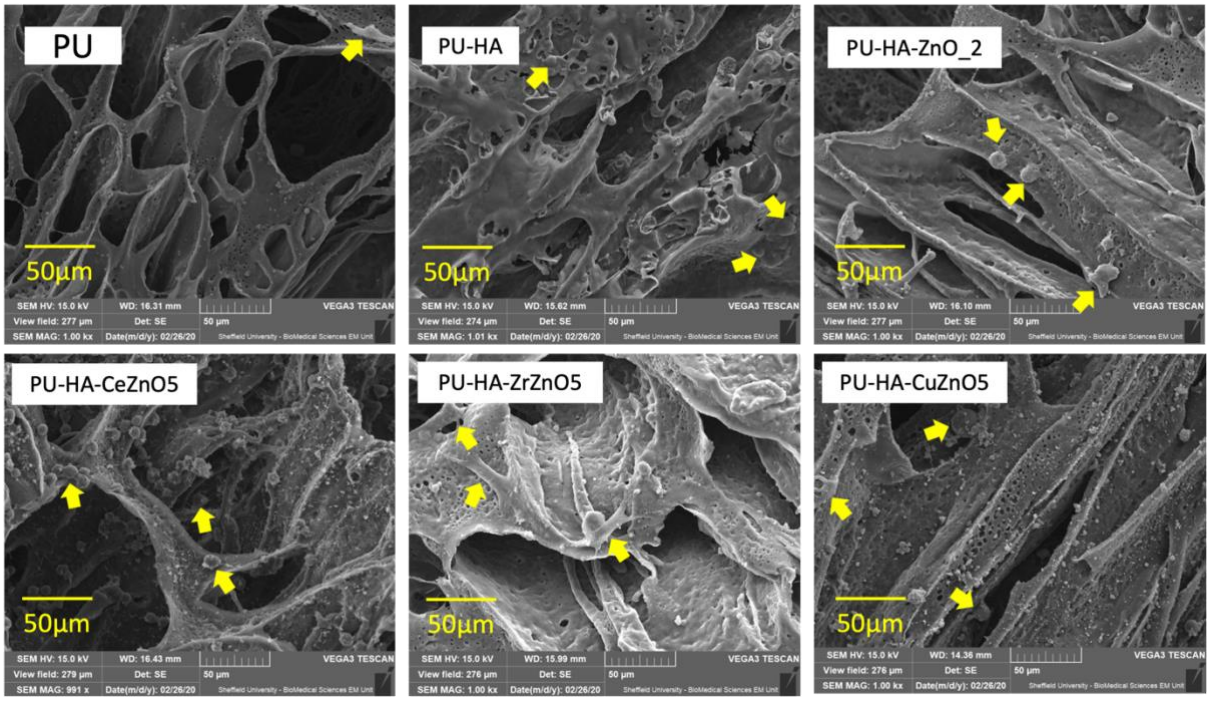

Figure 6.5: *SEM micrographs of cell attachment on Polyurethane porous scaffolds. Cells were seeded on scaffolds overnight. The scaffolds were dehydrated the next day and SEM analysis was performed at a magnification of 1000x.*

6.4.2.2 Cell seeding efficiency

Cell seeding efficiency of Y201s evaluated by resazurin assay which measured cell metabolic activity. The level of cell metabolic activity reflected cell number. The result showed maximum cell attachment on porous scaffolds incorporated with zinc oxide or doped zinc oxide nanoparticles. The polyurethane surface properties were improved with addition of doped zinc oxide nanoparticles, hence making the cell adherence more efficient. The copper doped zinc oxide and cerium doped zinc oxide incorporated scaffolds were found to be the most efficient when it comes to cell attachment as the highest cell metabolic activity was recorded. The lowest was recorded for PU scaffolds containing only hydroxyapatite. The results were compared with PU only scaffold which is the control.

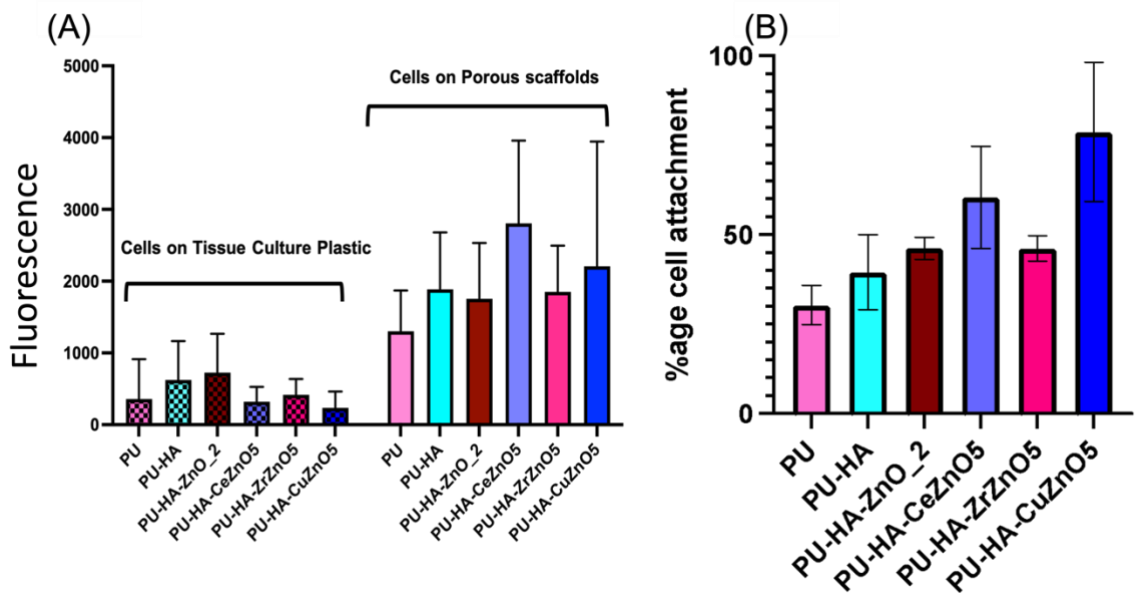

Figure 6.6: *Cell Seeding Efficiency after 16 hours incubation with Y201 cells. The metabolic activity assay was performed to identify viable cells attached on scaffolds and Tissue Culture plastic. A) The scaffolds were transferred to new well plate before performing resazurin assay. B) the percentage cell attachment is shown with control (PU, PU-HA & PU-HA-ZnO_2) being considered 100%. CuZnO5 incorporated scaffolds showed 80% cell attachment. Data represents mean±S.D, n= 3*3*

6.4.2.3 Cell metabolic activity assay

The Y201 cells were seeded on sterilised scaffolds and cell metabolic activity assay was performed at defined time point to evaluate the cell adhesion and proliferation on scaffolds. A Day 3 the highest cell metabolic activity was recorded for Zirconium doped zinc oxide and lowest was recorded for control Polyurethane only scaffold. The doped zinc oxide i.e. Cerium doped zinc oxide, Copper doped zinc oxide and Zirconium doped zinc oxide showed the highest cell metabolic activity demonstrating that the more cells were attached and proliferated on these scaffolds. CeZnO5, ZrZnO5 and CuZnO5 stimulated cell attachment and proliferation as compared to PU or PU HA scaffolds. Over the time of cell culture there was no cell inhibition or cell death with any of the scaffolds. Between day 14 and day 21 there was only a very small increase (if any) in metabolic activity this is likely to be because cells became confluent limiting their ability to proliferate. However, the CuZnO5 incorporated scaffold and CeZnO5 incorporated scaffolds which were lower at day 14 started to reach to the same level. Which clearly shows no cell inhibition or cell death. The data demonstrated that the ZrZnO5 likely stimulated the cells to proliferate at a faster rate as compared to cells on CeZnO5 and CuZnO5 containing scaffolds. Overall, the doped zinc oxide incorporated nanoparticles stimulated the Y201 cells to attach and proliferate better on scaffolds as compared to controls PU, PU-HA or PU-HA-ZnO_2.

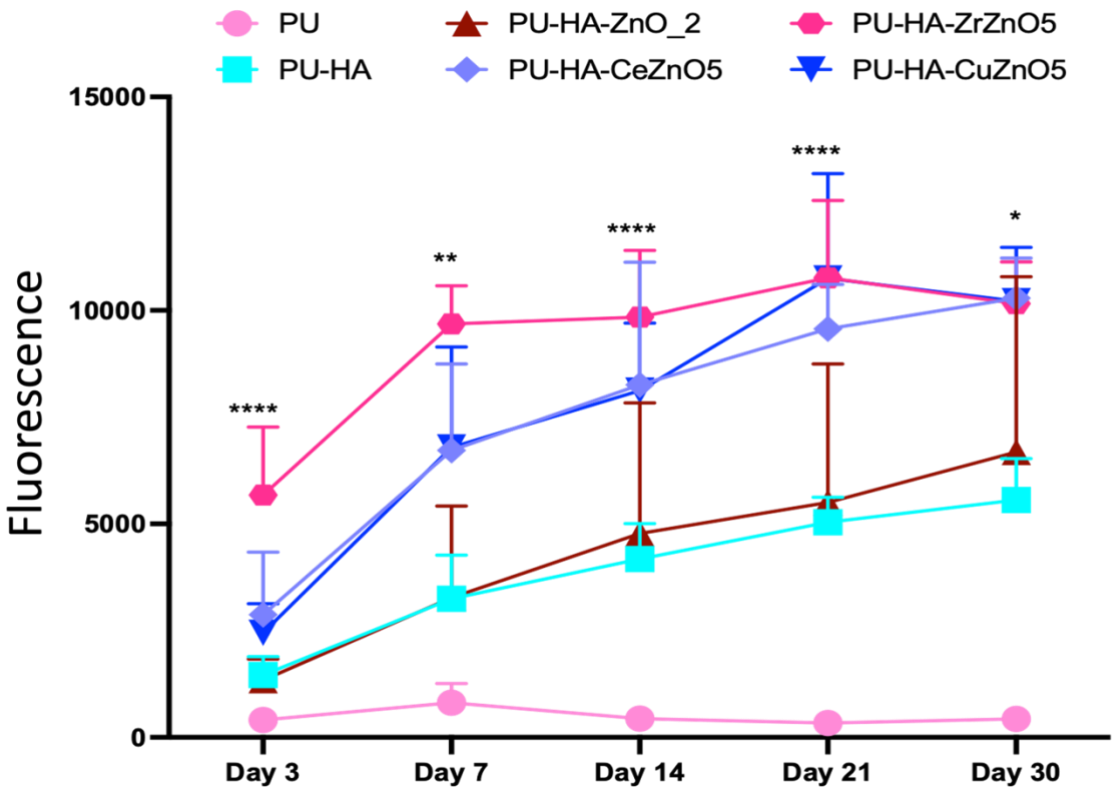

Figure 6.7: *Cell metabolic activity assay showing the proliferation of Y201 cell line on composite scaffolds for 30 days. Data represent ± SD, *p<0.05. n=3*3*

6.4.2.4 Comparison basal media Vs osteogenic media

The cell metabolic activity pattern was the same as fig 6.7. for basal media and osteogenic media supplementation. However, the cell metabolic activity was marginally higher in presence of basal media (fig 6.8).

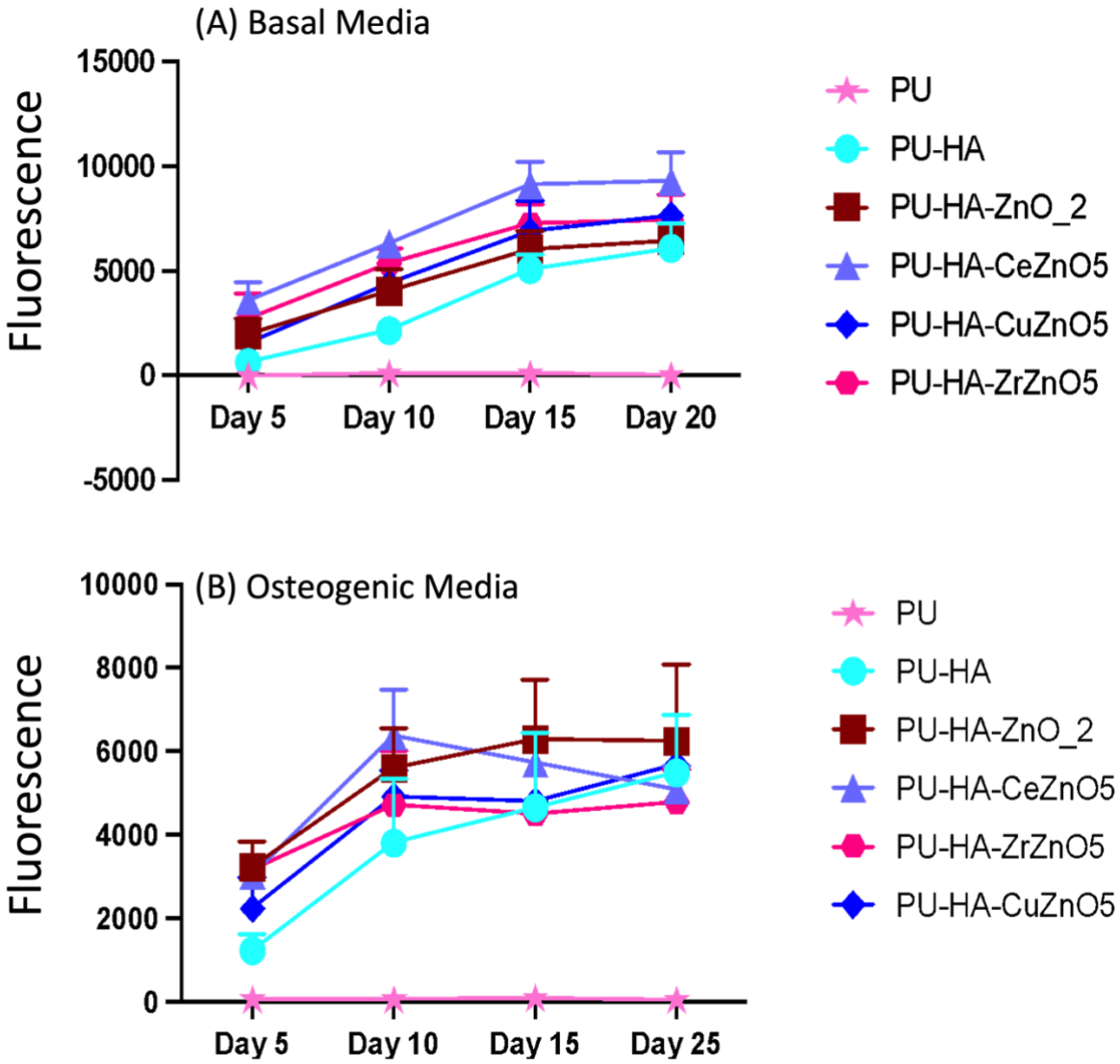

Figure 6.8: *Cell metabolic activity assay showing the proliferation of Y201 cell line on composite scaffolds for 30 days. (A) in Basal Media. (B) in Osteogenic Media. Data shows ± SD, n=3*

6.4.2.5 Alkaline Phosphatase Activity

Y201 cells were seeded on sterilised scaffolds for 20 days. The cell culture medium was changed every 2 days (details mentioned in the methodology chapter). One set of scaffolds was exposed to basal media, the other was exposed to osteogenic media. All the other parameters were kept identical. The experiment was repeated three times in triplicate and the mean is displayed in figure 6.8. The cells grown on scaffolds incorporating hydroxyapatite or ZnO_2 nanoparticles had higher ALP activity in basal medium than only PU scaffolds. The ZrZnO5 incorporated scaffolds elevated the ALP levels in cells in basal medium marginally as compared to CeZnO5 and CuZnO5 incorporated scaffolds.

A similar pattern was observed with osteogenic media, but the ALP levels recorded were significantly higher than for ones in basal media. The CeZnO5 incorporated scaffolds showed improved ALP levels in osteogenic media. Hydroxyapatite, ZnO_2, CeZnO5 and ZrZnO5 showed improved ALP levels with osteogenic media as compared to PU, PU-HA and PU-HA-CuZnO5 (fig 6.9).

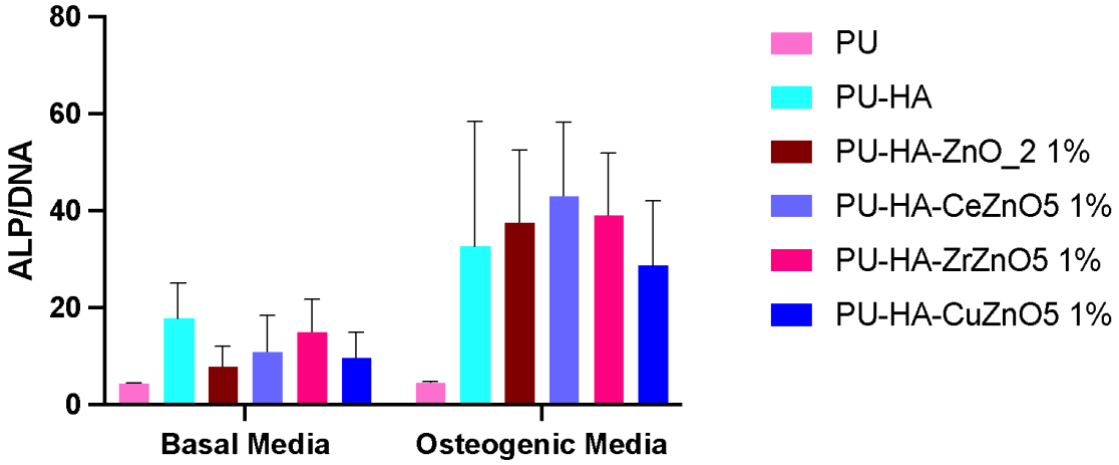

Figure 6.9: *Measurement of ALP enzyme activity in the Y201 cells seeded on Scaffolds incorporated with Polyurethane, Polyurethane Hydroxyapatite, Polyurethane Hydroxyapatite Zinc oxide, Polyurethane Hydroxyapatite CeZnO5, Polyurethane Hydroxyapatite ZrZnO5 and Polyurethane Hydroxyapatite CuZnO5. Data represent mean ± SD, n=3*3.*

6.4.2.6 Vascular Endothelial Growth factor release analysis – VEGF ELISA

The VEGF release in response to composite scaffolds is very important as it facilitates the local microcirculation leading to bone defect healing and regeneration. The data showed no significant change in VEGF release in response to different types of scaffolds. No VEGF release was recorded with Polyurethane only scaffolds which is associated with very low cells metabolic activity. The current data is not sufficient to conclude whether zinc oxide or doped zinc oxide incorporated scaffolds have the potential to encourage cells to release VEGF (fig.6.10). The previous literature reported burst release of VEGF in the first three days, in later days the release becomes steady. The initial burst release is associated with upregulation of BMP-2 which resulted in enhanced vascularisation and bone formation. The VEGF ELISA should be performed in the early days of the experiment to have some conclusive data (B. Li et al., 2017).

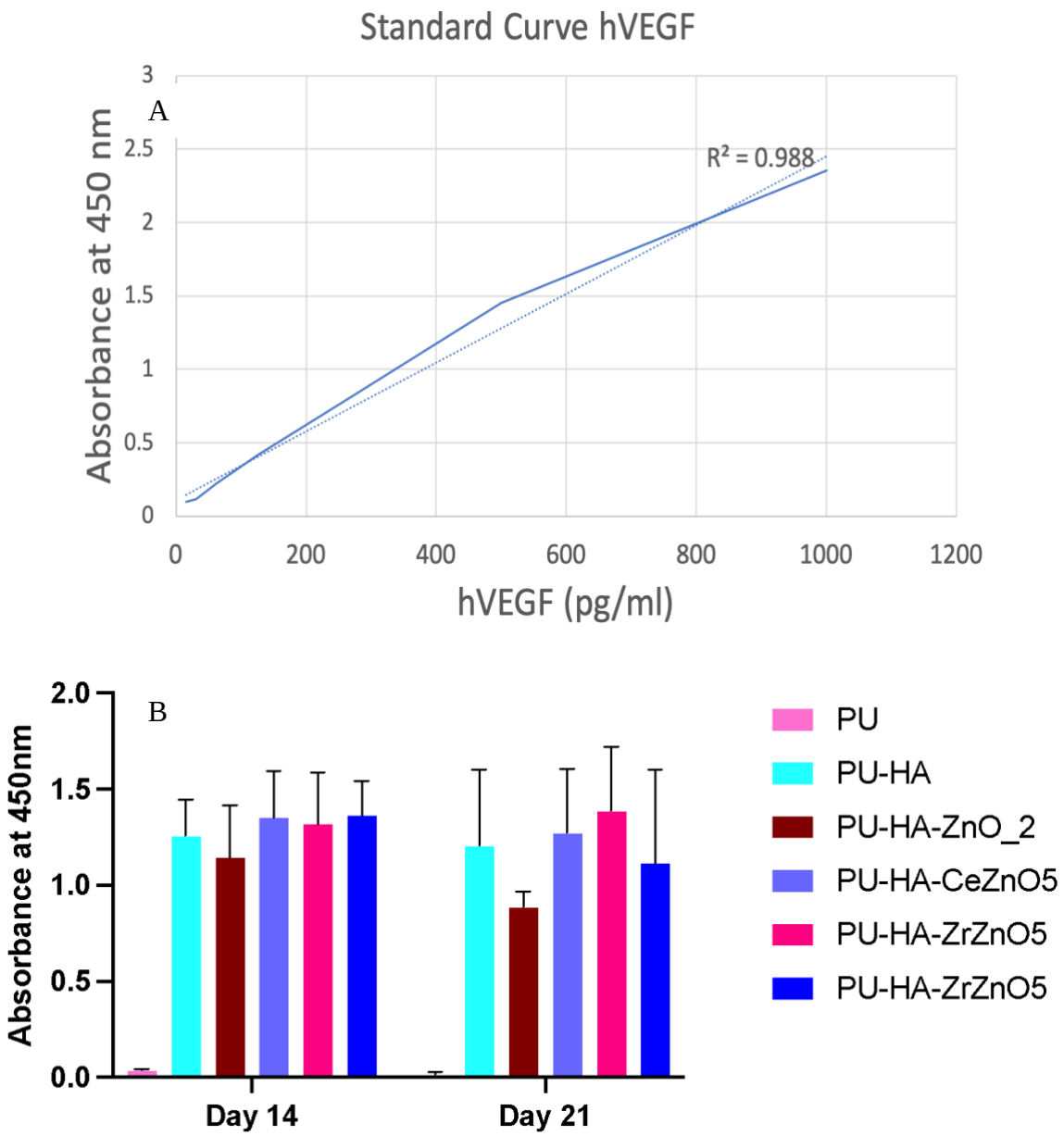

***Figure 6.10**: A) Standard curve for VEGF. B) Vascular Endothelial growth factor (VEGF) release from Y201 cells attached to porous scaffolds. The secreted VEGF concentrations were evaluated in cell culture supernatants at Day 14 and Day 21 (n=3) using VEGF ELISA Kit.*

6.5 Discussion

Composite mechanical properties depend upon the interaction of polymer and ceramic components present in the scaffold. If the interfacial bonding strength between nanoparticles and polymer is enhanced, the load bearing capability of the material improves. The tensile testing of composite scaffolds in this case led to changes in Polyurethane behaviour depending upon which nanoparticles were used. The pure PU scaffold was flexible, However, upon introduction of Hydroxyapatite, the break point was achieved earlier which means the scaffold became brittle with the addition of nanoparticles. The reason could be a weak interfacial interaction between the polymer and Hydroxyapatite (Rajzer, 2014 particles making the scaffold break. A comparative study using nano hydroxyapatite and micro hydroxyapatite polyurethane scaffolds was performed by a previous group member. The study reported higher Young's modulus for scaffolds containing nano hydroxyapatite as compared to the micro hydroxyapatite, osteoid bone formation was also recorded as early as day 7, however, with micro hydroxyapatite, it was recorded at day 45 (Gifty Tetteh, 2016). This data is not directly comparable to present study but does shed some light on importance of using nano particles as compared to micro to improve mechanical properties as well as biological properties to some extent.

The zinc oxide and Zirconium doped zinc oxide in present study was able to increase the yield strength and tensile strength as compared to only Polyurethane which might be a result of strong van der waals interaction (Rajzer, 2014). ZnO_2 and ZrZnO5 addition to PU led to defined porosity which could be the reason for increased ultimate stress levels. The load applied on PU-HA-ZnO_2 and PU-HA-ZrZnO5 might be distributed along the material delaying the break point, hence elongation at break point was recorded higher than the control scaffolds. The optimal tensile properties depend on the application of scaffolds. Fresh frozen cancellous bone strength is reported to have tensile strength 1.8-63.6 MPa, trabecular bone 1-13MPa and tibia 0.2 – 6.2 MPa was recorded respectively (Shkarina et al., 2018). The concentration of nanoparticles and polymer percentages can be adjusted to improve the yield strength and tensile strength to make them suitable for craniofacial bone regeneration purposes.

The nanoparticle addition to polymeric scaffolds also affects the microstructure of the resultant scaffold. The microstructure of the scaffold is very important in the field of bone tissue engineering. The interaction of particles with polymeric chains determines the nature of porosity in the resultant scaffolds. The optimal size of pores and interconnectivity is very important for cell attachment, proliferation, and bone infiltration (Gao et al., 2014). From nanosized pores to a maximum of 500 µm pore size was recorded for scaffolds incorporated with zirconium doped zinc oxide and Copper Doped zinc oxide. This pore size range is reported to influence the exchange of nutrients and waste along with bone ingrowth and angiogenesis. The larger pore size also promotes mineralisation as porosity increases the surface area for apatite formation (Lü et al., 2013).

Cell seeding efficiency and cell attachment assay performed showed that the Y201 cells adhered to scaffolds with bigger pores and higher surface roughness (CeZnO5, ZrZnO5 and CuZnO5). SEM images revealed that the cells started to attach (became flat and well spread) to the scaffolds however, on PU and PU-HA cells looked more globular and still were not attached properly to the surface. The interaction of cells with the scaffolds depends on several factors including surface charge, porosity, roughness and hydrophilicity. The cell friendly scaffold surface allows cells to attach in less time. Well attached cells generally seem flattened and tend to connect to each other, however cells on hydrophobic surfaces or surfaces that do not allow cell adhesion look more rounded. In this study, the cells adhered really well on scaffolds incorporated with ZrZnO5. The finding can be backed up with previous literature where myoblasts adhered to polyurethane scaffolds with higher surface roughness and larger pores (Vannozzi et al., 2017). The nature of adhesion, location and number of adhesion focal points affects the cell-matrix interaction and the cytoskeleton, which are the key factors for cell survival differentiation in bone tissue engineering (Carey et al., 2010). In vitro cell attachment and spreading depend on reorganisation of cytoskeleton in such a way that integrin mediated cell signalling is initiated. The cell adhesion to a surface generally happens in three phases. The first stage is cell attachment to the substrate, followed by flattening and spreading of the cell body, finally organisation of the actin cytoskeleton and formation of focal adhesion points between the cells and the scaffold surface (fig. 6.11) (Khalili & Ahmad, 2015).

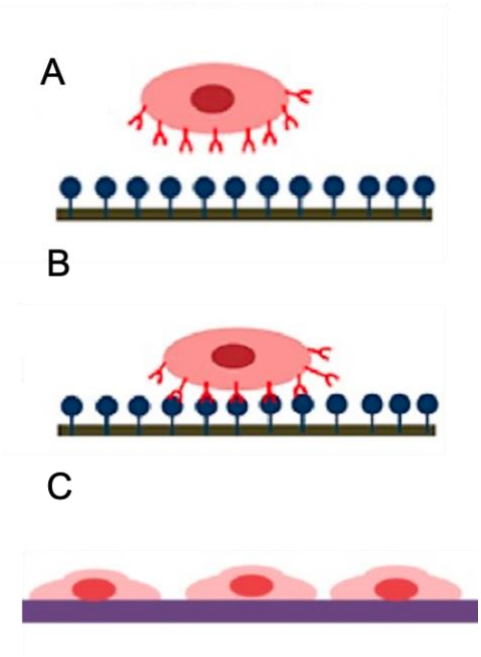

Figure 6.11: *Schematic of cell adhesion to the surface. A) Initial attachment of cells and surface. B) Flattening or cell onto the surface C) Fully spreading or cells on the surface.*

The Y201 cells were left to grow on scaffolds for up to 30 days to evaluate cell proliferation with reference to cell metabolic activity at regular intervals. The Cerium, Copper and Zirconium doping into zinc oxide individually had benefits on cell adhesion and proliferation as discussed in previous chapters. The CeZnO5 contained a CeO_2 phase which is a stable trivalent state and acts as an antioxidant, this means it regulates oxygen levels which are critical for cell growth. That might be the reason for better cell proliferation in the case of CeZnO5 incorporated scaffolds as compared to PU, PU-HA or ZnO_2.

The scaffold surface properties play an important role in cell adhesion and proliferation. The cells respond to macro roughness (100 µm to mm) or microroughness (100 nm-100 µm) in different manners. A study was performed on polycaprolactone rough membranes using osteoblast cells. Reduced or inhibited adhesion and proliferation was recorded with increased pore size due to surface discontinuity (fig. 6.12), however, an increase in microroughness (200 µm) resulted in improved cell differentiation, ALP activity and osteocalcin expression (De Bartolo et al., 2008).

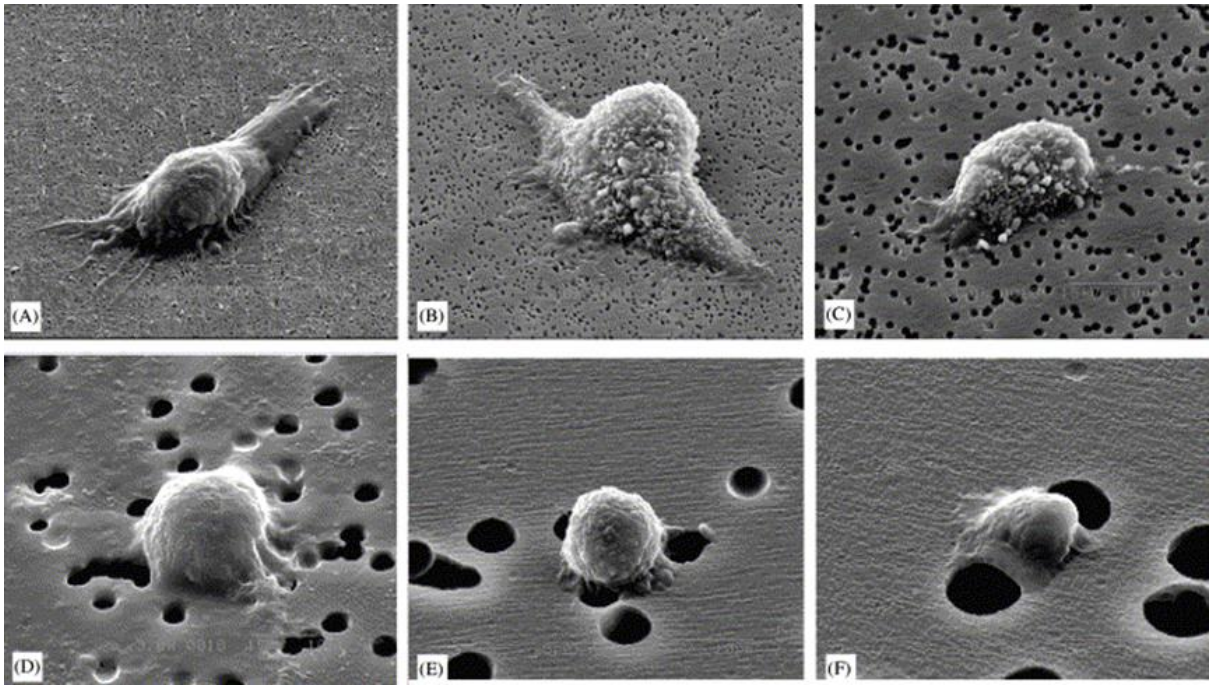

Figure 6.12: *MG63 cell attachment on micro and macrorough surfaces. A) 0.2 mm pores B) 0.4mm pores C) 1.0 mm Pores D) 3.0mm pores E) 5.0mm pores F) 8.0mm pore. Image is used under Creative Commons Attribution-NonCommercial-ShareAlike-3.0 License,* (S. J. Lee et al., 2004)

The size of individual pores has also been found to be important for cell seeding efficiency. As the size of pores aids cell attachment to the surface. PLA and PLGA scaffolds synthesised via a salt leaching process were synthesised, and the average pore size recorded was 160 µm. The 160 µm pore size was found to be optimal for attachment of human skin fibroblast cells. PMMA scaffolds with a pore size of 450 µm were found to be better for bone cell infiltration and growth (Ashman & Moss, 1977; Jian Yang et al., 2002). The pore interconnectivity is of huge importance especially when comes to cells infiltration, osteogenesis or angiogenesis. 150-300 µm porosity, highly interconnected polyurethane meniscal implants were investigated, and fibrocartilaginous tissue ingrowth was evidenced (C.-G. Wu et al., 1996). Another study reported that the osteoblast cells migrate at much faster rate when the porosity is 100 µm in polyHIPE scaffolds, however, no difference was observed for mineralisation or cell penetration. High pore interconnectivity is also essential for nutrient supply and oxygen exchange which is critical for cell viability (Akay et al., 2004).

The zirconium doped zinc oxide incorporation into scaffolds increased the porosity which is a favourable factor for cell attachment and proliferation as per literature available .(Ashman & Moss, 1977; Jian Yang et al., 2002). The pore interconnectivity was not investigated in this study so I can only speculate that the pores might be more interconnected leading to better cell metabolic activity relative to control scaffolds. Another likely reason could be the reduced zeta potential for ZrZnO5 or Zinc oxide leading to less repulsive forces between proteins (fibronectin) and scaffolds. Fibronectin increases the cell attachment capacity and hence leads to cell proliferation. Copper ions as mentioned in chapter 5 can induce bone regeneration when used in low quantities (Mourino et al., 2012). The CuZnO5 used in scaffolds was 1%is a very low quantity and it was found to be non-toxic for Y201 cells and hES-MPs (discussed in previous chapter). It also induces the proliferation of Y201 cells and higher metabolic activity was recorded compared to controls. The pathway by which copper induces proliferation is yet unclear. Based on literature and current data copper is proangiogenic. Copper ions induce formation of blood vessels resulting in recruitment of bone cells for bone formation. Upon comparison of all the doped zinc oxide scaffolds, Cerium and copper doped zinc oxide containing scaffolds demonstrated better cell attachment. The metabolic activity recorded was maximum for ZrZnO5 scaffold until Day 14 and cells in cerium and copper doped zinc oxide scaffolds reached the same confluence at Day 21. The data showed that the zirconium doped zinc oxide scaffold provided the cells with conditions to attach, proliferate and connect to each other. The reason might be better porosity and roughness for cell adhesion and proliferation leading to increase in metabolic activity. No cell death or growth inhibition was seen. However, the cell metabolic activity was recorded to be higher for cerium and copper as well as compared to control, and the scaffolds became confluent by Day 30 with no cell death or inhibition recorded. Further studies can be performed to explore the bone regenerative and angiogenic capacity of these scaffolds. But based on current data PU-HA-ZrZnO5 is overall more promising than PU-HA-CeZnO5 and PU-HA-CuZnO5.

6.6 Conclusions

The doped zinc oxide nanoparticles certainly are more effective under the conditions examined here compared to only zinc oxide nanoparticles. Ionic dopings into a zinc oxide lattice are a good way to prevent the burst release of ions which was reported to have toxic effects on cells. Cerium, copper, and zirconium dopings were performed and resulted in improved physical and biological properties. The scaffolds incorporated with doped zinc oxide nanoparticles resulted in uniform porous scaffolds with maximum pore size of about 500 µm. Nanosized pores or rough surfaces were obtained similar to that seen for cancellous bone. The cells attached better to these scaffolds with maximum cell attachment recorded for cerium and copper doped zinc oxide incorporated scaffolds. The zirconium doped zinc oxide incorporated scaffolds were found to have improved tensile properties and scaffold microstructure. Selecting a scaffold is a critical process as it involves balancing physical, chemical and biological properties.

Chapter 7 Final Discussion and Future work

Bone repair and regeneration is a complex process and involves a critical balance between upregulation of growth factors, recruitment of cells and bone formation. A need for composite scaffolds supporting this process and accelerating it is the purpose of bone tissue engineering research. Zinc oxide in the field of bone tissue engineering is becoming popular because of its effect on upregulation of fibroblast growth factor (FGF) and Vascular endothelial growth factor (VEGF) leading to angiogenesis and osteogenesis. A few studies on polyurethane and zinc oxide composite scaffolds have been published concluding the efficiency of the scaffolds for cell adhesion and proliferation. Polyurethane/zinc oxide composite scaffolds have been studied (discussed in the literature review section) and it was demonstrated that the lower zinc oxide concentration (0.5 to 5 wt %) improved the cell attachment and proliferation of the scaffolds (Y. Wang et al., 2020). This research was focused on doping cerium, zirconium and copper ions to zinc oxide. In the previous chapter, the synthesis of cerium, zirconium and copper doped zinc oxide have been discussed. The chemical, physical and biological characterisation of these nanoparticles were performed and porous composite scaffolds with polyurethane/hydroxyapatite base were synthesised. The 3D foam like scaffolds were investigated for its potential as a bone regenerative scaffold by performing cell seeding efficiency, cell metabolic activity assay, Alkaline Phosphate Activity (ALP) Assay and Vascular Endothelial Growth Factor detection ELISA analysis (VEGF). ALP and VEGF assays are the preliminary assays for mineralisation and angiogenesis, Increased levels of ALP and VEGF may contribute towards mineralisation and angiogenesis.

The novelty of the current study lies in synthesis of cerium, zirconium and copper doped zinc oxide for bone tissue engineering applications. The synthesis of these metallic dopings have been reported in a limited number of studies for photocatalysis applications. To my knowledge here we are the first to explore the biological properties of these dopants. The cell metabolic activity assay of cells exposed to compounds containing cerium, zirconium and copper doped zinc oxide was performed for the first time, and it was revealed that the presence of these nanoparticles does play an important role in supporting in cell metabolic activity compared to cells exposed only to standard cell culture media. The cell metabolic

activity of cells exposed to doped zinc oxide was comparable with the pure zinc oxide based on cell metabolic activity assays. So far cerium, zirconium and copper doped zinc oxide loaded scaffolds supported improved cell attachment and proliferation and stimulated ALP activity, a common marker of osteogenic differentiation. The data indicated that doped zinc oxides may improve osteogenesis compared to scaffolds containing only hydroxyapatite or pure zinc oxide. To date, this study is the first to report the lack of cytotoxicity and healthy cell metabolic activity of cells exposed to this composite formulation.

7.1 Limitations of the study:

1. The scaffolds were auto-fluorescent making it impossible to use immunostaining techniques such as DAPI/Phalloidin to investigate the number of nuclei and gross cell morphology on the scaffolds.
2. The composite scaffolds were retaining excess dye from Sirius red and Alizarin red hence we couldn't perform mineralisation study using this method.
2. The VEGF Assay was performed at late time points (Day 14 & Day 21). However, VEGF is typically burst release at early time points in cell culture and the release kinetics then become steady or constant over time. This means that the VEGF data is ambiguous. Also, the assay was performed with cell culture supernatant, and the media used for cell culture was supplemented with serum which can contain small amounts of VEGF that might have interfered with our data.

7.2 Short term future works

The short-term future work would be to rectify the limitations of the study which we were unable to do due to covid19.

7.2.1 Detection of PCR markers for osteogenesis:

The first and foremost priority would be to use RT-PCR to detect early markers of osteogenesis such as Runx-2, ON, OCN, OPN, BMP-2, and COL1 (Bou Assaf et al., 2019). We planned to perform quantitative real-time PCR at different time points to evaluate the osteoinductive potential of doped zinc oxide incorporated Scaffolds.

7.2.2 VEGF release detection:

To get a complete understanding of VEGF release and effect of doped zinc oxide incorporated scaffolds VEGF should be performed at different time points starting from Day 1. The test would be repeated at different timepoints and without serum supplementation. That way the data would be better interpretable.

7.2.3 Chicken Chorioallantoic membrane Assay (CAM):

Chicken Chorioallantoic membrane Assay (CAM) for Angiogenesis would be performed. To determine the ability of doped zinc oxide incorporated Polyurethane composite scaffolds to promote angiogenesis a CAM assay could be carried out. Fertilised chicken eggs will be taken and labelled carefully. The eggs will be incubated at 37°C 65% humidity. On day 8, 3 cm cut, or hole will be created to access the chorioallantoic membrane, 2 cm^2 sized scaffold (sterilised) will be carefully placed on the membrane. The hole will be closed using parafilm to prevent dehydration and possible contaminants. The eggs will be returned to an incubator and analysed after 2 days. The blood vessels will be counted manually around the scaffold in clockwise direction (Augustine, Malik, et al., 2014).

Finally, to better understand the properties and safety of the scaffolds, detailed characterisation is required such as degradation and wettability.

7.2.4. Degradation:

The degradation study would be based on mass loss over the time. The pre-weighed scaffolds would be submerged in PBS and the weight loss recorded every 5 days for up to 30 days. The PBS would be replaced every 5 days and analysed using UV Vis spectrophotometer, FTIR and HPLC for released substances. This study would provide a better understanding of the scaffold's degradation products and the ionic release profile.

7.3 The long-term future Goals:

7.3.1 Scaffold Fabrication Technique:

The scaffold synthesis was performed using a freeze extraction salt leaching process. The process is economical, but it is not easily reproducible and there can be batch to batch and scaffold to scaffold variability. The technique can be made better by controlling the conditions such as using Teflon moulds and dedicated freezer for freezing the moulds. This would allow the quick freeze of the scaffolds before the porogen starts to settle down. The porosity will be optimised and controlled by controlling the size of the porogen. The open pores with interconnectivity are very important for tissue engineering and angiogenesis. To determine the nature of porosity, Micro CT analysis will be performed to analyse if the pores are interconnective and what is the difference between different ionic dopings as the current study did give some information of change in porosity due to different dopings.

7.3.2 Cellular uptake of zinc oxide & doped zinc oxide:

Osteogenic cells will be grown for 24 hours in the presence of zinc oxide or doped zinc oxide suspension followed by PBS washing, trypsin treatment, collection of cells via centrifugation. The collected cells will be re-suspended in Trump's Fixative (A combination of Sodium Cacodylate, Formalin, and Glutaraldehyde used to fix cellular samples before Electron

Microscopy). The SEM will be performed to see if the nanoparticles are entering into the cells and if the type of particle is causing any change in cells' morphology. If reliable data is not obtained using SEM, thin sections will be cut and TEM will be performed.

7.3.3 Determination of Reactive Oxidative Species (ROS)

The reactive oxidative species plays an important role in angiogenesis. Y201 and hES-MPs cells will be treated with zinc oxide suspension for 24 hours followed by florescence microscopy. The samples will be excited at wavelength λEX = 488nm (blue) and green florescence emission will be detected λEM = 525 nm which indicates the presence of ROS.

7.3.4 Matrigel analysis for tubule formation:

Capillary tube formation Assay will be done using vascular endothelial cells (HUVEC). The cells will be cultured in presence of doped zinc oxide suspensions. For this test, 10 µL of Matrigel will be transferred to well plates followed by addition of 50 µL cell suspension/nanoparticle suspension. The plates will be stored in a CO2 incubator under standard cell culture conditions and analysed after 5- and 24-hours using phase-contrast inverted microscopy. This assay will demonstrate the effect of nanoparticles on HUVEC proliferation and microtubule formation. This would act as a model for neovascularisation. This is a two-dimensional in vitro assay and reliable results can be obtained in less amount of time as compared to CAM. The assay can be performed on all the nanoparticles to identify pro-angiogenic potential. Capillary tube formation assay can reliably detect the weak proangiogenic agents as compared to CAM assay (evaluation of angiogenesis assays).

After performing in vitro and in vivo testing, the scaffolds will be ready for animal testing and finally a clinical study for craniofacial bone repair and regeneration.

7.4 Conclusions

The focus of this thesis was on development of improved biomaterials for regenerative biomedicine. At first, a high throughput, eco-friendly synthesis method for nanoparticles was selected. The zinc oxide and doped zinc oxide nanoparticles were successfully synthesised using a pilot continuous hydrothermal flow system. All the ceramic particles obtained were under 100 nm and did not pose any cytotoxic effects on MG63 or hES-MP cells. The porous scaffolds synthesised using these nanoparticles were found to improve the cell adhesion and proliferation properties when tested with the Y201 cell line. Cell attachment was improved due to cerium, copper and zirconium doping of zinc oxide when compared with pure zinc oxide or Hydroxyapatite containing scaffolds. The three dopings individually were found to benefit cell adhesion and proliferation as compared to controls however, ZrZnO5 was found to improve the cell metabolic activity at early days. The doped zinc oxide nanoparticles were found to increase the ALP levels as well which is the early marker for osteogenesis. The highest VEGF was also recorded for ZrZnO5 incorporated scaffolds, hence making the doped zinc oxide a potential source for future bone regenerative scaffolds. The current research explored the biological properties of doped zinc oxide and the above-mentioned future work would lead to better understanding of these particles and their uses for tissue engineering applications. Better understanding of the physical, chemical and biological properties of cerium, zirconium and copper doped zinc oxide nanoparticles will lay the foundation of customisation of scaffolds for angiogenesis and osteogenesis.

References

Abd-Ellah, M., Moghimi, N., Zhang, L., Thomas, J. P., McGillivray, D., Srivastava, S., & Leung, K. T. (2016). Plasmonic gold nanoparticles for ZnO-nanotube photoanodes in dye-sensitized solar cell application. *Nanoscale*, *8*(3), 1658–1664.

Adair, THOMAS H, Gay, W. J., & Montani, J.-P. (1990). Growth regulation of the vascular system: evidence for a metabolic hypothesis. *American Journal of Physiology-Regulatory, Integrative and Comparative Physiology*, *259*(3), R393–R404.

Adair, Thomas H, & Montani, J.-P. (2010). Overview of angiogenesis. *Angiogenesis*, 1–8.

Ahtzaz, S., Nasir, M., Shahzadi, L., Amir, W., Anjum, A., Arshad, R., Iqbal, F., Chaudhry, A. A., Yar, M., & ur Rehman, I. (2017). A study on the effect of zinc oxide and zinc peroxide nanoparticles to enhance angiogenesis-pro-angiogenic grafts for tissue regeneration applications. *Materials & Design*, *132*, 409–418.

Akay, G., Birch, M. A., & Bokhari, M. A. (2004). Microcellular polyHIPE polymer supports osteoblast growth and bone formation in vitro. *Biomaterials*, *25*(18), 3991–4000.

Alhamoudi, F. H., Akhtar, H., Almoshawah, Y., Talari, A. C., Chaudhry, A. A., Reilly, G. C., & Rehman, I. U. (2021). *Bioactive Nano Hydroxyapatites for Orbital Floor Repair and Regeneration*.

Amna, T., Hassan, M. S., Sheikh, F. A., Lee, H. K., Seo, K.-S., Yoon, D., & Hwang, I. H. (2013). Zinc oxide-doped poly (urethane) spider web nanofibrous scaffold via one-step electrospinning: a novel matrix for tissue engineering. *Applied Microbiology and Biotechnology*, *97*(4), 1725–1734.

An, S.-H., Matsumoto, T., Miyajima, H., Nakahira, A., Kim, K.-H., & Imazato, S. (2012). Porous zirconia/hydroxyapatite scaffolds for bone reconstruction. *Dental Materials*, *28*(12), 1221–1231.

Anselme, K. (2000). Osteoblast adhesion on biomaterials. *Biomaterials*, *21*(7), 667–681.

Ashman, A., & Moss, M. L. (1977). Implantation of porous polymethylmethacrylate resin for tooth and bone replacement. *The Journal of Prosthetic Dentistry*, *37*(6), 657–665.

Augustine, R., Dan, P., Sosnik, A., Kalarikkal, N., Tran, N., Vincent, B., Thomas, S., Menu, P., & Rouxel, D. (2017). Electrospun poly (vinylidene fluoride-trifluoroethylene)/zinc oxide nanocomposite tissue engineering scaffolds with enhanced cell adhesion and blood vessel formation. *Nano Research*, *10*(10), 3358–3376.

Augustine, R., Dominic, E. A., Reju, I., Kaimal, B., Kalarikkal, N., & Thomas, S. (2014a). Electrospun polycaprolactone membranes incorporated with ZnO nanoparticles as skin

substitutes with enhanced fibroblast proliferation and wound healing. *RSC Advances*, *4*(47), 24777–24785.

Augustine, R., Dominic, E. A., Reju, I., Kaimal, B., Kalarikkal, N., & Thomas, S. (2014b). Investigation of angiogenesis and its mechanism using zinc oxide nanoparticle-loaded electrospun tissue engineering scaffolds. *RSC Advances*, *4*(93), 51528–51536.

Augustine, R., Malik, H. N., Singhal, D. K., Mukherjee, A., Malakar, D., Kalarikkal, N., & Thomas, S. (2014). Electrospun polycaprolactone/ZnO nanocomposite membranes as biomaterials with antibacterial and cell adhesion properties. *Journal of Polymer Research*, *21*(3), 1–17.

Baker, S. B., Weinzweig, J., Kirschner, R. E., & Bartlett, S. P. (2002). Applications of a new carbonated calcium phosphate bone cement: early experience in pediatric and adult craniofacial reconstruction. *Plastic and Reconstructive Surgery*, *109*(6), 1789–1796.

Bari, A., Bloise, N., Fiorilli, S., Novajra, G., Vallet-Regí, M., Bruni, G., Torres-Pardo, A., González-Calbet, J. M., Visai, L., & Vitale-Brovarone, C. (2017). Copper-containing mesoporous bioactive glass nanoparticles as multifunctional agent for bone regeneration. *Acta Biomaterialia*, *55*, 493–504.

Barui, A. K., Veeriah, V., Mukherjee, S., Manna, J., Patel, A. K., Patra, S., Pal, K., Murali, S., Rana, R. K., & Chatterjee, S. (2012). Zinc oxide nanoflowers make new blood vessels. *Nanoscale*, *4*(24), 7861–7869.

Baruwati, B., Kumar, D. K., & Manorama, S. V. (2006). Hydrothermal synthesis of highly crystalline ZnO nanoparticles: A competitive sensor for LPG and EtOH. *Sensors and Actuators B: Chemical*, *119*(2), 676–682.

Bejarano, J., Detsch, R., Boccaccini, A. R., & Palza, H. (2017). PDLLA scaffolds with Cu- and Zn-doped bioactive glasses having multifunctional properties for bone regeneration. *Journal of Biomedical Materials Research Part A*, *105*(3), 746–756.

Benic, G. I., Thoma, D. S., Sanz-Martin, I., Munoz, F., Hämmerle, C. H. F., Cantalapiedra, A., Fischer, J., & Jung, R. E. (2017). Guided bone regeneration at zirconia and titanium dental implants: a pilot histological investigation. *Clinical Oral Implants Research*, *28*(12), 1592–1599.

Bhadada, S. V, Goyal, B. R., & Patel, M. M. (2011). Angiogenic targets for potential disorders. *Fundamental & Clinical Pharmacology*, *25*(1), 29–47.

Bielenberg, D. R., & D'Amore, P. A. (2008). Judah Folkman's contribution to the inhibition of angiogenesis. *Lymphatic Research and Biology*, *6*(3–4), 203–207.

Bonewald, L. F. (2002). Transforming growth factor-β. In *Principles of Bone Biology (Second Edition)* (pp. 903–918). Elsevier.

Bou Assaf, R., Fayyad-Kazan, M., Al-Nemer, F., Makki, R., Fayyad-Kazan, H., Badran, B., & Berbéri, A. (2019). Evaluation of the osteogenic potential of different scaffolds embedded with human stem cells originated from Schneiderian membrane: an in vitro study. *BioMed Research International*, *2019*.

Boyan, B. D., Lohmann, C. H., Sisk, M., Liu, Y., Sylvia, V. L., Cochran, D. L., Dean, D. D., & Schwartz, Z. (2001). Both cyclooxygenase-1 and cyclooxygenase-2 mediate osteoblast response to titanium surface roughness. *Journal of Biomedical Materials Research Part A*, *55*(3), 350–359.

Bramfeld, H., Sabra, G., Centis, V., & Vermette, P. (2010). Scaffold vascularization: a challenge for three-dimensional tissue engineering. *Current Medicinal Chemistry*, *17*(33), 3944–3967.

Bueno-Ferrer, C., Parres-Esclapez, S., Lozano-Castelló, D., & Bueno-López, A. (2010). Relationship between surface area and crystal size of pure and doped cerium oxides. *Journal of Rare Earths*, *28*(5), 647–653.

Burke, M., & Goodman, S. (2008). Failure mechanisms in joint replacement. In *Joint replacement technology* (pp. 264–285). Elsevier.

Burkus, J. K., Transfeldt, E. E., Kitchel, S. H., Watkins, R. G., & Balderston, R. A. (2002). Clinical and radiographic outcomes of anterior lumbar interbody fusion using recombinant human bone morphogenetic protein-2. *Spine*, *27*(21), 2396–2408.

Burri, P. H., Hlushchuk, R., & Djonov, V. (2004). Intussusceptive angiogenesis: its emergence, its characteristics, and its significance. *Developmental Dynamics*, *231*(3), 474–488.

Butscher, A., Bohner, M., Hofmann, S., Gauckler, L., & Müller, R. (2011). Structural and material approaches to bone tissue engineering in powder-based three-dimensional printing. *Acta Biomaterialia*, *7*(3), 907–920.

Bužarovska, A., Dinescu, S., Lazar, A. D., Serban, M., Pircalabioru, G. G., Costache, M., Gualandi, C., & Avérous, L. (2019). Nanocomposite foams based on flexible biobased thermoplastic polyurethane and ZnO nanoparticles as potential wound dressing materials. *Materials Science and Engineering: C*, *104*, 109893.

Cai, K., Frant, M., Bossert, J., Hildebrand, G., Liefeith, K., & Jandt, K. D. (2006). Surface functionalized titanium thin films: zeta-potential, protein adsorption and cell

proliferation. *Colloids and Surfaces B: Biointerfaces*, *50*(1), 1–8.

Calestani, D., Zha, M., Mosca, R., Zappettini, A., Carotta, M. C., Di Natale, V., & Zanotti, L. (2010). Growth of ZnO tetrapods for nanostructure-based gas sensors. *Sensors and Actuators B: Chemical*, *144*(2), 472–478.

Cao, G. (2004). *Nanostructures & nanomaterials: synthesis, properties & applications*. Imperial college press.

Carey, S. P., Charest, J. M., & Reinhart-King, C. A. (2010). Forces during cell adhesion and spreading: implications for cellular homeostasis. In *Cellular and biomolecular mechanics and mechanobiology* (pp. 29–69). Springer.

Carmeliet, P. (2003). Angiogenesis in health and disease. *Nature Medicine*, *9*(6), 653.

Carmeliet, P., De Smet, F., Loges, S., & Mazzone, M. (2009). Branching morphogenesis and antiangiogenesis candidates: tip cells lead the way. *Nature Reviews Clinical Oncology*, *6*(6), 315.

Carragee, E. J., Hurwitz, E. L., & Weiner, B. K. (2011). A critical review of recombinant human bone morphogenetic protein-2 trials in spinal surgery: emerging safety concerns and lessons learned. *The Spine Journal*, *11*(6), 471–491.

Castañeda, L. (2013). Fabrication of transparent conductive zinc oxide Co-doped with fluorine and zirconium thin solid films by ultrasonic chemical pyrolysis: effects of precursor solution aging and substrate temperature. *Journal of Coatings*, *2013*.

Chatkaewsueb, S., Saysunee, N., & Tamaekong, N. (2017). The synthesis and characterization of p-CuO/n-ZnO nanoparticles synthesized by chemical method. *Materials Today: Proceedings*, *4*(5), 6111–6117.

Chen, P., Gu, L., Xue, X., Song, Y., Zhu, L., & Cao, X. (2010). Facile synthesis of highly uniform ZnO multipods as the supports of Au and Ag nanoparticles. *Materials Chemistry and Physics*, *122*(1), 41–48.

Chevalier, J. (2006). What future for zirconia as a biomaterial? *Biomaterials*, *27*(4), 535–543.

Chien, S. (2007). Mechanotransduction and endothelial cell homeostasis: the wisdom of the cell. *American Journal of Physiology-Heart and Circulatory Physiology*, *292*(3), H1209–H1224.

Chouchene, B., Chaabane, T. Ben, Balan, L., Girot, E., Mozet, K., Medjahdi, G., & Schneider, R. (2016). High performance Ce-doped ZnO nanorods for sunlight-driven photocatalysis. *Beilstein Journal of Nanotechnology*, *7*, 1338.

Choudhury, S. R., Ordaz, J., Lo, C.-L., Damayanti, N. P., Zhou, F., & Irudayaraj, J. (2017).

From the cover: zinc oxide nanoparticles-induced reactive oxygen species promotes multimodal cyto-and epigenetic toxicity. *Toxicological Sciences*, *156*(1), 261–274.

Clament Sagaya Selvam, N., Vijaya, J. J., & Kennedy, L. J. (2012). Effects of morphology and Zr doping on structural, optical, and photocatalytic properties of ZnO nanostructures. *Industrial & Engineering Chemistry Research*, *51*(50), 16333–16345.

Colon, G., Ward, B. C., & Webster, T. J. (2006). Increased osteoblast and decreased Staphylococcus epidermidis functions on nanophase ZnO and TiO2. *Journal of Biomedical Materials Research Part A*, *78*(3), 595–604.

Critchlow, M. A., Bland, Y. S., & Ashhurst, D. E. (1995). The effect of exogenous transforming growth factor-β2 on healing fractures in the rabbit. *Bone*, *16*(5), 521–527.

Cushing, B. L., Kolesnichenko, V. L., & O'Connor, C. J. (2004). Recent advances in the liquid-phase syntheses of inorganic nanoparticles. *Chemical Reviews*, *104*(9), 3893–3946.

D'Mello, S., Elangovan, S., Hong, L., Ross, R. D., Sumner, D. R., & Salem, A. K. (2015). Incorporation of copper into chitosan scaffolds promotes bone regeneration in rat calvarial defects. *Journal of Biomedical Materials Research Part B: Applied Biomaterials*, *103*(5), 1044–1049.

Dar, G. N., Umar, A., Zaidi, S. A., Ibrahim, A. A., Abaker, M., Baskoutas, S., & Al-Assiri, M. S. (2012). Ce-doped ZnO nanorods for the detection of hazardous chemical. *Sensors and Actuators B: Chemical*, *173*, 72–78.

Darr, J. A., Zhang, J., Makwana, N. M., & Weng, X. (2017). Continuous hydrothermal synthesis of inorganic nanoparticles: applications and future directions. *Chemical Reviews*, *117*(17), 11125–11238.

Das, S., Singh, S., Dowding, J. M., Oommen, S., Kumar, A., Sayle, T. X. T., Saraf, S., Patra, C. R., Vlahakis, N. E., & Sayle, D. C. (2012). The induction of angiogenesis by cerium oxide nanoparticles through the modulation of oxygen in intracellular environments. *Biomaterials*, *33*(31), 7746–7755.

De Bartolo, L., Rende, M., Morelli, S., Giusi, G., Salerno, S., Piscioneri, A., Gordano, A., Di Vito, A., Canonaco, M., & Drioli, E. (2008). Influence of membrane surface properties on the growth of neuronal cells isolated from hippocampus. *Journal of Membrane Science*, *325*(1), 139–149.

Delaine-Smith, R. M., MacNeil, S., & Reilly, G. C. (2012). Matrix production and collagen structure are enhanced in two types of osteogenic progenitor cells by a simple fluid shear

stress stimulus. *Eur Cell Mater*, *24*(4), 162–174.

Deliormanlı, A. M. (2015). Synthesis and characterization of cerium-and gallium-containing borate bioactive glass scaffolds for bone tissue engineering. *Journal of Materials Science: Materials in Medicine*, *26*(2), 67.

Desai, M. P., Labhasetwar, V., Amidon, G. L., & Levy, R. J. (1996). Gastrointestinal uptake of biodegradable microparticles: effect of particle size. *Pharmaceutical Research*, *13*(12), 1838–1845.

DeSaix, P., Betts, J. G., Johnson, E., Johnson, J. E., Korol, O., Kruse, D. H., Poe, B., Wise, J. A., & Young, K. A. (2013). *Anatomy & Physiology: OpenStax*.

Devescovi, V., Leonardi, E., Ciapetti, G., & Cenni, E. (2008). Growth factors in bone repair. *La Chirurgia Degli Organi Di Movimento*, *92*(3), 161–168.

Dias, R. C. M., Góes, A. M., Serakides, R., Ayres, E., & Oréfice, R. L. (2010). Porous biodegradable polyurethane nanocomposites: preparation, characterization, and biocompatibility tests. *Materials Research*, *13*(2), 211–218.

Dumontel, B., Canta, M., Engelke, H., Chiodoni, A., Racca, L., Ancona, A., Limongi, T., Canavese, G., & Cauda, V. (2017). Enhanced biostability and cellular uptake of zinc oxide nanocrystals shielded with a phospholipid bilayer. *Journal of Materials Chemistry B*, *5*(44), 8799–8813.

Feng, P., Wei, P., Shuai, C., & Peng, S. (2014). Characterization of mechanical and biological properties of 3-D scaffolds reinforced with zinc oxide for bone tissue engineering. *PloS One*, *9*(1), e87755.

Fernandes, D. M., Silva, R., Hechenleitner, A. A. W., Radovanovic, E., Melo, M. A. C., & Pineda, E. A. G. (2009). Synthesis and characterization of ZnO, CuO and a mixed Zn and Cu oxide. *Materials Chemistry and Physics*, *115*(1), 110–115.

Figg, W. D., & Folkman, J. (2008). *Angiogenesis: an integrative approach from science to medicine*. Springer Science & Business Media.

Florencio-Silva, R., Sasso, G. R. da S., Sasso-Cerri, E., Simões, M. J., & Cerri, P. S. (2015). Biology of bone tissue: structure, function, and factors that influence bone cells. *BioMed Research International*, *2015*.

Foroutan, T. (2014). The effects of zinc oxide nanoparticles on differentiation of human mesenchymal stem cells to osteoblast. *Nanomedicine Journal*, *1*(5), 308–314.

Frenot, A., & Chronakis, I. S. (2003). Polymer nanofibers assembled by electrospinning. *Current Opinion in Colloid & Interface Science*, *8*(1), 64–75.

Fuchs, R. K., Warden, S. J., & Turner, C. H. (2009). Bone anatomy, physiology and adaptation to mechanical loading. In *Bone repair biomaterials* (pp. 25–68). Elsevier.

Gao, C., Deng, Y., Feng, P., Mao, Z., Li, P., Yang, B., Deng, J., Cao, Y., Shuai, C., & Peng, S. (2014). Current progress in bioactive ceramic scaffolds for bone repair and regeneration. *International Journal of Molecular Sciences*, *15*(3), 4714–4732.

Garrison, K. R., Donell, S., Ryder, J., Shemilt, I., Mugford, M., Harvey, I., & Song, F. (2007). Clinical effectiveness and cost-effectiveness of bone morphogenetic proteins in the non-healing of fractures and spinal fusion: a systematic review. *Health Technology Assessment (Winchester, England)*, *11*(30), 1–150.

Gautschi, O. P., Frey, S. P., & Zellweger, R. (2007). Bone morphogenetic proteins in clinical applications. *ANZ Journal of Surgery*, *77*(8), 626–631.

Gazia, R., Chiodoni, A., Bianco, S., Lamberti, A., Quaglio, M., Sacco, A., Tresso, E., Mandracci, P., & Pirri, C. F. (2012). An easy method for the room-temperature growth of spongelike nanostructured Zn films as initial step for the fabrication of nanostructured ZnO. *Thin Solid Films*, *524*, 107–112.

Gerhardt, H. (2008). VEGF and endothelial guidance in angiogenic sprouting. In *VEGF in Development* (pp. 68–78). Springer.

Giahi, M., Badalpoor, N., Habibi, S., & Taghavi, H. (2013). Synthesis of CuO/ZnO nanoparticles and their application for photocatalytic degradation of lidocaine HCl by the trial-and-error and Taguchi methods. *Bulletin of the Korean Chemical Society*, *34*(7), 2176–2182.

Giannoudis, P. V, & Tzioupis, C. (2005). Clinical applications of BMP-7: the UK perspective. *Injury*, *36*(3), S47–S50.

Gogolewski, S., & Gorna, K. (2007). Biodegradable polyurethane cancellous bone graft substitutes in the treatment of iliac crest defects. *Journal of Biomedical Materials Research Part A: An Official Journal of The Society for Biomaterials, The Japanese Society for Biomaterials, and The Australian Society for Biomaterials and the Korean Society for Biomaterials*, *80*(1), 94–101.

Gong, T., Xie, J., Liao, J., Zhang, T., Lin, S., & Lin, Y. (2015). Nanomaterials and bone regeneration. *Bone Research*, *3*, 15029.

Gorna, K., & Gogolewski, S. (2003). Preparation, degradation, and calcification of biodegradable polyurethane foams for bone graft substitutes. *Journal of Biomedical Materials Research. Part A*, *67*(3), 813–827. https://doi.org/10.1002/jbm.a.10148

Govender, S., Csimma, C., Genant, H. K., Valentin-Opran, A., Amit, Y., Arbel, R., Aro, H., Atar, D., Bishay, M., & Börner, M. G. (2002). Recombinant human bone morphogenetic protein-2 for treatment of open tibial fractures: a prospective, controlled, randomized study of four hundred and fifty patients. *JBJS*, *84*(12), 2123–2134.

Grad, S., Kupcsik, L., Gorna, K., Gogolewski, S., & Alini, M. (2003). The use of biodegradable polyurethane scaffolds for cartilage tissue engineering: Potential and limitations. *Biomaterials*, *24*(28), 5163–5171. https://doi.org/10.1016/S0142-9612(03)00462-9

Guelcher, S. A. (2008). Biodegradable Polyurethanes: Synthesis and Applications in Regenerative Medicine. *Tissue Engineering Part B: Reviews*, *14*(1), 3–17. https://doi.org/10.1089/teb.2007.0133

Guelcher, S. a., Patel, V., Gallagher, K., Connolly, S., Didier, J. E., Doctor, J., & Hollinger, J. O. (2004). Synthesis of polyurethane foam scaffolds for bone tissue engineering. *AIChE Annual Meeting, Conference Proceedings*, *30*, 1087–1089.

Hollinger, J. O., Einhorn, T. A., Doll, B., & Sfeir, C. (2004). *Bone tissue engineering*. CRC press.

Hollister, S. J. (2005). Porous scaffold design for tissue engineering. *Nature Materials*, *4*(7), 518.

Hollister, S. J., Lin, C. Y., Saito, E., Lin, C. Y., Schek, R. D., Taboas, J. M., Williams, J. M., Partee, B., Flanagan, C. L., & Diggs, A. (2005). Engineering craniofacial scaffolds. *Orthodontics & Craniofacial Research*, *8*(3), 162–173.

Hornyak, G. L., Tibbals, H. F., Dutta, J., & Moore, J. J. (2008). *Introduction to nanoscience and nanotechnology*. CRC press.

Horowitz, A., & Simons, M. (2008). Branching morphogenesis. *Circulation Research*, *103*(8), 784–795.

Hosseini, M., & Mozafari, M. (2020). Cerium oxide nanoparticles: Recent advances in tissue engineering. *Materials*, *13*(14), 3072.

Howlett, C. R., Evans, M. D. M., Walsh, W. R., Johnson, G., & Steele, J. G. (1994). Mechanism of initial attachment of cells derived from human bone to commonly used prosthetic materials during cell culture. *Biomaterials*, *15*(3), 213–222.

Huang, S. H., Liu, P., Mokasdar, A., & Hou, L. (2013). Additive manufacturing and its societal impact: A literature review. *International Journal of Advanced Manufacturing Technology*, *67*(5–8), 1191–1203. https://doi.org/10.1007/s00170-012-4558-5

Im, O., Li, J., Wang, M., Zhang, L. G., & Keidar, M. (2012). Biomimetic three-dimensional nanocrystalline hydroxyapatite and magnetically synthesized single-walled carbon nanotube chitosan nanocomposite for bone regeneration. *International Journal of Nanomedicine*, *7*, 2087.

Jaidev, L. R., Kumar, S., & Chatterjee, K. (2017). Multi-biofunctional polymer graphene composite for bone tissue regeneration that elutes copper ions to impart angiogenic, osteogenic and bactericidal properties. *Colloids and Surfaces B: Biointerfaces*, *159*, 293–302.

James, A. W., LaChaud, G., Shen, J., Asatrian, G., Nguyen, V., Zhang, X., Ting, K., & Soo, C. (2016). A review of the clinical side effects of bone morphogenetic protein-2. *Tissue Engineering Part B: Reviews*, *22*(4), 284–297.

Jiang, J., Pi, J., & Cai, J. (2018). The advancing of zinc oxide nanoparticles for biomedical applications. *Bioinorganic Chemistry and Applications*, *2018*.

Johnson, E. E., Urist, M. R., & Finerman, G. A. (1992). Resistant nonunions and partial or complete segmental defects of long bones. Treatment with implants of a composite of human bone morphogenetic protein (BMP) and autolyzed, antigen-extracted, allogeneic (AAA) bone. *Clinical Orthopaedics and Related Research*, *277*, 229–237.

Jones, N. (1997). *Craniofacial trauma: An interdisciplinary approach*. Oxford University Press, USA.

Josset, Y., Oum'Hamed, Z., Zarrinpour, A., Lorenzato, M., Adnet, J.-J., & Laurent–Maquin, D. (1999). In vitro reactions of human osteoblasts in culture with zirconia and alumina ceramics. *Journal of Biomedical Materials Research: An Official Journal of The Society for Biomaterials, The Japanese Society for Biomaterials, and The Australian Society for Biomaterials and the Korean Society for Biomaterials*, *47*(4), 481–493.

Kandjani, A. E., Tabriz, M. F., & Pourabbas, B. (2008). Sonochemical synthesis of ZnO nanoparticles: The effect of temperature and sonication power. *Materials Research Bulletin*, *43*(3), 645–654.

Kang, T., Guan, R., Chen, X., Song, Y., Jiang, H., & Zhao, J. (2013). In vitro toxicity of different-sized ZnO nanoparticles in Caco-2 cells. *Nanoscale Research Letters*, *8*(1), 496.

Karsdal, M. A., Larsen, L., Engsig, M. T., Lou, H., Ferreras, M., Lochter, A., Delaissé, J.-M., & Foged, N. T. (2002). Matrix metalloproteinase-dependent activation of latent transforming growth factor-β controls the conversion of osteoblasts into osteocytes by

blocking osteoblast apoptosis. *Journal of Biological Chemistry*, *277*(46), 44061–44067.

Karsenty, G. (1999). The genetic transformation of bone biology. *Genes & Development*, *13*(23), 3037–3051.

Katagiri, T., & Takahashi, N. (2002). Regulatory mechanisms of osteoblast and osteoclast differentiation. *Oral Diseases*, *8*(3), 147–159.

Khalili, A. A., & Ahmad, M. R. (2015). A review of cell adhesion studies for biomedical and biological applications. *International Journal of Molecular Sciences*, *16*(8), 18149–18184.

Kołodziejska, B., Kaflak, A., & Kolmas, J. (2020). Biologically inspired collagen/apatite composite biomaterials for potential use in bone tissue regeneration—a review. *Materials*, *13*(7), 1748.

Kornu, R., Smith, R. L., Maloney, W. J., & Kelly, M. A. (1996). Osteoblast adhesion to orthopaedic implant alloys: Effects of cell adhesion molecules and diamond-like carbon coating. *Journal of Orthopaedic Research*, *14*(6), 871–877.

Kubota, K., Sakikawa, C., Katsumata, M., Nakamura, T., & Wakabayashi, K. (2002). Platelet-Derived Growth Factor BB Secreted From Osteoclasts Acts as an Osteoblastogenesis Inhibitory Factor. *Journal of Bone and Mineral Research*, *17*(2), 257–265.

Kulandaisamy, A. J., Elavalagan, V., Shankar, P., Mani, G. K., Babu, K. J., & Rayappan, J. B. B. (2016). Nanostructured Cerium-doped ZnO thin film–A breath sensor. *Ceramics International*, *42*(16), 18289–18295.

Kumar, R., Umar, A., Kumar, G., & Nalwa, H. S. (2017). Antimicrobial properties of ZnO nanomaterials: A review. *Ceramics International*, *43*(5), 3940–3961.

Kurz, H., Burri, P. H., & Djonov, V. G. (2003). Angiogenesis and vascular remodeling by intussusception: from form to function. *Physiology*, *18*(2), 65–70.

Kusakawa, Y., Yoshida, E., & Hayakawa, T. (2017). Protein adsorption to titanium and zirconia using a quartz crystal microbalance method. *BioMed Research International*, *2017*.

Kyurkchiev, D., Bochev, I., Ivanova-Todorova, E., Mourdjeva, M., Oreshkova, T., Belemezova, K., & Kyurkchiev, S. (2014). Secretion of immunoregulatory cytokines by mesenchymal stem cells. *World Journal of Stem Cells*, *6*(5), 552.

Laurenti, M., Verna, A., Fontana, M., Quaglio, M., & Porro, S. (2014). Selective growth of ZnO nanowires on substrates patterned by photolithography and inkjet printing. *Applied*

Physics A, *117*(2), 901–907.

Lee, J.-Y., Nam, S.-H., Im, S.-Y., Park, Y.-J., Lee, Y.-M., Seol, Y.-J., Chung, C.-P., & Lee, S.-J. (2002). Enhanced bone formation by controlled growth factor delivery from chitosan-based biomaterials. *Journal of Controlled Release*, *78*(1–3), 187–197.

Lee, S. J., San Choi, J., Park, K. S., Khang, G., Lee, Y. M., & Lee, H. B. (2004). Response of MG63 osteoblast-like cells onto polycarbonate membrane surfaces with different micropore sizes. *Biomaterials*, *25*(19), 4699–4707.

Leuning, D. G., Beijer, N. R. M., Du Fossé, N. A., Vermeulen, S., Lievers, E., Van Kooten, C., Rabelink, T. J., & De Boer, J. (2018). The cytokine secretion profile of mesenchymal stromal cells is determined by surface structure of the microenvironment. *Scientific Reports*, *8*(1), 1–9.

Lieberman, J. R., Daluiski, A., & Einhorn, T. A. (2002). The role of growth factors in the repair of bone: biology and clinical applications. *JBJS*, *84*(6), 1032–1044.

Lind, M., Schumacker, B., Søballe, K., Keller, J., Melsen, F., & Bünger, C. (1993). Transforming growth factor-β enhances fracture healing in rabbit tibiae. *Acta Orthopaedica Scandinavica*, *64*(5), 553–556.

Lindaman, L. M. (2001). Bone healing in children. *Clinics in Podiatric Medicine and Surgery*, *18*(1), 97–108.

Linh, N. T. B., Jang, D.-W., & Lee, B.-T. (2015). Collagen immobilization of multi-layered BCP-ZrO2 bone substitutes to enhance bone formation. *Applied Surface Science*, *345*, 238–248.

Liu, C., Fu, X., Pan, H., Wan, P., Wang, L., Tan, L., Wang, K., Zhao, Y., Yang, K., & Chu, P. K. (2016). Biodegradable Mg-Cu alloys with enhanced osteogenesis, angiogenesis, and long-lasting antibacterial effects. *Scientific Reports*, *6*, 27374.

Lü, R., Zhou, W., Shi, K., Yang, Y., Wang, L., Pan, K., Tian, C., Ren, Z., & Fu, H. (2013). Alumina decorated TiO 2 nanotubes with ordered mesoporous walls as high sensitivity NO x gas sensors at room temperature. *Nanoscale*, *5*(18), 8569–8576.

Macchetta, A., Turner, I. G., & Bowen, C. R. (2009). Fabrication of HA/TCP scaffolds with a graded and porous structure using a camphene-based freeze-casting method. *Acta Biomaterialia*, *5*(4), 1319–1327.

Malda, J., Rouwkema, J., Martens, D. E., le Comte, E. P., Kooy, F. K., Tramper, J., van Blitterswijk, C. A., & Riesle, J. (2004). Oxygen gradients in tissue-engineered Pegt/Pbt cartilaginous constructs: measurement and modeling. *Biotechnology and*

Bioengineering, *86*(1), 9–18.

Mansour, S. F., El-Dek, S. I., & Ahmed, M. K. (2017). Physico-mechanical and morphological features of zirconia substituted hydroxyapatite nano crystals. *Scientific Reports*, *7*, 43202.

McFarland, C. D., Thomas, C. H., DeFilippis, C., Steele, J. G., & Healy, K. E. (2000). Protein adsorption and cell attachment to patterned surfaces. *Journal of Biomedical Materials Research: An Official Journal of The Society for Biomaterials and The Japanese Society for Biomaterials*, *49*(2), 200–210.

Miccoli, B., Cauda, V., Bonanno, A., Sanginario, A., Bejtka, K., Bella, F., Fontana, M., & Demarchi, D. (2016). One-dimensional ZnO/gold junction for simultaneous and versatile multisensing measurements. *Scientific Reports*, *6*, 29763.

Mohamed, A. M. (2008). An overview of bone cells and their regulating factors of differentiation. *The Malaysian Journal of Medical Sciences: MJMS*, *15*(1), 4.

Mohan, A. C., & Renjanadevi, B. (2016). Preparation of zinc oxide nanoparticles and its characterization using scanning electron microscopy (SEM) and X-ray diffraction (XRD). *Procedia Technology*, *24*, 761–766.

Morra, M. (2001). *Water in biomaterials surface science*. John Wiley & Sons.

Mourino, V., Cattalini, J. P., & Boccaccini, A. R. (2012). Metallic ions as therapeutic agents in tissue engineering scaffolds: an overview of their biological applications and strategies for new developments. *Journal of the Royal Society Interface*, *9*(68), 401–419.

Naik, E. I., Naik, H. S. B., Viswanath, R., Kirthan, B. R., & Prabhakara, M. C. (2020). Effect of zirconium doping on the structural, optical, electrochemical and antibacterial properties of ZnO nanoparticles prepared by sol-gel method. *Chemical Data Collections*, *29*, 100505.

Naveed Ul Haq, A., Nadhman, A., Ullah, I., Mustafa, G., Yasinzai, M., & Khan, I. (2017). Synthesis approaches of zinc oxide nanoparticles: the dilemma of ecotoxicity. *Journal of Nanomaterials*, *2017*.

Nethi, S. K., Nanda, H. S., Steele, T. W. J., & Patra, C. R. (2017). Functionalized nanoceria exhibit improved angiogenic properties. *Journal of Materials Chemistry B*, *5*(47), 9371–9383.

Nielsen, H. M., Andreassen, T. T., Ledet, T., & Oxlund, H. (1994). Local injection of TGF-β increases the strength of tibial fractures in the rat. *Acta Orthopaedica Scandinavica*, *65*(1), 37–41.

Nordsletten, L. (2006). Recent developments in the use of bone morphogenetic protein in orthopaedic trauma surgery. *Current Medical Research and Opinion*, *22*(sup1), S13–S17.

Nordsletten, L., & Madsen, J. E. (2006). The effect of bone morphogenetic proteins in fracture healing. *Scandinavian Journal of Surgery*, *95*(2), 91–94.

Ong, K. L., Villarraga, M. L., Lau, E., Carreon, L. Y., Kurtz, S. M., & Glassman, S. D. (2010). Off-label use of bone morphogenetic proteins in the United States using administrative data. *Spine*, *35*(19), 1794–1800.

Pacholski, C., Kornowski, A., & Weller, H. (2002). Self-assembly of ZnO: from nanodots to nanorods. *Angewandte Chemie International Edition*, *41*(7), 1188–1191.

Panyam, J., & Labhasetwar, V. (2003). Biodegradable nanoparticles for drug and gene delivery to cells and tissue. *Advanced Drug Delivery Reviews*, *55*(3), 329–347.

Parisi, L., Toffoli, A., Ghezzi, B., Mozzoni, B., Lumetti, S., & Macaluso, G. M. (2020). A glance on the role of fibronectin in controlling cell response at biomaterial interface. *Japanese Dental Science Review*, *56*(1), 50–55.

Park, Y.-S., Kim, K.-N., Kim, K.-M., Choi, S.-H., Kim, C.-K., Legeros, R. Z., & Lee, Y.-K. (2006). Feasibility of three-dimensional macroporous scaffold using calcium phosphate glass and polyurethane sponge. *Journal of Materials Science*, *41*(13), 4357–4364.

Patil, S., Sandberg, A., Heckert, E., Self, W., & Seal, S. (2007). Protein adsorption and cellular uptake of cerium oxide nanoparticles as a function of zeta potential. *Biomaterials*, *28*(31), 4600–4607.

Pignolo, Robert J., Kaplan, F. S. (2008). No Title. In *Interventional Spine an algorithmic approach* (pp. 423–433). Elsevier. https://doi.org/10.1016/B978-0-7216-2872-1.50043-1

Rahyussalim, A. J., Supriadi, S., Marsetio, A. F., Pribadi, P. M., & Suharno, B. (2019). The potential of carbonate apatite as an alternative bone substitute material. *Medical Journal of Indonesia*, *28*(1), 92–97.

Rajzer, I. (2014). Fabrication of bioactive polycaprolactone/hydroxyapatite scaffolds with final bilayer nano-/micro-fibrous structures for tissue engineering application. *Journal of Materials Science*, *49*(16), 5799–5807.

Rasmussen, J. W., Martinez, E., Louka, P., & Wingett, D. G. (2010). Zinc oxide nanoparticles for selective destruction of tumor cells and potential for drug delivery applications. *Expert Opinion on Drug Delivery*, *7*(9), 1063–1077.

Rehman, I., & Bonfield, Wjj. (1997). Characterization of hydroxyapatite and carbonated

apatite by photo acoustic FTIR spectroscopy. *Journal of Materials Science: Materials in Medicine*, *8*(1), 1–4.

Rezaei, M., & Habibi-Yangjeh, A. (2013). Simple and large scale refluxing method for preparation of Ce-doped ZnO nanostructures as highly efficient photocatalyst. *Applied Surface Science*, *265*, 591–596.

Rezania, A., & Healy, K. E. (2000). The effect of peptide surface density on mineralization of a matrix deposited by osteogenic cells. *Journal of Biomedical Materials Research*, *52*(4), 595–600.

Risau, W. (1997). Mechanisms of angiogenesis. *Nature*, *386*(6626), 671.

Rizzo, D. C. (2015). *Fundamentals of anatomy and physiology*. Cengage Learning.

Roduner, E. (2006). Size matters: why nanomaterials are different. *Chemical Society Reviews*, *35*(7), 583–592.

Rouwkema, J., Rivron, N. C., & van Blitterswijk, C. A. (2008). Vascularization in tissue engineering. *Trends in Biotechnology*, *26*(8), 434–441.

Ruhrberg, C., Gerhardt, H., Golding, M., Watson, R., Ioannidou, S., Fujisawa, H., Betsholtz, C., & Shima, D. T. (2002). Spatially restricted patterning cues provided by heparin-binding VEGF-A control blood vessel branching morphogenesis. *Genes & Development*, *16*(20), 2684–2698.

Sadat-Shojai, M., Khorasani, M.-T., Dinpanah-Khoshdargi, E., & Jamshidi, A. (2013). Synthesis methods for nanosized hydroxyapatite with diverse structures. *Acta Biomaterialia*, *9*(8), 7591–7621.

Sajjad, M., Ullah, I., Khan, M. I., Khan, J., Khan, M. Y., & Qureshi, M. T. (2018). Structural and optical properties of pure and copper doped zinc oxide nanoparticles. *Results in Physics*, *9*, 1301–1309.

Salatin, S., Maleki Dizaj, S., & Yari Khosroushahi, A. (2015). Effect of the surface modification, size, and shape on cellular uptake of nanoparticles. *Cell Biology International*, *39*(8), 881–890.

Sanginario, A., Cauda, V., Bonanno, A., Bejtka, K., Sapienza, S., & Demarchi, D. (2016). An electronic platform for real-time detection of bovine serum albumin by means of amine-functionalized zinc oxide microwires. *RSC Advances*, *6*(2), 891–897.

Sapkal, P. S., Kuthe, A. M., Kashyap, R. S., Nayak, A. R., Kuthe, S. A., & Kawle, A. P. (2017). Indirect casting of patient-specific tricalcium phosphate zirconia scaffolds for bone tissue regeneration using rapid prototyping methodology. *Journal of Porous*

Materials, *24*(4), 1013–1023.

Schipani, E., Maes, C., Carmeliet, G., & Semenza, G. L. (2009). Regulation of osteogenesis-angiogenesis coupling by HIFs and VEGF. *Journal of Bone and Mineral Research*, *24*(8), 1347–1353.

Schmidt, A., Brixius, K., & Bloch, W. (2007). Endothelial precursor cell migration during vasculogenesis. *Circulation Research*, *101*(2), 125–136.

Sebastian, V., Arruebo, M., & Santamaria, J. (2014). Reaction engineering strategies for the production of inorganic nanomaterials. *Small*, *10*(5), 835–853.

Setiawati, R., & Rahardjo, P. (2019). Bone Development and Growth. In P. R. E.-H. Yang (Ed.), *Osteogenesis and Bone Regeneration* (p. Ch. 1). IntechOpen. https://doi.org/10.5772/intechopen.82452

Shafi, K. M., Vinodkumar, R., Bose, R. J., Uvais, V. N., & Pillai, V. P. M. (2013). Effect of Cu on the microstructure and electrical properties of Cu/ZnO thin films. *Journal of Alloys and Compounds*, *551*, 243–248.

Shi, R., Yang, P., Wang, J., Zhang, A., Zhu, Y., Cao, Y., & Ma, Q. (2012). Growth of flower-like ZnO via surfactant-free hydrothermal synthesis on ITO substrate at low temperature. *CrystEngComm*, *14*(18), 5996–6003.

Shimoaka, T., Ogasawara, T., Yonamine, A., Chikazu, D., Kawano, H., Nakamura, K., Itoh, N., & Kawaguchi, H. (2002). Regulation of osteoblast, chondrocyte, and osteoclast functions by fibroblast growth factor (FGF)-18 in comparison with FGF-2 and FGF-10. *Journal of Biological Chemistry*, *277*(9), 7493–7500.

Shitole, A. A., Raut, P. W., Sharma, N., Giram, P., Khandwekar, A. P., & Garnaik, B. (2019). Electrospun polycaprolactone/hydroxyapatite/ZnO nanofibers as potential biomaterials for bone tissue regeneration. *Journal of Materials Science: Materials in Medicine*, *30*(5), 1–17.

Shkarina, S., Shkarin, R., Weinhardt, V., Melnik, E., Vacun, G., Kluger, P. J., Loza, K., Epple, M., Ivlev, S. I., & Baumbach, T. (2018). 3D biodegradable scaffolds of polycaprolactone with silicate-containing hydroxyapatite microparticles for bone tissue engineering: High-resolution tomography and in vitro study. *Scientific Reports*, *8*(1), 1–13.

Shrestha, B. K., Shrestha, S., Tiwari, A. P., Kim, J.-I., Ko, S. W., Kim, H.-J., Park, C. H., & Kim, C. S. (2017). Bio-inspired hybrid scaffold of zinc oxide-functionalized multi-wall carbon nanotubes reinforced polyurethane nanofibers for bone tissue engineering.

Materials & Design, *133*, 69–81.

Shruti, S., Salinas, A. J., Lusvardi, G., Malavasi, G., Menabue, L., & Vallet-Regi, M. (2013). Mesoporous bioactive scaffolds prepared with cerium-, gallium-and zinc-containing glasses. *Acta Biomaterialia*, *9*(1), 4836–4844.

Simons, M. (2005). *Angiogenesis, arteriogenesis, and diabetes: paradigm reassessed?* Journal of the American College of Cardiology.

Sinha, N., Ray, G., Bhandari, S., Godara, S., & Kumar, B. (2014). Synthesis and enhanced properties of cerium doped ZnO nanorods. *Ceramics International*, *40*(8), 12337–12342.

Sittichockechaiwut, A., Scutt, A. M., Ryan, A. J., Bonewald, L. F., & Reilly, G. C. (2009). Use of rapidly mineralising osteoblasts and short periods of mechanical loading to accelerate matrix maturation in 3D scaffolds. *Bone*, *44*(5), 822–829. https://doi.org/10.1016/j.bone.2008.12.027

Sittichokechaiwut, a, Edwards, J. H., Scutt, a M., & Reilly, G. C. (2010). Short bouts of mechanical loading are as effective as dexamethasone at inducing matrix production by human bone marrow mesenchymal stem cell. *European Cells & Materials*, *20*, 45–57. https://doi.org/vol020a05 [pii]

Small, J. V., Stradal, T., Vignal, E., & Rottner, K. (2002). The lamellipodium: where motility begins. *Trends in Cell Biology*, *12*(3), 112–120.

Srisuvetha, V. T., Rayar, S. L., & Shanthi, G. (2020). Role of cerium (Ce) dopant on structural, optical and photocatalytic properties of MgO nanoparticles by wet chemical route. *Journal of Materials Science: Materials in Electronics*, *31*(4), 2799–2808.

Stegen, S., van Gastel, N., & Carmeliet, G. (2015). Bringing new life to damaged bone: the importance of angiogenesis in bone repair and regeneration. *Bone*, *70*, 19–27.

Stephansson, S. N., Byers, B. A., & García, A. J. (2002). Enhanced expression of the osteoblastic phenotype on substrates that modulate fibronectin conformation and integrin receptor binding. *Biomaterials*, *23*(12), 2527–2534.

Strick, D. M., Waycaster, R. L., Montani, J.-P., Gay, W. J., & Adair, T. H. (1991). Morphometric measurements of chorioallantoic membrane vascularity: effects of hypoxia and hyperoxia. *American Journal of Physiology-Heart and Circulatory Physiology*, *260*(4), H1385–H1389.

Sulaiman, S. Bin, Keong, T. K., Cheng, C. H., Saim, A. Bin, & Idrus, R. B. H. (2013). Tricalcium phosphate/hydroxyapatite (TCP-HA) bone scaffold as potential candidate for the formation of tissue engineered bone. *The Indian Journal of Medical Research*,

137(6), 1093.

Tallia, F., Gallo, M., Pontiroli, L., Baino, F., Fiorilli, S., Onida, B., Anselmetti, G. C., Manca, A., & Vitale-Brovarone, C. (2014). Zirconia-containing radiopaque mesoporous bioactive glasses. *Materials Letters*, *130*, 281–284.

Terjung, R. L., Zarzeczny, R., & Yang, H. T. (2002). Muscle blood flow and mitochondrial function: influence of aging. *International Journal of Sport Nutrition and Exercise Metabolism*, *12*(3), 368–378.

Tetteh, G., Khan, A. S., Delaine-Smith, R. M., Reilly, G. C., & Rehman, I. U. (2014). Electrospun polyurethane/hydroxyapatite bioactive Scaffolds for bone tissue engineering: The role of solvent and hydroxyapatite particles. *Journal of the Mechanical Behavior of Biomedical Materials*, *39*, 95–110. https://doi.org/10.1016/j.jmbbm.2014.06.019

Tetteh, Gifty. (2016). *Polyurethane-based Scaffolds for Bone Tissue Engineering. The Role of Hydroxyapatite Particles, Solvent Combinations, Electrospun Fibre Orientations, In Vivo & In Vitro Characterisation, and Particulate Leached Foams for creating 3-D Bone Models.* University of Sheffield.

Tosiriwatanapong, T., & Singhatanadgit, W. (2018). Zirconia-based biomaterials for hard tissue reconstruction. *Bone and Tissue Regeneration Insights*, *9*, 1179061X18767886.

Tsay, C.-Y., & Fan, K.-S. (2008). Optimization of Zr-doped ZnO thin films prepared by sol-gel method. *Materials Transactions*, *49*(8), 1900–1904.

Tsuzuki, T. (2009). Commercial scale production of inorganic nanoparticles. *International Journal of Nanotechnology*, *6*(5–6), 567–578.

Van Hinsbergh, V. W. M., & Koolwijk, P. (2007). Endothelial sprouting and angiogenesis: matrix metalloproteinases in the lead. *Cardiovascular Research*, *78*(2), 203–212.

Vannozzi, L., Ricotti, L., Santaniello, T., Terencio, T., Oropesa-Nunez, R., Canale, C., Borghi, F., Menciassi, A., Lenardi, C., & Gerges, I. (2017). 3D porous polyurethanes featured by different mechanical properties: Characterization and interaction with skeletal muscle cells. *Journal of the Mechanical Behavior of Biomedical Materials*, *75*, 147–159.

Vlad, S., Tanase, C., Macocinschi, D., Ciobanu, C., Balaes, T., Filip, D., Gostin, I. N., & Gradinaru, L. M. (2012). Antifungal behaviour of polyurethane membranes with zinc oxide nanoparticles. *Dig. J. Nanomater. Bios*, *7*, 51–58.

Vo, T. N., Kasper, F. K., & Mikos, A. G. (2012). Strategies for controlled delivery of growth

factors and cells for bone regeneration. *Advanced Drug Delivery Reviews*, *64*(12), 1292–1309.

Wagner, P. D. (2001). Skeletal muscle angiogenesis. In *Hypoxia* (pp. 21–38). Springer.

Wang, B., He, X., Zhang, Z., Zhao, Y., & Feng, W. (2012). Metabolism of nanomaterials in vivo: blood circulation and organ clearance. *Accounts of Chemical Research*, *46*(3), 761–769.

Wang, H.-J., Sun, Y.-Y., Cao, Y., Yu, X.-H., Ji, X.-M., & Yang, L. (2011). Porous zinc oxide films: controlled synthesis, cytotoxicity and photocatalytic activity. *Chemical Engineering Journal*, *178*, 8–14.

Wang, Y., Zhang, P., Zhao, Y., Dai, R., Huang, M., Liu, W., Liu, H., He, S., & Zhu, C. (2020). Shape memory composites composed of polyurethane/ZnO nanoparticles as potential smart biomaterials. *Polymer Composites*, *41*(5), 2094–2107.

Widiarti, N., Sae, J. K., & Wahyuni, S. (2017). Synthesis CuO-ZnO nanocomposite and its application as an antibacterial agent. *IOP Conference Series: Materials Science and Engineering*, *172*(1), 12036.

Wolff, J. (1870). Ueber die innere Architectur der Knochen und ihre Bedeutung für die Frage vom Knochenwachsthum. *Archiv Für Pathologische Anatomie Und Physiologie Und Für Klinische Medicin*, *50*(3), 389–450.

Wolff, J. (2010). The classic: on the inner architecture of bones and its importance for bone growth. *Clinical Orthopaedics and Related Research®*, *468*(4), 1056–1065.

Wu, C.-G., DeGroot, D. C., Marcy, H. O., Schindler, J. L., Kannewurf, C. R., Liu, Y.-J., Hirpo, W., & Kanatzidis, M. G. (1996). Redox intercalative polymerization of aniline in V2O5 xerogel. The postintercalative intralamellar polymer growth in polyaniline/metal oxide nanocomposites is facilitated by molecular oxygen. *Chemistry of Materials*, *8*(8), 1992–2004.

Wu, S., Liu, X., Yeung, K. W. K., Liu, C., & Yang, X. (2014). Biomimetic porous scaffolds for bone tissue engineering. *Materials Science and Engineering: R: Reports*, *80*, 1–36.

Xynos, I. D., Edgar, A. J., Buttery, L. D. K., Hench, L. L., & Polak, J. M. (2000). Ionic products of bioactive glass dissolution increase proliferation of human osteoblasts and induce insulin-like growth factor II mRNA expression and protein synthesis. *Biochemical and Biophysical Research Communications*, *276*(2), 461–465.

Yang, Jian, Shi, G., Bei, J., Wang, S., Cao, Y., Shang, Q., Yang, G., & Wang, W. (2002). Fabrication and surface modification of macroporous poly (L-lactic acid) and poly (L-

lactic-co-glycolic acid)(70/30) cell scaffolds for human skin fibroblast cell culture. *Journal of Biomedical Materials Research: An Official Journal of The Society for Biomaterials, The Japanese Society for Biomaterials, and The Australian Society for Biomaterials and the Korean Society for Biomaterials*, *62*(3), 438–446.

Yang, Jinghai, Gao, M., Yang, L., Zhang, Y., Lang, J., Wang, D., Wang, Y., Liu, H., & Fan, H. (2008). Low-temperature growth and optical properties of Ce-doped ZnO nanorods. *Applied Surface Science*, *255*(5), 2646–2650.

Yoganandan, N., & Pintar, F. A. (2004). Biomechanics of temporo-parietal skull fracture. *Clinical Biomechanics*, *19*(3), 225–239.

Yoshida, E., & Hayakawa, T. (2016). Adsorption analysis of lactoferrin to titanium, stainless steel, zirconia, and polymethyl methacrylate using the quartz crystal microbalance method. *BioMed Research International*, *2016*.

Yousefi, M., Amiri, M., Azimirad, R., & Moshfegh, A. Z. (2011). Enhanced photoelectrochemical activity of Ce doped ZnO nanocomposite thin films under visible light. *Journal of Electroanalytical Chemistry*, *661*(1), 106–112.

Yu, H.-D., Regulacio, M. D., Ye, E., & Han, M.-Y. (2013). Chemical routes to top-down nanofabrication. *Chemical Society Reviews*, *42*(14), 6006–6018.

Zamiri, R., Ahangar, H. A., Kaushal, A., Zakaria, A., Zamiri, G., Tobaldi, D., & Ferreira, J. M. F. (2015). Dielectrical properties of CeO2 Nanoparticles at different temperatures. *PLOS One*, *10*(4), e0122989.

Zauner, W., Farrow, N. A., & Haines, A. M. R. (2001). In vitro uptake of polystyrene microspheres: effect of particle size, cell line and cell density. *Journal of Controlled Release*, *71*(1), 39–51.

Zdrahala, R. J., & Zdrahala, I. J. (1999). Biomedical Applications of Polyurethanes: A Review of Past Promises, Present Realities, and a Vibrant Future. In *Journal of Biomaterials Applications* (Vol. 14, Issue 1, pp. 67–90). https://doi.org/10.1177/088532829901400104

Zeferino, R. S., Flores, M. B., & Pal, U. (2011). Photoluminescence and Raman scattering in Ag-doped ZnO nanoparticles. *Journal of Applied Physics*, *109*(1), 14308.

Zhang, J., Gao, D., Yang, G., Zhang, J., Shi, Z., Zhang, Z., Zhu, Z., & Xue, D. (2011). Synthesis and magnetic properties of Zr doped ZnO Nanoparticles. *Nanoscale Research Letters*, *6*(1), 587.

Zhu, P., Weng, Z., Li, X., Liu, X., Wu, S., Yeung, K. W. K., Wang, X., Cui, Z., Yang, X., &

Chu, P. (2016). Biomedical applications of functionalized ZnO nanomaterials: From biosensors to bioimaging. *Advanced Materials Interfaces*, *3*(1).